Centro de Biomateriales
Departament de Termodinàmica Aplicada
Universitat Politècnica de València

FORMULACIÓN DE IMPRIMACIONES EPOXI EN POLVO DE CURADO A BAJAS TEMPERATURAS BASADAS EN TRIFLATOS DE LANTÁNIDO. DESARROLLO DE UNA TÉCNICA ELECTROQUÍMICA PARA LA EVALUACIÓN ACELERADA DE LA PROTECCIÓN ANTICORROSIVA DE RECUBRIMIENTOS ORGÁNICOS: APLICACIÓN A RECUBRIMIENTOS EN POLVO Y CATAFORÉTICOS

Memoria Presentada para Optar al Grado de Doctor por:

Santiago J. García Espallargas

Bajo la dirección del Doctor:

Julio J. Suay Antón

València, 2006

A mi familia

"- Digo, pues, que los trabajos del estudiante son estos: principalmente pobreza (no porque todos sean pobres, sino por poner este caso en todo el extremo que pueda ser); y en haber dicho que padece pobreza me parece que no había que decir más de su mala ventura; porque quien es pobre no tiene cosa buena. Esta pobreza la padece por sus partes, ya en hambre, ya en frío, ya en desnudez, ya en todo junto; pero, con todo eso, no es tanta que no coma, aunque sea poco más tarde de lo que se usa; aunque sea de las sobras de los ricos; que es la mayor miseria del estudiante este que entre ellos llaman *andar a la sopa*; y no les falta algún ajeno brasero o chimenea, que, si no caliente, a lo menos entibie su frío, y, en fin, la noche duermen muy bien debajo de cubierta. No quiero llegar a otras menudencias, conviene a saber, de la falta de camisas y no sobra de zapatos, la caridad y poco pelo del vestido, ni aquel ahitarse con tanto gusto, cuando la buena suerte les depara algún banquete. Por este camino que he pintado, áspero y dificultoso, tropezando aquí, cayendo allí, levantándose acullá, tornando a caer acá, llegan al grado que desean; el cual alcanzado, a muchos hemos visto que habiendo pasado por estas sirtes y por estas Scilas y Caribdis, como llevados en vuelo de la favorable fortuna, digo que los hemos visto mandar y gobernar el mundo desde una silla, trocada su hambre en hartura, su frío en refrigerio, su desnudez en galas y su dormir en una estera en reposar en holandas y damascos, premio justamente merecido de su virtud…"

El Ingenioso Hidalgo Don Quijote de la Mancha
Capítulo XXXVII, Primera parte
Miguel de Cervantes Saavedra

Agradecimientos

Agradecimientos

Aquello que moldea la personalidad de un individuo es todo con lo que tiene contacto. Familia, amigos, entorno, estudios… De la misma forma, esta tesis, es, en función de todas las personas que han influido en su desarrollo de forma directa o indirecta.

Por este motivo mis agradecimientos se extienden a todos aquellos que de una forma u otra han influido en mí y en la propia tesis durante su desarrollo, aquellos que aquí señalo y aquellos de los que probablemente me olvide (lo siento…).

Agradecer a Julio que confiara en mí desde un principio, recordándome a menudo aquella frase mía de pipiolo: "no me quiero aburrir" y haciendo que se materializara en un "massa coses", facilitando el desarrollo de esta tesis. También le agradezco que me haya dado la oportunidad de tener contacto con tantas personas y grupos de trabajo. Y ¡cómo olvidar el famoso "master en recursos humanos"! En definitiva, gracias por darme la posibilidad de vivir la creación de una tesis doctoral.

En segundo lugar quiero hacer especial mención a una persona que ha sido, aún en la distancia, mi mentora en muchas más cosas de las que cree, no sólo en lo científico sino en lo personal. Gràcies Àngels.

To doctor Jochen Hollaender for his kindness in my short stay in Germany and for his availability to talk me about applied electrochemistry to coatings in any place and moment.

A Joseja por su tiempo y ayuda, y a las empresas Naber Polvo S.A. y PPG Ibérica por su financiación. A toda la gente del Centro de Biomateriales de la Universitat Politècnica de València por haberme prestado todo su apoyo, simpatía y equipos.

Agradecer a profesores, como Xavier Ramis, Juan Carlos Galván, Antonia Giménez, José Luis Gómez y Manolo Monleón, su ayuda desinteresada desde un inicio para poder ampliar mis conocimientos.

A mis compañeros del Área de Materiales de la Universitat Jaume I de Castelló: Quique, Raúl, Kudama, Juan, Iván, Chema, Carlos, Mohammad, Pepe, Raquel… y en especial a Eva por su gran apoyo en el laboratorio (ya quedaremos para extruir), a Maite por su experiencia, y a Lluís y Pili por su compañía en el despacho y gran amistad que hemos forjado.

Aussi remercier à Grace, Gilles, Inglèse et Virginia son hospitalité et amabilité pendant mon séjour en Bruxelles.

Ook veel dank aan alle metaianen van de Vrije Universiteit Brussel (Tim, Jan, Annette, Iris, Prof. Vereeken…) voor julie hulp en samenwerking.

A mis amigos que a pesar de no tener muy claro qué hago (cosa por otro lado normal) han comprendido mi dedicación.

Y finalmente a los más próximos a mí: mis padres, hermanos, abuelos y resto de familiares, y como no, Amanda, quien me ha acompañado en este viaje soportando como nadie mis nervios y crisis *tesiles* (y no *tesiles*) apoyándome y animándome en todo momento, aún desde la distancia.

A todos: Gracias.

I. RESUMEN / ABSTRACT

La corrosió dels metalls és un problema de gran importància i abast mundial, tant per a les institucions com per a l'usuari particular. En la lluita contra la tendència natural dels metalls, com l'acer, a oxidar-se, destaca l'aplicació de recobriments orgànics en un intent de ralentitzar el procés de corrosió degut a les elevades prestacions i varietat de productes que aquestos recobriments presenten. El camp dels recobriments en pols és el de major creixement dins del sector de les pintures orgàniques, degut principalment als seus avantatges mediambientals (menys d'un 4% de contingut en solvents volàtils (VOC)) i relatiu baix cost d'aplicació.

Els recobriments de tipus epoxi són els més estesos dins dels emprats per a proteccions anticorrosives de substrats metàl·lics com l'acer i l'alumini. Els sistemes epoxi en pols més utilitzats en l'actualitat empren agents de curat latents derivats de la diciandiamida (DICY), com l'orto-tolilbiguanida (TBG). No obstant, els rangs de temperatura i temps que aquest tipus de sistemes necessiten en el procés de curat són relativament elevats (amb temperatures superiors als 160ºC), presentant així dos limitacions substancials: elevats costos d'aplicació i impossibilitat d'aplicar aquests sistemes en substrats termosensibles com fusta i plàstic. D'aquesta manera es fa necessari desenvolupar nous sistemes orgànics en els què es reduïsca la temperatura i el temps de curat. L'ús d'àcids de Lewis com a iniciadors (o catalitzadors) de la reacció d'entrecreuament de la resina epoxi pareix ser una alternativa als sistemes actuals, a pesar que el seu ús en recobriments orgànics en pols anticorrosius no ha sigut encara investigat.

L'obtenció de les característiques anticorrosives d'una imprimació orgànica aplicada sobre substrat metàl·lic sol realitzar-se per mitjà d'assajos accelerats com el de resistència a boira salina. Al seu torn, atès que el procés de corrosió aquosa és un conjunt de reaccions oxidació-reducció, des dels anys 90 s'utilitzen distintes tècniques electroquímiques per a la seua avaluació, com ara la tècnica d'espectroscòpia d'impedància electroquímica (*Electrochemical Impedance Spectroscopy*, EIS). No obstant, ambdós tipus de tècniques presenten llargs períodes d'avaluació (entre 1 mes i 1 any), elevat nombre de provetes a assajar i elevats costos de desenvolupament. D'esta manera es planteja la necessitat clara en el sector industrial de trobar mètodes d'avaluació amb menors costos econòmics i de menors temps d'elaboració.

En la present tesi doctoral es proposa desenvolupar una tècnica electroquímica accelerada, denominada AC/DC/AC, i l'estudi de la seua viabilitat sobre distints tipus de recobriments orgànics (en pols i cataforétics), així com el seu ús com a ferramenta a l'hora de desenvolupar els recobriments o optimitzar processos d'aplicació i curat.

En el capítol II de la present tesi doctoral es fa un repàs al marc teòric i antecedents del tema trobats a la literatura, al mateix temps que s'estableixen els objectius marcats en el projecte. En el capítol III es presenten els materials emprats, i en el IV els equips, tècniques i assajos aplicats al llarg de la tesi. El capítol V és el cos principal de la tesi doctoral on es presenta, en forma d'articles, els resultats obtinguts en el transcurs de la realització de la tesi per a, en el capítol VI, presentar les conclusions obtingudes en funció dels objectius generals marcats en l'inici i els resultats del capítol V.

La corrosión de los metales es un problema de gran importancia y alcance mundial, tanto para las instituciones como para el usuario particular. En la lucha contra la tendencia natural de los metales, como el acero, a oxidarse, destaca la aplicación de recubrimientos orgánicos en un intento de ralentizar el proceso de corrosión debido a las elevadas prestaciones y variedad de productos que éstos recubrimientos presentan. El campo de los recubrimientos en polvo es el de mayor crecimiento dentro del sector de las pinturas orgánicas, debido principalmente a sus ventajas medioambientales (menos de un 4% de contenido en solventes volátiles (VOC)) y relativo bajo coste de aplicación.

Los recubrimientos de tipo epoxi son los más extendidos dentro de los empleados para protecciones anticorrosivas de substratos metálicos como el acero y el aluminio. Los sistemas epoxi en polvo más utilizados en la actualidad emplean agentes de curado latentes derivados de la diciandiamida (DICY), como la orto-tolilbiguanida (TBG). No obstante, los rangos de temperatura y tiempo que este tipo de sistemas necesitan en el proceso de curado son relativamente elevados (con temperaturas superiores a los 160ºC), presentando así dos limitaciones sustanciales: altos costes de aplicación e imposibilidad de aplicar estos sistemas en substratos termosensibles como madera y plástico. De esta forma se hace necesario desarrollar nuevos sistemas orgánicos en los que se reduzca la temperatura y tiempo de curado. El empleo de ácidos de Lewis como iniciadores (o catalizadores) de la reacción de entrecruzamiento de la resina epoxi parece ser una alternativa a los sistemas actuales, a pesar que su uso en recubrimientos orgánicos en polvo anticorrosivos no ha sido todavía investigado.

La obtención de las características anticorrosivas de una imprimación orgánica aplicada sobre substrato metálico suele realizarse mediante ensayos acelerados como el de resistencia a niebla salina. A su vez, dado que el proceso de corrosión acuosa es un conjunto de reacciones oxidación-reducción, desde los años 90 se utilizan distintas técnicas electroquímicas para su evaluación, como por ejemplo la técnica de espectroscopia de impedancia electroquímica (*Electrochemical Impedance Spectroscopy*, EIS). Sin embargo, ambos tipos de técnicas presentan largos periodos de evaluación (entre 1 mes y 1 año), elevado número de probetas a ensayar y elevados costes de desarrollo. De esta forma se plantea la necesidad clara en el sector industrial de encontrar métodos de evaluación con menores costes económicos y de menores tiempos de elaboración.

En la presente tesis doctoral se propone desarrollar una técnica electroquímica acelerada, denominada AC/DC/AC, y el estudio de su viabilidad sobre distintos tipos de recubrimientos orgánicos (en polvo y cataforéticos), así como su empleo como herramienta a la hora de desarrollar los recubrimientos u optimizar procesos de aplicación y curado.

En el capítulo II de la presente tesis doctoral se hace un repaso al marco teórico y antecedentes del tema encontrados en la literatura, a la vez que se establecen los objetivos marcados en el proyecto. En el capítulo III se presentan los materiales empleados, y en el IV los equipos, técnicas y ensayos aplicados a lo largo de la tesis. El capítulo V es el cuerpo principal de la tesis doctoral donde se presenta, en forma de artículos, los resultados obtenidos en el transcurso de la realización de la tesis para, en el capítulo VI, presentar las conclusiones obtenidas en función de los objetivos generales marcados en el inicio y los resultados del capítulo V.

Corrosion of metals is a problem of great importance and world's scale, for the institutions as well as for the user. In the fight against the natural trend of metals, such as steel, to corrode, the use of organic coatings is the most spread way to stop or decelerate the corrosion process due to the high performance and variety of products that these kind of coatings present. The field of powder coatings presents the major growing in the industry of organic paints, mainly due to their great environmental advantages (less than a 4% of volatile organic contents (VOC)) and relative low-costs application.

Epoxy coatings are the most extended coatings amongst those used for anticorrosive protection of metallic substrates such as steel and aluminium. The nowadays most employed powder epoxy systems, use compounds derived from dicyandiamide (DICY), such as orto-tolylbiguanide (TBG), as latent curing agents. Nevertheless, the ranges of curing temperature and time that this kind of systems need in the curing process are relatively high (with temperatures above 160ºC), thus presenting two main handicaps: high application costs, and the impossibility of using these systems on thermo-sensitive substrates such as wood or plastic. Therefore, it is necessary the development of new organic systems in which curing temperature and time are reduced. The use of Lewis acids as initiators (or catalysts) of the crosslinking reaction of the epoxy resin appears as an alternative to conventional systems, although if their use in powder anticorrosive organic coatings has not yet been investigated.

The anticorrosive characteristics of an organic primer applied on metallic substrates are usually obtained by accelerated tests such as the resistance to salt fog spray. Moreover, due to the fact that the aqueous corrosion process is a whole of oxidation-reduction reactions, since the 90's different electrochemical techniques are used for the evaluation, such as the electrochemical impedance spectroscopy (EIS). Nevertheless, both kinds of techniques present long evaluation periods (1 month to one year), high number of tested samples, and high evaluation costs. Thus, the industrial sector is still having the need to find new evaluation methods with lower economic costs and lower testing times.

In the present doctoral thesis it is proposed the development of an accelerated electrochemical technique, named AC/DC/AC, and the study of its viability on different kind of organic coatings (powder and cataphoretic ones), as well as its use as a tool to develop new coatings or to optimize the application and curing processes.

In chapter II of this doctoral thesis it is briefly presented the theoretical background and general knowledge of the topic of study found in the literature and at the same time the objectives of the study are presented. Chapter III shows the used materials, while chapter IV presents the techniques, equipment and applied tests used along the thesis. Chapter V is the main body text of the doctoral thesis where it is presented, in the form of articles, the obtained results in the course of the realization of this thesis for, in chapter VI, presenting the main conclusions obtained in function of the fixed general objectives and the results presented on chapter V.

II. MARCO TEÓRICO Y OBJETIVOS

2.1. CORROSIÓN

Según la IUPAC[1], se define corrosión como una reacción interfacial irreversible de un material (metal, cerámico o polímero) con su entorno, dando como resultado el consumo de material o la disolución de alguna especie del entorno en el seno del material [1].

Aunque la definición de corrosión por la IUPAC es general y aplicada a metales, polímeros o cerámicas, el término corrosión se emplea especialmente en el campo de la metalurgia. En este caso la corrosión es debida a la inestabilidad del metal en su forma elaborada, y se basa en la tendencia que el material tiene de volver a su estado natural o de equilibrio. El grado de corrosión de un sistema vendrá dado por la interacción entre un material determinado y su entorno, pudiendo existir cuatro grandes grupos de entornos: líquido, subterráneo, atmosférico y de elevada temperatura.

Debido al tipo de material y entorno presentes pueden existir numerosos tipos de corrosión [2-4]:

- Corrosión uniforme o general (ataque químico o electroquímico)
- Corrosión galvánica
- Corrosión localizada (picaduras, filiforme…)
- Corrosión intergranular
- Corrosión por deszincado y corrosión selectiva
- Corrosión a alta temperatura

El presente trabajo se ha centrado en los métodos de protección contra corrosión electroquímica, puesto que es el principal mecanismo de corrosión ambiental, por estar el agua siempre presente en el ambiente, ya sea en forma vapor o en su forma líquida.

La definición de corrosión electroquímica que la IUPAC ofrece es: “aquella corrosión que siempre incluye reacciones de electrodo, siendo habituales la formación de capa de óxido sobre el substrato o la disolución de los iones metálicos en el medio” [1].

En la corrosión electroquímica intervienen reacciones de tipo oxidación y reducción, de igual intensidad pero sentidos de reacción opuestos. En este tipo de reacciones se produce un intercambio de electrones, debido a una diferencia de potencial, entre una zona anódica (donde se produce la oxidación) y una zona catódica donde tiene lugar la reducción. En este proceso, los electrones desprendidos de la zona anódica se desplazan a través del metal conductor hacia el cátodo [5-6].

En el caso de la corrosión electrolítica del hierro se producen principalmente las reacciones de oxidación-reducción siguientes en presencia de agua:

Reacción anódica	$2\,Fe \longrightarrow 2\,Fe^{2+} + 4\,e^-$	(Medio ácido y básico)
Reacción catódica	$O_2 + 2\,H_2O + 4\,e^- \longrightarrow 4\,OH^-$	(Medio básico y neutro)
	$2\,H^+ + 2\,e^- \longrightarrow H_2$	(Medio ácido)

[1] IUPAC = International Union of Pure and Applied Chemistry

La reacción anódica de cesión de electrones se produce en medios ácidos y básicos. Sin embargo, la reacción catódica de reducción de oxígeno predomina en medios básicos y neutros mientras que la producción de hidrógeno sucede en medios ácidos. Cabe decir, que el tipo de reacciones que tienen lugar en una celda electroquímica depende de numerosos factores como el pH del medio, el tipo de electrolito, el metal… Así, otros ejemplos de procesos de reducción posibles serían:

$$Me^{2n} + z\ e^- \longrightarrow z\ Me$$

$$H_2O_2 + 2\ e^- \longrightarrow 2\ OH^-$$

$$NO^-_3 + 4\ H^+ + 3\ e^- \longrightarrow NO + 2\ H_2O$$

$$Fe^{3+} + e^- \longrightarrow Fe^{2+}$$

En la figura 2.1.1. se presenta un esquema idealizado del proceso de corrosión electroquímica para metales en general [7].

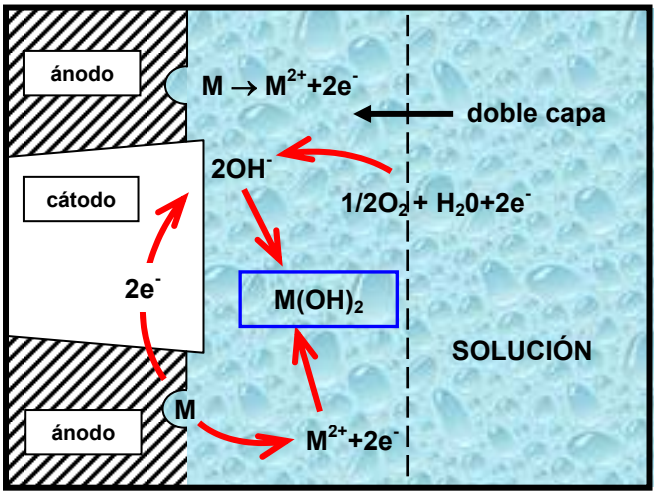

Fig. 2.1.1. Esquema idealizado de corrosión electrolítica.

Por tanto, en todo proceso electroquímico será necesaria la existencia de 4 componentes: ánodo, cátodo, electrolito (conductor del movimiento iónico) y conexión eléctrica entre cátodo y ánodo para el paso de corriente de electrones. Así pues, para poder luchar eficazmente contra la corrosión electroquímica bastaría con impedir la existencia de uno de los cuatro elementos.

Es por ello que la lucha contra la corrosión puede darse desde cuatro perspectivas diferentes [6]: sustituir el material que se corroe por otro más resistente, polarizar el material con una corriente externa y situarlo en zona noble, modificación del ambiente haciéndolo menos agresivo, y emplear recubrimientos protectores. El uso de un método u otro depende de diversos factores como son el económico y las prestaciones que el material debe ofrecer.

Los recubrimientos protectores (metálicos y no metálicos) son el campo más extenso dentro de la protección de metales. Los recubrimientos metálicos pueden actuar como ánodos de sacrificio protegiendo el substrato cuando éste actúa como cátodo (Ej. recubrimientos de zinc o cadmio), o bien ofrecer protección barrera cuando el substrato es quien actúa como ánodo (Ej. recubrimientos níquel, cromo o plomo). Los recubrimientos no metálicos engloban óxidos (como anodizados en aluminio), cerámicas, cromatos o fosfatos y en especial pinturas orgánicas [6].

Las pinturas orgánicas (compuestas generalmente de ligante, pigmentos y aditivos) pueden ser aplicadas como recubrimientos protectores o como acabado final, y son el campo de recubrimientos más amplio en la protección anticorrosiva de metales.

Las principales ventajas de los recubrimientos orgánicos son su relativo bajo coste, su amplio rango de acabados y la gran variedad de métodos de aplicación y formas que éstos pueden presentar (líquidas, polvo, cataforesis…), haciendo así que rara vez se presente como problema el tamaño o forma del metal a recubrir.

En la actualidad parece que la protección de metales reactivos (como acero y aluminio) con recubrimientos orgánicos es la forma más apropiada de aprovechar sus propiedades mecánicas, a la vez de ofrecer protección contra la corrosión e introducir una o varias propiedades superficiales extra (color, resistencia a desgaste, reducción de ruido, aislamiento electrónico, etc.) [8].

2.2. RECUBRIMIENTOS ORGÁNICOS

2.2.1. Generalidades

De forma general se define un recubrimiento como un "producto, en forma líquida, pasta o polvo, que al ser aplicado sobre un substrato forma una película con propiedades protectoras, decorativas y/u otras propiedades específicas" [9].

Un recubrimiento orgánico se puede definir de forma sencilla como un material donde el ligante es orgánico y que se aplica sobre un substrato con fin decorativo o protector. Normalmente estos recubrimientos suelen estar formados por un ligante o vehículo, un entrecruzante, y pigmentos o cargas, aunque se les puede incluir, a fin de modificar las propiedades del sistema, otros componentes como plastificantes, catalizadores... El vehículo, habitualmente un polímero de relativo bajo peso molecular, determina las propiedades físicas y químicas básicas del recubrimiento. La función de los pigmentos es mejorar esas propiedades a la vez que proporcionar color, actuar como barrera de las especies corrosivas y servir como especies inhibidoras de la corrosión [8].

En la protección del acero por medio de sistemas orgánicos es habitual emplear sistemas compuestos por una imprimación, una capa intermedia y una capa de acabado final, teniendo, cada una de ellas, funciones concretas pero relacionadas entre sí [6]:

1. La imprimación es la primera capa que se aplica sobre el substrato metálico teniendo funciones de:
    - Prevenir o retrasar la corrosión inicial
    - Formar una capa muy adherente al substrato (o a los óxidos del substrato) sobre la cual se adhieran fuertemente posteriores capas de pintura
    - Crear un sistema que selle las superficies activas para evitar ataques químicos de las posteriores capas orgánicas

2. La capa intermedia complementa las funciones anticorrosivas de la imprimación y a su vez proporciona las siguientes características:
    - Actuar de unión entre la imprimación y el acabado final
    - Proporcionar características próximas al acabado final

3. El acabado final proporciona características estéticas y una superficie resistente a las condiciones atmosféricas como radiación ultravioleta, ataque químico, rayado…

En la figura 2.2.1. se puede observar un esquema básico de un sistema orgánico-metal.

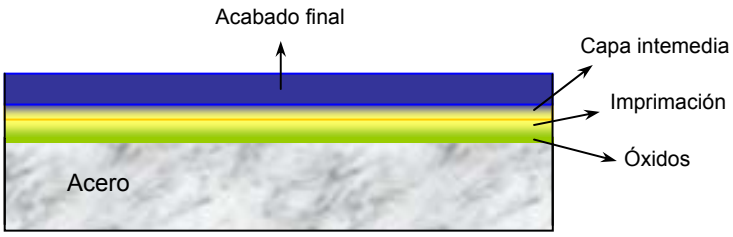

Fig. 2.2.1. Esquema sistema orgánico-metal.

La protección que ofrece un recubrimiento orgánico contra la corrosión de un metal es un proceso complejo y de difícil interpretación que depende de numerosos factores [10-13] como son: la calidad del recubrimiento (propiedades eléctricas, químicas y mecánicas de los polímeros, su adherencia al substrato, sus características de absorción, y la permeabilidad al agua, oxígeno e iones que presente…), el tipo de substrato y pre-tratamiento superficial aplicado, y la interfase metal/recubrimiento así como las propiedades inhibidoras de corrosión de los pigmentos en su seno [10, 14-19].

Los recubrimientos orgánicos proporcionan protección contra la corrosión por alguno o varios de los siguientes mecanismos [20, 8]:

1. Efecto barrera para los iones, dando lugar a una doble capa de difusión extendida
2. Adhesión al substrato
3. Bloqueo de caminos iónicos entre ánodos locales y cátodos a lo largo de la interfase metal/polímero
4. Vehículo de pigmentos activos e inhibidores que son liberados en caso de daño del recubrimiento

En presencia de soluciones acuosas, las propiedades barrera al transporte de agua, oxígeno e iones son muy importantes, puesto que su presencia en el recubrimiento orgánico podría activar los procesos de corrosión, pérdida de adherencia o formación de ampollas [21, 8].

Sin embargo, todos los polímeros son en alguna medida permeables al agua, oxígeno e iones, dependiendo de las características del recubrimiento polimérico, del tipo de substrato y tratamiento superficial, y de la interfase metal/recubrimiento [14, 22-24]. En un intento de incrementar la protección dada por los recubrimientos se introducen pigmentos en el sistema con la función de aumentar el efecto barrera (aumentando la tortuosidad de los caminos por los que se introduce el electrolito y resto de especies), o bien incluir un efecto inhibidor de los procesos de corrosión, o incluso una combinación de ambos [6].

En la figura 2.2.2. se muestra un esquema con los diferentes efectos protectores que los pigmentos ofrecen al sistema.

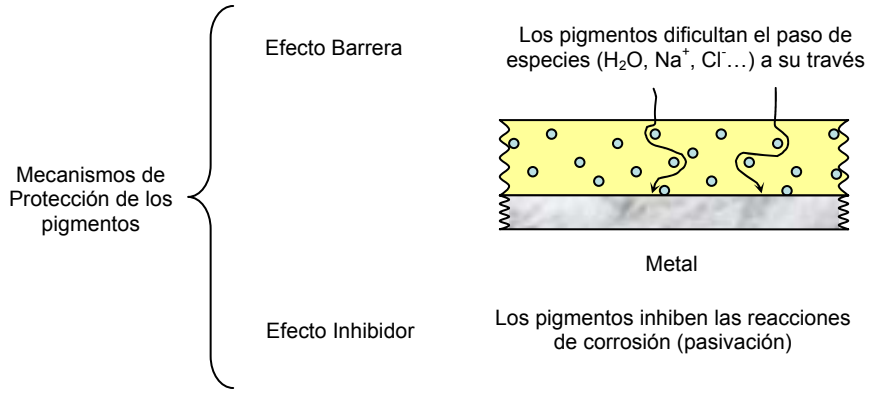

Fig. 2.2.2. Protección ofrecida por los pigmentos.

En general, la adición de pigmentación en el sistema (pigmentos inhibidores de corrosión y barrera) da lugar a una mejora de las propiedades anticorrosivas siempre que no se supere la concentración crítica de pigmentos en volumen (CCPV[2]), a partir de la cual distintas propiedades del sistema (entre ellas la protección) empeoran [25-28].

A pesar de la introducción de pigmentos en el sistema, en la actualidad no se ha conseguido el objetivo de impedir que las diferentes especies atraviesen el recubrimiento y alcancen la interfase puesto que todos los polímeros son de una forma u otra, porosos.

Según describió Mayne, para los recubrimientos orgánicos típicos empleados en la protección de corrosión, el grado de difusión de agua y oxígeno excede, con mucho, el valor límite de difusión para la reducción del oxígeno [29] (clave para que el proceso corrosivo tenga lugar). Por esto, al emplear recubrimientos orgánicos, es sólo cuestión de tiempo que se produzca corrosión en el substrato, debido a que las diferentes especies pasen a través de poros y canales del recubrimiento (inherentes al ligante o producidos durante la vida del recubrimiento, como impacto por piedras…) y alcancen la interfase.

2.2.2. Adherencia como parámetro en la lucha contra corrosión

Hoy en día hay cierto debate científico entorno a la importancia de la adherencia y del efecto barrera en la lucha contra la corrosión [30-38]. Se ha demostrado que el efecto barrera contra el paso del agua y oxígeno no puede ser considerado un efecto preventivo suficiente contra la corrosión, debido a que la permeabilidad de un recubrimiento contra una de estas especies es siempre mayor que el límite necesario para iniciar la corrosión [31, 32]. De esta forma, actualmente, se le da mayor importancia a la prevención del transporte de iones a través del recubrimiento y/o de las zonas anódicas a las catódicas (proceso relacionado con la adherencia). Funke [39], describe la adherencia como la propiedad más importante y decisiva de un recubrimiento. Así, se considera que los mejores recubrimientos contra

[2] CCPV = Concentración crítica de pigmentos en volumen

corrosión son aquellos que presentan una mayor adherencia al substrato, puesto que ésta es un factor crítico para evitar los procesos de corrosión [40]. Sin embargo, conviene tener en cuenta que la adherencia no es el único factor que influye en los procesos de corrosión, sino que la corrosión es un proceso que engloba múltiples variables.

Teorías como las del modelo mecánico, eléctrico, difusión, adsorción, enlace químico, ácido-base, reológico o de capas débiles de rotura preferente [6, 41] tratan de explicar los fenómenos de adhesión. Sin embargo, en la adhesión de recubrimientos orgánicos-metal, los modelos considerados más importantes son el mecánico y el de adsorción [6].

El modelo mecánico está basado en el anclaje por medio de ganchos y aros entre el recubrimiento y el substrato. Según este modelo cuanto mayor sea la irregularidad y porosidad del substrato mayor será la adherencia. Es la teoría más antigua y más establecida, sin embargo, se ha demostrado como los métodos de aumento de superficie favorecen la adherencia no sólo por aumento de área de contacto sino también por la eliminación de agentes contaminantes (que impedirían uniones químicas), por lo que realmente no se puede aplicar a todos los casos.

La teoría de la adsorción se basa en la existencia de fuerzas de enlace superficiales, en concreto, fuerzas de enlace primario o químicos (iónico, covalente y metálico) y secundario o físicos (van der Waals y puentes de hidrógeno).

Los enlaces iónicos y metálicos no ejercen demasiada influencia en la adherencia recubrimiento-metal [6]. Sin embargo, los enlaces covalentes que se forman por compartición de electrones y son típicos en componentes orgánicos, tienen gran importancia. Cuando este enlace se produce entre dos átomos similares se obtiene una molécula no polar (Ej. Polietileno), pero cuando se produce entre dos átomos diferentes se obtiene una molécula polar. Esto es de gran importancia en la adhesión puesto que polímeros polares presentan mejor adherencia que los no polares, a la vez que mayor solubilidad y compatibilidad con otras resinas y cohesión de la matriz polimérica. Sin embargo, a partir de la cohesión no se puede indicar la adherencia puesto que ésta no sólo depende de la polaridad.

Los enlaces secundarios, o de Van der Waals, son los predominantes en la adhesión de recubrimientos orgánicos a metales. Cuanto más asimétrico sea el polímero y más libre de contaminantes el substrato, mayor fuerza tendrán estos enlaces. Los enlaces de Van der Waals son enlaces débiles resultantes de campos aislados asociados a enlaces primarios, y pueden ser de tres tipos: Keesom, Debye y London [6].

Los enlaces Keesom (por orientación), se producen por la interacción de moléculas en el polímero, en las cuales los centros de masa de carga positiva y negativa están desequilibrados debido a la asimetría de la estructura molecular. Esta estructura polimérica tiene un momento eléctrico o dipolo permanente, pudiendo las moléculas que contienen dipolo, influir en la orientación de otras. Son muy importantes en la adhesión de recubrimientos orgánicos.

Las moléculas que contienen un dipolo y por tanto elevada adherencia a substratos metálicos, contienen enlaces C-O, como el grupo carbonilo o el grupo carboxilo (esquema 2.2.1.).

Grupo carbonilo Grupo carboxilo

Esquema 2.2.1. Grupos polares

Los enlaces London (por dispersión), son debidos a la interacción de una molécula con otra debido a la oscilación de electrones. Están presentes en todas las moléculas y suponen un 80% del total de las fuerzas de cohesión de la mayor parte de compuestos orgánicos.

Los enlaces Debye (por inducción), son debidos a la interacción (polarización) de moléculas que tienen dipolos inducidos resultantes de la interacción de una molécula con dipolo permanente con un sistema de enlace susceptible de ser polarizado. Son menores que las Keesom y las London, y por tanto, contribuyen poco a la adherencia y cohesión global.

Según esta teoría la mayor adherencia se produciría con la mayor mojabilidad del polímero en el substrato (mayor superficie de contacto) y con el mayor número de grupos polares en la molécula.

Por otro lado, se sabe que la presencia de grupos hidroxilo secundarios (grupos polares) a lo largo de la cadena, dan lugar a una fuerte adhesión al metal por medio de la formación de enlaces por puente de hidrógeno [40], más fuertes que los enlaces de Van der Waals, entre los grupos hidroxilo y la capa de óxido superficial del substrato (figura 2.2.3.).

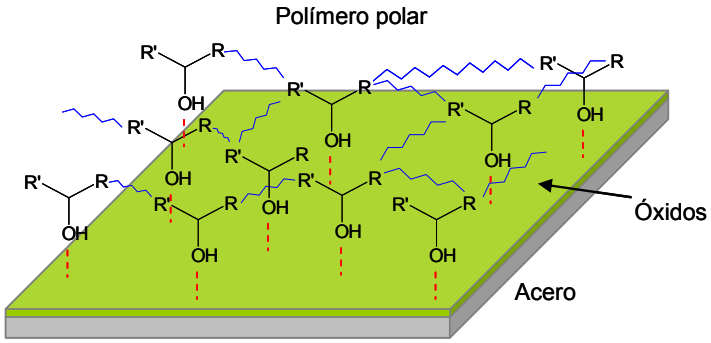

Fig. 2.2.3. Adherencia a substrato de red polimérica.

La pérdida de adherencia puede deberse al desarrollo de tensiones en el film por procesos de envejecimiento durante exposición, produciéndose la rotura del recubrimiento cuando estas tensiones internas superan a las fuerzas de adhesión entre recubrimiento y substrato [6]. Por otro lado, la pérdida de adherencia se produce casi totalmente cuando el recubrimiento epoxi se expone a agua o humedad [31, 35, 36, 42], ya que el agua penetra en el recubrimiento hasta la interfase metal/recubrimiento, o los compuestos resultantes de la descomposición electroquímica del agua se acumulan en la interfase. En ambos casos el enlace entre el grupo hidroxilo (u otro grupo polar) de la resina y la capa de óxido superficial del substrato se desestabiliza [40].

2.2.3. Fenómenos de degradación en sistemas metal/recubrimiento

En combinación con los fenómenos de corrosión de un substrato metálico recubierto, se dan los fenómenos de ampollamiento y delaminación que acaban por disminuir en gran medida la protección que el recubrimiento consigue ofrecer.

Leidheiser, describió los diferentes fenómenos de corrosión en sistemas metálicos recubiertos con polímeros [43] haciendo especial hincapié en la adherencia del recubrimiento al substrato. En un ambiente agresivo como puede ser el ambiente marino se producen principalmente el ampollamiento y/o la delaminación del recubrimiento [44]. Por lo general, se producen los dos procesos juntos, sin embargo, se pueden tratar sus principios por separado.

2.2.3.1. Ampollamiento

En general, para que se produzca la formación de ampollamiento, en el sistema se dan las siguientes etapas [45]:

1. El film embebe agua de la solución, conteniendo ésta sales disueltas
2. En un momento dado, una cantidad suficiente de agua con iones Cl^- pasa a través del recubrimiento hasta alcanzar la interfase y activa los emplazamientos de corrosión primaria
3. Conforme la corrosión sucede en las zonas anódicas bajo el film, se crean iones hidroxilo en zonas catódicas del substrato
4. El ambiente alcalino en las zonas catódicas debilita o destruye la adherencia del film al producir sustancias osmóticamente activas en la interfase con el metal
5. La presencia de estas substancias en la interfase favorece al paso endosmótico de agua a través del film

Aunque en bibliografía (y también en este trabajo) por lo general se trata el ampollamiento producido por procesos catódicos, se han descrito tres tipos de ampollamiento: osmótico, catódico y anódico [45].

El osmótico sucede como consecuencia de la existencia de un substrato contaminado con sales solubles que favorecen la entrada de agua a través del recubrimiento para equilibrar la presión osmótica entre ampolla y solución exterior, así va aumentando la ampolla debido a la entrada de agua por efecto osmótico [43, 46, 47].

El ampollamiento anódico, parte de la idea de considerar las ampollas rellenas de líquido como de naturaleza anódica [48]. Este tipo de ampollamiento se produce cuando el pH del medio es muy bajo, como sucede en bebidas y comida enlatada.

El ampollamiento catódico es el más comentado en bibliografía y es debido a un entorno alcalino debajo de un recubrimiento provocado por la reacción catódica asociada a zonas dañadas del recubrimiento donde se produce la corrosión anódica [49-51].

2.2.3.2. Delaminación

La delaminación catódica es un proceso que se origina debido a la alcalinidad en la interfase (como el ampollamiento catódico) producida por la actividad catódica bajo el recubrimiento. El mecanismo por el cual se produce la delaminación es objeto de debate junto con el proceso que posibilita a las diferentes especies involucradas en el fenómeno corrosivo alcanzar la interfase. Para explicar el proceso de delaminación se han propuesto numerosas teorías. Teorías que van desde la disolución del óxido de la interfase [52, 53], hasta el ataque químico del medio básico al recubrimiento provocando el fallo cohesivo [54, 55]. Según Koehler, la delaminación tiene lugar entre la capa de óxido superficial (formada por exposición al aire previo recubrimiento) y el recubrimiento, y es un fenómeno que afecta a todo el sistema. Koehler postuló, que sólo se puede producir la delaminación cuando se encuentran cationes metálicos alcalinos (como el Na^+) en el medio capaces de actuar como contraiones de los recién formados OH^- en las zonas catódicas, y una película de agua bajo el recubrimiento.

2.2.3.3. Proceso global de degradación metal /recubrimiento

Con todo esto, el proceso global de corrosión de sistemas metálicos, como el acero, recubiertos con pinturas se inicia en un defecto del film (poros o grietas) que posibilita una reacción anódica:

$$2\,Fe \longrightarrow 2\,Fe^{2+} + 4\,e^- \qquad (1)$$

A fin de mantener la electroneutralidad del sistema se produce la reacción catódica en zonas cercanas a la anódica, siendo esta reacción normalmente la de reducción del oxígeno (medios no ácidos):

$$O_2 + 2\,H_2O + 4\,e^- \longrightarrow 4\,OH^- \qquad (2)$$

Inicialmente las dos reacciones tienen lugar de forma adyacente, pero conforme avanza la corrosión la zona catódica se desplaza por debajo del recubrimiento orgánico a zonas más alejadas, de forma que los procesos de corrosión se complican. En esta situación, se producen productos de corrosión en la zona dañada del recubrimiento (zona anódica), y delaminación catódica alrededor de la zona anódica y, a su vez, por conducción de electrones, se produce ampollamiento catódico en otros lugares más alejados del metal recubierto.

Los iones de hierro formados en la zona anódica reaccionan con iones hidroxilo y oxígeno que alcanzan la interfase formando así los productos de corrosión. En las zonas catódicas se siguen produciendo iones hidroxilo que reaccionarán con los iones hierro formando así más productos de corrosión y delaminación catódica.

Por otro lado, en zonas del recubrimiento alejadas al defecto se dan más reacciones catódicas que producen iones hidroxilo, que al reaccionar con iones sodio (procedentes del electrolito) provocarán un aumento de la presión osmótica y pH bajo film, lo cual favorecerá la entrada de más especies de la disolución (agua y sales) a través del recubrimiento, formando así el ampollamiento catódico.

En la figura 2.2.4. se muestran los dos procesos principales de delaminación y ampollamiento propuestos por Schwenk [49].

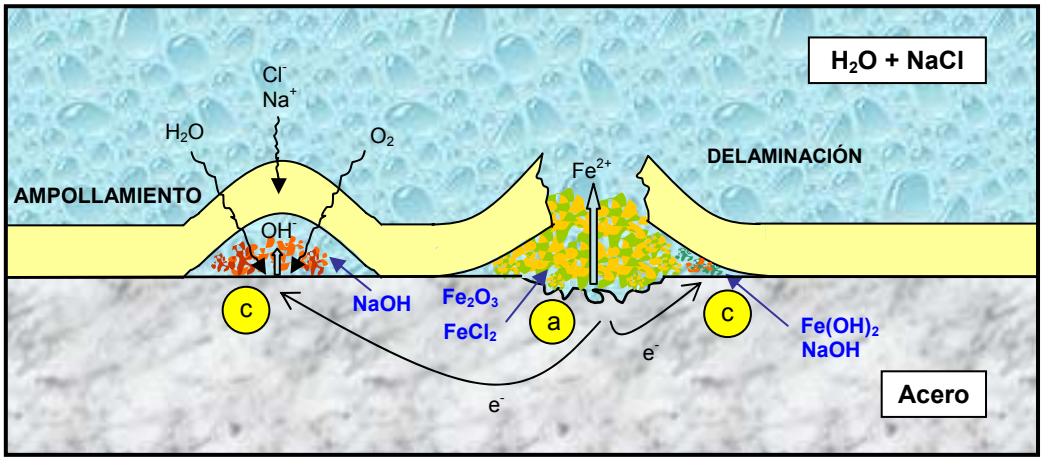

Fig. 2.2.4. Procesos de degradación en recubrimientos orgánico.

En esta figura se puede observar como los hidroxilos producidos de forma catódica se presentan tanto en el ampollamiento como en los puntos de delaminación. La naturaleza alcalina de la solución resultante en estos sitios se considera el factor principal en el fallo del recubrimiento [44] debido a la alcalinización del recubrimiento, disolución de la capa de óxido en la interfase y alteración de la resistencia iónica del film [56-59]. Ante la presencia de electrolito y cloruro sódico en el cátodo y el ánodo se producen reacciones de formación de productos de corrosión:

Ánodo: $Fe^{2+} + 4\ Cl^- \rightarrow 2\ FeCl_2$

$Fe^{2+} + 3/2O_2 \rightarrow Fe_2O_3$

Cátodo: $2OH^- + 2Na^+ \rightarrow 2NaOH$

$4OH^- + Fe^{2+} \rightarrow 2\ Fe(OH)_2$

En general se observa que hay un periodo de tiempo previo al inicio de la corrosión debajo del recubrimiento e inicio del ampollamiento y delaminación (tiempo *onset*), tras la exposición a un ambiente corrosivo. Estos fenómenos han sido interpretados por dos teorías igualmente válidas. La primera, propuesta por Leidheiser [60], justifica este retraso debido a un tiempo de estabilización de los procesos de difusión a través del recubrimiento, ya sea de oxígeno, agua o iones. Por otro lado, la segunda, descrita por Nguyen [51], justifica este retraso indicando que la ruta realmente limitante de la difusión es aquella de los cationes a lo largo de la interfase metal/recubrimiento.

2.2.4. Clasificación de recubrimientos orgánicos

Los recubrimientos orgánicos se pueden clasificar en función de su procedimiento de aplicación, finalidad del recubrimiento, composición (tipo de ligante empleado, disolvente, según el pigmento)…

En este trabajo se ha atendido a su clasificación en función del procedimiento de aplicación, debido a que a escala industrial parece ser la forma más práctica de clasificación. Los diferentes tipos de aplicación actuales son [6, 61]:

- Pintado con brocha
- Pintado por spray (pistola de alimentación por succión, alimentación por gravedad, alimentación por presión, spray sin aire…)
- Pintado por inmersión
- Pintado por flujo
- Electrodeposición
- Pintado electrostático
- Pintado por rodillos

El uso de uno u otro sistema de aplicación depende de la velocidad deseada de producción, de la inversión económica y propiedades finales del recubrimiento así como del tipo de recubrimiento.

Atendiendo a las demandas actuales tanto económicas como ecológicas, dos han sido las técnicas de aplicación estudiadas, cada una desde un punto de vista diferente.

El pintado por electrodeposición (en concreto la deposición catódica) se ha estudiado desde el punto de vista de la mejora de la aplicación a fin de reducir costes y disminuir el impacto medioambiental en su aplicación dentro de la industria del automóvil. El pintado electrostático se ha estudiado desde el punto de vista de la mejora de las pinturas en polvo empleadas en este tipo de aplicación. La elección del estudio de este tipo de pinturas se basa, sobretodo, en sus ventajas económicas y ecológicas frente a las pinturas líquidas.

2.3. PINTADO POR ELECTRODEPOSICIÓN

2.3.1. Generalidades

Los recubrimientos por electrodeposición son de dos tipos: aniónicos o catiónicos (en función de si el substrato actúa como ánodo o como cátodo, respectivamente, en el proceso de deposición), y se pueden conocer por nombres como E-coat, electrocoat, electropaint, ED o ELPO. La electroforesis (anaforesis y cataforesis) es un método de pintado ampliamente empleado en grandes series de producción, principalmente en la industria del acero, debido a su gran versatilidad y excelentes resultados. La cataforesis es la variante actualmente más empleada en procesos industriales de medio y gran volumen [62]. En la actualidad se han introducido pinturas sin plomo, y más recientemente libres de estaño. A su vez, el contenido en VOCs de las imprimaciones cataforéticas ha descendido de forma significativa y supone menos de un 2% en la mayoría de aplicaciones [63]. Otro factor que hace del pintado por electrodeposición una técnica respetuosa con el medio ambiente es la reducción de aguas residuales, hasta eliminarlas en algunas líneas de pintado por cataforesis gracias a la introducción de sistemas de aclarado apropiados y al uso de un aclarado final con ultrafiltrado [64].

El proceso de electrodeposición de una pintura consiste en la inmersión de la pieza a recubrir en un tanque que contiene una dispersión acuosa de la pintura, donde, tras la aplicación de una diferencia de potencial entre el ánodo y el cátodo, las partículas cargadas se depositan sobre la pieza creando un recubrimiento de espesor uniforme. En el tanque, la pieza a recubrir podrá actuar como ánodo (deposición anódica) o como cátodo (deposición catódica o cataforesis). Los aspectos fundamentales del proceso de electrodeposición fueron claramente descritos por Beck [65-67].

Habitualmente se emplean pinturas tipo epoxi o tipo acrílico. El contenido en sólidos es cercano al 10% y el de los solventes orgánicos por debajo del 5% (y en algunos casos 0%), siendo la viscosidad de los recubrimientos por electrodeposición muy baja, cercana a la del agua [68].

Durante la electrodeposición, la resina y pigmento, en suspensión en agua, se cargan siendo entonces obligadas a dirigirse hacia la pieza que se encuentra con la carga opuesta. Así, el recubrimiento coagula en la superficie del metal, formando un recubrimiento de gran adherencia, libre de poros y de espesor uniforme debido a que las superficies pintadas ven reducida su conductividad forzando a las partículas a dirigirse a zonas no cubiertas.

Tras la deposición, la pieza se limpia con agua y se cura en un horno entre 5 y 30 minutos a una temperatura entre 120 y 200ºC [68]. En la figura 2.3.1. se muestra un diagrama de pintado por electroforesis, en este caso por cataforesis en la industria del automóvil.

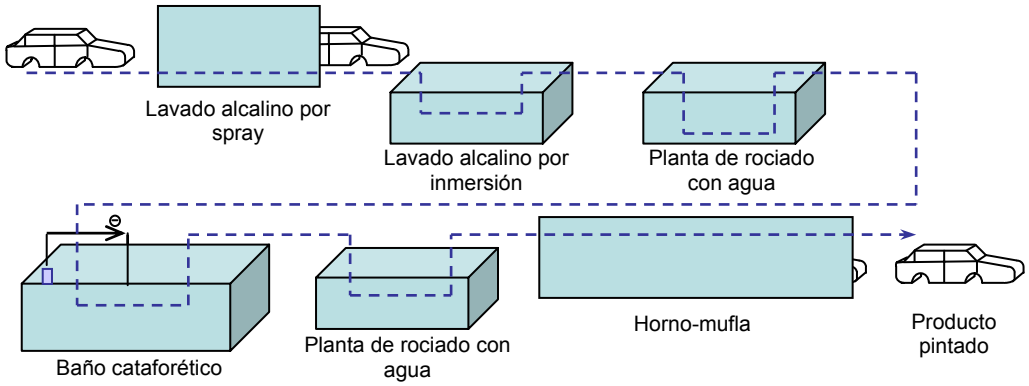

Fig. 2.3.1. Proceso pintado por cataforesis.

Esta técnica está muy extendida en las líneas de aplicación tanto de imprimaciones como de pintura de acabado de una sola capa [6], siendo sus principales ventajas [6, 15, 61, 68] frente a otros métodos las aquí enumeradas:

- Uso de pequeñas cantidades de VOCs, y control de sus emisiones menos caro que en otros métodos de aplicación
- Recuperación de un 90% del exceso de pintura (ahorro en costes de materia prima)
- Obtención de recubrimientos anticorrosivos uniformes y de espesores muy bajos
- Posibilidad de automatizar todo el proceso
- Facilidad a la hora de recubrir zonas ocultas, como huecos o interior de cajas
- Posibilidad de aplicar una segunda capa de pintura, basada en agua o en disolvente, sobre el electro-recubrimiento no curado
- Empleado en producciones a gran escala

Sin embargo, esta técnica también presenta algunas desventajas [68], como son la necesidad de separar líneas de diferentes colores (un tanque para cada color), costes de operación y precios de equipos relativamente elevados, gran formación de los empleados…

La industria del automóvil requiere recubrimientos protectores con elevada resistencia a degradación. En este sector, el recubrimiento debe proteger el substrato contra ataques corrosivos y mantener, por un largo periodo, buenas propiedades estéticas, lo que supone una elevada estabilidad ante degradación foto-oxidativa y abrasión mecánica [69]. Por estos motivos el principal sector donde se aplica la electroforesis es el automovilístico, pudiéndose afirmar que hoy en día la protección de casi toda carrocería de coche y una gran variedad de piezas incluye una imprimación cataforética [15].

La electrodeposición anódica se introdujo en la industria automovilística en los años 60, siendo desbancada rápidamente en los años 70 por la electrodeposición catódica debido a las mejores propiedades que confería a los recubrimientos como, por ejemplo, una mayor protección anticorrosiva

(se conseguían propiedades nunca alcanzadas por otras técnicas). Las características que han hecho que el proceso de cataforesis gane tanta aceptación frente a otros procesos son su carácter automatizado, el bajo nivel de polución y su elevada capacidad para pintar zonas difíciles del substrato.

En el inicio de la década de los 90, los sistemas catódicos estaban basados en resinas epoxi modificadas con grupos amino. Estas resinas se dispersaban en agua por protonación del grupo amino con ácidos orgánicos y entrecruzaban con isocianatos saturados. Los pigmentos empleados se basaban en dióxido de titanio a la vez que se introducía plomo, contenido en silicatos, como agente anticorrosivo y como catalizador de las reacciones de curado del sistema, y el contenido en disolventes orgánicos tan sólo suponía un 2% en volumen del total.

A pesar que esta técnica ha sido considerada como casi plenamente desarrollada durante mucho tiempo, en la actualidad se sigue mejorando. No es sino, a mediados de la década de los 90 cuando aparecen en el mercado los primeros sistemas libres de plomo, coincidiendo con los intentos por conseguir imprimaciones medioambientalmente aceptables, reducciones en el contenido de solventes orgánicos volátiles (VOC's), y reducciones en las temperaturas de curado de los sistemas [70-72].

El proceso de electrodeposición y las características de los recubrimientos están controlados por numerosos parámetros, como la concentración de resina en el baño de electrodeposición, el potencial aplicado entre electrodos, la distancia ánodo-cátodo, el área de los mismos o la temperatura del baño, así como la temperatura de curado posterior. Todos estos parámetros tienen una gran importancia en el comportamiento final de las imprimaciones. Por ejemplo, para poder alcanzar zonas de difícil acceso de una pieza a recubrir, se pueden aplicar mayores potenciales consiguiendo que el sistema pueda cubrir las citadas zonas, sin embargo, este alto potencial puede provocar el fenómeno llamado "ruptura de film", que se caracteriza por causar imperfecciones o manchas en el recubrimiento [73-75]. De esta forma se hace necesario alcanzar un compromiso entre la posibilidad de aplicar el recubrimiento y la calidad obtenida de éste.

2.3.2. Deposición anódica (anaforesis)

El sistema orgánico que se utiliza en el proceso de deposición anódica está compuesto por agua, resina y pigmentos. La dispersión acuosa contiene partículas de pigmento sin carga y partículas de resina ionizada (cargada negativamente). En la fabricación de la pintura, las partículas de resina cargada son absorbidas por la superficie de los pigmentos, de forma que éstos adquieren carga negativa. Esta carga de los sistemas resina-pigmento facilita que al circular una corriente a través de la celda, la pintura se deposite en el ánodo (pieza a recubrir) con un ratio pigmento/ligante adecuado.

La pintura se deposita en el ánodo adoptando características de esponja, y ocluyendo así agua en su seno. Durante el proceso de electro-ósmosis esta agua es eliminada, dejando una película de pintura uniforme sobre la pieza.

Tras la inmersión de la pieza en el tanque, se prosigue con el soplado de la pintura sobrante y su posterior curado en un horno durante 20-30 minutos a 150-160ºC, produciéndose así la reacción de los grupos carbonilo y la polimerización del ligante [6].

2.3.3. Deposición catódica (cataforesis)

La deposición catódica surge como respuesta a los problemas que presenta la deposición anódica, tales como la formación de acabados decolorados por la formación de precipitados Fe^{2+}/resina y la oclusión de iones metálicos en la pintura [6].

El término cataforesis hace referencia al principal proceso que tiene lugar en este método, esto es, el desplazamiento "hacia el cátodo" de las micelas de pintura. La cataforesis es un proceso de deposición de un film protector sobre una superficie conductora empleando una dispersión coloidal de partículas poliméricas en agua [76, 77].

Las principales ventajas que presenta son [15, 77]:

- Excelente poder cubriente de superficies complejas
- Casi absoluta inexistencia de VOCs
- Eliminación de disolución de metal
- Imposibilidad de oxidación electroquímica de la resina en el substrato
- Mejor protección contra corrosión

Sin embargo, también presenta ciertas desventajas frente a otros métodos como son [77]:

- Elevado coste de la planta industrial
- Las resinas que se utilizan tienen una formulación compleja
- Dificultad de obtener espesores elevados

En el caso de las pinturas aplicadas por cataforesis (en adelante cataforéticas) el sistema a aplicar es ligeramente ácido (pH 5.7-6.5), con las partículas de resina ionizadas positivamente de forma que al aplicar la corriente se depositan sobre el cátodo, que en este caso es la pieza a recubrir [6]. En la figura 2.3.2. se muestra un esquema de un baño cataforético. Se observan las moléculas de resina cargadas, los pigmentos (*P*), el ánodo (*A*), y el cátodo (*C*), que será la pieza a pintar. Al aplicar una diferencia de potencial determinada se produce un paso de electrones en dirección al cátodo provocando el inicio del proceso de cataforesis, tal y como se explica a continuación.

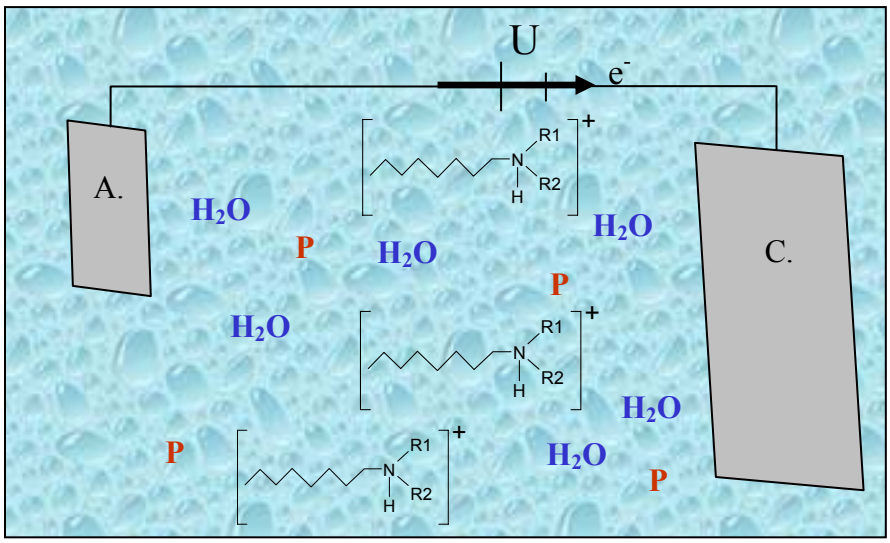

Fig. 2.3.2. Esquema baño cataforético.

Tradicionalmente, las pinturas empleadas en cataforesis consisten en una resina básica (empleada como ligante) y unos pigmentos. La resina, inicialmente insoluble en agua, se hace soluble por protonación mediante el uso de ácidos débiles como el acético o el fórmico. En el esquema 2.3.1. se muestra la protonación de la resina con ácido débil de bajo peso molecular dando lugar a una resina cargada positivamente y soluble en agua.

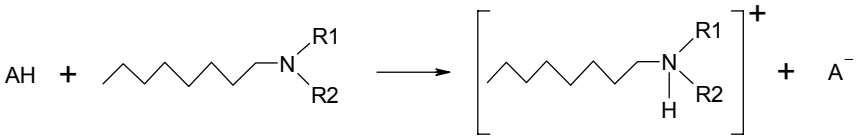

Esquema 2.3.1. Solubilización de la resina

Una vez se tiene la resina dispersada en agua se produce la electrodeposición, que es un proceso complicado que incluye las siguientes etapas [15, 66, 71, 73, 78]:

1. *Inducción*: Es el primer paso de la cataforesis (una vez aplicada la corriente a la celda) y consiste en la electrolisis del agua en el cátodo (pieza a pintar) con la formación de iones hidroxilo e H_2 gas (esquema 2.3.2.).

$$2\ H_2O + 2\ e^- \rightarrow H_2 + 2\ OH^-$$

Esquema 2.3.2. Inducción

2. *Migración electroforética*: Una vez aplicada la corriente y obtenida la inducción en el cátodo se producirá la migración electroforética de las micelas de resina y pigmentos asociados hacia el cátodo.

3. *Electrocoagulación*: Durante la inducción, y a consecuencia de la electrolisis del agua, en el cátodo se produce un aumento del pH del medio, de forma que cuando se alcanza un pH crítico (concentración adecuada de OH^- generados electroquímicamente) se produce la neutralización de las micelas de resina cargadas positivamente mediante los iones OH^- generados, depositándose así la resina sobre la superficie del cátodo (esquema 2.3.3.).

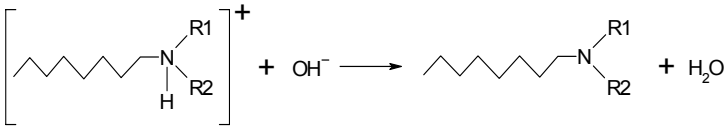

Esquema 2.3.3. Electrocoagulación

4. *Electroósmosis*: En los poros del film depositado, se produce la electroósmosis del agua debido a la diferencia de potencial a lo largo del film, y a las cargas superficiales en las paredes de los poros.

5. *Heterogulación*: Esto es la deposición del film en el substrato metálico.

6. *Adagulación*: Es la deposición de posteriores capas de pintura sobre las capas ya depositadas.

Todo este proceso de precipitación de la resina ocurre como consecuencia de la baja solubilidad de la amina base en comparación con su sal [79], y sin producirse reacciones adicionales.

La coagulación del ligante requiere de una concentración mínima de iones hidroxilo en la superficie del cátodo. Para alcanzar esta concentración crítica por medio de la electrolisis del agua se debe hacer circular una cantidad específica de electricidad, durante un tiempo específico (t_i, *tiempo de inducción*) y a una densidad de corriente determinada. Así, el tiempo de inducción se define como el tiempo necesario para que se produzca la deposición de la resina.

Para un electrolito estático, el tiempo de inducción se puede calcular mediante la ecuación propuesta por Sand [80]:

$$t_i = \frac{\left(\left[OH^-\right]_c\right)^2 F^2}{D_{OH^-} \Pi 4 j^2} \qquad \text{Ec. 2.3.1}$$

Donde,

$[OH^-]_c$ = Concentración crítica de iones OH^-

D_{OH-} = Coeficiente de difusión de los iones hidroxilo

F = Constante de Faraday

j = Densidad de corriente

Teniendo en cuenta las constantes, la ecuación 2.3.1 se puede reescribir en la forma de la ecuación 2.3.2. Donde K es una constante.

$$t_i j^2 = K \qquad \text{Ec. 2.3.2}$$

A esta ecuación, Kubo [81] propuso una modificación debido a que parte de los iones OH^- producidos se emplean para neutralizar los grupos catiónicos en el material ligante (lo cual varía en función del tipo de resina y grado de neutralización). Así, la ecuación 2.3.2 quedaría como:

$$t_i j^2 = K + K_1 j^2 \qquad \text{Ec. 2.3.3}$$

Donde, K_1 es una constante cuyo valor numérico depende de las propiedades de la resina empleada.

La concentración necesaria de iones OH^- en las proximidades del cátodo para iniciar la coagulación es aquella que causa un pH 12 en el medio, según estimaciones de varios autores [80, 82].

Bajo un voltaje de deposición constante, la ecuación matemática para el crecimiento de film es:

$$db / dt = cj \qquad \text{Ec. 2.3.4}$$

Siendo,

b = espesor de film

c = rendimiento culómbico (cm^3/C)

Si el film tiene características ohmnicas, entonces se puede emplear la ecuación 2.3.5:

$$j = kU / b \qquad \text{Ec. 2.3.5}$$

Donde U es el potencial de deposición (prácticamente localizado a lo largo del film) y k es la conductividad del film. Si se sustituye 2.3.5 en 2.3.4 obtenemos:

$$\frac{db}{dt} = \frac{ckU}{b} \quad \rightarrow \quad bdb = ckUdt$$

$$\int_0^b bdb = \int_{t_i}^{t} ckUdt \quad \rightarrow \quad \frac{1}{2}b^2 = ckU(t - t_i)$$

$$b = (2ckU)^{1/2}(t - t_i)^{1/2} \qquad \text{Ec. 2.3.6}$$

La ecuación 2.3.6 sugiere que el espesor del film es proporcional a la raíz cuadrada del tiempo de deposición (para un voltaje constante).

En el caso de una resina epoxi modificada con amina aplicada sobre acero, el tiempo de inducción está estimado en ser de aproximadamente 0.35 segundos [78], aunque depende de numerosos factores y, por tanto, no es constante para un tipo de substrato dado, aunque sí aproximado el orden de magnitud.

Puesto que la película depositada tiene baja conductividad (o elevada resistividad) la diferencia de potencial se encuentra localizada prácticamente en su totalidad a lo largo del film, de forma que se puede esperar que durante la deposición se libere calor por efecto Joule, cuya magnitud dependerá de la densidad de corriente de deposición, resistividad y espesor del film. Debido a este efecto, la temperatura en la superficie del cátodo aumenta.

Este aumento localizado de la temperatura ha sido objeto de estudio [78], destacándose algunas de las consecuencias del mismo, como por ejemplo la formación de agujeros y cráteres [83].

Estos efectos tienen gran influencia en la protección frente a corrosión que un recubrimiento epoxi electrodepositado puede ofrecer. Cabría distinguir en todo caso entre la importancia de la existencia de microporos o de macroporos, creados por el efecto Joule. En general se asume que los microporos existentes en todo recubrimiento no afectan en gran medida a las propiedades anticorrosivas del mismo, sin embargo, si se analiza el comportamiento de un recubrimiento frente a la absorción de agua se puede intuir el problema que supone para las propiedades anticorrosivas el aumento de los macroporos.

Este hecho quedó demostrado empíricamente por el trabajo de Miskovic-Stankovic [84] donde quedó patente cómo el electrolito en los microporos no afecta a la conductividad ni a la resistencia del recubrimiento (a pesar que sean entorno a un orden de magnitud más numerosos que los macroporos), debido a que las cadenas poliméricas impiden la movilidad de los iones y agua, y a pesar que saturan el recubrimiento por absorción de agua. Sin embargo, el aumento en el número y tamaño de canales y macroporos en el recubrimiento producido por la liberación de calor por efecto Joule, sí que afectará enormemente a las propiedades anticorrosivas del mismo, empeorándolas.

2.3.4. Composición de pinturas cataforéticas

Las pinturas cataforéticas se preparan por dispersión o solución. Por lo general las resinas empleadas en este tipo de pinturas son conocidas únicamente por los productores. Sin embargo, se sabe que principalmente están basadas en resinas epoxi de bisfenol-A que ha reaccionado con poliaminas para dar lugar a resinas con grupos amino terciarios y secundarios así como grupos hidroxilo.

En primer lugar se prepara un aducto[3] de resina poliepoxídica (resina catiónica) con poliaminas empleando un exceso de amina. A fin de promover el curado se introduce toluendiisocianato saturado con un alcohol. Al aplicar temperatura se consigue que el isocianato reaccione con los grupos amino secundarios obteniendo una urea sustituida entrecruzada, o reaccionando con grupos hidroxilo para formar uretano entrecruzado.

2.3.5. Variables de aplicación y limitaciones

El proceso de cataforesis es ampliamente empleado en la producción de automóviles, industria de gran importancia a nivel mundial y, particularmente en España y la Comunidad Valenciana.

[3] Aducto: Se refiere a una entidad química que se produce por la unión de dos moléculas mediante enlace covalente.

Para la obtención de las mejores propiedades anticorrosivas de las pinturas cataforéticas, es de gran importancia la optimización de dos parámetros en el proceso de aplicación: el potencial de deposición y la temperatura de curado.

A la hora de proceder a la optimización del proceso de aplicación de cataforesis y del posterior curado, es importante conocer como afectan a las propiedades ambas variables.

2.3.5.1. Potencial de deposición

Tal y como se ha indicado anteriormente, es conocido que la capacidad del proceso de cataforesis para depositar capas de recubrimiento en las zonas más internas y difíciles de una pieza, aumenta con el potencial de deposición empleado, siendo el límite del mismo aquel para el que se produce el fenómeno de "ruptura de film". Éste es un fenómeno producido por un exceso de diferencia de potencial entre electrodos que causa la ruptura del film (que actúa como dieléctrico) a la vez que provoca la aparición de defectos (*pinholes*) y manchas en el recubrimiento.

La deposición cataforética de pinturas se realiza normalmente a un potencial medio inicial entre 250 y 275 V, seguido por un potencial posterior mayor (325-375V). Un aumento del potencial de aplicación trae consigo un aumento de la densidad de corriente en el recubrimiento con el peligro de ruptura del film, dando lugar a cráteres y defectos similares [73].

Estudios previos referentes a este efecto demostraron que los cráteres aparecían en el momento de la deposición y persistían durante el proceso de curado. Este hecho es debido a que durante la deposición cataforética a altas diferencias de potencial, el sistema desprende calor por efecto Joule, aumentando así la temperatura y promoviendo el curado parcial. Las partes de resina que polimerizan, al menos parcialmente, tendrán una viscosidad suficientemente elevada como para que la aplicación de temperatura no pueda eliminar los cráteres formados durante la electrodeposición. Ensayos experimentales en este campo encontraron, en el film electrodepositado, una ruptura dieléctrica localizada, producida durante las duras condiciones iniciales de la electrodeposición [73].

Por otro lado, la dependencia del espesor del film con el potencial y el tiempo de aplicación, es una función compleja donde interviene tanto el potencial catódico aplicado como la conductividad térmica del substrato. Mayores corrientes de deposición (con mayores potenciales) producen un mayor calor por efecto Joule y, como consecuencia, mayores temperaturas en la superficie durante la deposición. Conforme la temperatura del film aumenta, el hidrógeno acumulado en el film tiene una mayor tendencia a salir de éste creando burbujas y provocando defectos. Además, si la temperatura aumenta en exceso, se puede producir una evaporación muy rápida de los disolventes dando lugar a poros. A su vez, tal y como se ha indicado antes, el aumento de temperatura puede promover un curado prematuro de la pintura durante el proceso de cataforesis, reduciendo así la fluidez del film durante el posterior proceso de curado. Este último proceso es un factor fundamental en la calidad final de la pintura.

En definitiva diferencias de potencial demasiado elevadas provocarán que el recubrimiento tenga bajas propiedades y calidad (poros, cráteres…) [73, 78] dando lugar a una baja protección anticorrosiva.

De esta forma será necesario encontrar un potencial de aplicación óptimo, suficientemente alto como para permitir la deposición de pintura en zonas complicadas de la pieza, pero lo suficientemente bajo como para no producir problemas de pérdida de propiedades anticorrosivas.

2.3.5.2. Temperatura de curado

Es bien sabido que las propiedades finales de una resina termoestable dependen, entre otros parámetros, del proceso de curado (tiempo y temperatura) que se emplea. A fin de obtener buenas propiedades mecánicas y anticorrosivas, las imprimaciones epoxídicas depositadas por cataforesis necesitan curar a temperaturas suficientemente elevadas para dar lugar a una buena reticulación pero, a su vez, lo suficientemente bajas como por un lado no provocar un exceso de fragilidad en el film depositado y adicionalmente no dañar los componentes plásticos presentes en la carrocería a pintar.

Una temperatura excesiva provocará reacciones de curado rápidas, una gran contracción de la resina y a consecuencia de todo ello tensiones internas, pudiendo provocar por estos motivos una elevada fragilidad del film que tendrá como consecuencia delaminaciones locales, agrietamiento y pérdida de adherencia.

Sin embargo, una temperatura de curado excesivamente baja (aplicada a fin de evitar los efectos anteriores) dará lugar a una menor densidad de entrecruzamiento (mayor volumen libre y menor T_g), proporcionando así una menor protección barrera.

Por tanto, será necesario encontrar una temperatura de curado óptima, que por un lado consiga un grado de reticulación suficientemente elevado como para que la permeabilidad a las especies reactivas no sea excesiva, pero siempre evitando la aparición de tensiones internas en el material que den lugar a una elevada fragilidad.

2.4. PINTADO ELECTROSTÁTICO

2.4.1. Generalidades

Junto con el pintado por lecho fluidizado, lecho fluidizado electrostático y spray-llama, el pintado electrostático es uno de los cuatro métodos actuales de aplicación de pinturas en polvo [85].

El pintado electrostático, desarrollado en Alemania por Ransberg durante la Segunda Guerra Mundial, es un proceso automático de aplicación del recubrimiento basado en la atracción de partículas de pintura cargadas negativamente hacia un objeto (pieza a pintar) conectado a tierra [6]. En la actualidad es el proceso de aplicación más empleado en pinturas en polvo [85].

Esta técnica de pintado ofrece una gran eficiencia (65%-95%) y un gran ahorro económico, principalmente debido a la inexistencia de sobre-pintado y posibilidad de reciclaje de los excesos. Otra ventaja de este tipo de pintado es la gran uniformidad de espesores que se consigue.

La principal desventaja que presenta es la dificultad que los sistemas mecánicos tienen para conseguir que la pintura alcance las zonas difíciles de la pieza (hay zonas que, a parte de su complicado acceso, actúan como cajas de Faraday y no pueden ser pintadas con facilidad).

El equipo para el pintado electrostático [85] se basa en un tubo a través del cual se transporta el polvo con aire hasta un orificio donde se encuentra un electrodo. Este electrodo está conectado a una fuente de elevado voltaje (40-100kV) y bajo amperaje. Los electrones emitidos por el electrodo reaccionan con las moléculas de aire generando así una nube de iones, llamada corona, alrededor del orificio. La corona está probablemente compuesta por una mayoría de iones OH^- (y tal vez O_2^-). Al pasar las partículas de polvo a su través, recogen aniones de la corona (aunque sólo un 0.5% de las moléculas quedan cargadas [86]). Como el objeto a pintar está conectado a tierra, se crea una diferencia de potencial que atrae las partículas cargadas hacia la pieza a pintar. Así, las partículas de polvo se adhieren formando un film incluso en objetos con formas irregulares, estando las partículas de menor tamaño más cercanas al substrato [87].

En la figura 2.4.1. se muestra una instalación habitual de pistola electrostática. El funcionamiento consiste en la propulsión del polvo de forma neumática hacia la pistola de proyección (otros sistemas para aplicaciones a pequeña escala lo realizan directamente en la pistola por carga superior, como el empleado en el desarrollo de este trabajo).

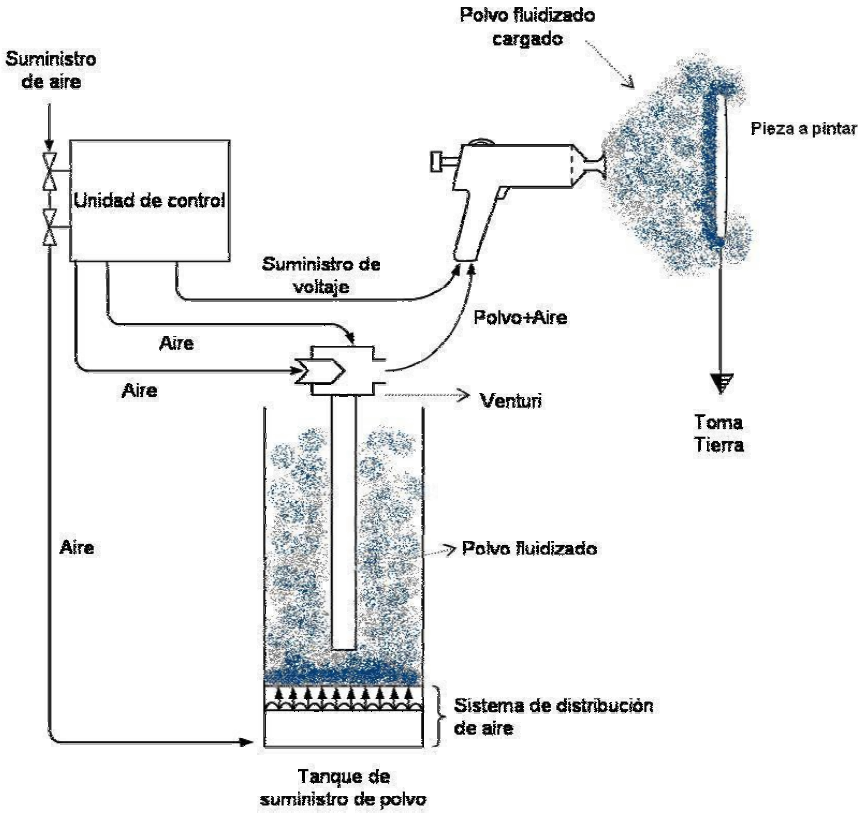

Fig. 2.4.1. Esquema de aplicación con pistola electrostática neumática.

Las partículas se adhieren lo suficientemente fuerte a la superficie del substrato como para poder transportar la pieza recubierta a un horno, donde se mantiene durante un tiempo y temperatura determinados. Bajo estas condiciones las partículas primero reblandecen y se fusionan, dando lugar a un recubrimiento blando pero coherente. Posteriormente comienza el proceso de curado obteniendo así el recubrimiento final sobre el substrato. El curado puede ser por temperatura en un horno de convección convencional o bien por radiación ultravioleta [68, 88].

En sistemas industriales, el polvo extra que no se adhiere a la pieza (sobre-pintado) se recolecta mediante un sistema de filtrado de aire y se devuelve al tanque de suministro para su reutilización, dando lugar así a una baja pérdida de material y una disminución de costes de aplicación.

El espesor de film obtenido aumentará conforme se emplee un mayor voltaje y la aplicación se realice a menor distancia entre la pistola y la pieza. También se pueden conseguir mayores espesores calentando el objeto a pintar antes de aplicar el polvo. El límite de espesor es aquel para el que el recubrimiento actúa como aislante y no atrae más partículas.

2.4.2. Pinturas en polvo

Las pinturas en polvo empezaron a utilizarse en los años 50, y en la actualidad se consideran como la opción más adecuada para reducir los VOCs en el sector de los recubrimientos [89] (contienen un máximo de VOC entre 0.5 y 5%, mientras que las pinturas líquidas contienen cerca de 60% [90, 91]).

Los recubrimientos en polvo son actualmente el sector de pinturas industriales de mayor crecimiento [89] debido a sus propiedades técnicas y a ser respetuosas con el medioambiente, por su baja emisión de disolventes y por reducir los requisitos de limpieza con éstos. A su vez, se eliminan las pérdidas de material por ser éste reutilizable casi en su totalidad [68]. Estos recubrimientos se adaptan perfectamente a los principales objetivos estratégicos de la industria de las pinturas como son la protección contra la corrosión, mejoras en la durabilidad, eliminación de disolventes orgánicos, reducción de deshechos tóxicos, ahorro energético y reducción global de costes [92, 93]. En los últimos años se han realizado numerosos avances tanto en el campo de la formulación y producción como en de la aplicación [94-98] y se estima que en el futuro serán posibles mayores desarrollos.

Comparadas con las pinturas líquidas, el proceso de formación de la película a partir de partículas en polvo es diferente ya que se produce en la fase reblandecida de la resina. Fusión, flujo, punto de gel y curado, son las principales etapas de la formación de film de los recubrimientos en polvo y determinan las propiedades estéticas y protectoras de la pintura, encontrándose la duración de estas etapas directamente afectada por la composición de la pintura: tipo de ligante y entrecruzante, naturaleza, tamaño y distribución de pigmentos, iniciadores, aditivos, y condiciones de aplicación y curado. Estas variables determinan a su vez algunas características del recubrimiento como rugosidad, adherencia, brillo, resistencia química y durabilidad exterior [99-108].

Las principales ventajas que presentan las pinturas en polvo frente a las convencionales de base disolvente son [6, 68, 89]:

- Eficiencias de hasta 95%-99% si el diseño del sistema es apropiado
- Pocos problemas de polución de aire
- Escasos problemas de sobre pintado tóxico, aguas contaminadas o basuras tóxicas
- No se requieren disolventes ni para pintura ni para limpieza
- Se pueden aplicar recubrimientos pesados a superficies complejas
- Facilidad de crear superficies lisas sobre superficies rugosas
- Posible obtención de películas gruesas (75-1300μm) mediante el uso de lecho fluidizado y pinturas termoplásticas
- Recubrimiento de los bordes continuo y uniforme
- Respeto por el medio ambiente

Sin embargo, las pinturas en polvo y sus aplicaciones también presentan ciertas desventajas, como son la dificultad de obtener recubrimientos de espesores bajos (25-50μm) o la dificultad de reciclar el sobre pintado. También presentan dificultades a la hora de conseguir uniformidad de color y pintar esquinas y zonas donde se produce efecto celda de Faraday. A su vez, la necesidad de una limpieza total del sistema antes de cambiar de color en los sistemas de aplicación requiere tiempo.

Finalmente, en una comparación de costes entre diferentes tipos de pintura [109], se puede observar como desde el punto de vista del coste de material por metro cuadrado de substrato recubierto, las pinturas en polvo se muestran como la opción más económica:

	Bajo contenido en sólidos	Alto contenido en sólidos	Base agua	Polvo
Coste €/m^2	0.708	0.491	0.688	0.461

2.4.2.1. Composición y propiedades de pinturas en polvo

Los recubrimientos en polvo pueden ser termoestables o termoplásticos [64], aunque más de un 90% de los recubrimientos en polvo en el mercado son termoestables (resina termoplástica que se convierte en termoestable mediante un entrecruzante, llamado también agente de curado), sin embargo, para espesores muy gruesos (entorno a 1,5mm) también se pueden emplear resinas termoplásticas como el nylon, cloruro de polivinilo, poliolefinas y polímeros fluorados.

Los componentes básicos de las pinturas en polvo termoestables son [6, 110, 111]:

1. Resina

   Es el componente clave de las pinturas en polvo, confiriendo, junto al agente de curado, las propiedades básicas del recubrimiento. Pueden ser de diversos tipos dependiendo de la aplicación que se le vaya a dar. En las pinturas en polvo se emplean especialmente tres tipos de resina: las resinas epoxi que debido a su buen comportamiento ante abrasión y degradación química se emplean en industria, marina y embalaje; las resinas de uretano, que presentan muy buena resistencia al agua, disolventes, aceites y otros, y una muy buena adherencia, aunque tienen peor resistencia a las bases que las resinas epoxi; y las resinas tipo poliéster empleadas esencialmente en recubrimientos de elevadas prestaciones como en la industria del automóvil o acabados en madera.

2. Entrecruzante (o agente de curado)

   Junto con la resina forma el ligante o matriz de la pintura en polvo. Se emplea un tipo de entrecruzante u otro en función del tipo de resina del sistema y de las propiedades finales del recubrimiento. Algunos entrecruzantes pueden ser isocianatos, poliaminas, poliamidas o TGIC (triglicidil isocianurato).

3. Catalizador

   Se emplean a fin de mejorar la cinética de los procesos de reacción de curado, debido a que disminuyen la energía de activación y aceleran el curado. Pueden ser estimulados por calentamiento o por fotoirradiación siendo, desde un punto de vista práctico, el calentamiento, la opción más sencilla ya que un calentamiento homogéneo se puede alcanzar con facilidad [112]. A su vez, las reacciones elementales se aceleran y la viscosidad de la mezcla de reacción disminuye. Esto reduce el tiempo de reacción, especialmente en aquellos sistemas en

los que el gradiente de curado está controlado por procesos de difusión. Un ejemplo de catalizador tradicionalmente empleado son las aminas terciarias para resinas epoxi.

Entre los nuevos tipos de catalizadores/iniciadores latentes, destacan los ácidos de Lewis por su capacidad de homopolimerizar resinas epoxi por mecanismos catiónicos [113] a bajas temperaturas y tiempos.

4. Agente de flujo

   Pueden ser agentes de flujo en seco, para mejorar el transporte de la pintura en polvo en los sistemas de producción. O bien, agentes de flujo en húmedo, para minimizar/eliminar defectos superficiales mejorando la mojabilidad del recubrimiento reblandecido. Algunos ejemplos son poli-acrilatos, siliconas y surfactantes.

5. Desgasificante

   Se emplean para disipar y eliminar burbujas de aire/gas que puedan causar porosidad y fragilidad o malos acabados. Son especialmente importantes en sistemas con alta velocidad de curado. El desgasificante más empleado en la actualidad en pinturas en polvo es la benzoína (esquema 2.4.1.) debido a ser altamente eficaz y bastante económica. La benzoína, a parte de facilitar la desgasificación, también tiene un efecto "*antipinholing*". A pesar que se ha publicado muy poco respecto al funcionamiento de la benzoína [114], se ha demostrado que desaparece de la red entrecruzada en los primeros minutos del curado, liberando con ella los gases ocluidos en la mezcla. Sin embargo, el lado negativo del uso de la benzoína es que afecta ligeramente al curado del sistema [115, 116] (ralentizándolo). Normalmente se emplea en proporciones entre 0.1 y 1%.

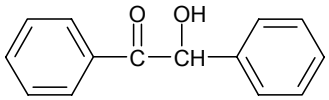

Esquema 2.4.1. Benzoína

6. Pigmentos

   Son partículas sólidas (normalmente cristalinas) encargadas de dar color, opacidad o tener funciones de protección en los recubrimientos (o bien por inhibición o por efecto barrera). Algunos ejemplos son: dióxido de titanio, óxido de zinc, negro de carbono o fosfato de zinc.

7. Cargas

   Se emplean para reducir el coste de formulación de un recubrimiento y/o para mejorar propiedades específicas como flujo, textura superficial, resistencia bacteriana, brillo, lubricación, etc. Algunas cargas comunes son, barita, calcita, mica, talco, silicato de alúmina y wollastonita.

2.4.2.2. Clasificación de pinturas en polvo

Según el tipo de ligante (sistema resina/agente de curado) se puede establecer una clasificación de las pinturas en polvo termoestables como de tipo epoxi, híbrido epoxi/poliéster, poliéster-TGIC, acrílico-uretano, poliéster-uretano y pinturas ultravioleta [6, 68, 110, 111, 117, 118]:

1. Recubrimientos Epoxi

   Sobretodo se emplean resinas basadas en Bisfenol-A y resinas de novolaca, entrecruzadas generalmente con diciandiamida (DICY) y derivados, o con endurecedores fenólicos o anhídridos para aplicaciones de mayores prestaciones. Se emplean tanto como recubrimientos funcionales como decorativos. Las aplicaciones funcionales de mayor tecnología son recubrimientos aislantes de electricidad, recubrimientos para tuberías y recubrimientos para las barras de refuerzo de cemento en construcción de puentes y muelles. Estos recubrimientos funcionales proporcionan excelentes propiedades eléctricas y anticorrosivas. Otras aplicaciones funcionales son como recubrimientos anticorrosivos de carrocerías, muebles y otros enseres cotidianos.

   Los recubrimientos epoxi ofrecen acabados atractivos, manteniendo las propiedades típicas de la familia epoxi como son las buenas propiedades mecánicas, anticorrosivas y buena adherencia. En la actualidad estos sistemas pueden curar a temperaturas mínimas de 120ºC durante 30-50 minutos, o a mayores temperaturas y menores tiempos.

   Estos recubrimientos no son recomendables en usos de exposición directa a radiación solar debido a su tendencia a amarillear cuando se someten a luz UV.
   A pesar de no ser los más empleados, son los primeros recubrimientos en polvo desarrollados y sobre los que se basan los posteriores tipos de recubrimientos. Por este motivo, a estos recubrimientos se les ha prestado especial atención y se les tratará con más detalle a lo largo de este trabajo.

2. Recubrimientos híbridos epoxi/poliéster

   Se formulan con resinas basadas en Bisfenol-A curadas con resinas poliéster con ácido carboxílico terminal, por reacción de apertura del anillo oxirano con los ácidos carboxílicos. Los híbridos ofrecen mejor resistencia al fallo por amarilleamiento y resistencia a UV que los recubrimientos epoxi estándar, aunque tampoco tienen buena durabilidad exterior. Son menos rígidos que los epoxis, pero mantienen en gran parte sus propiedades mecánicas y de resistencia a corrosión con el tiempo. Tienen la ventaja de penetrar bien en esquinas complicadas de piezas a recubrir. Su uso está dirigido a calentadores de agua, extintores y radiadores entre otros. Son los más empleados en la actualidad [119].

3. Recubrimientos poliéster-TGIC

   Se formulan con resinas poliéster con ácidos carboxílicos terminales entrecruzadas con TGIC (triglicidil isocianurato). Son sistemas que presentan mejor comportamiento a exposición ambiental que los sistemas híbridos epoxi-poliéster descritos arriba, debido a que el agente de curado, TGIC, es un compuesto trifuncional de bajo peso molecular resistente a la exposición ambiental. Los recubrimientos formulados empleando estas resinas ofrecen excelentes propiedades mecánicas a espesores elevados, buena protección contra corrosión, buen poder cubriente de vértices, y bajo rango de temperaturas de curado. El mayor problema de este tipo de pinturas radica en la toxicidad del entrecruzador. Este tipo de recubrimientos tienen gran aplicación en ventanas y puertas expuestas a la intemperie debido a su excelente resistencia a exposición ambiental.

4. Recubrimientos acrílicos-uretano

   Generalmente se formulan con comonómeros de resinas epoxi acrílicas funcionales y glicidil metacrilato (GMA) entrecruzados con ácido dicarboxílico, aunque pueden formularse a partir de resinas acrílicas hidroxi-funcionales entrecruzadas con isocianatos saturados. Otra opción de formulación es con resinas acrílicas con grupos funcionales ácido carboxílico curadas con resinas epoxi. Presentan excelente color, brillo, dureza, resistencia ambiental y resistencia química. Se caracterizan por un excelente acabado de film manteniendo buena flexibilidad, sin embargo, presentan menor flexibilidad y resistencia a impacto que los poliésteres. Un uso muy extendido de estos recubrimientos es su aplicación en lavadoras.

5. Recubrimientos poliéster-uretano

   Los recubrimientos de poliuretano se forman por polimerización de resina de poliéster hidroxilada entrecruzada con isocianatos. Los recubrimientos de poliuretano combinan una buena apariencia del film (similar a la obtenida con pinturas líquidas) y dureza, con sus excelentes propiedades ante la exposición ambiental. Su buen acabado y propiedades hacen que sea empleada en una gran variedad de campos.

   Este tipo de pinturas se recomienda para aplicaciones de espesores finos, debido a que el isocianato empleado tiende a volatilizarse, causando agujeros en recubrimientos gruesos.

6. Recubrimientos de curado UV

   Pueden formularse empleando resinas epoxi acrílicas y/o poliésteres acrílicos curados por medio de radicales libres, o bien empleando resina epoxi basada en bisfenol-A con curado catiónico. En la formulación se deben incluir fotoiniciadores que activen el proceso de reacción. Son pinturas estables en ausencia de luz, se producen pocas reacciones prematuras antes del curado que se realiza mediante lámparas UV o en infrarrojo curando a 120ºC.

Se emplean solamente como recubrimientos clear-coat (sistemas libres de pigmento), sin pigmentos, debido a que éstos afectan al curado por absorber parte de la luz ultravioleta [117] reduciendo la reactividad del sistema y dificultando el curado total.

En la tabla 2.4.1. se resumen los tipos de ligante empelados en cada tipo de recubrimiento [118].

Tabla 2.4.1. Resumen de sistemas ligantes

Recubrimiento	Resina primaria	Agente de curado
Epoxi	Epoxi bisfenol-A o novolac	Poliaminas, anhídridos o fenólicos
Híbrido epoxi/poliéster	Poliéster con COOH funcional	Epoxi bisfenol-A
Poliéster/TGIC	Poliéster con COOH funcional	Triglicidilisocianurato o hidroxialquilamina
Poliéster/uretano	Poliéster con OH funcional	Isocianato saturado o resina aminada
Acrílico	Acrílica con epoxi funcional	Ácido dibásico
	Acrílica con OH funcional	Isocianato saturado o resina aminada
Curado UV	Resina con acrilato funcional	Radical libre
	Resina con epoxi funcional	Catiónico

En la tabla 2.4.2. se comparan algunas propiedades de las pinturas en polvo termoestables [117].

Tabla 2.4.2. Comparación de propiedades de pinturas en polvo termoestables

Propiedad	Epoxi	Híbrido epoxi/ poliéster	Poliéster TGIC	Poliéster uretano	Acrílica uretano
Espesor (μm)	25-500[1]	25-250	25-250	25-90	25-90
Ciclo de curado[2] (temperaturas del metal)	230ºC/3' 120ºC/30'	230ºC/3' 160ºC/25'	200ºC/7' 150ºC/20'	200ºC/7' 180ºC/17'	200ºC/7' 182ºC/25'
Resistencia exposición ambiental[3]	Pobre	Pobre	Excelente	Muy buena	Muy buena
Dureza-lápiz[3]	HB - 5H	HB - 2H	HB - 2H	HB - 3H	H - 3H
Adherencia[3]	Excelente	Excelente	Excelente	Excelente	Excelente
Resistencia química	Excelente	Muy buena	Buena	Buena	Muy buena

(1) Espesor hasta 4mm si aplicación de múltiples capas en lecho fluidizado
(2) El tiempo y la temperatura se pueden reducir empleando sistemas acelerados
(3) Ensayo realizado en un recubrimiento de 50μm de espesor

En lo que respecta a las mejoras en la formulación de pinturas en polvo, los principales retos a conseguir son aumentar el "pot-life[4]", así como evitar la sinterización durante el almacenaje, la disminución de coalescencia, desgasificación y nivelación durante el horneado, y la disminución de temperatura y tiempo de curado [114]. En esta tesis doctoral uno de los objetivos ha sido reducir la

[4] Pot-life = vida del producto almacenado sin ser usado

temperatura y tiempo de curado de recubrimientos epoxi. Para conseguir este objetivo se debe tener en cuenta las limitaciones tecnológicas actuales (debidas fundamentalmente al proceso de extrusión) que ocasionan que la menor temperatura de curado posible se sitúe 50ºC por encima de la temperatura de fundido en la extrusión, y 70-80ºC por encima de la T_g del polvo no curado. Así, para un polvo con T_g de 55ºC, la mínima temperatura de curado será 125-135ºC [114].

2.4.2.3. Pinturas en polvo tipo epoxi

Las resinas epoxi tienen una gran aplicación en el campo de los recubrimientos debido a su excelente adhesión, resistencia química, estabilidad térmica y buenas propiedades mecánicas [120-123].

La resina epoxi, junto con el agente de curado y posibles catalizadores, conforma el ligante de la pintura, cuyas propiedades dependerán en gran medida de la estructura de la red final.

Según Tanaka y Bauer [124, 125], una resina epoxi comercial se define como un compuesto o mezcla de oligómeros que contienen uno o más grupos 1,2-epoxi u oxirano (esquema 2.4.2.) por molécula y son capaces de convertirse en termoestables o redes de estructura tridimensional por medio de un agente de curado. El término se emplea tanto para designar resinas en estado termoplástico no curado, como resinas termoestables curadas.

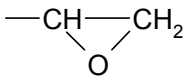

Esquema 2.4.2. Anillo oxiránico

Las ventajas que las resinas epoxi ofrecen en su uso como ligantes frente a otras resinas son [125]:

- excelente adherencia a gran variedad de substratos (gracias a la presencia de grupos hidroxilo)
- baja contracción en curado (menores tensiones ayudando a la adherencia)
- no emiten volátiles en el curado
- excelentes propiedades mecánicas y eléctricas
- buena resistencia química y a los disolventes
- estabilidad térmica
- buena resistencia a la humedad
- buena estabilidad dimensional y resistencia a fatiga
- gran versatilidad (muchas formas de curado, tipos de resina y amplio rango de posibles modificaciones)

En su uso como recubrimientos, estas resinas ofrecen una elevada adherencia, resistencia química, tenacidad, estabilidad térmica y rigidez, de forma que se emplean en usos industriales muy variados (Ej. automóviles, ferrocarriles, electrodomésticos, equipamiento…). Sin embargo, el amarilleamiento que presentan limita su uso a imprimaciones o capa intermedia, pero nunca como capa final [6, 110, 111].

La gran resistencia química que presentan estos sistemas se debe a la presencia de los enlaces C-C y enlaces tipo éter en la columna vertebral del polímero. Y su gran adherencia a casi todos los metales se debe a la polaridad de la molécula y a la existencia de grupos OH^-.

Las resinas epoxi pueden ser principalmente de tres tipos [125]:

1. Resinas epoxi cicloalifáticas: El átomo de oxígeno del anillo oxirano está unido a dos carbonos de un anillo alifático
2. Aceites (triglicéridos) y otros ésteres epoxidados. El anillo epoxi está unido a ácidos como el ácido oleico
3. Resinas epoxi glicídicas (grupo 1,2-epoxipropilo), donde el anillo epoxi está unido a compuestos polihidroxílicos, polifenólicos, ácidos polibásicos o poliaminas. Son las resinas más empleadas

Las resinas epoxi glicidícas, se distinguen por tener el anillo oxirano enlazado a una cadena orgánica a través de un grupo funcional generalmente éter o éster [126]. Estas resinas son polímeros polares, de baja solubilidad en sustancias no polares, que contienen grupos oxirano o glicidilo terminales (esquema 2.4.2.). Estos grupos oxirano son reactivos ante grupos hidroxilo, carboxilo y amino, entre otros [120, 121] debido a la polaridad del enlace C-O y su estado tensionado [125]. Así, el anillo oxirano se puede abrir mediante agentes de curado, para proceder al entrecruzamiento de la cadena polimérica y obtener una red tridimensional termoestable.

Los agentes de curado más habituales suelen ser aminas (alifáticas, cicloalifáticas, aromáticas, terciarias o imidazoles), anhídridos de ácido o ácidos de Lewis. Las aminas y los anhídridos de ácido reaccionan con el anillo epoxi por sustitución nucleófila al carbono metilénico del anillo oxirano o con el grupo hidroxilo, mientras que los ácidos de Lewis lo hacen esencialmente por homopolimerización de la resina mediante activación de los anillos oxirano [125]. En las pinturas en polvo se emplean como agentes de curado anhídridos de ácido, ácidos de Lewis y derivados de la diciandiamida (DICY).

Entre las resinas epoxi glicidícas más empleadas destacan las obtenidas por condensación de bisfenol-A (difenilol propano) con epiclorhidrina (1-cloro-2,3-epoxipropano) en presencia de NaOH (para deshidrohalogenar la bisclorohidrina intermedia) y bajo reflujo (esquema 2.4.3.), conociéndose el producto como resina DGEBA (diglicidiléter de bisfenol A) [120, 125, 127].

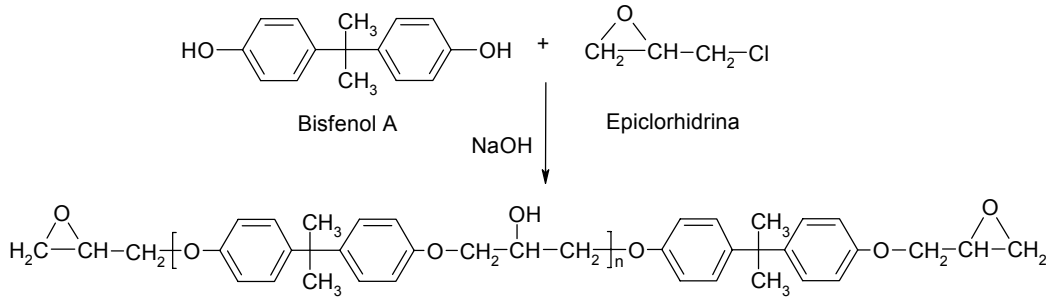

Esquema 2.4.3. Reacción de obtención de una resina epoxi glicidílica tipo DGEBA

Las resinas epoxi sólidas, basadas en Bisfenol A, (para uso en pinturas en polvo) se obtienen con proporciones equimoleculares de reactantes (excesos de epiclorhidrina dan lugar a resinas líquidas). La longitud de la cadena vendrá también dada por la proporción entre reactantes, pudiendo estar "n" entre 0 y 100 (esquema 2.4.3). Cuando "n" está entre 0 y 1, las resinas son líquidas, y si se encuentra entre 2 y 100, serán sólidas. Sin embargo, resinas con valores de n superiores a 18, debido al elevado peso molecular, son de naturaleza termoplástica y no requieren de agente de curado. Así, en función de la longitud de cadena, las propiedades de las resinas epoxi variarán en gran medida (tabla 2.4.3.) [6, 125].

Tabla 2.4.3. Propiedades de las resinas epoxi en función de la longitud de cadena

Longitud de cadena (n)	Peso molecular (aprox.)	Punto de reblandecimiento (ºC)	Grupo reactivo principal	Usos
0-1	400	Líquidas	Oxirano	Curado a temperatura ambiente con aminas para recubrimientos
2	1000	70	Oxirano	
4	2000	100	Oxirano-Hidroxilo	Ésteres epoxídicos
8	3500	130	Hidroxilo	Secado por temperatura con resinas amínicas o fenólicas
12	6000	150	Hidroxilo	

Una resina de un valor "n" determinado, realmente es una mezcla de oligómeros con diferentes longitudes de cadena o "n" y a la que se le da un valor "n" promedio de toda la dispersión de oligómeros obtenida en su procesado [125].

Por lo general las resinas con "n" bajos serán curadas con agentes de curado que reaccionen con grupos epoxi, mientras que las resinas con "n" elevados lo harán con agentes de curado que reaccionen con los grupos hidroxilo [125].

En el curado de una resina de estas características se crea una red tridimensional entrecruzada unida por enlaces covalentes, cuya morfología, estructura química y densidad de entrecruzamiento vienen determinadas por el agente de curado, el mecanismo de entrecruzamiento y la cinética de la reacción [121,122, 128].

En el caso de las pinturas en polvo tipo epoxi se requiere de un entrecruzante sólido (normalmente un derivado de la diciandiamida) para obtener una red entrecruzada como la red idealizada mostrada en la figura 2.4.2., donde las líneas naranja simulan las cadenas de resina DGEBA y los grupos negros simulan el agente de curado.

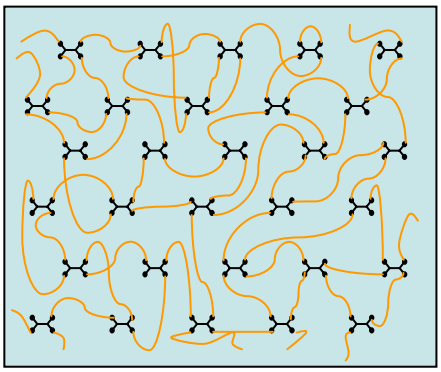

Fig. 2.4.2. Red entrecruzada.

En el proceso de curado nucleófilo por reacción entre una resina epoxi y un agente de curado, como puede ser un derivado de diciandiamida (DICY) o una amina, pueden tener lugar tres tipos de reacciones según Shechter, Wynstra y Kurkjy [129] (esquema 2.4.4.).

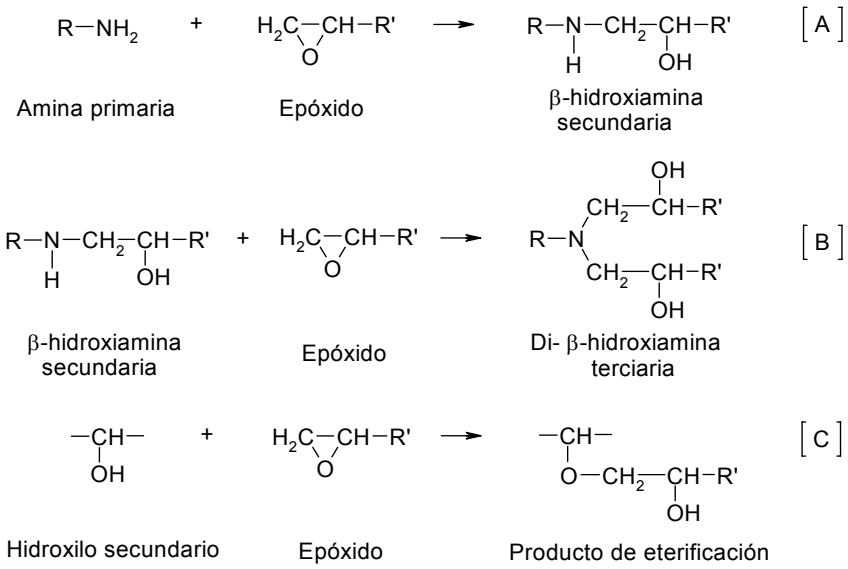

Esquema 2.4.4. Reacciones de curado de un sistema tradicional epoxi/amina

Donde las reacciones son de tres tipos:

- Reacción de sustitución nucleófila (reacción A de apertura de anillo y creación de amina secundaria y alcohol secundario en el carbono β)
- Reacción de sustitución nucleófila tipo B, a partir de la amina secundaria. Esta reacción es simultánea a la reacción A aunque más impedida estéricamente, por lo que es más lenta [130]
- Reacción C de eterificación. Es una reacción secundaria minoritaria que sólo se produce cuando la temperatura de curado está por encima de los 140ºC [131] y cuando la proporción epoxi/diamina es muy elevada [132]

La existencia de reacciones de eterificación afecta a las propiedades mecánicas y químicas de la red polimérica [131]. Sin embargo, su importancia no es excesiva puesto que el grado de la reacción tipo C es hasta 10 veces menor que la reacción de adición (A y B), y bajo condiciones de curado normales (temperaturas no excesivamente elevadas) su efecto sólo es notable al final del proceso principal (reacción A) [131]. A su vez, la importancia de esta reacción sólo es elevada en sistemas no-estequiométricos, con exceso de componentes epoxi, esto es, en sistemas donde P<0.8 [131]. Siendo:

$$P = [NH]_o / [EP]_o$$

$[NH]_o$ = concentración inicial de grupo amina
$[EP]_o$ = concentración de grupos epoxi

Las aminas cíclicas más empleadas son la diamina isoforona y la 1,2-ciclohexandiamida, aunque su uso en resinas en polvo es restringido. Algunos ejemplos de aminas alifáticas son la dietilentriamina (DETA), la trietilentetraamina (TETA) o la polioxipropilendiamina. A pesar de ser los agentes de curado más extendidos, las aminas alifáticas no se emplean en pinturas en polvo debido a que reaccionan a temperatura ambiente. Sin embargo, algunas poliamidas (derivados de las aminas por reacción con ácidos grasos para reducir su toxicidad) pueden ser empleadas en pinturas en polvo. El caso más claro es el de la diciandiamida o cianoguanida (DICY) (esquema 2.4.5.) que fue uno de los primeros agentes de curado térmico latentes para resinas epoxi. Sus derivados son actualmente los agentes de curado para pinturas en polvo más empleados, obteniéndose grupos hidroxilo y amina al reaccionar con los anillos oxirano. Su proporción recomendada suele estar entorno a 4-6phr[5] y el curado superior a 175ºC [125].

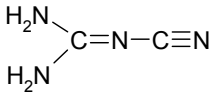

Esquema 2.4.5. Diciandiamida (DICY)

A pesar de estos sistemas tan empleados, las tendencias actuales de mercado impulsan a la búsqueda de reducciones en costes de aplicación de los recubrimientos en polvo, y esto es, crear sistemas alternativos con menores temperaturas y/o tiempos de curado.

Las reacciones de curado, ya sea por adición o por condensación, presentan el problema de la contracción [133] debido a que las moléculas se encuentran separadas por distancias Van der Waals y al polimerizar pasan a ser distancias covalentes, más próximas entre sí [134-136].

Estas contracciones comportan el empeoramiento de las propiedades mecánicas de las redes creadas, por aparecer tensiones internas y, en consecuencia, pérdida de adhesión, poros, grietas, etc. Así, la eliminación o control de la contracción en la polimerización es uno de los problemas a solventar en las aplicaciones industriales [137, 138]. Actualmente se emplean cargas para cumplir esta función, el problema es que afectan a la homogeneidad de la red y a la fragilidad de la misma [139].

[5] p.h.r = parts per hundred resin: gramos de compuesto por 100 gramos de resina

De esta forma la formulación de recubrimientos en polvo epoxídicos de baja temperatura de curado y con nula o menor contracción (empleando nuevos catalizadores, iniciadores y agentes de curado) se ha convertido en una de las principales líneas de investigación en industrias y centros relacionados. Como ya se ha mencionado en esta tesis doctoral, se intentará obtener sistemas epoxi de bajo curado y baja o nula contracción.

Una de las líneas enfocada a la disminución de la temperatura de curado de las pinturas en polvo gira en torno a los iniciadores catiónicos (como los ácidos de Lewis[6]). A su vez, los ácidos de Lewis, por provocar el curado por homo-polimerización (curado por apertura de anillo), se presentan como alternativa a eliminar la contracción ofrecida por el curado por adición con aminas o amidas [126].

En los iniciadores catiónicos empleados como agentes de curado en pinturas en polvo, el orden de reactividad depende tanto del catión como de las características nucleófilas del contraión (Cl^-, BF^-, SbF_3^- …), siendo más activo el compuesto con el anión menos nucleófilo porque se minimizan o eliminan las reacciones de terminación de cadena por formación de enlace covalente con anión [112, 140]. Entre estos iniciadores, los más ampliamente empleados son agentes de curado latentes como el BF_3/amina (ej. BF_3·MEA [7]), debido a que crean mezclas con las resinas epoxi que son estables a temperatura ambiente (lo que aumenta su pot-life) pero de curado rápido al aplicar elevadas temperaturas (a 120ºC el sistema cura en pocos minutos). El inconveniente que presentan es que estos compuestos catiónicos son altamente higroscópicos, se descomponen o desactivan en presencia de humedad, no pueden ser reutilizados y las propiedades eléctricas de los sistemas formados se deterioran a temperaturas elevadas y con la humedad [124, 141-143].

Como alternativa a los iniciadores catiónicos actuales se han propuesto nuevos sistemas promotores también de polimerización catiónica, como los triflatos de lantánido, usados principalmente por ser estables y comportarse como ácidos de Lewis incluso en presencia de humedad, aunque su aplicación en la actualidad sea tan solo a escala de laboratorio.

En el año 1954 comienza el desarrollo de estos iniciadores con la descripción del ácido trifluorometanosulfónico o ácido tríflico (TfOH) por Haszeldine y Kidd [144]. Así los triflatos de lantánido se preparan principalmente a partir de calentar el óxido o cloruro de lantánido en una solución acuosa de ácido trifluorometanosulfónico (TfOH) [145-149].

La formula general de los triflatos de lantánido es $Ln(OSO_2CF_3)_n$ donde n, valencia del lantánido, suele ser 3 debido a ser su estado de oxidación más estable [150]. De forma abreviada se puede escribir como $Ln(TfO)_n$. Los trifluorometanosulfonatos de lantánido son ácidos de Lewisfuertes, potenciados por el carácter electro-atractor del grupo trifluorometanosulfonilo (TfO) [151].

[6] Ácido de Lewis: sustancia capaz de aceptar y compartir un par electrónico
[7] BF_3·MEA = trifluoruro de boro monoetilamina

En 1991 aparece por primera vez un trabajo donde se nombra su compatibilidad con el agua [152-154]. Desde entonces han mostrado un gran desarrollo y producido diversos tipos de derivados [155-159].

Los triflatos de lantánido se han utilizado en la polimerización catiónica del p-metoxiestireno [160-163] y otros monómeros vinílicos [164]. También se ha estudiado la preparación de poliésteres a temperatura ambiente por policondensación directa de diácidos y dioles en presencia de triflatos de escandio, que tiene una reactividad muy parecida a los triflatos de lantánido [165].

Por otra parte, los triflatos de lantánido se han propuesto como excelentes catalizadores en la apertura de anillos oxirano en presencia de agentes nucleófilos como aminas [166-168], indoles [169] o alcoholes [170].

El efecto catalítico de los triflatos de lantánido en el curado de resinas líquidas también ha sido objeto de estudio [113, 126, 171]. En este trabajo se trata el uso de triflatos de lantánido como iniciadores para resinas epoxi en polvo, ya que el efecto de los triflatos de lantánido en el curado de resinas en polvo para recubrimientos orgánicos no ha sido estudiado hasta la fecha y parece ser de notable importancia por las posibles reducciones económicas de coste de aplicación.

Los cationes lantánido (Ln(III)) tienen una elevada capacidad de coordinación [172, 173], gracias a su gran afinidad hacia el oxígeno del anillo oxirano, debilitan el enlace C-O del anillo [151, 174, 175] favoreciendo así mecanismos catiónicos de reacción. Su eficiencia catalítica depende de la acidez de Lewis relativa de cada lantánido

Los aniones triflato presentan una nucleofilia pobre, una baja basicidad y una habilidad coordinativa pobre, de forma que, tal y como se ha explicado más arriba para los iniciadores catiónicos, es de esperar la existencia de pocos procesos de finalización de cadena [176].

Las mayores ventajas [126, 160, 173-178] que estos iniciadores presentan frente a otros ácidos de Lewis como el $AlCl_3$, BF_3 y $TiCl_4$ son las siguientes:

- Son estables en presencia de agua, pudiéndose emplear en medios acuosos
- Son estables a temperatura ambiente
- No es necesario su almacenaje en atmósfera inerte
- Son bastante solubles en compuestos orgánicos
- La toxicidad de los lantánidos es menor que la de los metales de transición y similar a la de los metales alcalinos
- Son reutilizables. Esto es, una vez finalizada la reacción en síntesis orgánica (no en polimerización, donde quedan anclados a la red) pueden ser recuperados por extracción con agua y ser reutilizados, lo cual comporta una ventaja medioambiental frente a otros ácidos de Lewis

Según diversos autores [126, 139, 179, 180] que han estudiado los mecanismos de polimerización catiónica de epóxidos se producen dos tipos de reacciones: las que siguen un mecanismo tipo ACE (activated chain-end mechanism), esquema 2.4.6., y las de tipo AM (activated monomer mechanism), esquema 2.4.7. Donde "I" es el catión iniciador (lantánido) que activa el oxígeno del anillo oxirano (creando una deficiencia electrónica).

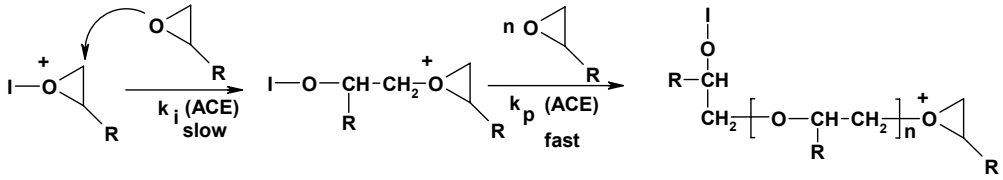

Esquema 2.4.6. Reacción ACE (activated chain-end mechanism)

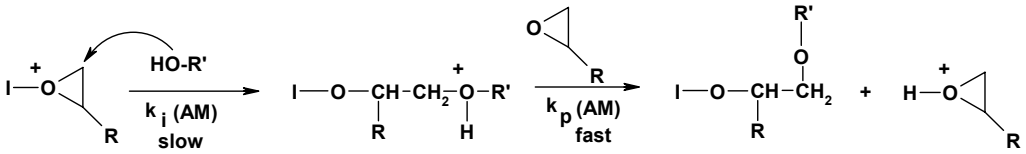

Esquema 2.4.7. Reacción AM (activated monomer mechanism)

Los iniciadores tipo ácidos de Lewis conducen a una polimerización por apertura de anillo de los compuestos epoxi, la cual procede principalmente por el mecanismo ACE del esquema 2.4.6, donde el anillo oxirano de la resina DGEBA se abre por coordinación del oxígeno oxirano con el iniciador y ataque nucleófilo de otro anillo oxirano. En polimerización catiónica está aceptado que el verdadero iniciador cuando se usa ácidos de Lewis es un catión hidrogenónio, H^+ [181], sin embargo, el mecanismo cuando se emplean triflatos de lantánido no se ha estudiado aún, aunque debido a no introducir protones, una posible teoría, pendiente de justificación, es que el iniciador sea el propio lantánido.

Por otro lado, la presencia de grupos hidroxilo puede llevar a procesos de polieterificación por el mecanismo AM, lo que puede cambiar la cinética de la reacción y las propiedades del material. No obstante, este tipo de reacciones es menos importante que las ACE por el bajo contenido en hidroxilos. El mecanismo AM puede verse favorecido en presencia de protones en el medio [126, 139], lo cual sucedería sobretodo en sistemas en base disolvente prótico pero no en sistemas en polvo, como es nuestro caso de estudio, donde la presencia de protones procede tan solo del agua de hidratación del triflato de lantánido o de los grupos hidroxílicos de la resina y no de agua en el medio, si bien es cierto que por ser la resina epoxi polar, cierta cantidad de humedad se encuentra retenida en la red. Un aumento de hidroxilos en el medio produciría un aumento del mecanismo AM (como ocurriría en el caso de resinas epoxi con mayor peso molecular). Otro efecto que puede favorecer las reacciones tipo AM es una mayor inclusión de triflato de lantánido en el sistema. Esto se debe a un mayor aumento de grupos epóxido activos, reduciendo los grupos epóxido no catiónicos capaces de reaccionar por el mecanismo ACE y, favoreciendo así el mecanismo AM por reacción de los grupos hidroxilo.

En lo que respecta al efecto de los triflatos de lantánido en la contracción de la resina epoxi durante el curado se puede explicar a partir del esquema 2.4.8. Donde se observa como por cada enlace que pasa de una distancia Van der Waals a una distancia covalente (contracción), hay otro que lo hace de una distancia covalente a una distancia próxima a la de Van der Waals (expansión) [133, 134, 182, 183], produciéndose así una disminución de la contracción del sistema, a diferencia de lo que ocurre en el curado con DICY por ejemplo.

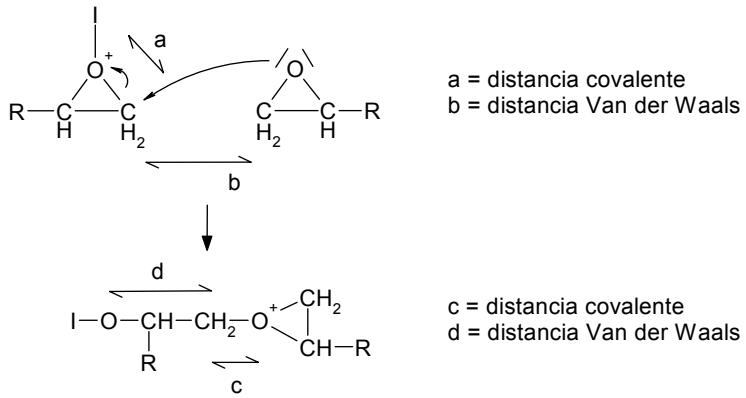

Esquema 2.4.8. Esquema del cambio de distancias en homopolimerización

Durante el curado se rompe un enlace covalente en el oxirano (a) y se reduce una distancia de Van der Waals de separación entre las dos moléculas (b), pero en la red formada se crea un nuevo enlace covalente (c) y al abrirse el anillo se pasa a una distancia próxima a la de Van der Waals (d) de forma que no se produce sino una ligera contracción del sistema.

Sin embargo, para aplicaciones donde se requiera evitar totalmente la contracción o incluso favorecer cierta expansión es necesario el uso de otros materiales como son los compuestos bicíclicos o *monómeros expandibles*, definidos en 1973 por Bailey [184, 185], en los que por cada distancia que pasa de Van der Waals a covalente hay por lo menos dos distancias que pasan de covalente a Van der Waals de forma que el polímero sufre una ligera expansión [135, 136, 186].

Un monómero de tipo expandible tiene que cumplir tres características para poder evitar la contracción de la resina epoxi durante el curado [133, 184]:

- Los anillos deben estar fusionados, es decir, cada anillo del monómero bicíclico debe tener como mínimo un átomo en común
- Cada anillo debe tener como mínimo un heteroátomo
- Los anillos no se pueden abrir simétricamente (no deben dar el mismo tipo de grupo los dos anillos al abrirse)

Ejemplos de este tipo de material son los espiroésteres (SOEs), espirocarbonatos (SOCs) y los bicicloortoésteres (BOEs) [133, 137, 187-190]. Los SOEs, esquema 2.4.9., se obtienen a partir de la reacción directa de una lactona y un grupo epoxi en presencia de un iniciador ácido de Lewis [126, 191-

194]. De esta forma se consigue la polimerización con una cierta expansión. Si esta estrategia se aplica a la preparación de termoestables se limitan así problemas de aparición de micro-grietas y pérdidas de adherencia. Algunos autores han conseguido interesantes resultados cinéticos y mecánicos con la polimerización de una resina de DGEBA líquida, empleando una lactona de cinco miembros y triflatos de lantánido como iniciadores [126, 195-198], sin embargo, en sistemas epoxi en polvo (sistemas sólidos) todavía no se ha realizado investigación alguna.

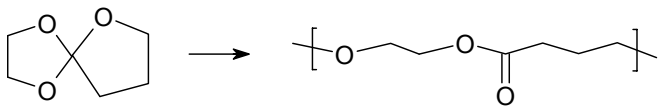

Esquema 2.4.9. Polimerización de un SOE

2.4.2.4. Procesado de pinturas en polvo

El procesado de las pinturas en polvo (fundamentos desarrollados en 1961 [98]) consiste en el mezclado de las diferentes materias primas sólidas siguiendo los pasos de pre-mezclado, extrusión, granulado, molienda y clasificación, y almacenaje [68, 199]. En la figura 2.4.3. se muestra un esquema del proceso de producción a escala industrial.

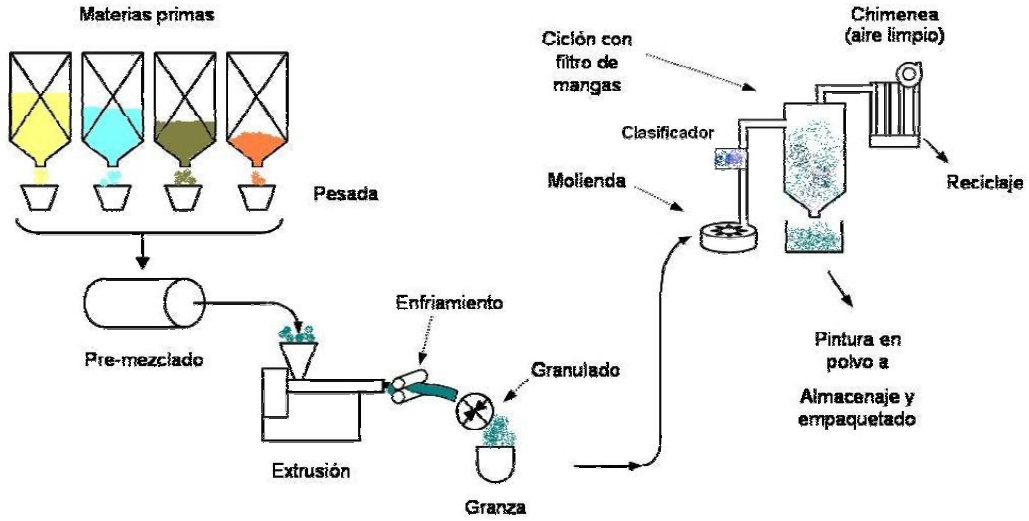

Fig. 2.4.3. Esquema producción pinturas en polvo.

1. *Pre-mezclado*

   Consiste en la pesada de las diferentes materias primas y su mezclado por agitación obteniendo un mezclado uniforme de los componentes. Por lo general las materias primas son sólidas pero cuando se emplea algún aditivo líquido se debe mezclar con algún otro componente sólido (normalmente resina) para formar un masterbatch sólido.

2. *Extrusión*

Es el verdadero mezclado de las materias primas y se suele llevar a cabo en una extrusora (ver figura 2.4.4). Se puede definir una extrusora como un equipo empleado para homogeneizar materiales plásticos, incluyendo colorantes y aditivos, en la fase fundida/reblandecida. Para llevar a cabo esta homogeneización la extrusora emplea calor y esfuerzos de cizalla para lo cual se vale de un tornillo sin fin (o dos) que arrastrará el material y aumentará la cizalla según las necesidades por medio de su morfología, de forma que, el tornillo comprime, funde y homogeneiza el material.

Así existen dos tipos de extrusora, las mono-usillo (un tornillo) donde se incluye una zona de recirculación a parte del giro radial para mejorar el mezclado y dispersión, y las doble usillo (dos tornillos) en las que los tornillos combinan zonas de arrastre con zonas de amasado. Un motor potente gira los tornillos para conducir el material a través de un tubo. El tubo y los tornillos están configurados para conseguir mezclar el material adecuadamente y aplicar una gran cizalla para separar agregados de partículas. Ambos sistemas consiguen una excelente dispersión.

La pre-mezcla se introduce en la extrusora donde se compacta y reblandece. Las fuerzas de tensión de cizalla rompen los agregados de pigmentos obteniéndose una dispersión homogénea de los diferentes elementos en el seno de la resina reblandecida.

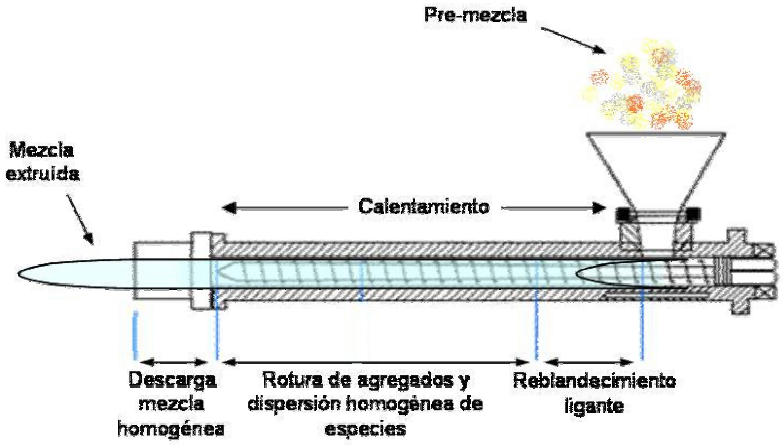

Fig. 2.4.4. Extrusión pintura en polvo.

3. *Enfriado/granulado*

Consiste en el enfriado de la mezcla extruída mediante rodillos de enfriamiento, pudiendo emplearse una banda de enfriado en equipos de elevada producción. La operación de enfriado termina con la rotura del material extruído, frágil y frío, en trozos de entre 5 y 15mm, mediante molinos de palas.

4. *Molienda/clasificación*

Las etapas finales del procesado son la molienda (o pulverización) y posterior clasificación. Estos procesos convierten los trozos de 15 mm (granza) en polvo fino con un tamaño de partícula determinado. Normalmente se emplean micro-pulverizadores en la industria (*pin-disk mills*), y a escala de laboratorio, molinos ultra-centrífugos (*hammer mills*). Sin embargo, recientemente se han desarrollado los *opposed jet mills*, en los que la reducción de tamaño se fuerza por colisiones entre las propias partículas en lugar de con palas o *plugs*.

Tras la molienda se separan los gruesos de los finos en un clasificador (tamiz), donde los gruesos se recirculan al molino/pulverizador y los finos se transportan hasta sistemas de aire (ciclones) donde se vuelven a clasificar, enviándose la fracción con tamaño de partícula deseado (tamaño entre 40 y 100μm) a las zonas de almacenaje, y los finos a un filtro de mangas para su recuperación y recirculación.

Especial atención se presta al tamaño de partícula puesto que puede tener influencia en el comportamiento del material en el proceso de reparto, carga, aplicación, conformación y propiedades finales del film.

Se buscará una distribución de tamaño de partícula (campana de Gauss) en la que el tamaño predominante sea menor que el espesor deseado de film, y los más grandes no sean más de dos veces el espesor del film [85]. Por ejemplo, en un film deseado de 50μm, la campana de distribución de diámetros estará centrada en 45μm, siendo el máximo 100μm. Se ha demostrado que es el rango intermedio de distribución de partículas el que se adhiere al substrato [200], ya que los menores tamaños de partícula son arrastradas por el aire de la campana de pintado, y las de mayor peso por la gravedad. De esta forma el sobre-pintado lo componen esas partículas gruesas y finas que se recircularán, disminuyendo a menos de un 5% las pérdidas por sobre pintado. De esta forma los tamaños de partícula que se adherirán al substrato están entre 20 y 60μm.

5. *Almacenaje*

El polvo procedente del ciclón se almacena en cámaras de almacenaje, desde donde se distribuirá para su empaquetamiento y posterior aplicación.

2.5. OBJETIVOS

A raíz de los antecedentes presentados en el marco teórico, para la realización de la presente tesis doctoral se plantearon los siguientes objetivos generales:

1. Formular una imprimación epoxi en polvo de curado a bajas temperaturas basada en triflatos de lantánido, a fin de abaratar costes de aplicación y facilitar el uso de las pinturas en polvo en substratos termosensibles, presentando a su vez, buenas propiedades anticorrosivas.
2. Desarrollar una técnica electroquímica de evaluación acelerada del comportamiento anticorrosivo de recubrimientos orgánicos, con la finalidad de reducir en gran medida el tiempo de evaluación de los recubrimientos, abaratando costes y facilitando la formulación de recubrimientos orgánicos.
3. Optimizar el sistema de aplicación y curado de pinturas cataforéticas en la industria del automóvil mediante el uso de técnicas electroquímicas.

A fin de alcanzar los objetivos generales se establecieron diversos objetivos parciales:

1. Caracterizar los nuevos sistemas orgánicos en polvo desarrollados, que servirán de ligante en las imprimaciones anticorrosivas, mediante técnicas de caracterización cinética, térmica (DSC, TGA), mecánica (caída de dardo, DMTA, rayado, ensayos de tracción, adherencia), superficial (SEM, XPS), química (FTIR) y electroquímica (EIS, Niebla Salina, AC/DC/AC).
2. Estudiar las posibilidades de uso de la técnica electroquímica acelerada desarrollada, mediante su uso en imprimaciones en polvo y cataforéticas.
3. Evaluar la correlación entre la técnica acelerada desarrollada y otras técnicas de evaluación anticorrosiva actuales (EIS y Niebla Salina).

Los objetivos marcados se alcanzaron mediante el establecimiento de una metodología de trabajo que consta de dos líneas directas de investigación y una línea transversal.

1. *Línea Transversal*: Desarrollo de técnica electroquímica acelerada de evaluación anticorrosiva (AC/DC/AC). Estudio de su viabilidad de uso en la formulación de pinturas en polvo y pinturas cataforéticas. Aplicación a la optimización de sistemas de aplicación: cataforesis.
   La técnica desarrollada se empleará para evaluar las características anticorrosivas de las imprimaciones formuladas, a la vez que se buscará la correlación existente entre ésta y las técnicas existentes actuales (EIS y Niebla Salina).

2. *Línea directa*: Evaluación de pinturas cataforéticas. Optimización del proceso de cataforesis (esquema 2.5.1).

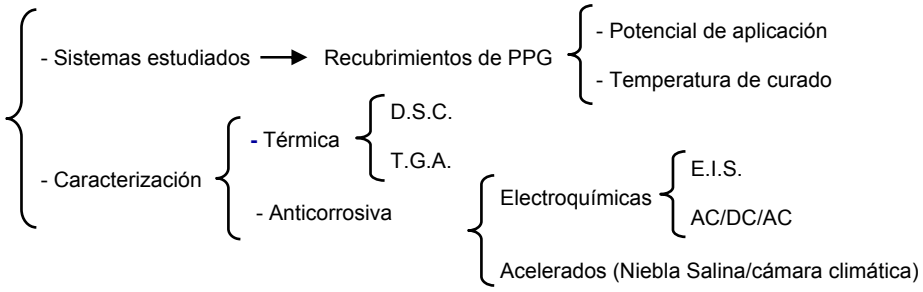

Esquema 2.5.1. Diagrama optimización cataforesis

En primer lugar se establecieron los sistemas que se iban a emplear en el estudio, para lo cual se contó con el apoyo de una industria líder del sector (PPG Ibérica) con la cual se acordó emplear un recubrimiento fabricado por la empresa. La empresa PPG Ibérica fue la encargada de aplicar el recubrimiento sobre substrato acero variando dos parámetros: el potencial de aplicación (manteniendo el resto de variables constante) y la temperatura de curado posterior (manteniendo el resto de variables constante).

Una vez preparadas las muestras se procedió a su evaluación térmica por medio de un DSC (Dynamic Scanning Calorimeter) a fin de determinar la influencia de la temperatura de curado y potencial de aplicación en la temperatura de transición vítrea del sistema, así como de un TGA (Thermogravimetric analyzer) para determinar la influencia de las variables sobre la estabilidad térmica y contenido de pigmentos depositado.

En paralelo se realizó el estudio de propiedades anticorrosivas y la influencia de la variación de las dos variables en éstas. Para esto se empleó una técnica acelerada tradicional (empleada en la industria PPG, en la que se combina resistencia a niebla salina y cámara climática) y una técnica electroquímica muy extendida a nivel científico (Electrochemical Impedance Spectroscopy, EIS). A su vez se desarrolló una técnica electroquímica de evaluación rápida (AC/DC/AC) capaz de evaluar de forma rápida y eficaz las propiedades anticorrosivas y clasificar así los sistemas en función de sus propiedades.

Por medio de la combinación de estas técnicas se pudo ofrecer un rango de temperaturas de curado y potenciales de aplicación adecuados con los que optimizar el proceso de cataforesis.

3. *Línea directa*: Formulación y evaluación de imprimaciones epoxi en polvo. Obtención de una imprimación de curado a bajas temperaturas (empleo de ácidos de Lewis). Adición de ácido de Meldrum para mejorar en gran medida las prestaciones del recubrimiento.

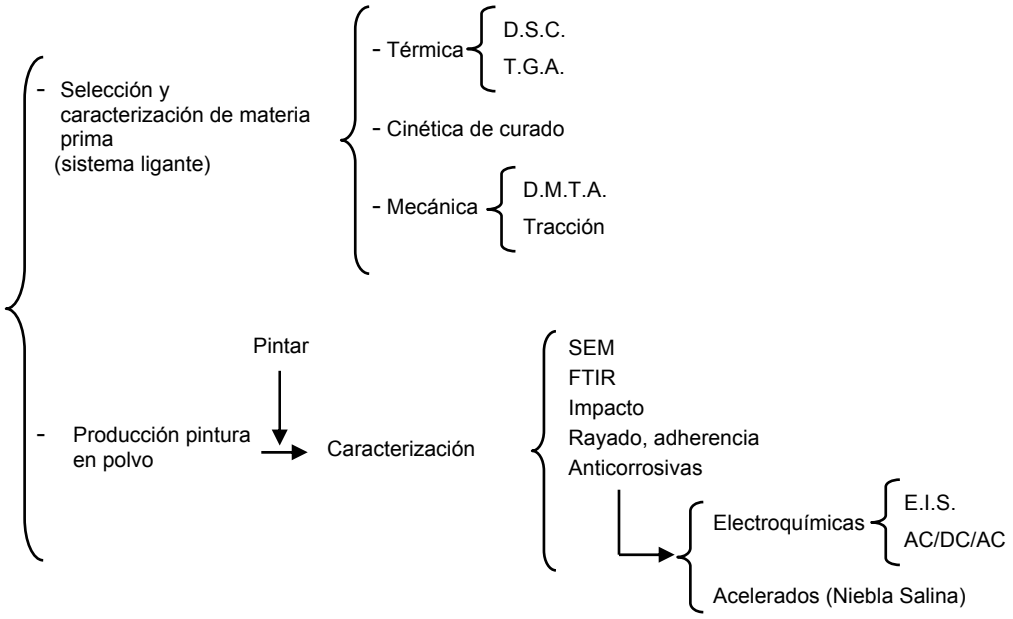

Esquema 2.5.2. Diagrama formulación pinturas en polvo

El objetivo principal de este trabajo fue formular un recubrimiento en polvo basado en triflatos de lantánido, de curado a baja temperatura y con buenas propiedades mecánicas, térmicas y anticorrosivas. Para alcanzar este objetivo se emplearon triflatos de erbio e iterbio como iniciadores de homopolimerización de una resina epoxi y como catalizadores de un sistema convencional epoxi/o-tolilbiguanida.

En primer lugar se establecieron las formulaciones a preparar basándose en la literatura. La preparación de los sistemas se realizó por medio de extrusión y posterior molienda/tamizado. Los sistemas tuvieron dos tratamientos de curado en función de los ensayos a realizar: como film libre, o como recubrimiento sobre substrato acero.

A las muestras en film libre se les realizó una caracterización cinética, térmica y mecánica mediante técnicas como DSC, SEM, FTIR, TGA, tracción y DMTA. Sobre las muestras aplicadas sobre substrato acero se realizaron ensayos de impacto, adherencia, rallado y, principalmente, estudios de propiedades anticorrosivas mediante ensayos acelerados tradicionales (Niebla Salina) y electroquímicos (EIS y la técnica desarrollada para pinturas cataforéticas AC/DC/AC).

Toda la caracterización térmica, mecánica y anticorrosiva permitió establecer la formulación más apropiada y orientar el siguiente paso, consistente en la mejora del producto empleando ácidos de Lewis. Así se introdujo el uso de ácido de Meldrum en dos formulaciones, desarrollando para estos nuevos sistemas el mismo esquema de trabajo presentado en esquema 2.5.2., y estableciendo así un producto que cumpliera los objetivos marcados en un inicio: elevada velocidad de curado y buenas propiedades anticorrosivas y mecánicas.

1. Electrochemical Corrosion Nomenclature (IUPAC Recommendations 1988), Prepared for publication by K.E. Heusler, D. Landolt, S. Trasatti, *Pure* & *Appl. Chem.,* 61 (1) (1989) 19
2. M.G. Fontana, *Corrosion Engineering*, McGraw-Hill Book Co., 3rd Edition
3. NACE Basic Corrosion Course. NACE ETC-10 Committee, 1996 Rev
4. H.H. Uhlig, *Corrosión y Control de Corrosión*, Urmo S.A. Ediciones 1979
5. K.R. Trethewey, J. Chamberlain, *Corrosion for Science and Engineering*, Longman 1995, 2nd Edition
6. J.A. von Fraunhofer, J. Boxall, *Protective Paint Coatings for Metals*, Portcullis Press Ltd. 1976
7. J.A. González-Fernández, *Control de la Corrosión – Estudio y medida por técnicas electroquímicas,* CNIM-CSIC 1989
8. G. Grundmeier, W. Schmidt, M. Stratmann, *Electrochim. Acta,* 45 (2000) 2515
9. UNE-EN 971-1, *Pinturas y Barnices*
10. J.B. Bajat, V.B. Miskovic-Stankovic, *Prog. Org. Coat.*, 49 (2004) 183
11. H. Leidheiser, *Prog. Org. Coat.*, 7 (1979) 79
12. G.W. Walter, *Corros. Sci.*, 26 (1986) 27
13. E.P.M. Van Westing, G.M. Ferrari, J.H.W. de Wit, *Corros. Sci.*, 37 (1994) 957
14. V.B.Miskovic-Stankovic, M.R. Stanic, D.M. Drazic, *Prog. Org. Coat.*, 36 (1999) 53
15. V.B. Miskovic-Stankovic, *J. Serb. Chem. Soc.,* 67 (5) (2002) 305
16. F. Deflorian, L. Fedrizzi, P.L. Bonora*, Corrosion,* 50 (1994) 113
17. L. Fedrizzi, F. Deflorian, P.L. Bonora, *Electrochim. Acta,* 42 (1997) 969
18. E.P.M. van Westing, G.M. Ferrari, F.M. Geenen, J.H.W. de Wit, *Prog. Org. Coat.,* 23 (1993) 89
19. F.M. Geenen, E.P.M. van Westing, J.H.W. de Wit, *Prog. Org. Coat.,* 18 (19990) 295
20. M. Kendig, J. Scully, *Corros. Sci.*, 39 (1997) 25
21. F. Deflorian, L. Fedrizzi, S. Rossi, P.L. Bonora, *Electrochim. Acta*, 44 (1999) 25
22. U. Rammelt, G.Reinhard, *Prog. Org. Coat.*, 21 (1992) 205
23. T. Monetta, F. Bellucci, L. Nicodemo, L. Nicolais, *Prog. Org. Coat.*, 21 (1993) 353
24. P.L. Bonora, F. Deflorian, L. Fedrizzi, *Electrochim. Acta*, 41 (1996) 1073
25. M.T. Rodríguez, *"Formulación y evaluación de imprimaciones epoxis anticorrosivas, curables a temperatura ambiente"*, tesis doctoral, Universitat Jaume I, Castelló (2004)
26. W.K. Asbeck, M. van Loo, *Ind. Eng. Chem.*, 41 (1949) 1470
27. G.P. Bierwagen, *J. Paint Tech.*, 44 (1972) 45
28. G.P. Bierwagen, *J. Coat. Tech.*, 64 (1992) 71
29. J.E.O. Mayne, *JOCCA*, 32 (352) (1949) 481
30. W. Kaiser, S. Pietsch, A. Rudolf, *Farbe Lack*, 98 (1992) 182
31. W. Funke, H. Leidheiser, R. Dickie, H. Dinger, W. Fisher, H. Haagen, K. Herrmann, H. Moslé, W. Oechsner, J. Ruf, J. Scantlebury, M. Svoboda, J. Sykes, *J. Coat. Technol.*, 58 (1986) 79
32. N.L. Thomas, *Prog. Org. Coat.*, 19 (1991)101
33. H. Yamabe, A. Tsutsumi, *Farbe Lack*, 99-n1 (1993) 16
34. W. Funke, *ACS Symp. Ser. Polym. Mater. Corros. Control*, 322 (1986) 222
35. W. Fürbeth, G. Grandmeier, M. Stratmann, *Farbe Lack*, 102 (1) (1996) 78
36. H. Leidheiser, W. Funke, *J. Oil Col. Chem. Assoc.*, 70 (5) (1987) 121
37. J.E.O. Mayne, D.J. Mill, *Surf. Coat. Int.*, 77 (4) (1994) 154
38. G.P. Bierwagen, *Prog. Org. Coat.*, 28 (1996) 43
39. W. Funke, *JOCCA*, 68 (9) (1985) 229
40. A.C. Rouw, *Prog.Org. Coat.*, 34 (1998) 181
41. J.M. Martí-Martínez, M. Madrid-Vega, *Teoría de la adhesión, Tema 2: Propiedades de los adhesivos y los selladores antes del curado*, Loctite España
42. A. Rudolf, *Farbe Lack*, 103 (1) (1997) 75
43. H. Leidheiser Jr., *Corrosion*, 38 (7) (1982) 374
44. D. Greenfield, J. D. Scantleburry, *JCSE*, 2 paper 26 (2000)
45. D. Greenfield, J. D. Scantleburry, *JCSE*, 3 paper 5 (2000)
46. B.R. Appleman, *J. Prot. Coat. Lin.*, Oct. (1987) 68
47. C.H. Hare, *J. Prot. Coat. Lin.*, Feb. (1998) 45
48. E.L. Koehler, "Underfilm corrosion currents as the cause of failure of protective organic coatings", Corrosion Control by Organic Coatings, Ed. H. Leidheiser Jr. (1981) 87
49. W. Schwenk, "Adhesion Loss for Organic Coatings, Causes and consequences for Corrosion Protection", Corrosion Control by Organic Coatings, Ed H. Leidheiser Jr. (1981) 103
50. C.H. Hare, *J. Prot. Coat. Lin.*, Mar. (1998) 17
51. T. Nguyen, J.B. Hubbard, G.B. McFadden, *J. Coat. Tech.,* 63 (794) (1991) 63
52. R.A. Dickie, *"Chemical studies of the organic coating/steel interface alter exposure to aggressive environments"*, Critical issues in reducing the corrosion of steels, (1985) 379

53. J.J. Ritter, *J. Coat. Tech.*, 54 (695) (1982) 51
54. E.L. Koehler, *Corrosion-NACE*, 33 (6) (1977) 209
55. E.L. Koehler, *Corrosion*, 40 (1) (1984) 5
56. J.E. Castle, J.F. Watts, "Cathodic Disbondment of Well Characterised Steel/Coating Interfaces". Corrosion Control by Organic Coatings. Ed H. Leidheiser Jr. (1981) 78
57. J.J.Ritter, *J. Coat. Tech.*, 54 (695) (1982) 51
58. J.E.O. Mayne, D.J. Mills, *JOCCA*, 58 (1975) 155
59. J.I. Skar, U. Steinsmo, *Corrosion Science*, 35 (5-8) (1993) 1385
60. H. Leidheiser Jr., W. Wang,L. Igtoft, *Prog. Org. Coat.*, 11 (1983) 19
61. S.B. Levinson, "Application of Paints and Coatings", *Federation Series on Coatings Technology, Federation of Societies for Coatings Technology*, 1998
62. A.M. Cabral, E. Almeida, C.C. Marzues, *Corros. Prot. Mater.*, 8 (1) (1989) 12
63. H. Gehmecker, *Corros. Prev., SAC, SP-1265*, 45 (1997)
64. E. Almeida, *J. Coat. Tech.*, 72 (911) (2000) 73
65. F. Beck, *Chem. Ing. Techn.*, 40 (1968) 575
66. F. Beck, *Prog. Org. Coat.*, 4 (1976) 1
67. F. Beck, in J.O.M. Bockris, B.E. Conwey, E. Yeager, R.E. White (Eds.), *Comprehensive Treatise of Electrochemistry*, vol.2, Plenum, New York, 1981, p.537
68. *Technical Reference Manual on Techniques for reducing or eliminating releases of toxic chemicals in metal painting,* U.S. Enviromental Protection Agency Center for Environmental Research Information, 1995
69. D.R. Bauer, *J. Coat. Tech.*, 66 (1994) 57
70. K.M. Wernstahl, B. Carlsson, *J. Coat. Tech.,* 69 (865) (1997) 69
71. E. Almeida, I. Alves, C. Brites, L. Fedrizzi, *Prog. Org. Coat.,* 46 (2003) 8
72. J.J. Suay, M.T. Rodríguez, R. Izquierdo, A.H. Kudama, J.J. Saura, *J. Coat. Tech.,* 75 (945) (2003) 103
73. N. Vatistas, *Prog. Org. Coat.,* 33 (1998) 14
74. G.E.F. Brewer, R.F. Hines, *J. Paint Tech.,* 43 (1971) 71
75. W.B. Brown, *J. Paint Tech.,* 47 (1975) 43
76. L. Fedrizzi, F.J. Rodríguez, S. Rossi, F. Deflorian, *Prog. Org. Coat.*, 46 (2003) 62
77. J. Leir, *Application of Paints and Coatings*, FSCT, Pittsburgh, 1991, p.35
78. N.M. Acamovic, D.M. Drazic, V.B. Miskovic-Stankovic, *Prog. Org. Coat.*, 25 (1995) 293
79. N.U. Schenck, Y. Stoelting, *JOCCA*, 63 (1980) 482
80. P.E. Pierce, *J. Coat. Tech.,* 53 (1981) 52
81. M. Kubo, R. Tagaki, H. Ushieda, *Denki Kagaku*, 32 (1974) 650
82. D.M. Drazic, N.M. Acamovic, O.D. Stojanovic, *J. Coat. Technol.*, 61 (1989) 27
83. C.K. Schoff, *J. Coat. Technol.*, 62 (1990) 115
84. V.B. Miskovic-Stankovic, D.M. Drazic, M.J.Teodorovic, *Corros. Sci.,* 37 (1995) 241
85. Z.W. Wicks, Jr., F.N. Jones, S.P. Pappas, *J. Coat. Tech.: Educational Series*, 71 nº895 (1999) 67
86. E.F. III Meyer, *Polym. Mater. Sci. Eng.*, 67 (1992) 220
87. Z. Huang, L.E. Scriven, H.T. Davis, *Proc. International Waterborne, High-Solids & Powder Coatings*, *Symp.*, New Orleans, L.A. 1997, 328
88. The Coatings Guide™, U.S. EPA Guide to Application of Clean Technologies for Replacement Coating Materials, *RTI International in cooperation with the U.S. EPA Office of Research and Development, The National Risk Management Research Laboratory's Air Pollution Prevention and Control Division*,1992
89. C. Rodríguez-Santamarta, *Química e Industria*, Julio-Agosto (2001) 436
90. R.A. Dickie, D.R. Bauer, S.M. Ward, D.A. Wagner, *Prog. Org. Coat.,* 31 (1997) 209
91. Sang Sun Lee et al, *Prog. Org. Coat.,* 36 (1999) 79
92. E. Bodner, *Eur. Coat. Tech.,* 44 (1997)
93. A. Schütz, W.-D. Kaiser, *Macromol. Symp.* 187 (2002) 781
94. T.A. Misev, R. van der Linde, *Prog. Org. Coat.*, 34 (1998) 160
95. B. Wojcik, F. Teymour, H. Arastoopour, S. Mostovoy, *Polym. Eng. Sci.*, 42 nº6 (2002) 1286
96. F.M. Witte, C.D. Goemans, R. van der Linde, D.A. Stanssens, *Prog. Org. Coat.*, 32 (1997) 241
97. M. Gedan-Smolka, D. Lehmann, S.Çetin, *Prog. Org. Coat.*, 33 (1998) 177
98. E. Weidner, M. Petermann, K. Blatter, V. Rekowski, *Chem. Eng. Technol.*, 24 nº5 (2001) 529
99. E.G. Belder, H.J.J. Rutten, D.Y. Perera, *Prog. Org. Coat.,* 42 (2001) 142
100. J. Hess, Powder everywhere, *Coatings World*, (36) 1999
101. T.A. Misec (Ed.), *Powder Coatings Chemistry and technology*, Wiley, New York, 1991
102. R. van der Linde, B.J.R. Scholtens, E.G. Belder, *Proceedings of the 11th International Conference on Organic Coatings in Science and Technology*, pp. 147, Athens, Greece, 1985
103. F.M. Witte, C.D. Goemans, R. van der Linde, D.A. Stanssens, *Prog. Org. Coat.,* 32 (1997) 241
104. M. Osterhold, F. Niggemann, *Prog. Org. Coat.,* 33 (1998) 55

105. M. Johansson, H. Falken, A. Irestedt, A. Hult, *J. Coat. Tech.,* 70 (884) (1998) 57
106. S.S. Lee, H.Z.Y. Han, J.G. Hilborn, J.-A.E. Manson, *Prog. Org. Coat.,* 36 (1999) 79
107. R. van der Linde, E.G. Belder, D.Y. Perera, *Prog. Org. Coat.,* 40 (2000) 215
108. D. Maetens, L. Moens, L. Boogaerts, K. Buysens, *Eur. Coat. J.,* 5 (1999) 26
109. Powder coating – A Pollution Prevention Alternative from The Powder Coating Institute, *The Powder Coating Institute, U.S.A.* 1999.
110. J. Boxall, J.A. von Fraunhofer, *Paint Formulation – Principles and Practice*, George Godwin Limited 1980
111. R. Woodbridge, *Principles of Paint Formulation*, Blackie & Son Limited, New York, 1991
112. T. Endo, F. Sanda, *Macromol. Symp.,* 107 (1996) 237
113. C. Mas, A. Serra, A. Mantecón, J.M. Salla, X. Ramis, *Macromol. Chem. Phys.,* 202 (2001) 2554
114. Z.W. Wicks, Jr., F.N. Jones, S.P. Pappas, *J. Coat. Tech.: Educational Series*, 71 nº893 (1999) 47
115. B.E. Maxwell, R.C. Wilson, H.A. Taylor, D.E. Williams, *26th International Conference in Organic Coatings*, Athens, 2000
116. B.E. Maxwell, R.C. Wilson, H.A. Taylor, D.E. Williams, J. Tria, *Prog. Org. Coat.*, 43 (2001) 158
117. PCI Technical Brief No. 1, *The Powder Coating Institute, U.S.A.*
118. Z.W. Wicks, Jr., F.N. Jones, S.P. Pappas, *J. Coat. Tech.: Educational Series*, 71 nº892 (1999) 41
119. E. Bodnar, *EuroCoat.*, 1 (1991) 206
120. B. Ellis, *Chemistry and Technology of Epoxy Resins*, Blackie Academic & Professional, New York, 1993
121. S.Wu, M.D. Soucek, *J. Coat. Tech.*, 69 (1997) 43
122. S.Wu, M.D. Soucek, *Polymer*, 39 (1998) 23
123. M.D. Soucek, O.L. Abu-Shanab, C.D. Anderson, S. Wu, *Macromol. Chem. Phys.,* 199 (1998) 1035
124. C.A. May, *Epoxy Resins: Chemistry and Technology,* Marcel Dekker, New York, 1988, 2nd Edition
125. R.S. Bauer, L.S. Corley, *Epoxy Resins: Composites Technology*. Ed. Stuart M. Lee, Technomid Publishing Company. Inc. Pennsylvania, 1989
126. C. Mas, "*Modificació Química de Reïnes Epoxi amb Lactones"*, tesis doctoral, Departament de Química Analítica i Química Orgànica, Universitat Rovira i Virgili, Tarragona (2004)
127. J.H. Jilek, *Powder Coatings, Federation Series on Coating Technology*, FSCT, October, 1991
128. L. Matjeka, S. Podzimek, K. Dusek, *J. Polym. Sci. Part A.: Polym. Chem.*, 33 (1995) 473
129. L. Shechter, J. Wynstra, R.P. Kurkjy, *Ind. Eng. Chem.*, 48(1) (1956) 94
130. J.J. King, J.P. Bell, *Reactions in a Typical Epoxy-Aliphatic Diamine System*, in *Epoxy Resin Chemistry*. R.S. Bauer, ed. American Chemical Society 1979
131. E.F. Oleinik, *Advances in Polym. Sci.*, 80 (1986) 49
132. E. Girard-Reydet, C.C. Riccardi, M. Sautereau, J.P. Pascault, *Macromolecules*, 18 (1995) 7599
133. R.K. Sadhir, M.R. Luck, Ed., *Expanding Monomers. Synthesis, Characterization and Applications,* CRC Press, Boca Raton, 1992
134. W.J. Bailey, H. Iwama, R.Tsushima, *J. Polym. Sci.: Polym. Symp.*, 56 (1976) 117
135. W.J. Bailey, T. Endo, *J. Polym. Sci.: Polym. Symp.*, 64 (1978) 17
136. H. Nishida, F. Sanda, T. Endo, T. Nakarahara, T. Ogata, K. Kusumoto, *Polym. Sci.: Part A: Polym. Chem.,* 37 (1999) 4502
137. K. Chung, T. Takata, T. Endo, *Macromolecules*, 28 (1995) 3048
138. A.M. Sikes, R.F. Brady, *J. Polym. Sci.: Part A: Poly. Chem.*, 28 (1990) 2533
139. L. Matejka, P. Chabanne, L. Tighzert, J.P. Pascault, *J. Polym. Sci.: Polym. Chem.*, 32 (1994) 1447
140. I. Ideisan, A. Abdoun, A. Ali, *Eur. Polym J.,* 28 (1992) 73
141. S. Kobayashi, M. Sugiura, H. Kitagawa, W. W.-L.Lam, *Chem. Rev.*, 102 (2002) 2227
142. M. Tokizawa, H. Okada, N. Wakabayaski, *J. Appl. Polym. Sci.,* 50 (1993) 875
143. K. Morio, H. Murase, H. Tsuchiya*, J. Appl. Polym. Sci.,* 32 (1986) 5727
144. R.N. Haszeldine, J.M. Kidd, *J. Chem. Soc.*, (1954) 4228
145. K.F. Thom, *U.S. Patent 3615169 1971*; *Chem. Abstr.,* 76 (1972) 5436a
146. J.H. Forsberg, V.T. Spaziano, T.M. Balasubramanian, G.K. Liu, S.A. Kinsley, C.A. Duckworth, J.J. Poteruca, P.S. Brown, J.L. Miller, *J. Org. Chem*., 52 (1987) 1017
147. S. Collins, Y. Hong, *Tetrahedron Lett*., 28 (1987) 4391
148. M.-C. Almasio, F. Arnaud-Neu, M.-J. Schwing-Weill, *Helv. Chim. Acta*., 66 (1983) 1296
149. J.M. Harrowfield, D.L. Kepert, J.M. Patrick, A.H. White, *Aust. J. Chem., 36 (*1983) 483
150. S. Kobayaski, *Lanthanides: Chemistry and Use in Organic Synthesis*, Springer, Berlin, 1999
151. V.K. Aggarwal, G.P. Vennall, *Tetrahedron Lett.*, 37 (1996) 3745
152. S. Kobayashi, *Synlett,* (1994) 689
153. R.W. Marshman, *Aldrichimica Acta,* 28 (1995) 77
154. S. Kobayashi, *S. Chem. Lett., (*1991) 2187
155. N. Yanagihara, S. Nakamura, M. Nakayama, *Polyhedron*, 17 (1998) 3625
156. G.A. Molander, *Chem. Rev*., 92 (1992) 29

157. J.E. Roberts, *J. Am. Chem. Soc.*, 83 (1961) 83
158. G.A. Olah, O. Farooq, C.X. Li, A.M. Farnia, J.J. Aklonis, *J. Appl. Polym. Sci.*, 45 (1992) 1355
159. H.C. Aspinall, N. Greeves, E.G.McIver, *J. Alloys and Compounds*, 275 (1998) 773
160. K. Satoh, M. Kamigaito, M. Sawamoto, *Macromolecules*, 33 (2000) 4660
161. K. Satoh, M. Kamigaito, M. Sawamoto, *Macromolecules*, 33 (2000) 5836
162. K. Satoh, M. Kamigaito, M. Sawamoto, *J. Polym. Sci: Part A: Polym. Chem.*, 38 (2000) 2728
163. S. Cauvin, F. Ganachaud, V. Tiuchard, P. Hémery, F. Leising, *Macromolecules*, 37 (2004) 3214
164. R. Faust, T.D. Shaffer, Eds. *Cationic Polymerization*, ACS Symposium Series 665, Chap. 10, págs. 106
165. A. Takasu, Y. I, Y. Oishi, Y. Narukawa, T. Hirabayashi, *Macromolecules,* 38 (2005) 1048
166. M. Chini, P. Crotti, L. Favero, F. Macchia, M. Pineschi, *Tetrahedron Lett.,* 35 (1994) 433
167. M. Meguro, N. Asao, Y. Yamamoto, *Chem. Soc. Perkin Trans.*, I (1994) 2597
168. S. Lou, B. Zhang, P.G. Wang, J. Cheng, *Synth. Commun.*, 33 (2003) 2989
169. H. Kotsuki, M. Teraguchi, N. Shimomoto, M. Ochi, *Tetrahedron Lett.*, 37 (1996) 3727
170. N. Iranpoor, M. Shekarriz, F. Shiriny, *Synth. Commun.,* 28 (1998) 347
171. P. Castell, M. Galià, A. Serra, J.M. Salla, X. Ramis, *Polymer*, 41 (2000) 8465
172. K. Satoh, M. Kamigaito, M. Sawamoto, *Macromolecules*, 32 (1999) 3827
173. S. Kobayaski, I. Hachiya, *J. Org. Chem.*, 59 (1994) 3590
174. S. Kobayaski, *Synlett*, (1994) 689
175. T. Imamoto, *Lanthanides in Organic Synthesis*, Academic Press, London, 1994
176. H.C. Aspinall, J.L. Dwyer, N. Greeves, E.G. McIver, J.C. Woolley, *Organometallics*, 17 (1998) 1884
177. S. Kobayaski, T. Wakabayashi, S. Nagayama, H. Oyamada, *Tetrahedron Lett.*, 38 (1997) 26
178. S. Kobayaski, Eur. *J. Org. Chem.*, (1999) 15
179. P. Kubisa, S. Penczek, *Prog. Polym. Sci.*, 24 (1999) 1409
180. S. Penczek, *J.Polym. Sci: Part A: Polym. Chem.*, 38 (2000) 1919
181. M. Ghaemy, *Eur. Polym. J.,* 34 (1998) 1151
182. W.J. Bailey, *J. Macromol. Sci- Chem,* A9 (5) (1975) 849
183. F. Fukuda, M. Hiriota, T. Endo, M. Okawa, W. Bailey, *J. Polym. Sci.: Polym. Chem.*, Ed. 20 (1982) 2935
184. W.J. Bailey, *J. Elastoplast.,* 5 (1973) 142
185. W. Bailey, R.L.-J. Sun, H. Katsuki, T. Endo, H. Iwama, R. Tsushima, K. Saigou, M.M. Bitritto, *Ring-Opening Polymerization*, ACS Symp. Ser. 59, Saegusa. T.; Goethals, E. Eds. ACS, Washington, 1977
186. F. Sanda, M. Hitomi, T. Endo, *J. Polym. Sci.: Part A: Polym. Chem.*, 39 (2001) 3159
187. T. Endo, F. Sanda, *Angew. Macromol. Chem.*, 240 (1996) 171
188. K. Saigo, W.J. Bailey, T. Endo, M. Okawara, *J. Polym. Sci.: Polym. Chem.*, 39 (2001) 3159
189. K. Chung, T. Takata, T. Endo, *Macromolecules,* 28 (1995) 1711
190. N. Kitamura, T. Takata, T. Endo, T. Nishikubo, *J. Polym. Sci.: Part A: Polym. Chem.*, 29 (1991) 1151
191. K. Bodendenner, *Ann.*, 625 (1959) 183
192. L. Matejka, K. Dusek, P. Chabanne, J.P. Pascault, *J. Polym. Sci.: Part A: Polym. Chem.*, 35 (1997) 665
193. M. Igarashi, T. Takata, T. Endo, *Macromolecules*, 27 (1994) 2628
194. H. Nishida, F. Sanda, T. Endo, T. Nakahara, T. Ogata, K. Kusumoto, *J. Polym. Sci.: Part A: Polym. Chem.*, 38 (2000) 68
195. C. Mas, X. Ramis, J.M. Salla, A. Mantecón, A. Serra, *J. Polym. Sci.: Part A: Polym. Chem.*, 41 (2003) 2794
196. X. Ramis, J.M. Salla, C. Mas, A. Mantecón, A. Serra, *J. Appl. Polym. Sci.*, 92 (2004) 381
197. C. Mas, A. Mantecón, A. Serra, X. Ramis, J.M. Salla, *J. Polym. Sci.: Part A: Polym. Chem.*, 42 (2004) 3782
198. C. Mas, A. Mantecón, A. Serra, X. Ramis, J.M. Salla, *J. Polym. Sci.: Part A: Polym. Chem.*, 43 (2005) 2337
199. Z.W. Wicks Jr., F.N. Jones, S.P. Pappas, *J. Coat. Tech.: Educational Series*, 71 nº894 (1999) 43
200. H. Bauch, *Polym. Mater. Sci. Eng.*, 67 (1992) 34

III. MATERIALES

Los materiales empleados en esta tesis dependieron del tipo de estudio realizado, así están los materiales empleados en el estudio de optimización del proceso de cataforesis, y los empleados en el desarrollo de pinturas en polvo de baja temperatura de curado.

3.1. ESTUDIO PINTURAS CATAFORÉTICAS

La empresa *Industrias PPG Ibérica* proporcionó las muestras a ensayar en este estudio. Estas muestras consistieron en recubrimientos epoxídicos (tipo Generación 6ª sin plomo) catiónicamente depositados sobre planchas de acero tipo ACT AR 10160 de dimensiones 210 x 110 x 1 mm. Previo a la deposición catódica de las pinturas sobre los substratos, las planchas de acero fueron tratadas mediante limpieza mecánica (pulido), desengrasadas con metil-etil-cetona y finalmente rociadas con agua destilada.

La composición de las pinturas en el baño de deposición fue de 47% de agua, 45.3% de ligante (aducto de resina catiónica poliepoxídica (basada en bisfenol A) con poliamina, curado con un entrecruzador en base poliuretano), y 7.7% de pigmentos y cargas. En la deposición catódica, el ánodo (carbono) se situó paralelo al cátodo (plancha de acero a pintar) a una distancia de 1.5cm, y en un ratio de área ánodo/cátodo de 1:4. Durante la deposición, la temperatura del baño se mantuvo a 30ºC.

En este trabajo dos fueron las variables estudiadas: el voltaje de aplicación y la temperatura de curado. En la tabla 3.1.1 se muestran los detalles de las condiciones de aplicación y de curado aplicadas a las diferentes muestras.

Tabla 3.1.1. Muestras proporcionadas por Industrias PPG Ibérica

Muestra	Voltaje de aplicación (V)	Tiempo de aplicación de voltaje (s)	Temperatura de curado (ºC)	Tiempo de curado (min)	Espesor (µm)
220V	220	120	180	10	20
245V	245	90			
270V	270	75			
295V	295	61			
320V	320	50			
345V	345	31			
145ºC	200	120	145	15	
155ºC			155		
165ºC			165		
175ºC			175		
185ºC			185		
195ºC			195		

3.2. ESTUDIO PINTURAS EN POLVO

Los materiales que se emplearon en el desarrollo de este estudio se escogieron en función de experiencia de fabricantes, seleccionando como material de referencia una pintura comercial. Tal y como se ha comentado en la introducción, el sistema ligante de las pinturas en polvo epoxi está compuesto por resina epoxi, un agente de curado y aditivos con diferentes funciones. Todas las materias primas empleadas en esta tesis se describen a continuación.

3.2.1. Resina Epoxi

Como resina epoxi en polvo, se empleó una resina de peso molecular medio basada en bisfenol-A (esquema 3.2.1) y con referencia comercial Araldite GT7004 de la empresa Huntsman. Las principales propiedades de la resina se muestran a continuación:

Índice epoxi (ISO 3001)	1.33-1.40	[eq/kg]
Equivalente epoxi (ISO 3001)	714-752	[g/Eq]

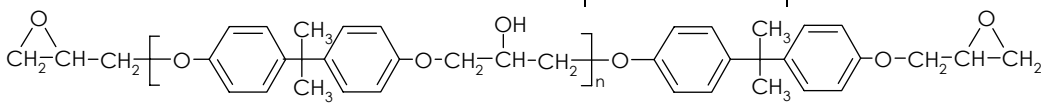

Esquema 3.2.1. Estructura de resina epoxi tipo DGEBA

3.2.2. Agentes de curado

Se emplearon dos tipos de agente de curado en polvo latentes. La o-tolilbiguanida se empleó en base a indicaciones técnicas de fabricantes para la resina epoxi escogida. Los ácidos de Lewis se emplearon en función de la literatura encontrada al respecto para sistemas líquidos así como gracias a sugerencias de especialistas en el campo.

3.2.2.1. Orto-tolilbiguanida (TBG)

La orto-tolilbiguanida (esquema 3.2.2) es un derivado de la dicianodiamida (DICY) de relativa elevada reactividad, el cual es uno de los principales endurecedores empleados en el campo de las pinturas en epoxi en polvo. En concreto se empleó el producto comercial Arador GT2844 de la empresa Huntsman con un equivalente en peso de H^+ activos de 37g/Eq.

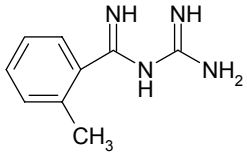

Esquema 3.2.2. Estructura de la o-tolilbiguanida, TBG

A fin de calcular la proporción adecuada de este compuesto se recurrió a datos del fabricante y fichas técnicas de los productos. Según éstos, la proporción apropiada para la resina epoxi empleada en el estudio es de 4.8phr, cantidad algo por debajo del valor estequiométrico calculado establecido en 5phr.

3.2.2.2. Ácidos de Lewis

En el desarrollo de esta tesis se emplearon dos tipos diferentes de ácidos de Lewis: trifluorometanosulfonato de erbio (III) al 98% y trifluorometanosulfonato de iterbio (III) al 98%, ambos proporcionados por Sigma-Aldrich Química S.A. A lo largo de la tesis se referenciarán como triflatos de erbio e iterbio, o $(TfO)_3Er$ y $(TfO)_3Yb$, respectivamente (esquema 3.2.3).

Ácido de Lewis	Fórmula química	Peso molecular (gr/mol)
Trifluorometanosulfonato de erbio (III)	$(CF_3SO_3)_3Er$	614.47
Trifluorometanosulfonato de iterbio (III)	$(CF_3SO_3)_3Yb{\cdot}xH_2O$	620.25

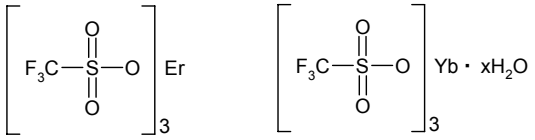

Esquema 3.2.3. Estructura de los trifluormetanosulfonatos de erbio e iterbio

3.2.3. Aditivos

Tal y como se ha dicho en la introducción, los aditivos tienen diversas funciones en la formulación de las pinturas en polvo, y su principal objetivo es el de mejorar las prestaciones del film final. Sin embargo, cabe destacar que su inclusión en los sistemas puede producir variaciones en la cinética y otras propiedades. Por ese motivo, estos aditivos sólo se añadieron en las formulaciones que se emplearon para pintar sobre substrato acero.

3.2.3.1. Benzoína

La benzoína (2-hidroxil-1,2-difeniletanona, 212,2gr/mol) es el desgasificante más empleado en pinturas en polvo en la actualidad (esquema 3.2.4). Se introdujo en la red polimérica a fin de eliminar las burbujas y aire ocluido que puede causar porosidad en el recubrimiento una vez aplicado, en una proporción recomendada según fabricantes (0.18phr).

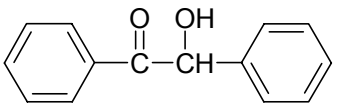

Esquema 3.2.4. Benzoína

3.2.3.2. Agente de Flujo (Powdermate 486CFL)

Los agentes de flujo se emplean para minimizar/eliminar defectos superficiales mejorando la mojabilidad del recubrimiento reblandecido a la vez que facilitan el transporte del material en polvo. En esta tesis se empleó un agente de flujo comercial de la empresa Troy, el powdermate 486CFL, empleándolo en proporciones según recomendaciones de fabricantes de pinturas en polvo (1.27phr).

3.2.3.3. Ácido de Meldrum

Tal y como se ha indicado en la introducción, uno de los problemas que pueden presentar las pinturas en polvo de base epoxi es la ligera contracción que presentan, creando al curar un material tensionado, con los problemas que aporta a su comportamiento anticorrosivo. Una posible alternativa es introducir en la red materiales que no produzcan contracción, más bien una ligera expansión. Las lactonas son ejemplos de estos materiales ya que en presencia de ácidos de Lewis reaccionan con la resina epoxi dando ligar a un producto intermedio (SOE) que al avanzar la reacción provoca una ligera expansión. El ácido de Meldrum (esquema 3.2.5) es un tipo comercial de lactona.

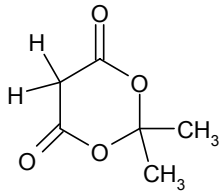

Esquema 3.2.5. Ácido de Meldrum

En esta tesis se empleó 2,2Dimetil-1,3 Dioxano-4,6 Diona, de fórmula química $C_6H_8O_4$ y peso molecular 144.13 gr/mol, proporcionado por la empresa Sigma-Aldrich Química S.A.

3.2.4. Substrato

Para los ensayos de propiedades anticorrosivas, los sistemas preparados fueron aplicados por medio de pistola electrostática sobre planchas de acero de bajo contenido en carbono (SAE 1010) previamente desengrasadas con acetona, de dimensiones 150 x 75 x 1mm.

3.2.5. Preparación de los sistemas estudiados

La formulaciones que se prepararon se pesaron y pre-mezclaron mediante agitación manual hasta que se consiguió un buen pre-mezclado. Tras esto, el material se procesó en una extrusora mono-usillo (Haake Rheomex 254) a 80ºC a lo largo de la extrusora y 60rpm. Una vez extruído, el material se molturó en un molino ultracentrífugo ZM100 y tamizó a 100micras, obteniendo así los materiales en polvo preparados para ser aplicados (figura 3.2.1).

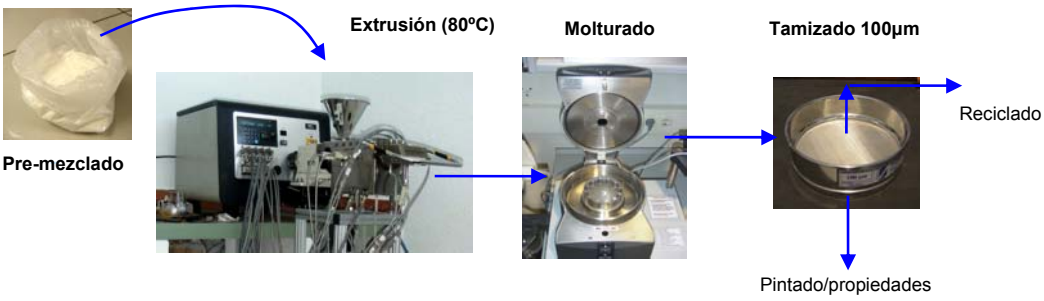

Fig. 3.2.1. Proceso de preparación de muestras.

En la tabla 3.2.1 se muestran los sistemas preparados para realizar el desarrollo de nuevas pinturas epoxi de bajo curado y que fueron aplicados sobre substratos metálicos. Muestras de la misma composición, pero sin benzoína ni agente de flujo, fueron también preparadas a fin de determinar las propiedades mecánicas y térmicas.

Tabla 3.2.1. Muestras preparadas. Proporciones en phr en base a 100gr de resina epoxi

Muestra	$(TfO)_3Er$	$(TfO)_3Yb$	TBG	Benzoína	Agente de Flujo	Ácido de Meldrum
TBG (referencia)	-	-	4.8	0.18	1.27	-
TBG/$Er(TfO)_3$ 1phr	1	-	4.8	0.18	1.27	-
TBG/$Yb(TfO)_3$ 1phr	-	1	4.8	0.18	1.27	-
$Er(TfO)_3$ 0.5phr	0.5	-	-	0.18	1.27	-
$Er(TfO)_3$ 1phr	1	-	-	0.18	1.27	-
$Er(TfO)_3$ 2phr	2	-	-	0.18	1.27	-
$Yb(TfO)_3$ 0.5phr	-	0.5	-	0.18	1.27	-
$Yb(TfO)_3$ 1phr	-	1	-	0.18	1.27	-
$Yb(TfO)_3$ 2phr	-	2	-	0.18	1.27	-
AM1	0.5	-	-	0.18	1.27	3.3
AM2	0.5	-	-	0.18	1.27	5

3.2.6. Aplicación y curado

El polvo tamizado a 100µm sigue tres tipos de preparación en función del ensayo de caracterización que se vaya a realizar:

- Directamente en polvo (muestras sin benzoína ni agente de flujo), para realizar ensayos de calorimetría diferencial y estudio cinético
- Como película libre. La muestra en polvo es depositada sobre una plancha de polipropileno con cargas y curada en estufa a 150ºC durante una hora (muestras sin benzoína ni agente de flujo), para, una vez curada, liberar la película del substrato gracias a su falta de adherencia al polipropileno y poder realizar sobre el film libre de substrato ensayos de TGA, DMTA, tracción, T_g por DSC… Las películas libres presentaron espesores de 1mm.
- Sistemas en polvo aplicados con pistola electrostática tipo corona modelo Easy 1-C, sobre substrato acero y curado en estufa a 150ºC durante 15 minutos, o 25 minutos para las muestras con TBG, para ensayos de resistencia a corrosión, impacto… Se obtuvieron recubrimientos de espesores en el rango 60±5 µm.

IV. ESTUDIO DE PROPIEDADES

4.1. PROPIEDADES TÉRMICAS

Un parte fundamental de esta tesis es el estudio de la viabilidad del uso de triflatos de lantánido como iniciadores y/o catalizadores de sistemas epoxi en polvo. Por este motivo, el estudio exhaustivo de la cinética de la reacción de curado en sistemas epoxi donde se encuentran presentes en distintas proporciones y con presencia o no de TBG o ácido de Meldrum adquiere gran importancia.

4.1.1. Cinética de curado

A fin de realizar el estudio cinético de los sistemas se empleó un Calorímetro Diferencial de Barrido (DSC, en siglas inglesas) tipo Perkin-Elmer DSC7 (figura 4.1.1).

Fig. 4.1.1. Calorímetro Diferencial de Barrido (DSC).

El DSC mide el flujo de calor de o hacia la muestra como una función de temperatura y tiempo. Una pequeña proporción del material se sitúa en una cápsula de aluminio y se calienta o enfría de forma controlada. Se emplea un material de referencia (normalmente una cápsula de aluminio vacía) que sigue simultáneamente la misma rutina de temperatura y tiempo. Las medidas calorimétricas se realizan durante el ciclo calentamiento/enfriamiento [1].

Para realizar las medidas calorimétricas se pueden emplear dos métodos diferentes. En el primero se miden las diferencias de temperatura entre la muestra estudiada y la de referencia conforme se les aplica la misma cantidad de calor (calorías). En el segundo método, se miden las diferencias de energía añadida a ó desprendida por cada una de las muestras para mantener constante e igual la temperatura de las dos. En ambos casos, el flujo de calor y temperatura de la muestra estudiada se monitorizan y comparan con el material de referencia obteniéndose gráficos como la figura 4.1.2. La cantidad de energía absorbida (endorterma) o desprendida (exoterma) conforme la muestra sufre cambios físicos o químicos (fusión, transición vítrea, cristalización, curado…) se mide como flujo de calor en función de la temperatura.

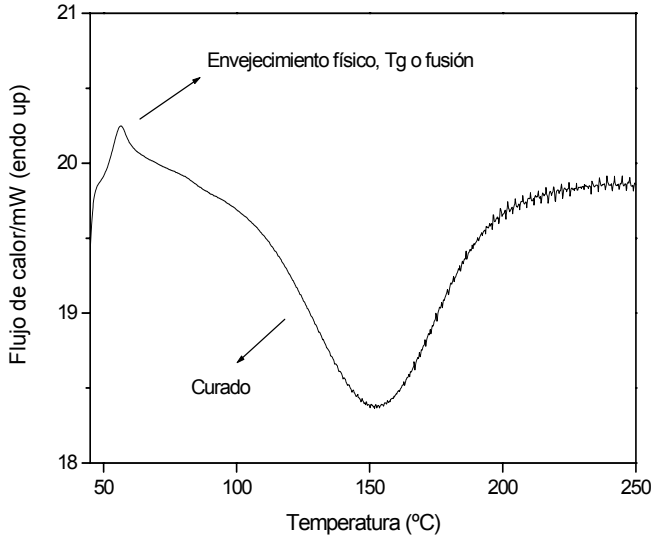

Fig. 4.1.2. Diagrama curado de muestra en DSC.

Para realizar el estudio de cinética de curado se ensayaron muestras en polvo no curadas de los distintos sistemas formulados según la tabla 3.2.1 introducidos en cápsulas de aluminio de 50µL, con un peso entre los 9 y los 10mg en presencia de atmósfera de gas argón. Se realizaron dos estudios: uno isotermo a diferentes temperaturas como se verá en el capítulo de resultados y otro no isotermo con barridos a 2.5, 5, 10 y 15 K/min entre 25 y 300ºC.

Una vez aplicados los barridos se procedió a realizar el estudio cinético mediante el método isoconversional de Coats-Redfern [2, 3] y el método del IKR [4, 5] a fin de calcular el triplete cinético (factor preexponencial A, energía de activación E, e integral del modelo cinético en función del grado de conversión g(α)) de cada sistema y así tener una idea sobre los procesos de reacción.

El software STARe de Mettler-Toledo se empleó para calcular los grados de conversión y cinéticas de los procesos sin necesidad de cálculos manuales (como el método model-free). La principal desventaja de este software es que no ofrece completa información sobre el triplete cinético del sistema (no ofrece información sobre el modelo cinético).

4.1.2. Temperatura de transición vítrea (T_g)

La influencia sobre los cambios de estructura de red (representados por variaciones de temperatura de transición vítrea, T_g) del uso de catalizadores o iniciadores en sistemas epoxi en polvo se estudió por calorimetría diferencial de barrido (DSC).

Para la determinación de T_g se empleó un equipo Perkin-Elmer DSC7. Las muestras, previamente curadas, pesaron alrededor de 10mg. Como gas de purga se empleó argón en un caudal de 20 cm^3/min. Los barridos se realizaron a 10ºC/min en el rango 25-220ºC. De las curvas calorimétricas se obtuvo la temperatura de transición vítrea (T_g) calculada a partir del valor de Cp medio extrapolado (*half Cp extrapolated*). En la figura 4.1.3 se muestra un ejemplo de cálculo de T_g.

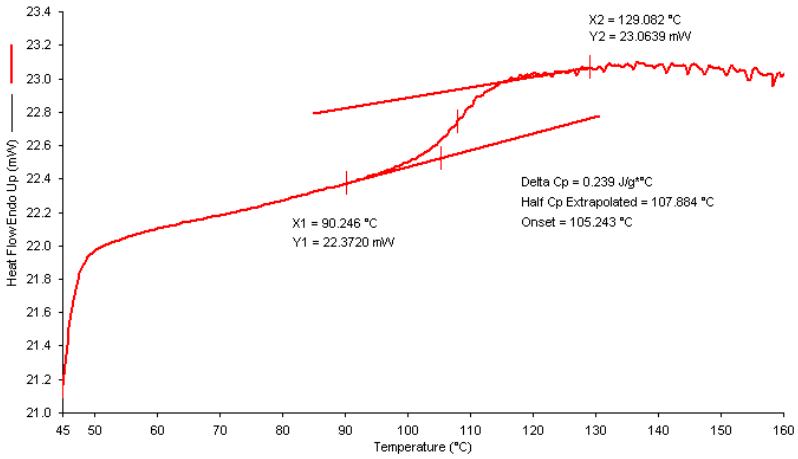

Fig. 4.1.3. Curva análisis T_g por medio de DSC.

La temperatura de transición vítrea, T_g, indica la temperatura por debajo de la cual un material exhibe propiedades propias de vidrio. A temperaturas por encima de T_g la movilidad molecular es suficiente en el material como para tener las propiedades (entalpía, volumen específico…) características del estado de equilibrio goma o líquido. El valor de T_g es orientativo y en realidad representa todo un rango de temperaturas. La temperatura de transición vítrea depende del tipo de ensayo experimental que utilicemos en su determinación, la velocidad con que se eleve la temperatura y finalmente el historial de la muestra en el estado vidrio. Se puede determinar la T_g del sistema como el cambio de pendiente de una propiedad como la entalpía o el volumen con la temperatura.

El principio físico de la T_g se basa en la posibilidad de que una macromolécula alcance grados de libertad de manera que los segmentos de las cadenas puedan desarrollar movimientos conjuntos. A temperaturas por debajo de T_g, el sistema se encuentra en una situación de no-equilibrio en el que únicamente están permitidos movimientos de tipo vibracional de los átomos. Cuando se alcanza la T_g, los movimientos adquieren tal amplitud que llegan a producirse deformaciones locales en las cadenas. A nivel macroscópico, un material presenta un comportamiento rígido y frágil por debajo de su T_g, aumentando su capacidad de deformación por encima de este valor.

4.1.3. Estabilidad térmica. Análisis termogravimétrico (TGA)

El análisis termogravimétrico se empleó para estudiar la estabilidad de las muestras y en el caso de las muestras cataforéticas para observar la influencia de los pigmentos así como de la temperatura de curado. El estudio de las curvas termogravimétricas también permite asociar los resultados de estabilidad con la red formada durante el curado.

Para los ensayos se empleó un equipo TGA 92-16.18 Setaram (figura 4.1.4). Las muestras empleadas (previamente curadas) se introdujeron en el crisol del equipo en un peso de

aproximadamente 15-20mg, realizándose barridos de 25ºC a 900ºC a una velocidad de calentamiento de 10K/min. En todos los ensayos se empleó argón como gas atmósfera en un caudal de 50 cm^3/min.

Fig. 4.1.4. Balanza de termogravimetría (TGA).

El análisis termogravimétrico mide continuamente el peso de la muestra como función de la temperatura y tiempo. La muestra se sitúa en un pequeño crisol de vidrio conectado a una microbalanza donde se calienta de forma controlada durante un tiempo específico (ensayos TGA isotermos), o bien se realiza un calentamiento a una velocidad determinada entre valores de temperatura especificados (ensayo TGA dinámico). Los cambios de peso observados a temperaturas específicas correlacionan la volatilización de componentes de la muestra, descomposición, reacciones de oxidación/reducción, y otros cambios o reacciones [1].

4.2. PROPIEDADES MECÁNICAS

4.2.1. Ensayos tensión-deformación (σ-ε)

Los ensayos tensión-deformación se realizaron a fin de obtener información sobre el comportamiento mecánico a tracción de las distintas composiciones. Este tipo de ensayos, por tanto, suele emplearse para la determinación de parámetros ingenieriles del material (módulo de elasticidad, límite elástico, tenacidad…).

Los ensayos de tensión-deformación son los más empleados entre los diversos ensayos de tipo mecánico (fluencia, microdurezas, dinámico-mecánico, impacto…). Sin embargo, los resultados obtenidos son, en ocasiones, de difícil interpretación tecnológica debido a las fluctuaciones del esfuerzo [6] originadas por defectos en el material y posible concurrencia de diferentes procesos durante la deformación (como la reestructuración de entidades cristalinas en polímeros semicristalinos, y la reorientación de los segmentos de cadena en polímeros amorfos).

Los ensayos se llevaron a cabo en una máquina de ensayos universales tipo Adamel-Lomargy DY34 (figura 4.2.1). Se prepararon 5 muestras curadas (1hora a 150ºC) en forma de alterio (de acuerdo con la Norma ASTM D 1708-96) de cada material, y se ensayaron a temperatura ambiente a una velocidad constante de 10mm/min empleando una célula de carga de 1KN. Así se obtuvieron los gráficos en forma de tensión (MPa) vs deformación (%).

Fig. 4.2.1. Máquina de ensayos universales tipo Adamel.

De este tipo de ensayos la principal información mecánica sobre el material es su rigidez, la resistencia a tracción y la tenacidad a fractura. En todas estas medidas influye la velocidad de desplazamiento de la cruceta.

La rigidez es la resistencia que el material ofrece cuando se le aplican fuerzas externas y evidencia el comportamiento elástico de la macromolécula en la región de bajas deformaciones. Una medida de la rigidez es el denominado módulo elástico o de Young, ecuación 4.2.1, que se define como la relación

entre el esfuerzo aplicado (σ) y la deformación resultante (ε), midiéndose en la zona de bajas deformaciones (menores al 1%).

$$E = \frac{\sigma}{\varepsilon} \qquad \text{Ec. 4.2.1.}$$

A partir de este valor (pendiente) se puede obtener los datos del límite elástico (tensión y deformación elásticas), que definen el momento en el que el material pasa a tener deformación plástica. Estos valores se obtienen trazando una paralela al módulo para una deformación del 0.02% y obteniendo el corte de esta recta con la curva de tensión.

La resistencia a tracción es el esfuerzo máximo que presenta un material antes de romper. La tenacidad representa el trabajo requerido para romper el material y se define como el área debajo de la curva tensión-deformación. La tenacidad es la energía que el material absorbe antes de romper.

Por lo general la forma que los materiales termoestables presentan en las curvas tensión-deformación es la típica de un material frágil ya que presentan poca deformación plástica antes de rotura.

4.2.2. Análisis termodinamomecánico (DMTA)

La gran ventaja de este tipo de ensayos mecánicos es poder realizar un ensayo sobre un amplio rango de temperaturas y frecuencias en un periodo de tiempo relativamente corto y, a partir de los resultados, predecir todo el comportamiento del material así como estimar otras propiedades mecánicas. El estudio de los módulos y pérdida mecánica en un amplio rango de frecuencias y temperaturas permite un conocimiento profundo de la estructura químico-física de los polímeros así como de la variación de sus propiedades (T_g, grado de entrecruzamiento, grado de cristalinidad, orientación molecular, separación de fases, cambios estructurales consecuencia del procesado, composición química…).

En los ensayos DMTA se obtienen distintos tipos de parámetros: módulo dinámico o de almacenamiento E’ (relacionado con la energía retenida por el polímero en cada periodo), módulo de pérdida E’’ (fracción de la energía disipada), y la pérdida o fricción interna $\tan\delta = E''/E'$.

El intervalo de temperaturas de estudio fue de 25ºC a 220ºC a una velocidad de calentamiento de 1ºC/min y una frecuencia de 1Hz. Las probetas ensayadas midieron 5x1x10mm (ancho x espesor x longitud). Los ensayos se realizaron en un equipo Seiko DMS210U (figura 4.2.2) con módulo de flexión en tres puntos.

Fig. 4.2.2. Equipo termodinamomecánico (DMTA).

Mediante los resultados también se obtuvieron valores de temperatura de transición mecánica (T_α), que es un valor que puede llegar a ser unos 15-20ºC mayor que el valor de T_g obtenido por medidas calorimétricas [7] aunque se basa en el mismo principio de movilidad de cadenas. Se considera la T_α como la temperatura para el máximo de tanδ (en la relajación principal α). A su vez, con los datos obtenidos por medio de este tipo de ensayos se puede adquirir una idea sobre el estado de la red formada (densidad de entrecruzamiento, heterogeneidad…).

Esta técnica se basa en la aplicación de una fuerza oscilatoria sobre la muestra y la evaluación de su respuesta, dándonos información sobre su estructura, tanto a nivel local como a nivel global. Estos ensayos se pueden hacer en condiciones isotérmicas a una temperatura prefijada, o bien en condiciones dinámicas, variando la temperatura obteniéndose información del comportamiento mecánico del material en todo el rango de temperaturas. Este último método de ensayo fue el elegido en la presente tesis.

Las fuerzas oscilatorias aplicadas en los ensayos dinamo-mecánicos (vibraciones) pueden ser de cuatro tipos [8]: vibraciones libres, vibraciones de resonancia, propagación de ondas y excitación sinusoidal y respuesta. Este último tipo de vibraciones son las empleadas habitualmente en ensayos de materiales poliméricos viscoelásticos (como el caso de estudio de esta tesis). En los ensayos de excitación sinusoidal y respuesta, las fuerzas y las deformaciones resultantes varían sinusoidalmente con el tiempo, con desfase para materiales viscoelásticos y sin desfase para materiales elásticos.

Un material viscoelástico se define como aquel que no tiene un comportamiento elástico ni viscoso ideales, esto es que el desfase entre la onda sinusoidal señal y la respuesta está entre 0º (sólido elástico ideal) y 90º (líquido viscoso ideal) ya que parte de la energía señal se disipa como calor y parte se almacena.

Los materiales termoestables estudiados presentan comportamiento viscoelástico, y por tanto, la deformación que experimenta el material no es instantánea sino que se produce a lo largo del tiempo. Así el módulo medido depende del momento en el que se realice la medida pues las cadenas o sus segmentos tienden a adoptar la configuración de equilibrio que corresponde al estado de tensión aplicada en el proceso conocido como relajación. La tensión aplicada es del tipo sinusoidal y se expresa como:

$$\sigma = \sigma_o sen(\omega t)$$ Ec. 4.2.2.

Donde t es el tiempo de aplicación de la tensión, ω la frecuencia angular de la tensión aplicada (ω=2πf) y σ_o la amplitud de la tensión.

La tensión aplicada provoca una deformación en la muestra de tipo sinusoidal pero con un ángulo de desfase entre la tensión y la deformación, δ:

$$\varepsilon = \varepsilon_o sen(\omega t + \delta)$$ Ec. 4.2.3.

Donde ε_o representa la máxima deformación sufrida por la muestra (y es igual a $E\sigma_o$ debido a la dependencia lineal entre tensión y deformación.

En la figura 4.2.3, se representa cualitativamente la tensión aplicada y la deformación obtenida, así como el desfase de la respuesta respecto la señal, debida al tiempo que necesita el material para responder con deformación a la tensión aplicada. Si el material fuera completamente elástico no existiría desfase.

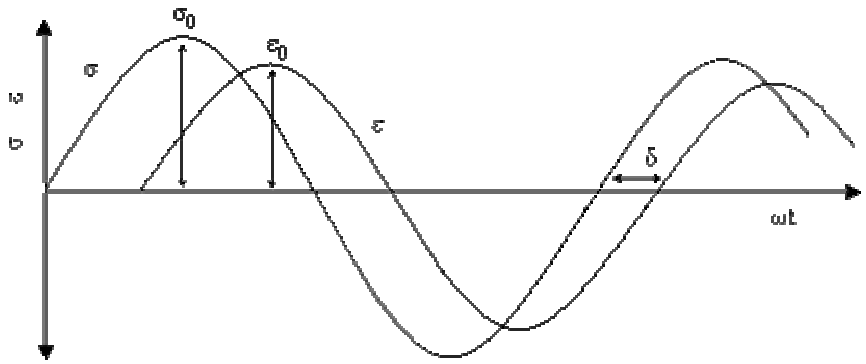

Fig. 4.2.3. Representación esquemática de la relación entre esfuerzo y deformación para una excitación sinusoidal.

La expresión 4.2.3 se puede reescribir como:

$$\varepsilon = \varepsilon_o \left[sen(\omega t)\cos\delta + \cos(\omega t) sen\delta \right]$$ Ec. 4.2.4.

A partir de esta ecuación se puede calcular el módulo elástico o de almacenamiento (E'), el módulo imaginario o de pérdida (E'') y el módulo complejo (E*), ecuaciones 4.2.5, 4.2.6 y 4.2.7 respectivamente.

$$E' = \varepsilon_o sen(\delta)$$ Ec. 4.2.5.

$$E'' = \varepsilon_o \cos(\delta)$$ Ec. 4.2.6.

$$E^* = E' + iE''$$ Ec. 4.2.7.

El módulo de almacenamiento (E') representa la parte de la energía que el material absorbe en cada ciclo de deformación y después devuelve al sistema como energía de recuperación, asociándose a la parte del material que se comporta de forma elástica (cuando la respuesta entra en fase con la señal). El módulo de pérdida representa la parte de la energía que no se recupera y que se disipa en forma de calor, asociándose a la parte viscosa del material (cuando la respuesta presenta un desfase δ respecto la señal). El módulo de pérdida es nulo para los materiales puramente elásticos, y el módulo de almacenamiento es nulo para los materiales puramente viscosos.

La relación entre el módulo de almacenamiento (energía potencial máxima almacenada) y el de pérdida (energía disipada) se conoce como tangente de pérdida (ecuación 4.2.8) y refleja la relación entre la energía disipada y la que se almacena en cada ciclo de deformación.

$$\tan\delta = \frac{E''}{E'} \qquad \text{Ec. 4.2.8.}$$

En materiales poliméricos se suelen emplear los parámetros E' y tanδ para definir el comportamiento dinámico-mecánico del material.

El factor de pérdida tanδ es sensible a movimientos moleculares y transiciones, y variando la temperatura en los ensayos DMTA, este factor nos puede mostrar las transiciones activadas térmicamente que tienen lugar en el material. Estas transiciones se nominan α, β, γ… en orden decreciente de temperatura y están asociadas a diferentes tipos de movimiento de cadena principal o grupos laterales. A la relajación principal (relajación α) se la asocia con movimientos cooperativos de segmentos de cadena principal, y así, se la relaciona con la temperatura de transición vítrea.

Cuando la medida se realiza a una temperatura inferior a la que tiene lugar la transición, la tangente de pérdidas presenta valores bajos debido a que la frecuencia fijada es mucho mayor que la velocidad a la cual el material tiende hacia el equilibrio, es decir, su tiempo de relajación es mucho mayor. La estructura se comporta de forma rígida y elástica y presenta valores altos para E'. Si por el contrario la medida se efectúa a temperaturas superiores a las de la transición, el sistema alcanza el estado de equilibrio de manera mucho más rápida que la que impone la frecuencia del experimento, es decir, el tiempo de relajación es mucho más pequeño, por lo que tanδ y E' presentan valores bajos. En la zona de la transición, a medida que aumenta la temperatura se activa el movimiento molecular de la cadena o de los segmentos involucrados en la transición, implicando un aumento del rozamiento y de la energía disipada, lo que se traduce en un aumento de E''. Esta situación se mantiene hasta que la frecuencia impuesta coincide con la tendencia del sistema a alcanzar la conformación de equilibrio, punto en el que E'' presenta un máximo, correspondiente al máximo de energía que el sistema puede disipar debido al rozamiento. Superado este máximo, la estructura, que ahora tiene más movilidad, tiende al equilibrio más fácilmente y de forma más rápida que la que impone la frecuencia de deformación, disipando así menos energía y presentando valores cada vez más bajos de E'' (y por tanto de tanδ).

A partir de los ensayos dinamo-mecánicos también se puede calcular el peso molecular medio entre nudos ($\overline{M_c}$) y hacerse así una idea del empaquetamiento de la red, densidad de entrecruzamiento y volumen libre del sistema. Para realizar este cálculo se puede emplear la teoría de elasticidad del caucho [9] suponiendo a su vez que el sistema epoxi se comporta como un caucho ideal. La ecuación 4.2.9 fue la empleada para este cálculo:

$$\overline{M}_c = \frac{3\nu\rho RT}{E'} \qquad \text{Ec. 4.2.9.}$$

Donde, E' es el módulo de almacenamiento en la zona caucho (E' relajado, obtenido para T_g+50ºC, ν es el denominado "front factor", cuyo valor es la unidad para cauchos ideales y es el empleado en este estudio, R es la constante de los gases ideales, T es T_g+50ºC (valor de medida de E') y ρ es la densidad aparente de la muestra curada. Esta teoría es estrictamente válida para materiales de baja densidad de entrecruzamiento, por tanto sólo se puede usar de forma cualitativa para materiales termoestables [10].

La densidad aparente de la muestra se midió mediante un aparato de medida de densidades acoplado a balanza y empleando la ecuación 4.2.10.

$$\rho_{ap} = \frac{m_{aire}}{m_{aire} - m_{liq}}(\rho_0 - \rho_L) + \rho_L \qquad \text{Ec. 4.2.10.}$$

Donde, ρ_0 es la densidad del líquido, ρ_L es la densidad del aire (0.0012g/cm^3), m_{aire} es el peso de la muestra en aire y m_{liq} es el peso de la muestra sumergida en el líquido.

4.2.3. Ensayos de adherencia

A fin de obtener una idea de la influencia de los triflatos de lantánido, TBG y ácido de Meldrum en la adherencia de un sistema epoxi en polvo a substratos metálicos tipo acero, se realizaron ensayos de adherencia por tracción en máquina de ensayos universales Instron 4469-H1907 (figura 4.2.4). Los ensayos están basados en la norma para adhesivos ISO 4587 (1979).

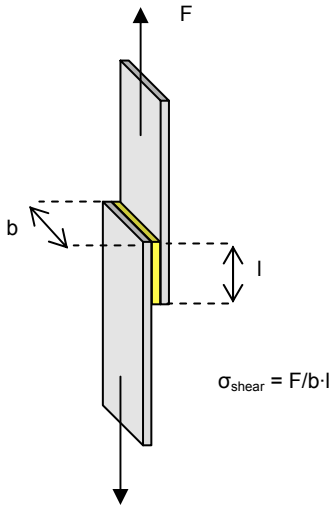

Fig. 4.2.4. y 4.2.5. Máquina de ensayos universales tipo Instron y esquema probeta de ensayo.

La idea general del ensayo consiste en unir dos planchas de acero al carbono (similares a las empleadas en el resto de ensayos) de medidas determinadas mediante una cantidad pre-establecida de material (recubrimiento en polvo). Las planchas se unen mediante los sistemas formulados y se curan durante 1 hora a 150ºC, que junto a 3 días a temperatura ambiente permitirá asegurar el curado total de los sistemas. Una vez transcurrido este periodo, las probetas (5 por cada pintura) se someten a ensayos de tracción a una velocidad de 1mm/min empleando una célula de carga de 50kN.

A partir del ensayo se emplea el valor de la fuerza aplicada hasta rotura (pérdida de adherencia) y del área de unión (13x25mm) para calcular así la tensión de cizalla, σ_{shear}, en MPa, como el cociente entre ambos parámteros (figura 4.2.5.).

4.2.4. Ensayos de impacto (caída de dardo)

La resistencia a impacto puede calcularse mediante el método de ensayo de caída de masa, siguiendo la Norma ISO 6272:1993.

De este tipo de ensayos se obtiene información de la resistencia que ejercerá el recubrimiento a un impacto de una masa dada a una determinada altura, detectándose así, de forma al menos cualitativa, la resistencia a impacto del material, su cohesión y su adherencia.

Los ensayos de caída de masa se realizaron con un impactómetro de caída de dardo (figura 4.2.6).

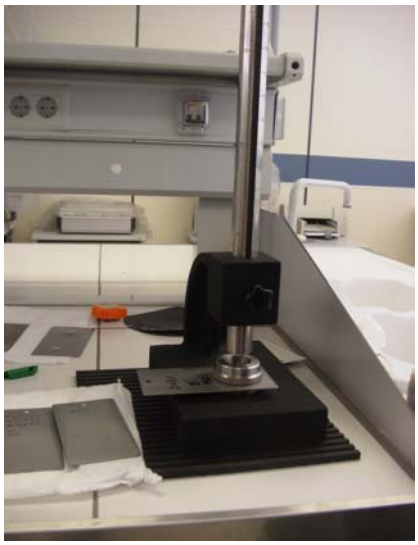

Fig. 4.2.6. Aparato de caída de dardo.

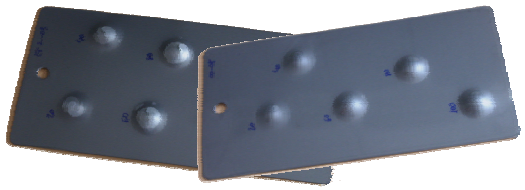

Fig. 4.2.7. Planchas impactadas por caída de dardo.

Los ensayos se efectuaron impactando las muestras por la zona no pintada mediante un cabezal semiesférico de 12.5mm de diámetro y 1kg de peso, a diferentes alturas (20, 40, 60, 80 y 100cm). Los resultados de esta técnica se obtienen por observación directa del recubrimiento ensayado (figura 4.2.7). El mayor inconveniente que presenta es la difícil interpretación de los resultados, en algunos casos, muy subjetiva.

4.3. PROPIEDADES ANTICORROSIVAS

4.3.1. Ensayos de niebla salina (Salt Fog Spray)

Los ensayos acelerados tipo niebla salina suponen el método de evaluación de propiedades anticorrosivas más extendido a nivel industrial. Sin embargo, este método requiere de largo tiempos de ejecución (superiores a un mes) para indicar el buen comportamiento de algunas pinturas, su interpretación es en parte subjetiva y no ofrece resultados sobre los procesos de corrosión que tienen lugar en el sistema metal/recubrimiento.

El ensayo consiste en crear un ambiente marino (altamente corrosivo) por generación de niebla salina en una cámara cerrada con temperatura y humedad controlada, e introducir en su interior las muestras a ensayar. Posteriormente se irán recogiendo muestras conforme pasen las horas de exposición. En la presente tesis se siguió la norma ASTM B117-85 y se empleó un equipo ACS-DCTC600P (figura 4.3.1).

Fig. 4.3.1. Cámara de Niebla Salina.

Fig. 4.3.2. Cruz de San Andrés practicada a plancha pintada para ensayo en Niebla Salina y plancha tras ensayo.

De cada uno de los sistemas formulados preparadas se prepararon 5 planchas. Previamente a la introducción de las planchas en la cámara de niebla salina se les practicó una Cruz de San Andrés a fin de dejar al descubierto el substrato metálico (figura 4.3.2). Las condiciones que se establecieron en la cámara de ensayo fueron de una humedad al 100% de disolución 5%NaCl en agua desionizada y unas temperaturas de 35ºC del agua y 37ºC de la cámara. Las muestras se recogieron tras 46, 94, 166, 214 y 293 horas. Tras cada recogida las muestras se secaron y 24horas después se evaluó el ampollamiento, la delaminación (tras aplicar una cinta adhesiva normalizada en un brazo de la cruz, estirar y ver el área delaminada) y la corrosión.

4.3.2. Espectroscopia de Impedancia Electroquímica (EIS)

En el caso de corriente continua (dc), los circuitos eléctricos presentan oposición al flujo de electrones por la existencia de resistencias (cumpliéndose la Ley de Ohm). En el caso de la corriente

alterna (ac) aparecen dos nuevos componentes que dificultan el paso de la corriente a través del circuito, éstos son las capacitancias y las inductancias [11, 12].

La impedancia es en la corriente alterna lo que la resistencia es en la corriente continua. Es la oposición del sistema al flujo de corriente o electrones y comprende elementos como resistencias, capacitancias e inductancias.

A fin de determinar la impedancia (en función de la frecuencia) de un sistema se emplea la corriente alterna en ensayos de espectroscopia de impedancia electroquímica (EIS), donde se emplean excitaciones de amplitudes bajas (entre 5 y 10mV), dando lugar a una pequeña perturbación del sistema electroquímico, asegurando que éste siga encontrándose en régimen lineal y no se haya desplazado fuera de su equilibrio electroquímico.

El sistema electroquímico se puede relacionar con un circuito eléctrico a fin de modelizar su comportamiento a partir de ajustar los datos de impedancia obtenidos de la medida EIS a los parámetros de un circuito equivalente elegido en función de la realidad física de los fenómenos físicos y químicos que tienen lugar.

De esta forma la técnica conocida como EIS se ha convertido en una herramienta poderosa en el estudio de corrosión, recubrimientos orgánicos, electrodeposición, semiconductores, baterías, *electroplatting*, y síntesis electro-orgánica.

Debido a que en la corriente alterna la impedancia (y todos los componentes) depende de la frecuencia de estudio, en las medidas EIS se aplican excitaciones de amplitud en el rango de frecuencias más amplio posible y que normalmente suele variar entre 0.001 y $1 \cdot 10^5$ Hz. Al utilizar excitación sinusoidal pequeña (baja amplitud) se consigue que la respuesta del sistema tenga un comportamiento pseudo-lineal, y de esta forma la respuesta de corriente frente a un estímulo de potencial sinusoidal, será también sinusoidal a la misma frecuencia pero con un ligero desfase.

La aplicación de la espectroscopia de impedancia electroquímica a metales con recubrimiento orgánico de función anticorrosiva se basa en la habilidad de la técnica para distinguir entre distintos procesos que suceden, de forma simultánea y/o consecutiva, en el sistema [12-25]. Para ello se introduce el concepto de constante de tiempo (τ). La constante de tiempo es el parámetro característico a cada fenómeno que sucede en el sistema metal/recubrimiento y consiste en el tiempo que un determinado proceso toma desde la perturbación causada mediante la medida EIS hasta su relajación. El análisis de estos procesos de relajación proporciona información acerca del sistema.

Así, en metales recubiertos, los procesos rápidos, con τ bajas, que son los relacionados con las propiedades dieléctricas de los polímeros, tienen lugar a frecuencias elevadas. En cambio, los procesos lentos, con τ elevadas, como es el caso de las reacciones de corrosión en la interfase metal-recubrimiento, tendrán lugar a frecuencias bajas [24]. Cada proceso, por lo tanto, se relaciona con una frecuencia característica:

$$f = \frac{1}{2\pi\tau}$$ Ec. 4.3.1.

Con la espectroscopia de impedancia es posible hacer barridos de frecuencia muy amplios, que pongan de manifiesto, tanto los fenómenos que tienen lugar a alta frecuencia como aquellos que ocurren a bajas frecuencias, dentro del sistema objeto de estudio.

Las perturbaciones aplicadas al sistema en el ensayo EIS pueden ser de corriente (galvanostático) o de potencial (potenciostático).

Supongamos una perturbación sinusoidal de potencial, de forma que la respuesta será una corriente en forma sinusoidal, pero desfasada por la desviación respecto al caso ideal (caso de un sistema puramente resistivo no habría desfase). Así tendremos una figura como la 4.3.3 y las ecuaciones que de ella se extraen.

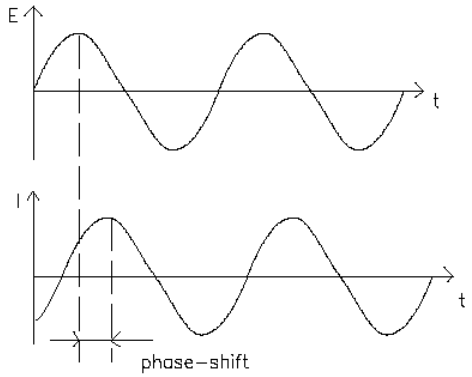

Fig. 4.3.3. Respuesta sinusoidal de corriente en sistema lineal.

Perturbación: $E_t = E_0\, sen(\omega t)$ Ec. 4.3.2.

Si el sistema es lineal, la respuesta será una corriente sinusoidal pura:

Respuesta: $I_t = I_0\, sen(\omega t - \phi)$ Ec. 4.3.3.

Donde, E_t e I_t son el potencial y la intensidad a un tiempo t. E_o e I_o son las amplitudes de señal y respuesta, respectivamente, ω es la frecuencia angular en radianes ($\omega=2\pi f$) de la señal, y ϕ es el ángulo de desfase (grados) entre el potencial de perturbación y la corriente de respuesta.

Mediante la relación de Euler:

$$\exp(j\phi) = \cos\phi + j\, sen\phi$$ Ec. 4.3.4.

Se puede expresar la impedancia como una función compleja, quedando las ecuaciones 4.3.2 y 4.3.3 como:

$$E_t = E_0 \exp(j\omega t)$$ Ec. 4.3.5.

$$I_t = I_0 \exp(j\omega t - \phi)$$ Ec. 4.3.6.

Teniendo en cuenta la Ley de Ohm y su aplicación a la impedancia en corriente alterna se puede escribir con las ecuaciones anteriores:

$$Z(\Omega) = \frac{E}{I} = Z_0 \exp^{j\phi} = |Z|\left(\cos\phi + j\,sen\,\phi\right) = Z' + jZ''$$ Ec. 4.3.7.

Los datos de las medidas de impedancia electroquímica se pueden representar en el plano complejo, donde la impedancia se representa con un vector de módulo $|Z|$ y de ángulo ϕ formado por el vector y el eje real, tal y como se muestra en la figura 4.3.4. Esta representación de un número complejo en un plano recibe el nombre de "diagrama de Argand". Z' es la parte real de la impedancia y hace referencia a su componente resistiva, mientras que Z'' es la parte imaginaria y representa su componente capacitiva. Así, cuanto mayor sea el ángulo de desfase más capacitivo será el sistema, mientras que a menor ángulo de desfase más resistivo será, es decir, tendrá un comportamiento más ideal, más próximo a la ley de Ohm.

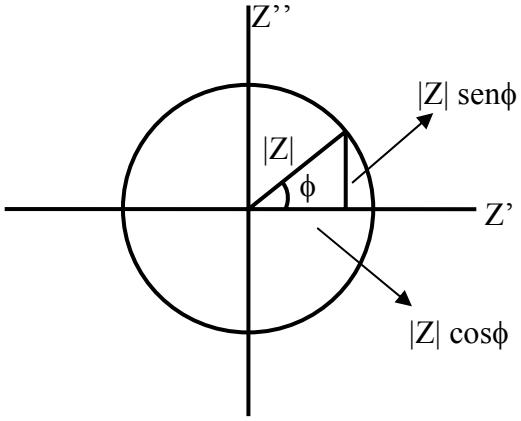

Fig. 4.3.4. Diagrama de Argand de la impedancia.

Cada vector define un punto de longitud |Z| y ángulo ϕ por lo que se puede representar por medio de los gráficos de Nyquist (parte imaginaria de la impedancia frente parte real para todo el rango de frecuencias), como la figura 4.3.5., el comportamiento de la impedancia del sistema en función de la frecuencia.

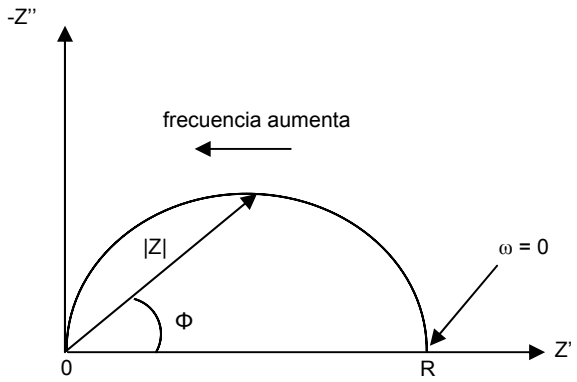

Fig. 4.3.5. Diagrama de Nyquist.

Cada semicírculo del diagrama de Nyquist está relacionado con una constante de tiempo, τ. La figura 4.3.5 se puede equiparar a un circuito eléctrico de una sola constante de tiempo, esto es con una resistencia y un condensador en paralelo.

Otra forma de representar los datos es mediante los gráficos de Bode, donde se representa el logaritmo del módulo de la impedancia (|Z|) y ángulo de fase (ϕ) en función del logaritmo de la frecuencia. Este tipo de gráficos presenta información más clara y menos ambigua que los de Nyquist, a la vez que distingue entre diferentes constantes de tiempo y procesos que tienen lugar en el sistema, por lo que es preferido por algunos investigadores [26] frente los gráficos de Nyquist. En la figura 4.3.6 se muestra un gráfico de Bode con dos constantes de tiempo.

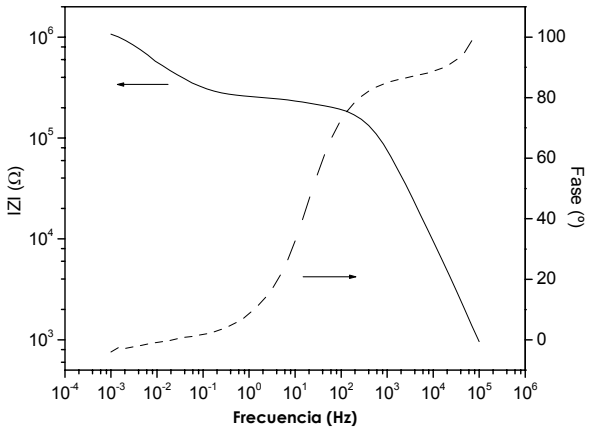

Fig. 4.3.6. Diagrama de Bode con dos constantes de tiempo.

Uno de los aspectos más importantes de la técnica EIS como herramienta para investigar las propiedades electroquímicas de los sistemas, es que, en muchos casos, el comportamiento de un sistema real se puede modelizar mediante un circuito constituido por un conjunto discreto de componentes eléctricos, denominado circuito equivalente, y de esta forma estudiar su comportamiento.

Esta relación es lógica si se tiene en cuenta que las leyes fundamentales que relacionan la carga y el potencial, que definen un sistema lineal, no cambian al pasar de componentes eléctricos (como los del circuito equivalente) a materiales iónicos (los que constituyen el sistema real). Esta afirmación, sin embargo, sólo es cierta bajo determinadas condiciones experimentales: cuando el comportamiento del sistema es lineal, razón por la cual se emplean señales de pequeña amplitud que aseguran dicha linealidad.

La interpretación de las medidas de EIS consiste, generalmente, en el ajuste de los datos experimentales a ese circuito equivalente, representativo de los procesos físicos y/o químicos que tienen lugar en el sistema objeto de estudio. Dicho circuito está constituido por combinaciones más o menos complejas de elementos resistivos, capacitivos e inductivos y debe tener la misma impedancia que el sistema medido.

En el caso de recubrimientos orgánicos aplicados sobre substratos metálicos, la técnica de espectroscopia de impedancia electroquímica se ha utilizado con éxito para la caracterización de sus propiedades protectoras [24-26].

El objetivo final de la técnica es ofrecer información acerca de las propiedades del sistema, tales como la presencia de defectos, la reactividad de la interfase, la adherencia metal-pintura, las propiedades barrera del recubrimiento... El conocimiento de estos parámetros resulta esencial para poder predecir las características anticorrosivas de dichos sistemas durante su vida de servicio y sentar las bases científicas para la mejora en la formulación de las pinturas.

Sin embargo, es necesario tener en cuenta una serie de limitaciones a la hora de aplicar la técnica EIS al estudio de los sistemas metal-recubrimiento:

1. Puede existir ambigüedad en los datos obtenidos e, incluso, no ponerse de manifiesto toda la información del sistema debido al solape de constantes de tiempo correspondientes a distintos procesos. Por otro lado, la elección del circuito equivalente adecuado exige, en muchas ocasiones, la utilización de técnicas complementarias. La técnica EIS, por si sola, no es suficiente en muchos casos para caracterizar el sistema metal-recubrimiento.
2. Los diagramas de Nyquist casi siempre se corresponden con semicírculos achatados de la distribución de las constantes de tiempo del sistema alrededor de un valor central. Esa distribución puede ser debida a la rugosidad de la superficie del electrodo, que genera una distribución no uniforme de la densidad de corriente sobre la superficie. Otra posible causa es debida a la formación de productos de corrosión sólidos que se sitúen en los defectos de la película orgánica o, simplemente, a la heterogeneidad intrínseca de la pintura.

Los espectros de impedancia de un sistema metal-recubrimiento presentan una evolución típica dependiendo del estado de la pintura. Si atendemos esta evolución en un gráfico de Nyquist ideal, observaremos la tendencia que tomaría el sistema con la evolución del tiempo (figura 4.3.7).

Inicialmente, la pintura está intacta, mostrando un comportamiento típicamente capacitivo (fig. 4.3.7.a) esto es con un ángulo ϕ lo más cercano a 90º posible, a medida que el electrolito atraviesa el recubrimiento el arco se cierra y se transforma en un semicírculo (fig. 4.3.7.b), es decir el ángulo es diferente a 90º y la componente resistiva-real comienza a tener más importancia, el material está dejando de ser un condensador perfecto y el electrolito empieza a introducirse en su seno. A mayores períodos de exposición, el electrolito ya ha penetrado en el recubrimiento y alcanzado la interfase de forma que se inician los procesos de corrosión en la interfase metal-recubrimiento, con la aparición de otra constante de tiempo a frecuencias inferiores (fig. 4.3.7.c-d). Esta segunda constante de tiempo también podrá tener un comportamiento completamente capacitivo (fig. 4.3.7.d) o bien la forma de un arco (fig. 4.3.7.c) y se ve totalmente afectada por los procesos que tienen lugar en la interfase, pudiendo existir una componente difusiva como la línea recta de la figura 4.3.7.d.

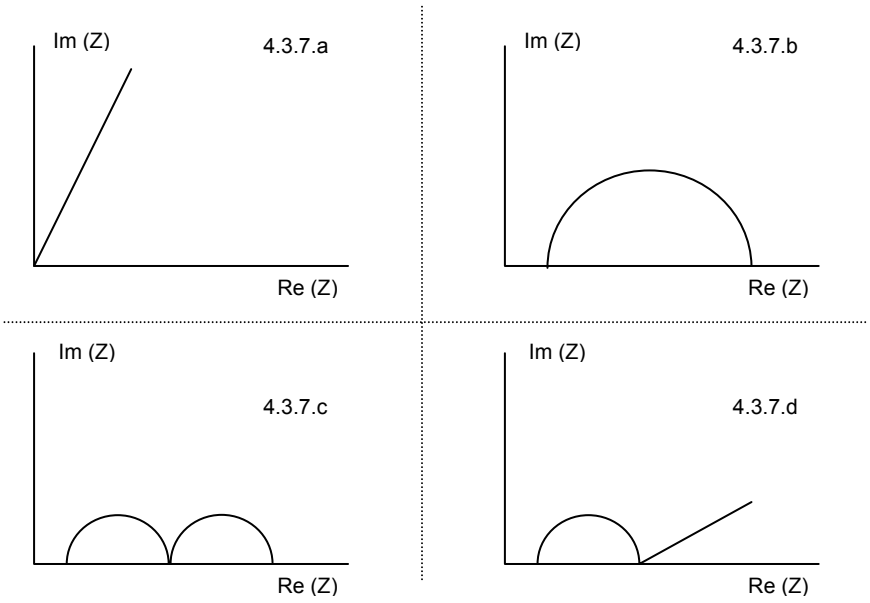

Fig. 4.3.7. (a-d). Evolución típica de los diagramas de Nyquist para un sistema metal/recubrimiento orgánico.

Los recubrimientos orgánicos se comportan idealmente como un dieléctrico, dando lugar a una impedancia capacitiva caracterizada por una dependencia en frecuencia tipo ω^{-1}. Este comportamiento es eléctricamente equivalente a la capacidad del recubrimiento polimérico C_c en paralelo con la resistencia del citado recubrimiento R_{po}.

No obstante, la mayor parte de los espectros de impedancia de metales recubiertos inmersos en una disolución electrolítica (de resistencia R_s) muestran desviaciones respecto a este comportamiento simple de la impedancia como resultado de la formación de poros con conductividad iónica [12] y reacciones consecutivas en la interfase. Este nuevo comportamiento puede ser descrito por el circuito equivalente mostrado en la figura 4.3.8. de amplio uso en la modelización de espectros EIS en metales recubiertos con pinturas orgánicas [26].

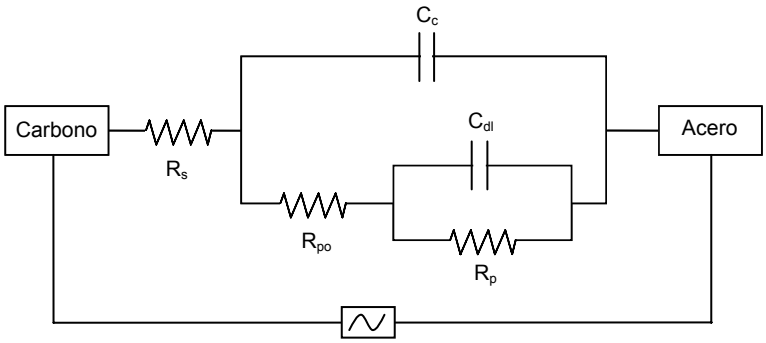

Fig. 4.3.8. Circuito equivalente con dos constantes de tiempo utilizado en la modelización de espectros de impedancia de sistemas recubrimiento orgánico/metal.

Cada uno de los parámetros del circuito eléctrico tiene una interpretación física dentro de los procesos del sistema orgánico/metal. De esta forma ajustando los espectros de impedancia a este circuito eléctrico equivalente se puede obtener información referente al comportamiento electroquímico del recubrimiento:

- R_s, es la resistencia del electrolito al flujo de corriente. En el estudio de recubrimientos orgánicos y empleando un potenciostato de 3 electrodos (trabajo, contra-electrodo y referencia) este valor es constante y despreciable frente al resto de los valores.

- R_{po} es una medida de la porosidad y deterioro del recubrimiento. Este parámetro se relaciona habitualmente con el número de poros y canales perpendiculares a la superficie del substrato a través de los cuales el electrolito alcanza la interfaz metal-recubrimiento [24]. Aunque R_{po} puede aumentar con el tiempo de inmersión, probablemente debido a la obstrucción de los poros por los productos de corrosión, normalmente decrece. Algunos autores [26, 27] han distinguido tres regiones en la tendencia dependiente del tiempo de R_{po}. Así, inicialmente decrece muy rápido, después despacio (mostrando una meseta o *plateau*) y posteriormente rápido de nuevo, coincidiendo con la aparición de un segundo semicírculo en el espectro de EIS. La meseta se explica asumiendo que el número de canales formados es prácticamente constante.

- C_c es la capacitancia del recubrimiento y puede emplearse como una medida de la permeabilidad del recubrimiento al electrolito. Este parámetro viene dado por la ecuación:

$$C_c = \varepsilon \cdot \varepsilon_0 \cdot A/d \qquad \text{Ec. 4.3.8.}$$

Donde, ε es la constante dieléctrica del recubrimiento, ε_o es la constante dieléctrica del vacío ($8.85 \cdot 10^{-12}$ F/m), *A* es el área del recubrimiento expuesta al electrolito y *d* es el espesor del recubrimiento. C_c variará normalmente con la absorción de electrolito, debido a que la constante dieléctrica del agua es aproximadamente 20 veces mayor que la de un recubrimiento típico (conforme aumenta el tiempo aumenta ε por la entrada de electrolito en el recubrimiento).

Habitualmente C_c aumenta en la etapa inicial de exposición, mostrándose así como una medida de la absorción de agua, esta etapa indica la entrada del electrolito a través de los microporos del recubrimiento (área superficial del mismo). Etapa controlada por la ley de difusión de Fick. No se produce la entrada de iones como el Cl^- debido a que su coeficiente de difusión ($4.7 \cdot 10^{-12}$ cm^2/s) es un orden de magnitud menor que el del agua ($3.16 \cdot 10^{-11}$ cm^2/s). En una segunda etapa, aparece C_c constante, notando que el recubrimiento está saturado de electrolito. Indica la entrada de agua e iones por los macroporos. Cuando el sistema metal/recubrimiento se ha expuesto durante un largo periodo de tiempo se puede relacionar con la delaminación y el deterioro del sistema ya que los macroporos han alcanzado la interfase, y con ellos el electrolito [28].

- R_p y C_{dl} son dos parámetros empleados para determinar la delaminación del recubrimiento y la actividad corrosiva que tiene lugar en la interfase. Sólo pueden ser calculados adecuadamente cuando se observan por lo menos dos constantes de tiempo en el espectro. R_p está asociada a la transferencia de carga existente en la superficie del substrato metálico y suele disminuir conforme avanza el tiempo, aunque depende de numerosos factores como la pasivación del substrato.
  C_{dl} es una medida del área de substrato delaminada. La tendencia del parámetro C_{dl} es muy compleja, y sus cambios de valor pueden ser asociados a la competición entre dos procesos opuestos como son, por un lado la delaminación y por otro la acumulación de productos de corrosión en la interfase. Este parámetro aumenta conforme el agua se introduce y extiende en la interfase y conforme el área delaminada aumenta. Por otro lado, el valor disminuye conforme la acumulación de productos de corrosión en la interfase disminuye el área del condensador de la doble capa. Por lo tanto, un cambio de tendencia de C_{dl} dependerá de qué factor es el dominante en el proceso de corrosión. Sin embargo, cabe destacar que tanto un aumento como un descenso de este valor son resultado del desarrollo de procesos de corrosión en la superficie del substrato metal, mientras que cuando C_{dl} es constante indica que la interfase del sistema es estable [20].

La figura 4.3.8 muestra un circuito equivalente ideal, en el que se emplean capacitores ideales en paralelo a resistencias. Sin embargo, tal y como se ha explicado más arriba, los sistemas metal/recubrimiento muestran numerosas imperfecciones (ej. inhomogeneidades) que hacen que no se comporten de forma ideal, esto es ya no se comportan como dos placas conductoras paralelas se paradas por un dieléctrico. Esta realidad de los sistemas provoca que a la hora de modelizar los circuitos equivalentes con softwares apropiados (como el Z-View) no se puedan emplear capacitores en el circuito equivalente y se tenga que introducir un nuevo elemento conocido como “elemento de fase constante” (CPE), que al fin y al cabo actúa como distribuidor de impedancia. La introducción de estos elementos en el circuito permite un ajuste de los parámetros mucho más exacto.

La distribución de capacitancia (por medio de CPEs) se ha discutido ampliamente en la literatura [29], y su origen se relaciona con diferentes causas como rugosidad y heterogeneidades, porosidad del electrodo (distribución de poros…), variación de la composición del recubrimiento (inhomogeneidades de

las propiedades de film…), reacciones de adsopción lentas (en el substrato o recubrimiento) y distribución no uniforme de potencial y corriente. Así el origen del comportamiento de los CPE debe ser una distribución de constantes de tiempo [29].

Al emplear CPE en lugar de capacitores, los softwares disponibles en el mercado como el Z-View, ofrecen un valor de capacitancia resultado del ajuste, que sin embargo, no es exactamente la capacitancia (conocida como efectiva) debido a que el uso de CPE introduce errores. Esto es especialmente cierto en el caso de los parámetros de la interfase (C_{dl}). Al ajustar el circuito equivalente con CPE, la capacitancia obtenida viene acompañada de un valor denominado "n", el cual es el exponente de la ecuación dada por Brug et al. [30] para la impedancia de un CPE:

$$Z_{CPE} = Y_0^{-1}(j\omega)^{-n} \qquad \text{Ec. 4.3.9.}$$

Donde Z_{CPE} es la impedancia del CPE, Y_0 es un parámetro con unidades s^n/Ω (es la capacitancia obtenida mediante el software), j es el número imaginario j ($j=(-1)^{1/2}$) y, ω es la frecuencia angular ($\omega=2\pi f$, siendo f la frecuencia). El parámetro n da una idea de las desviación del CPE con respecto a la capacitancia ideal (donde n=1), así cuando n es 1, el CPE se comporta como una capacitancia, mientras que cuando es 0 lo hace como un resistor (más distribución de capacitancia).

Debido la desviación de valores de la capacitancia ajustada con respecto la capacitancia efectiva (sistema ideal), algunos autores propusieron ecuaciones para calcular la capacitancia efectiva (C_{dl}) mediante el valor del ajuste (Y_0) y los valores de n y frecuencia angular. Esta relación fue propuesta por primera vez por E. Van Westing (ecuación 4.3.10) [31].

$$C_{dl} = Y_0(\omega)^{n-1} / \sin(n\pi/2) \qquad \text{Ec. 4.3.10.}$$

Posteriormente, Mansfeld y Hsu [32], propusieron una nueva ecuación, ecuación 4.3.11, como la apropiada para una conexión paralela de CPE con resistencia (como el caso de estudio en la tesis).

$$C_{dl} = Y_0(\omega''_{\max})^{n-1} \qquad \text{Ec. 4.3.11.}$$

Donde ω''_{max} es la frecuencia del máximo en la representación –Z'' (impedancia imaginaria) frente ω (frecuencia angular).

A fin de saber qué ecuación de todas las propuestas para calcular la relación entre C_{dl} e Y_0, Jovic [33] estudió el uso de las más importantes, llegando a la conclusión que la propuesta por Mansfeld y Hsu era la más apropiada (ec. 4.3.11).

A parte, las diferencias entre Y_0 y C_{dl} puede ser significante dependiendo de los valores de frecuencia y n [33]. Así, se recomienda el uso de la ecuación 4.3.11 cuando los valores de n están muy por debajo de 1, lo cual supondría el uso de esta ecuación para calcular los valores de capacitancia de la interfase efectivos (C_{dl}) ya que en el caso del recubrimiento los valores de n suelen ser muy cercanos a 1. También en el caso de los sistemas aplicados por cataforesis los valores de n suelen ser muy próximos a 1, tanto en recubrimiento como en interfase. Por lo que el uso de la ecuación 4.3.11 no se hace necesario, entendiendo los valores dados por el software como iguales a los reales obtenidos por dicha ecuación.

Por otro lado, la necesidad de uso de la ecuación 4.3.11 tiene mucha importancia cuando se pretende obtener cuantitativamente parámetros del sistema como el espesor de capas de anodizado en aleaciones de aluminio o la constante dieléctrica de materiales de baja constante dieléctrica [32]. En esta tesis los valores de capacitancia se emplearon tan sólo para tener una idea cualitativa de la resistencia del sistema a los diferentes procesos, por lo que no se presentaba necesario dichos cálculos. A pesar de esto se calcularon las capacitancias efectivas para las muestras con iterbio, observándose ningún cambio de tendencia, aunque sí ligeros cambios de valores. Debido a estos hechos, no se consideró necesario el cálculo de las capacitancias efectivas de todas las muestras, dejándose los valores obtenidos por el software con unidades tipo s^n/Ω en lugar de las propias de la capacitancia (F o s/Ω).

A fin de realizar los ensayos EIS se empleó un potenciostato-galvanostato tipo AUTOLAB PGSTAT30 (figura 4.3.9) en control potenciostático y al potencial libre de corrosión. Las medidas de impedancia se efectuaron en un rango de frecuencias entre 1mHz y 100 kHz, con un voltaje sinusoidal de amplitud 10 mV y en el interior de una celda de Faraday para evitar interferencias con el exterior.

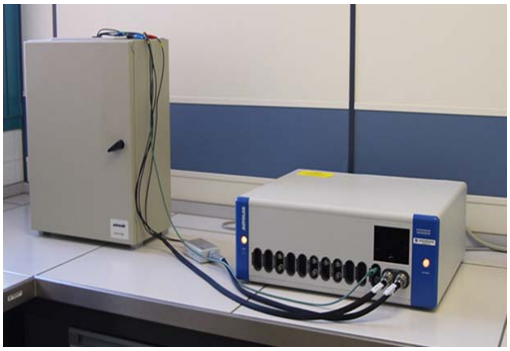

Fig. 4.3.9. Equipo de impedancias y celda de Faraday.

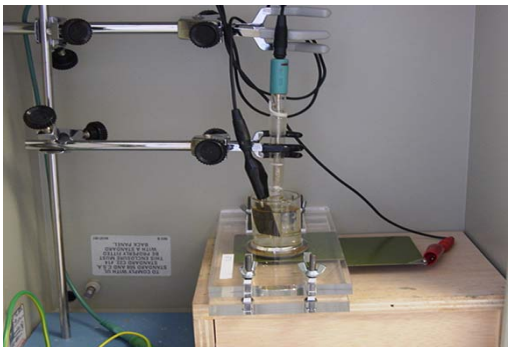

Fig. 4.3.10. Montaje experimental de la celda electroquímica.

Tal y como se ha indicado en el apartado de materiales los recubrimientos se depositaron mediante pistola electrostática y por electrodeposición (en el caso de las pinturas para la industria del automóvil) sobre substrato acero al carbono. En el caso de las pinturas en polvo el espesor medio conseguido fue de 60± 5µm, mientras que en las pinturas cataforéticas fue de 20± 1µm. Tras las respectivas condiciones de curado se seleccionaron las zonas de estudio de impedancia.

Sobre las áreas seleccionadas se fija un cilindro de vidrio de 16.6cm^2 de área donde se introduce la disolución electrolito (solución 3.5%NaCl en peso en agua desionizada) y el triple-electrodo compuesto por electrodo de trabajo (el acero substrato), contra-electrodo (hoja de carbono grafito), electrodo de referencia (Ag/AgCl) formándose así la celda electroquímica mediante la cual se medirá la evolución de la impedancia de los sistemas con el tiempo de exposición a la disolución (figura 4.3.10).

4.3.3. Ensayo electroquímico acelerado AC/DC/AC

La técnica EIS presentada en el punto 4.3.2 es de amplio uso en la evaluación de recubrimientos y presenta buenos resultados, aunque en ocasiones son complicados de interpretar y requieren de elevados periodos de exposición cuando los sistemas tienen excelentes propiedades anticorrosivas. De esta forma esta técnica, aunque bastante eficaz, tiene poca aplicación industrial.

Por otro lado los ensayos tradicionales como los de niebla salina mostrados en el apartado 4.3.1 son caros de realizar, requieren de tiempos relativamente elevados (en ocasiones más de un mes), son altamente subjetivos y requieren de experiencia para ser llevados a cabo de forma eficaz.

Con estos antecedentes en el año 1999 el doctor alemán Jochen Hollaender [34] presentó un método de ensayo de evaluación rápida de aplicación en la industria de los envases de alimentos, técnica que se presentó como AC-DC-AC. Desde entonces, esta técnica (basada en un sistema de dos electrodos sólidos) se ha probado y adaptado en sistemas orgánicos anticorrosivos en líquido aplicados sobre substrato acero al carbono [35-37], llegando a aparecer en una tesis doctoral [38] en el año 2004.

En este trabajo doctoral se ha empleado esta técnica, que a continuación se detallará, en pinturas en polvo y cataforéticas alcanzando una mayor comprensión de los fenómenos que tienen lugar así como el perfeccionamiento de la misma.

En términos generales la técnica AC/DC/AC permite obtener información objetiva y cuantitativa sobre las propiedades anticorrosivas de un sistema orgánico en menos de 24 horas (información sobre propiedades barrera y adhesiva). A su vez puede ser totalmente automatizado en un equipo de medidas de impedancia. Todas estas características la convierten en una técnica con grandes ventajas frente a la habitual EIS y ensayos acelerados tradicionales (como resistencia a niebla salina).

La técnica se basa en la provocación de un ciclo tensión/relajación al sistema recubrimiento/metal para acelerar su degradación. Mediante esta técnica se fuerza el paso de los iones y electrolito a través del recubrimiento hasta alcanzar la interfase, de esta forma se detectan fallos del recubrimiento (como delaminaciones locales o grietas) que otras técnicas no son capaces de detectar a no ser en periodos muy largos de tiempo. La técnica es capaz de evaluar el comportamiento dieléctrico del material y principalmente su adherencia al substrato.

La técnica AC/DC/AC es una combinación de medidas EIS, en corriente alterna (AC), y polarizaciones catódicas, en corriente continua (DC), tomándose entre polarización y medida EIS un tiempo denominado de relajación en el cual el sistema alcanza un nuevo estado de equilibrio tras el estrés provocado en la polarización. El ciclo se puede repetir hasta la degradación del recubrimiento o bien un número dado de ciclos para los que se pueden tener resultados comparativos entre diferentes sistemas.

En la figura 4.3.11 se puede observar un esquema de ensayo de la técnica de impedancia electroquímica de evaluación rápida AC/DC/AC.

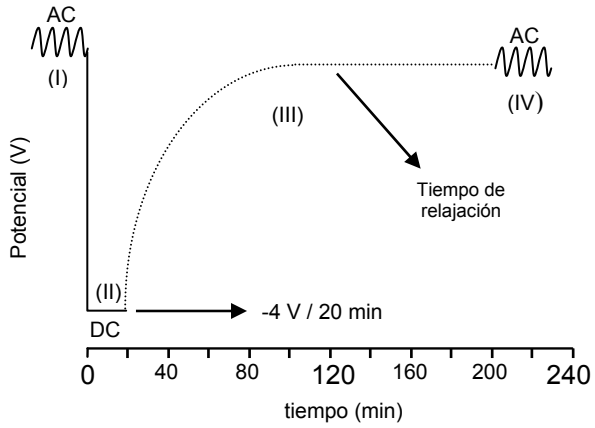

Fig. 4.3.11. Esquema de ensayo de la técnica AC/DC/AC versus tiempo.

Las etapas de la técnica AC/DC/AC son:

I. Medida EIS al potencial libre de corrosión (AC). De esta forma se obtiene la impedancia inicial del sistema recubrimiento/substrato.

II. Polarización catódica (DC). Se fuerza la entrada de electrolito e iones en el recubrimiento así como que el substrato metálico actúe como cátodo de forma que se promueven las reacciones catódicas superficiales en cuanto agua y oxígeno alcanzan la interfase. Su finalidad es provocar la degradación del recubrimiento y la corrosión del sustrato. En pinturas en polvo se aplicó un potencial de -2V mientras que en pinturas cataforéticas, por ser de mucha mayor calidad, se emplearon -4V de polarización, ambas durante 20 minutos.

III. Periodo de estabilización (t_{relax}). Durante la polarización el sistema se desequilibra así que antes de medir la nueva impedancia del sistema se deja que éste estabilice durante un periodo determinado. Se considera que el sistema es estable cuando el potencial a circuito abierto lo es. Al final de periodo de estabilización el potencial de corrosión será diferente (por lo general menor) al obtenido en la anterior medida EIS. Después de realizar ensayos a diferentes tiempos de relajación finalmente éste se fijó en 10800 segundos para todos los casos.

IV. Medida EIS al potencial libre de corrosión (AC). Tras la relajación se mide la nueva impedancia del sistema obteniendo así cómo ha variado el sistema tras el estrés aplicado (polarización).

Esta secuencia de ensayos se programó en el equipo (PGSTAT 30) de forma que fuera repetido automáticamente 6 veces, llegando a un tiempo de ensayo máximo de 24horas.

Del ensayo se obtiene dos tipos de información: la obtenida de las medidas de impedancia EIS de donde se determinan los parámetros característicos de un circuito equivalente (se utilizó de nuevo el de la figura 4.3.8 empleando CPE en lugar de C) y por otro lado, la información obtenida durante el tiempo de relajación, información en forma de gráficos E_{oc}=f(tiempo).

La técnica tiene sus bases en la influencia que la reacción catódica de la hidrólisis del agua (producida cuando el potencial es más negativo que -1V (vs SCE) [39]) tiene sobre la adherencia por la formación de H_2 (gas) y OH^-.

En la figura 4.3.12 se muestra un esquema de los procesos físicos y químicos que tienen lugar durante la polarización y relajación en la técnica AC/DC/AC.

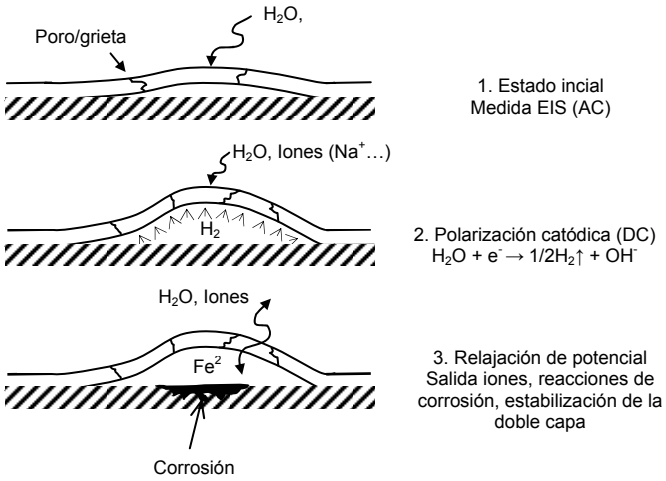

Fig. 4.3.12. Efecto físico de la polarización catódica sobre un substrato recubierto. Fallo de un recubrimiento orgánico.

En la polarización, la entrada de electrolito promoverá el desprendimiento de H_2 lo que aumentará las delaminaciones locales dando lugar al fallo del recubrimiento, situación que se detecta en la medida de impedancia tras la relajación.

Cuando cesa la reacción catódica, y la producción de H_2 ha tenido lugar, la corrosión electroquímica del sistema tiene lugar en presencia de electrolito, con producción de óxidos e hidróxidos de hierro. Por otro lado la polarización forzada hace que la doble capa en la interfase se distorsione y necesite reorganización, lo cual se refleja en la variación del potencial en el proceso de relajación. A su vez, los diferentes iones dentro del recubrimiento lo abandonarán produciendo equilibrio de cargas y reordenación de los dipolos moleculares del polímero, produciendo así la variación del potencial con el tiempo. Así el sistema se degrada por la pérdida de adherencia (formación de H_2), la apertura de poros por la introducción de las diferentes especies desde el electrolito, y la formación de productos de corrosión durante los procesos electroquímicos.

Los efectos que la polarización tiene sobre el sistema recubrimiento/metal son:

a. La introducción y el paso de diferentes iones (H^+, Na^+...) desde el electrolito a la película, debido al potencial negativo establecido en el sustrato metálico (por la polarización catódica impuesta). Esto puede producir una concentración de cationes en la imprimación que deberá ser neutralizada alcanzando un equilibrio a través de la entrada de aniones (como Cl^-). El paso de iones (que pueden ser hidratados) a través del recubrimiento puede causar su deterioro.

b. La reacción catódica que tiene lugar en la superficie metálica considerando el grado de polarización impuesto y el tipo de electrolito es [39]:

$$2H_2O\ (l) + 2\ e^- \rightarrow H_2\ (g) + 2\ OH^-$$

Esta reacción tendrá lugar antes si el electrolito es capaz de pasar a través del recubrimiento y alcanzar la interfase. Esto dependerá de las propiedades de la película (permeabilidad a los iones, adherencia al substrato, existencia de áreas de delaminación localizada, posibilidad de agrietamiento debido al alto grado de rigidez...) y, por supuesto, del potencial aplicado.

Obviamente, una alta calidad de la imprimación (impermeabilidad y ductilidad de la película y gran adhesión al sustrato), disminuye la probabilidad de que el electrolito alcance la interfase y de que la reacción catódica tenga lugar. El deterioro del recubrimiento debido a la polarización catódica puede estar provocado principalmente por el proceso de delaminación de la película en la interfase metálica si la reacción catódica de producción de H_2 (g) y/o OH^- finalmente ocurre, aunque el paso de iones a través de la película también debe ser considerado. Así, el potencial de polarización aplicado es función de la calidad del sistema debiéndose alcanzar un equilibrio entre dañar el recubrimiento en un tiempo no muy largo (inferior a 24horas) y un tiempo demasiado corto como para no observar una evolución clara del sistema con las polarizaciones.

Si fuera posible averiguar si la reacción catódica ha tenido lugar durante la polarización, esta información podría utilizarse para conocer mejor el comportamiento y el nivel de calidad de la imprimación. Una forma de detectar la producción de H_2 (g) en la interfase es estudiar la relajación del potencial a circuito abierto después de la polarización. Una vez ha finalizado la polarización catódica, el potencial del metal recubierto se relaja siguiendo los dos o uno de lo mecanismos siguientes:

a. Si la reacción catódica ha tenido lugar (producción de H_2), el potencial presentará una relajación rápida entorno a -1 V [39] (con ligeras variaciones dependiendo de la composición de la imprimación) que corresponde con el final de la reacción. Posteriormente se observa una segunda relajación que se asocia con la salida de iones y electrolito de la película, y posiblemente la formación de una nueva doble capa en la superficie metálica. En cualquier caso, la reacción catódica produce la entrada de electrolito a través del recubrimiento y la producción de H_2 (g) y OH^- en la interfase metal/recubrimiento. El tiempo necesario para que el electrolito y los iones abandonen la película será elevado dado que deben atravesar la imprimación.
b. Si la reacción catódica no se ha producido, tan sólo tendrá lugar una relajación correspondiente a la salida de iones y electrolito del recubrimiento. Esta relajación tendrá lugar a periodos de tiempo más altos en función de la penetración de éstos en la película, pero probablemente necesitarán menos tiempo que en el caso anterior.

4.4. PROPIEDADES ÓPTICAS Y QUÍMICAS

4.4.1. Espectroscopia de infrarrojo por transformada de Fourier (FTIR)

En el estudio se empleó un espectrofotómetro de infrarrojo por transformada de Fourier (FT/IR), modelo 680Plus de Jasco (figura 4.4.1) con una resolución de 4cm^{-1} en el modo de absorbancia. Las muestras previamente curadas se pusieron en un accesorio de reflexión atenuada con control térmico y cristal diamante (Golden Gate Heated Single Reflection Diamond ATR, Specac-Teknokroma). Los ensayos se llevaron a cabo a temperatura ambiente.

Fig. 4.4.1. Equipo de espectrofotometría (FT/IR).

La espectrofotometría [1] es una técnica analítica empleada para identificar materiales orgánicos (por detección de los grupos funcionales). Mide la absorción de la radiación infrarroja por el material en función de la longitud de onda. Las bandas de absorción infrarroja identifican componentes y estructuras moleculares.

Cuando el material se somete a radiación infrarroja, la radiación IR es absorbida por el material y excita las moléculas a un estado vibracional mayor. La longitud de onda de la luz absorbida por una molécula determinada es función de la diferencia de energía entre los estados vibracionales de reposo y excitado. Las longitudes de onda absorbidas por la muestra son características de la estructura molecular.

Los espectros de FTIR se suelen presentar como gráficos de intensidad (*absorbance*) frente número de cuentas, en cm^{-1} (*wavenumber*). El número de cuentas (número de ondas) es el recíproco de la longitud de onda. La intensidad se puede representar como el porcentaje de luz transmitida o absorbancia para cada número de cuenta.

4.4.2. Microscopio Electrónico de Barrido (MEB o SEM)

El microscopio electrónico de barrido es un método de elevada resolución para imágenes de superficie en el que se emplean electrones para crear las imágenes. A parte de las imágenes también se

puede obtener un análisis químico cualitativo y cuantitativo empleando junto al SEM un EDS (energy dispersive x-ray spectrometer).

En esta tesis se empleó un SEM modelo JEOL-JSM6300 Scanning Microscope (figura 4.4.2) para observar la influencia de la inclusión de triflatos de lantánido y ácido de Meldrum en la macro-porosidad del sistema. Para poder ensayar las muestras en el microscopio, éstas, en forma de película libre, se fragilizaron mediante N_2 líquido para provocar una rotura frágil y así observar correctamente el corte.

Fig. 4.4.2. Equipo SEM.

1. "*Handbook of analytical methods for materials*", Materials Evaluation and Engineering, Inc. Plymouth, EE.UU. (2001)
2. A.W. Coats, J. Redfern, *Nature*, 207 (1964) 290
3. X. Ramis, J.M. Salla, A. Cadenato, J.M. Morancho, *J. Therm. Anal. Calorim.*, 72 (2003) 707
4. X. Ramis, J.M. Salla, C. Mas, A. Mantecón, A. Serra, *J. Appl. Polym. Sci.*, 92 (2004) 381
5. X. Ramis, A. Cadenato, J.M. Morancho, J.M. Salla, *Polymer*, 44 (2003) 2067
6. I.M. Ward, *"Mechanical Properties of Solid Polymers"*, 2nd Ed., John Wiley and Sons, Chischester (1990)
7. J.M. Pereña, *Rev. Plast. Mod.*, 350, (1985) 167
8. Ferry J.D., *"Viscoelastic Properties of Polymers"*, Wiley, New York (1961)
9. A.V. Tobolsky, D.W. Carlson, N. Indictor, *J. Polymer Sci.*, 54 (1960) 175
10. C. Mas, A. Serra, A. Mantecón, J.M. Salla, X. Ramis, *Macromol. Chem. Phys.*, 202 (2001) 2554
11. "Electrochemical Impedance Spectroscopy Primer", *Gamry Instruments Inc.*
12. Basics of Electrochemical Impedance Spectroscopy", Application Note AC-1, *Princeton Applied Research*
13. U. Rammelt, G. Reinhard, *Prog. Org. Coat.*, 24 (1994) 309
14. I.M. Zin, R.L. Howard, S.J. Badger, J.D. Scantlebury, S.B. Lyon, *Prog. Org. Coat.*, 33 (1998) 203
15. L.S. Hernández, G. García, C. López, B. del Amo, R. Romagnoli, *Surf. Coat., Intern.*, 1 (1998) 19
16. G. Adrian, A. Bittner, *J. Coat. Tech.*, 58 (740) (1986) 59
17. T. Monetta, F. Bellucci, L. Nicodemo, L. Nicolais, *Prog. Org. Coat.*, 21 (1993) 353
18. I. Sekine, *Prog. Org. Coat.*, 31 (1997) 73
19. V.B. Miskovic-Stankovic, M.R. Stanic, D.M. Drazic, *Prog. Org Coat.*, 36 (1999) 53
20. N. Tang, W.J. van Ooij, G. Górecki, *Prog. Org. Coat.*, 30 (1997) 255
21. V.B. Miskovic-Stankovic, M.D. Maksimovic, Z. Kacarevic-Popovic, J.B. Zotovic, *Prog. Org. Coat.*, 33 (1998) 68
22. F. Deflorian, L. Fedrizzi, S. Rossi, P.L. Bonora, *Electrochim. Acta*, 44 (1999) 4243
23. F. Deflorian, V.B. Miskovic-Stankovic, P.L. Bonora, L. Fedrizzi, *Corr. Sci.*, 50 (1994) 438
24. A. Amirudin, D. Thierry, *Prog. Org. Coat.*, 26 (1995) 1
25. M.C. Pérez, *"Estudio de los sistemas de protección de las superficies metálicas expuestas a la intemperie"*, tesis doctoral, Universidad Santiago de Compostela, Santiago de Compostela (1998)
26. M. Kendig, F. Mansfeld, S. Tsai, *Corr. Sci.*, 23 (1983) 317
27. G.W. Walter, *Corr. Sci.*, 32 (1991) 1059
28. V.B. Miskovic-Stankovic, *J. Serb. Chem. Soc.*, 67, 5 (2002) 305
29. J.-B. Jorcin, M.E. Orazem, N. Pébère, B. Tribollet, *Electrochim. Acta*, 51 (2006) 1473
30. G.J. Brug, A.L.G. van Eeden, M. Sluyters-Rehbach, J. Sluyters, *J. Electroanal. Chem.*, 176 (1984) 275
31. E. Van Westing, *"Determination of coating performance with impedance measurements"*, tesis doctoral, Technical University of Delft, Delft (1992)
32. C.H. Hsu, F. Mansfeld, *Corrosion*, 57 (2001) 747
33. V.D. Jovic, "Determination of the correct value of Cdl from the impedance results fitted by the commercially available software", *Gamry Instruments Inc.* (2003)
34. J. Hollaender, C.A. Schiller, W. Strunz, *Food additives and contaminants*, 14, 6-7 (1999) 617
35. M.T. Rodriguez, J.J. Gracenea, J.J. Saura, J.J. Suay, *Prog. Org. Coat.*, 50 (2004) 68
36. J.J. Suay, M.T. Rodriguez, K.A. Razzaq, J.J. Carpio, J.J. Saura, *Prog. Org. Coat.*, 46 (2003) 121
37. M.T. Rodriguez, J.J. Gracenea, S.J. García, J.J. Saura, J.J. Suay, *Prog. Org. Coat.*, 50 (2004) 123
38. M.T. Rodríguez, *"Formulación y evaluación de imprimaciones epoxis anticorrosivas, curables a temperatura ambiente"*, tesis doctoral, Universitat Jaume I, Castellón (2004)
39. H. Leidheiser, *J. Adhesion Sci. Tech.*, 1 (1987) 79

V. RESULTADOS

5.1. OPTIMIZACIÓN DEL PROCESO DE CATAFORESIS

Este primer apartado del capítulo de *resultados y discusión* está dedicado a pinturas cataforéticas para la industria del automóvil.

Por medio de dos artículos se muestra el trabajo realizado entorno a la optimización del proceso de cataforesis, desde el punto de vista de las variables de deposición (potencial de aplicación) como desde el punto de vista de la temperatura de curado.

A fin de alcanzar los objetivos empleados se hizo uso de técnicas tradicionales de medidas anticorrosivas, como son los ensayos acelerados (tipo niebla salina/cámara climática) y las técnicas electroquímicas (EIS). A su vez, se estudió el uso de la técnica acelerada AC/DC/AC como técnica eficaz y eficiente a la hora de evaluar las propiedades anticorrosivas de los sistemas metal/recubrimiento orgánico.

Por medio de este estudio se consiguió establecer un intervalo de temperatura de curado y de potencial de aplicación óptimos para las pinturas cataforéticas aplicadas que confieran las mejores propiedades anticorrosivas. Por otro lado, se estableció la utilidad de la técnica AC/DC/AC en la optimización de las condiciones de aplicación por comparación de los resultados dados por esta técnica con aquellos dados por las técnicas tradicionales.

El primero de los artículos hace referencia al estudio efectuado para optimizar el potencial de aplicación, mientras que el segundo está referido a la temperatura de curado.

Validity of an electrochemical accelerated technique (AC/DC/AC) for rapid assessment of automotive primers

S. J. García[1], M. Rodríguez[1], R. Izquierdo[1], F. Romero[2] & J. Suay[3]

[1] Àrea de Ciència dels Materials i Enginyeria Metal·lúrgica, Departamento de Ingeniería de Sistemas Industriales y Diseño, Universitat Jaume I, Avda. Vicent Sos Baynat s/n, 12071 Castelló, Spain

[2] Departamento de Física Aplicada, Universitat Politècnica de València, Camino de Vera s/n, 46022 Valencia, Spain

[3] Centro de Biomateriales, Universitat Politècnica de València, Camino de Vera s/n, E-46071 Valencia, Spain

Corrosion Science XXX (2007) XXX
Enviado diciembre 2004. Bajo segunda revisión

Abstract

This paper deals with the evaluation of the anticorrosive properties of a cataphoretic paint and its dependence on the applied deposition voltage. In order to study it, three methods have been employed: the so-called EIS measurements; an accelerated cyclic test used in the automotive industry; and a rapid electrochemical test (AC/DC/AC) which combines EIS measurements with cathodic polarizations. The accelerated cyclic test seem to be not able to distinguish the influence of the deposition voltage on the anticorrosive properties. The AC/DC/AC test obtained the same results as EIS tests but in only 24 hours instead of months of evaluation. The technique AC/DC/AC was used to establish the optimum range of voltages needed to perform the cathodic deposition of the coating that offers the higher anticorrosive properties of an epoxy primer.

1. Introduction

Protection against corrosion in automobiles is of great importance from the point of view of both the national economy and the private car owner. The automotive industry requires organic protective coatings with very high resistance to degradation. Coatings must protect the substrate against corrosion attack and keep it undamaged for a long time, while at the same offering persistently good aesthetic properties, which means a high level of stability towards photo-oxidative degradation, mechanical abrasion and other harmful processes.

As is well known, the automotive sector has contributed on large scale to achieving compliance with increasingly restrictive environmental legislation in the field of surface treatments, above all in anticorrosive coatings. Today it can be stated that the anticorrosive protection of almost all-automobile bodywork includes a cataphoretic primer (98% of cars are primed with cathodic electrocoat) [1].

Although electrodeposition was introduced in the automotive industry in the 1960s, cathodic electrodeposition rapidly replaced anodic electrodeposition in the 1970s due to the greater anticorrosive protection that it conferred (its high level of automation, low levels of pollution, high throw power and homogeneity of the coating) [2-4]. At the beginning of the 1990s, cathodic systems were based on modified epoxy resins containing amino groups, systems which were described by Pierce [3]. These were dispersed in water by neutralising the amino group with organic acids. The resins were cross-linked by blocked isocyanates. Pigmentation was based on titanium dioxide and extender pigments. Special lead-containing pigments, such as silicates, were used as anticorrosive agents, although lead was also used to catalyze the curing reactions. The first lead-free systems came onto the market only in the 1990s, coinciding with attempts to meet other challenges such as achieving reductions in the volatile organic solvent content and lowering the curing temperature [5-7].

The electrodeposition process is controlled by many parameters, such as mean applied voltage, rectified ripple voltage, anode to sample distance or temperature. All of these have an important effect on the final performance of the primers. For example, it is well known that the ability of the cataphoretic process to deposit a film of paint in highly recessed areas increases with the deposition voltage, but the upper limit of the applicable deposition voltage is usually set by a phenomenon called film rupture, which causes blemishes [8-10].

Companies producing organic coatings for the automotive industry often need to test newly formulated products or materials, which may have different production parameters, in order to determine their actual behaviour before starting large-scale production of a coating. A correct selection of the test for this characterisation and the method of evaluation of the test results is critical. This choice is important because it is often necessary to distinguish between coatings with very similar performances [11].

In predicting the interaction stability properties of the primer, the main problem arises from the complexity of the overall process itself. Due to this complexity, the main routines of interaction testing and material assessment were developed experimentally by using different exposure processes and techniques for the measurement of properties. The main types of exposure processes are the accelerated aging test and field exposure experiments (which must be planned for long times and are

very expensive to run). Measurements of properties can be electrochemical, mechanical, chemical, and so on. Only if the exposure process and measurement test are well defined and programmed will it be possible to obtain information about the coating deterioration process, reproducible results and a time consumption that is not excessively long. Various electrochemical techniques have been used to evaluate the performance of organic coating/metal systems. The application of electrochemical impedance spectroscopy (EIS) to coated metals has proved to be a useful technique in the study of the corrosion performance of anticorrosive primers [12-19], although time is needed to perform this type of test because it takes days, weeks and sometimes months to obtain good results.

Therefore, it still exist an explicit interest in rapid assessment methods for practical applications that provide a faster indication of corrosion processes in the surface of coated metallic substrates. Hollaender et al. [20-22] developed a rapid method for testing coated metals in food packaging consisting in a combination of DC and AC measurements (AC/DC/AC procedure) which has been successfully adapted and used by Suay, Rodríguez and García in liquid paints applied to steel substrates [23-25]. After a first AC measurement, the test sample is treated for a short time by a constant cathodic current (DC) and, following that, an AC spectrum is recorded again. The change in the characteristics of the impedance spectrum can be attributed to a coating deterioration (pore formation) and a delamination process in the metallic surface due to hydrogen and OH^- production (if a cathodic reaction takes place).

The present work will mainly be focused on: The evaluation of an epoxy cathodic primer applied to metallic substrates at a given range of voltages, using different techniques in order to determine anticorrosion properties; The development of an electrochemical test procedure (AC/DC/AC) which can be applied to coated metals and offers results in a short time; and the comparison between the different evaluation procedures applied to the coated metals in order to determine whether the conclusions offered by each of them coincide.

Principles of cataphoretic deposition

Traditionally, the paint used in cataphoresis [6, 8, 26] consists of a basic resin and a pigment or paste. The resin is initially water-insoluble, but is made soluble by protoning it with weak acids like formic or acetic acid:

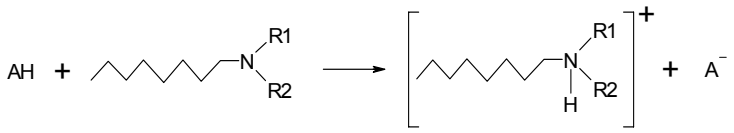

During the process of cataphoresis, water electrolysis takes place at the cathode with the formation of hydroxyl ions and evolvement of H_2. This initial step of the electrocoating process is known as the induction step:

$$2\ H_2O + 2\ e^- \rightarrow H_2 + 2\ OH^-$$

There will then be an electrophoretic migration of the resin micelles and associated pigments towards the cathode. The cathodic decomposition of water increases the pH value in this region. When this parameter reaches a critical value, an electrocoagulation of the resin micelles at the cathode surface will take place by neutralisation of positively charged groups in the resin with electrochemically generated OH^- ions:

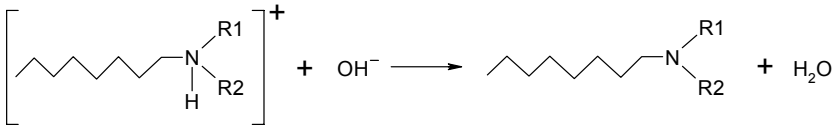

This mechanism occurs as a consequence of the low solubility of the base amine in comparison with its salt. The time needed to reach the critical pH value is known as the induction time.

The electrophoresis process continues with:

- Electroosmosis of water in the pores of the deposited films, caused by the voltage difference across the film and surface charges on the pore walls
- Heterocoagulation, which is film deposition on the metal substrate
- Adagulation, which is further film deposition upon already-deposited layers

Coagulation of the binder (resin) requires a minimum concentration of OH^- ions at the cathode surface. To reach this critical concentration by the electrolysis of water, a specific quantity of electricity must be applied, for a specific time (induction time) at a given current density. For a static electrolyte, induction time can be calculated by using Sand's equation [27, 28]:

$$t_i = \frac{\left(C_{OH^-}\right)^2 F^2}{D_{OH^-} \Pi 4 j^2} \tag{1}$$

where:

C_{OH-} = the critical OH^- ion concentration

D_{OH-} = the diffusion coefficient for hydroxyl ions

F = Faraday constant

j = current density

Equation (1) can be written in a shorter form:

$$t_i j^2 = K \tag{2}$$

K being a constant.

The critical concentration of OH^- ions in the vicinity of the cathode needed to initiate coagulation has been estimated by several authors [27] to be that which causes a pH = 12.

It is to be expected that the equation for film growth under a constant deposition voltage is:

$$db / dt = cj \tag{3}$$

being:

b = the film thickness

c = the coulombic yield (cm^3/C)

If the film has ohmnic characteristics, then relation "4" can be used:

$$j = kU / b \tag{4}$$

where U is the deposition voltage (which is located across practically all the film and k is the conductivity of the film). Replacing (4) in (3):

$$\frac{db}{dt} = \frac{ckU}{b} \quad \rightarrow \quad bdb = ckUdt$$

$$\int_0^b bdb = \int_{t_i}^{t} ckUdt \quad \rightarrow \quad \frac{1}{2}b^2 = ckU(t - t_i)$$

$$b = (2ckU)^{1/2}(t - t_i)^{1/2} \tag{5}$$

Equation (5) suggests that film thickness is proportional to the square root of the deposition time and the deposition voltage.

Since the deposited film has low conductivity (or high resistivity) so that the applied voltage is located across almost all the film, one can expect Joule heat to be evolved during deposition, the magnitude of which will depend on the deposition current density, resistivity and the thickness of the film. The local increase in temperature at the cathode surface has been measured and some consequences of this effect (like pinhole formation and cratering) have been discussed elsewhere [26].

Problems in the cathodic deposition when changing applied voltage

As stated above, it is well known that the ability of the cataphoretic process to deposit the film of paint in highly recessed areas increases with the deposition voltage, the upper limit of the applicable deposition voltage usually being set by a phenomenon called film rupture, which causes blemishes.

The cataphoretic deposition of paints normally occurs [8] at an initial medium voltage (250-275V), followed by a higher one (325-375V). The initial values of the applied voltage create sharply increasing conditions due to the high current during the induction time. These conditions affect not only the mechanism of the induction stage but the whole electrocoating process and, consequently, the rupture of the paint film as well as its cratering.

Cataphoretic paints display a further tendency towards the formation of crater-like features when applied over steel substrates under typical automotive application conditions. Previous studies concerning this type of defect (in zinc-coated steels) have shown that the craters appeared at the instant of fusion, during the baking, and persisted over a long heating time. The non-elimination of the defect during baking is attributed to the low fluidity of the deposited film due to its heating to a high degree during the previous cataphoretic deposition. Experimental runs in this field have localised dielectric breakdown of the electrocoat film during the sharp initial conditions of the electrocoating.

On the other hand, the observed temperature-time dependences are complex functions of the increase of the film thickness during deposition, the cathodic voltage applied, and the thermal conductivity of substrates. Higher deposition currents (with higher voltages) produce more Joule heat and consequently higher temperatures at the surface during deposition. As the temperature of the film increases by the Joule effect, the hydrogen accumulated in the film has a higher probability of creating bubbles, thus making the film unstable. Moreover, the evaporation of solvents can occur if the temperature increases further, giving rise to pinholes. Additionally, as has been indicated above, the increase in temperature can also create the conditions of a partial premature baking of the paint during the cataphoretic process, thus reducing the fluidity of the film during the next baking process. This last condition is a fundamental factor in the final quality of the paint.

Therefore, temperature is one of the reasons why the coating breaks down (pinholes, cratering and viscous flow of the deposited film) [8, 26].

2. Experimental

2.1. Materials

A commercial anticorrosive epoxy coating (supplied by *Industrias PPG Ibérica* and with commercial reference “Lead Free Generation 6”) was cationically deposited over steel substrates (cathode), type ACT APR 10160, with different cathodic voltages (220, 245, 270, 295, 320 and 345V). Steel test panels (210 x 110 x 1 mm) were pre-treated by mechanical cleaning (polishing), degreased with methyl-ethyl-ketone, and rinsed with distilled water. The composition of the cataphoretic bath was 47% of water, 45.3% of binder (adduct of cationic polyepoxydic resin (based on bisphenol-A) with polyamine cured with a polyurethane-based crosslinker) and 7.7% of pigments and charges. As anode, graphite was used.

Coatings were galvanostatically deposited at different current densities (giving different cathodic voltages) and different times in order to obtain a thickness of 20μm. Anodes were placed parallel to the working electrode (steel panels) at a distance of 1.5cm. The temperature of the electrolyte bath was kept at 30ºC throughout the complete cationic process. There was an anode/cathode area ratio of 1:4. The conditions of the cationic process, sample identification and curing conditions are summarised in Table 1. At least five samples were obtained under each condition.

When the painted samples were removed from the cationic bath, they were cured for 10 minutes at 180ºC, as shown in Table 1.

Table1. Identification and specifications (deposition voltage, time of voltage application, curing temperature and time) of the cataphoretically coated samples that were studied

Sample Identification	Deposition Voltage (V)	Time of voltage application (s)	Curing Temperature (ºC)	Curing time (min)
A	220	120	180	10
B	245	90	180	10
C	270	75	180	10
D	295	61	180	10
E	320	50	180	10
F	345	31	180	10

2.2. Testing Methods and Equipment

2.2.1. Thermogravimetric Analysis (TGA)

In order to determine the degradation process and the pigment content of each of the coatings applied at different voltages, thermogravimetric tests were carried out. To do so, a Setaram thermogravimetric analyzer (TGA) was used. The samples were obtained by peeling back the coating from the steel substrate. Samples between 15 and 20 mg were scanned up to 900ºC at 10 $K \cdot min^{-1}$. All scans were performed with an argon flow of 50 $cm^3 \cdot min^{-1}$.

2.2.2. Differential scanning calorimetry (DSC)

A Perkin Elmer DSC7 differential scanning calorimeter was employed for dynamic scans in order to measure the T_g of coatings applied under different cathodic voltages. The DSC was calibrated with a high purity indium sample. The samples were peeled back form the steel substrates and weighed from 8 to 12 mg. A flow of 20 $cm^3 min^{-1}$ of argon was used as purge gas. DSC scans at 10ºCmin^{-1} were performed on cured primers to determine the midpoint T_g.

2.2.3. Electrochemical impedance spectroscopy (EIS)

Electrochemical Impedance Spectroscopy (EIS) tests were carried out on coated samples exposed to 3.5% NaCl (by weight) in deionised water for periods up to three months. The three-electrode electrochemical cell was obtained by sticking a glass cylinder on the sample sheet and filling it with the test solution. The exposed surface area was 16.6 cm^2. A carbon sheet acted as the counter electrode and an Ag/AgCl electrode was used as the reference one.

The AC impedance data were obtained at the free corrosion potential using an AUTOLAB PGSTAT30 potentiostat and a frequency response analyser. The impedance tests were carried out over a frequency range of 100 kHz down to 1 mHz using a sinusoidal voltage of 10 mV as amplitude inside a Faraday cage in order to minimise external interferences on the system. The impedance spectrum was analyzed using Z-view software.

The equivalent circuit model, shown in Figure 1, was employed to analyze the EIS spectra. The circuit consisted of a working electrode (metal substrate), a reference electrode (Ag/AgCl), electrolyte resistance R_s, pore resistance R_{po}, constant phase element of the coating capacitance CPE_c, polarisation resistance R_p and constant phase element of the double layer capacitance CPE_{dl}.

Fitting the EIS data to the circuit determined the values of the equivalent circuit elements. The chi-squared parameter of the fit was usually below 0.1. When modelling the equivalent circuit with CPE, the software gives values of capacitance in units s^n/Ω together with a parameter known as “n”. When n is close to 1 (ideal capacitor), it can be considered that the values of capacitances given by the software match with the effective capacitances (ideal). Thus, it is not necessary to calculate the effective capacitances, and results can be interpreted as capacitances but with units s^n/Ω instead of those for effective/real capacitances (s/Ω or F).

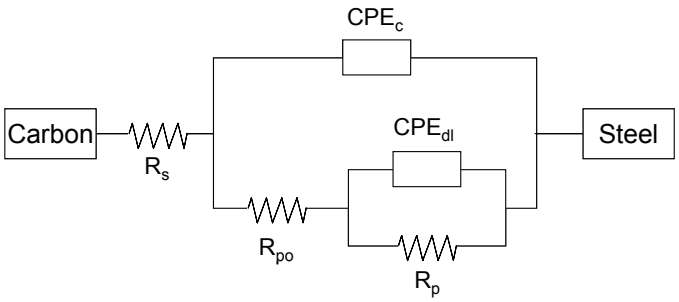

Fig. 1. Equivalent circuit used to model EIS and AC/DC/AC impedance data where passive parameters (R_s = electrolyte resistance, CPE_c = constant phase element of the coating capacitance, CPE_{dl} = constant phase element of the double layer capacitance, R_{po} = pore resistance, R_p = polarization resistance) can be defined.

2.2.4. AC/DC/AC test

The AC/DC/AC procedure consists in a combination of DC and AC measurements. First, an AC test is applied to the sample under the same conditions as described above in EIS. This measurement also allows knowing the impedance modulus of the tested sample. Following the first AC measurement, the test sample is treated for a short time with a constant cathodic voltage (–4V) for 20 minutes (DC conditions in order to force the production of H_2 and produce the degradation of the coating). After that, a registration of the system's open circuit potential variation with time was performed (relaxation time) until the sample reaches a new steady state and the potential is once more stabilised. In this case, the relaxation time was of 3 hours. Finally, a new EIS measurement (AC) is made to the sample in order to determine the new impedance modulus of the system. A schematic representation of the AC/DC/AC procedure is shown in Figure 2.

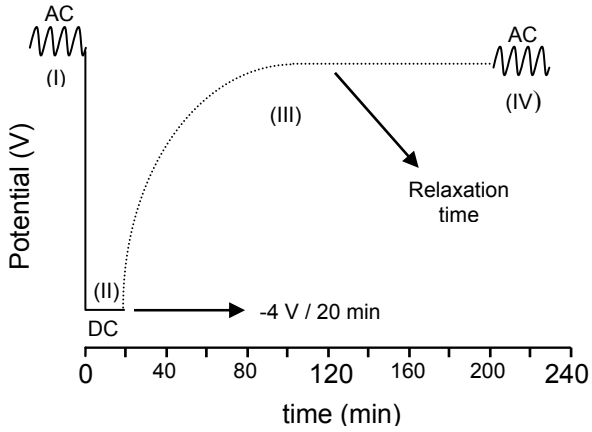

Fig. 2. AC/DC/AC test schematic figure versus time.

This test sequence is repeated at least 6 times, which means that almost 24 hours are needed for this purpose. The AC/DC/AC procedure was absolutely automated in PSTAT 30 AUTOLAB equipment.

Experimental results obtained in EIS measurements (AC) were modelled using the equivalent circuit shown in Figure 1 and with the same procedure as described above.

2.2.5. Equivalent circuit interpretation

It is generally assumed that there is a correlation between the elements of the equivalent circuit and the corrosion properties of the system [29].

Pore resistance R_{po} is a measure of the porosity and deterioration of the coating. R_{po} values have usually been related to the number of pores or capillary channels perpendicular to the substrate surface through which the electrolyte reaches the interface [30]. Although R_{po} can also increase with immersion time, probably as a result of pore or defect blockage by corrosion products, it usually decreases. Some authors, as Walter [31, 32], have found three regions in the time-dependent trend of R_{po}. It initially decreases rapidly, then slowly (displaying a plateau) and then rapidly again, coinciding with the appearance of the second semi-circle. The plateau is explained by making the assumption that the number of pathways formed is approximately constant with time.

C_c is the capacitance of the coating and this should be a measure of the permeation of water into the coating and is given by:

$$C_c = \varepsilon\varepsilon_0 A/d \quad (6)$$

where ε is the dielectric constant of the coating, ε_o is the vacuum permittivity, *A* is the area of the coating exposed to the electrolyte and *d* is the thickness. The coating capacitance will usually change during electrolyte absorption because the dielectric constant of water is approximately twenty times greater than that of a typical coating.

C_c usually increases at the initial stage of exposure and seems to be a measure of water absorption. When the coating has been exposed for a long time, it can be correlated to disbonding and deterioration.

The polarisation resistance R_p and double layer capacitance C_{dl} are two parameters used to specify the disbonding of the top coat and the onset of corrosion at the interface. The specific polarisation resistance is associated with the charge transfer behaviour of the metal substrate. R_p, like C_{dl}, can only be calculated well when at least two time constants are evident in the spectrum.

C_{dl}, the double layer capacitance, is a measure of the area over which the coating has disbonded. It can only be correctly measured at advanced stages of coating deterioration. The trend of C_{dl} is complex. A change in the C_{dl} value can be associated with the competition between disbonding and corrosion product accumulation at the interface. The C_{dl} value increases as water spreads at the interface and the delaminated area extends. On the other hand, the accumulation of corrosion products at the interface reduces the area of the double layer capacitor, which will lead to a decrease in the C_{dl} value. Therefore, the change of trend in C_{dl} may depend on which factor, disbonding or corrosion product accumulation, was more dominant during the corrosion process. However, it should be pointed out that both the increase and the decrease in C_{dl} are the results of the development of corrosion at the metal surface, while a constant C_{dl} is an indication of a stable interface [33].

2.2.6. Accelerated cyclic test

These kind of accelerated tests are mostly used in industries in order to study the anticorrosive properties of coatings. In this study, one accelerated cyclic test was carried out in order to study the correlation of electrochemical tests (EIS and AC/DC/AC) with the accelerated cyclic test used in the industry. It consisted on three consecutive steps, which were:

(1) Four hours in a salt fog chamber, in accordance with ASTM B117.
(2) Four hours at ambient exposure (temperature 18-28ºC and relative humidity 40-60%), in accordance with DIN 50014-23 / 50-2.
(3) Sixteen hours in humidity chamber at 40±3ºC and 100% relative humidity, in accordance with DIN 50017KK.

Coated samples were scribed through the paint down to the bare metal before testing them. The scribe marks were made at right angles to form a 6 x 6 cm cross.

The samples were evaluated after 40 cycles of exposure (repeating the three steps) by considering two parameters:

(1) Corrosion: normally determined by measuring the distance between the centre of the scribed line and the furthest points where the cataphoretic coating had been delaminated.
(2) Blistering: typically determined by measuring the distance between the centre of the scribed line and the furthest points where the cataphoretic coating had been damaged by blistering.

3. Results and Discussion

3.1. Thermogravimetric Analysis (TGA)

Figure 3 shows thermogravimetric analysis results for cured coatings deposited at different cathodic voltages (220, 245, 295, 320 and 345V).

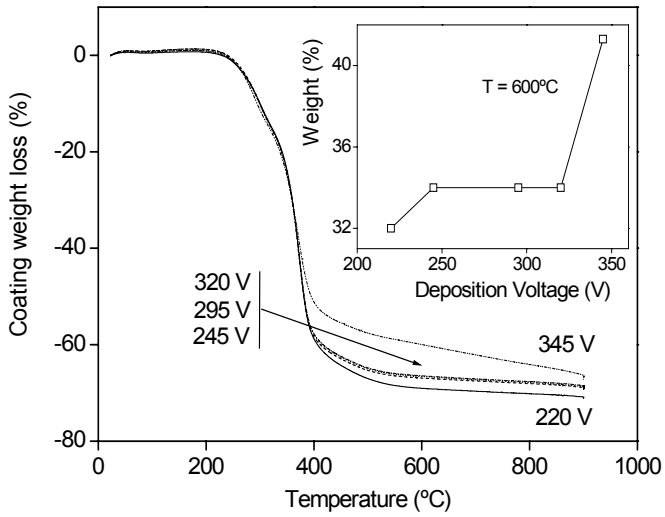

Fig. 3. TG signal (percentage of coating weight loss) versus temperature of samples cataphoretically deposited at different voltages. Percentage of weight of samples at 600ºC versus deposition voltage.

There is almost no change in weight loss until 210ºC. Yet, between 210 and 600ºC weight loss becomes significant (TG signal decreases), which corresponds to epoxy resin (used as a binder) degradation.

It can be seen quite clearly that the spectra of the coatings deposited at the different voltages are quite similar and that, as the cathodic voltage increases it is detected higher weight (around 32% for 220V, 34% for 245, 295 and 320V and finally 41% for 345V at 600ºC), meaning less degradation with temperature. It seems that as the deposition voltage increases, the resin micelles which migrate towards the cathode, are able to transport more and more pigments to the metallic substrates. There is a range of voltages (245-320V) where the change in voltages does not produce a variation in the final pigment content of the coating. Raising the voltage over 320V (345V), increases the quantity of pigment in the coating.

3.2. Thermal Analysis (DSC)

It can be seen in Figure 4 that the T_g value varied with the deposition voltage used in the cataphoretic process, decreasing as the deposition voltage increases.

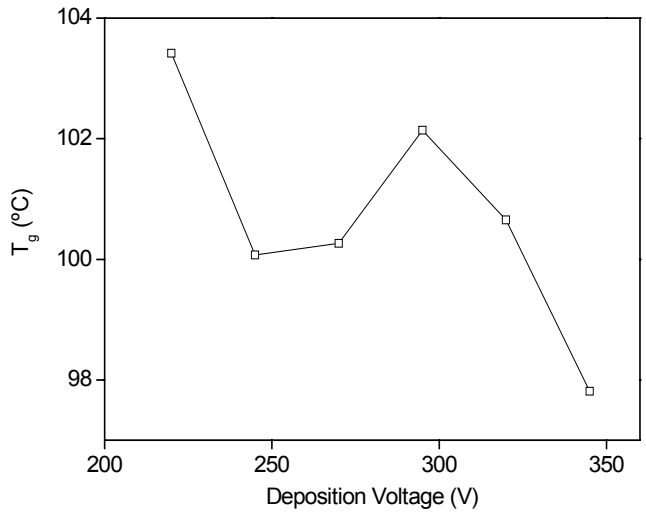

Fig. 4. Glass transition temperature versus deposition voltage.

It is well known that the T_g of an epoxy system increases with cross-linking density as the curing reaction progresses [34, 35], so T_g is a good indicator of the curing degree reached by the system. This is especially true in the last stages of the reaction, when, in other thermal tests (like isothermal or dynamic scans), the heat flow signal is below the sensitivity of the apparatus [36].

As observed in the results, T_g does not change too much when deposition voltages are within the 245-320V range. When cathodic voltage is below this range (220V), there is an increase in T_g which can be correlated with a higher cross-linking density. If the deposition voltage increases above 320V, T_g drops almost 3ºC, which reflects a decrease in cross-linking density. One possible reason for this behaviour is that, as primers are deposited with higher deposition voltages, the pigment content in the coating is also higher and a trapping effect exerted by the pigments can reduce the mobility of the molecules of the reactive system. This decreases the probability of an encounter between the epoxy resin and the curing agent species, which gives rise to a proportional increase in viscosity of the medium. Regions where epoxy and cross-linking agent groups remain non-reactive can thus be formed in the bulk material and then exert a plasticizing effect and reduce T_g [37-39].

3.3. Electrochemical Impedance Spectroscopy (EIS)

Figure 5 shows a Bode plot representing the impedance response (impedance modulus Z and phase angle) versus frequency for coatings deposited at different deposition voltages and after 100 days' exposure to electrolyte. As can be observed, the coatings deposited at low voltages (220 and 245V) have a lower impedance modulus at low frequencies than coatings deposited at higher ones. On the other hand, the coating deposited at the highest voltage (345V) has a lower impedance than those deposited at 295 and 320V. Coatings deposited in the 295-320V range have the best performance, showing capacitive response over the entire frequency interval.

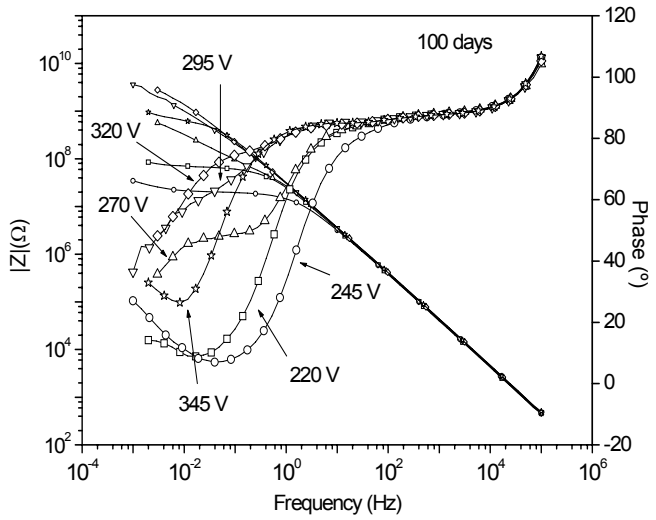

Fig. 5. Bode plot (impedance modulus and phase angle versus frequency) for primers applied with different voltages (V): 220 (□), 245 (O), 270 (Δ), 295 (∇), 320 (◊) and 345 (☆) applied on metal substrates after 100 days' exposure to electrolyte (deionised water with 3.5% NaCl by weight). EIS test.

Figure 6 (a, b, c) shows the equivalent circuit parameters modelled for EIS results and corresponding to pore resistance R_{po}, polarization resistance R_p and double layer capacitance C_{dl}. Results of coating capacitance C_c are not shown because they present slight differences between samples and an almost constant value over the exposure time interval of $4 \cdot 10^{-9}$ s^n/Ω. It can also be seen that coatings in the 295-320V range of voltages had the best anticorrosion properties, with the maximum R_{po} and R_p, and minimum C_{dl}. If the deposition voltage is under 270V (220 and 245V), the primer/metallic substrate interphase is more active (R_p is not stable and there is a small increase in C_{dl}, which means a greater tendency towards coating delamination). When using a deposition voltage over 320V (345V) anticorrosive properties slightly decrease.

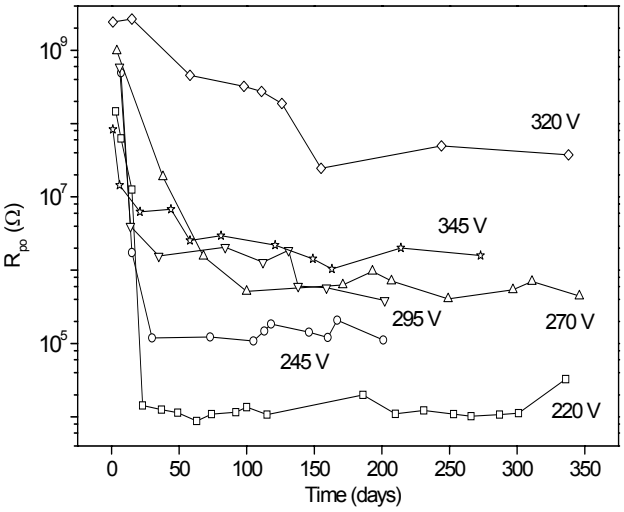

Fig. 6a. Evolution of pore resistance R_{po} versus time of exposure to electrolyte (deionised water with 3.5% NaCl by weight) for primers applied with different voltages: 220 (□), 245 (O), 270 (Δ), 295 (∇), 320 (◊) and 345 V (☆) applied on metal substrates. EIS test.

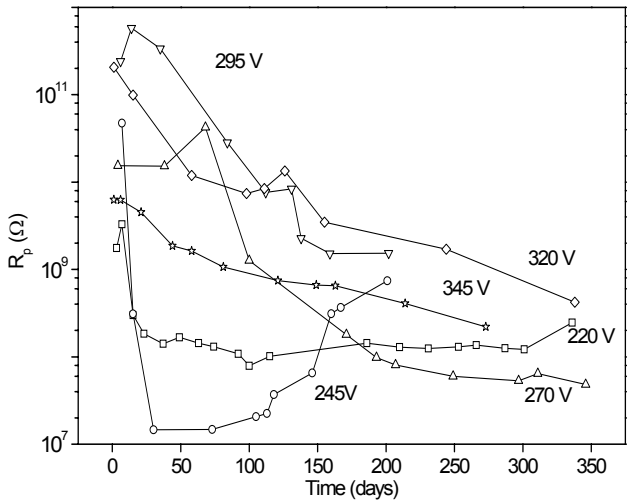

Fig. 6b. Evolution of polarisation resistance R_p versus time of exposure to electrolyte (deionised water with 3.5% NaCl by weight) for primers applied with different voltages: 220 (□), 245 (O), 270 (Δ), 295 (∇), 320 (◊) and 345 V (☆) applied on metal substrates. EIS test.

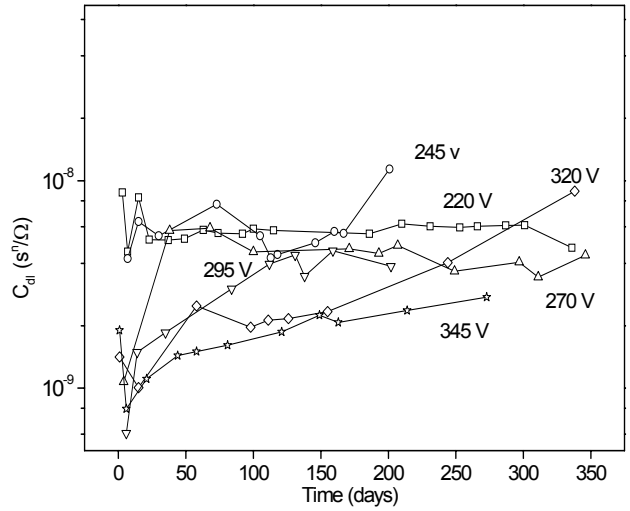

Fig. 6c. Evolution of double layer capacitance C_{dl} versus time of exposure to electrolyte (deionised water with 3.5% NaCl by weight) for primers applied with different voltages: 220 (□), 245 (O), 270 (Δ), 295 (∇), 320 (◊) and 345 V (☆) applied on metal substrates. EIS test.

If low voltages are used in the cataphoretic process, the electrolysis of water in the cathode is less vigorous and so the induction step will not take place so easily. This means that it will be more difficult for the resin micelles to migrate towards the cathode; there will be less production of OH^- (the pH increase in the region will be lower) and electrocoagulation of the resin micelles will be reduced because their neutralisation by OH^- ions will be more difficult.

As has been studied in this paper, the upper limit of the deposition voltage is set by a phenomenon called film rupture. If the deposition voltage increases, the current and Joule heat produced in the metallic surface also increases, which means higher temperatures at the interface. This increase in temperature can cause the evaporation of solvents and the release of the produced hydrogen, giving rise to pinholes.

This increase in temperature causes a partial premature baking, which reduces the final quality of the paint.

3.4. AC/DC/AC test

Figure 7 shows a Bode graph (impedance modulus and phase angle versus frequency) for coatings deposited at different voltages and after 4 cathodic polarisations. It can be observed that the results are very similar to those obtained by the EIS technique, showing that the maximum impedance modulus is obtained when the paint is deposited in the range of voltages 270-320V and how the impedance decreases significantly when low voltages (220 and 245V) are applied. The impedance modulus of a coating deposited at 345V is slightly lower than those found in the optimum range.

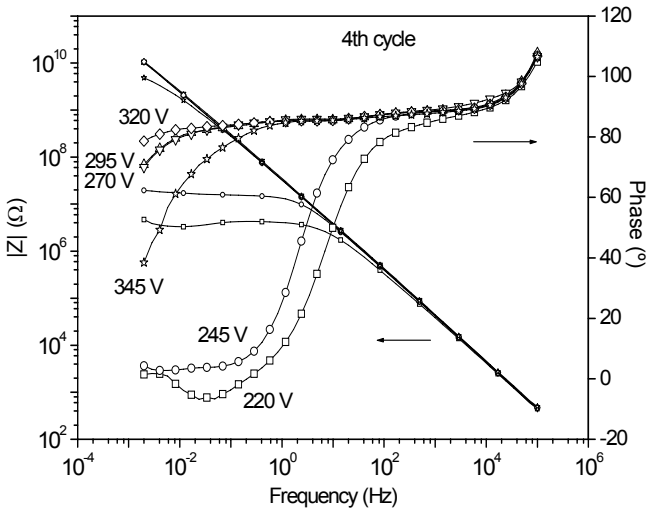

Fig. 7. Bode plot (impedance modulus and phase angle versus frequency) for primers applied with different voltages (V): 220 (□), 245 (O), 270 (Δ), 295 (∇), 320 (◊) and 345 (☆) applied on metal substrates after 4 cycles of cathodic polarisations. AC/DC/AC test.

Figure 8 (a and b) shows the Bode plots (impedance modulus and phase angle versus frequency) for a coating deposited at 220V, 8a corresponding to an EIS test performed over different intervals of time and 8b to the response of the sample after different cathodic polarisations. Figure 9 (a and b) shows the same Bode plots as Figure 8 but for a coating deposited at 320V. As can be seen in these Bode plots, coatings deposited at 220V do not have a very good anticorrosion performance and their impedance decreases with the time of exposure to the electrolyte and with the cathodic polarisations. The coating deposited at 320V is of very good quality and its impedance hardly changes with time or polarisations. The results from the two techniques concerning a very good performance coating (320V) and another of not such good quality (220V) largely coincide.

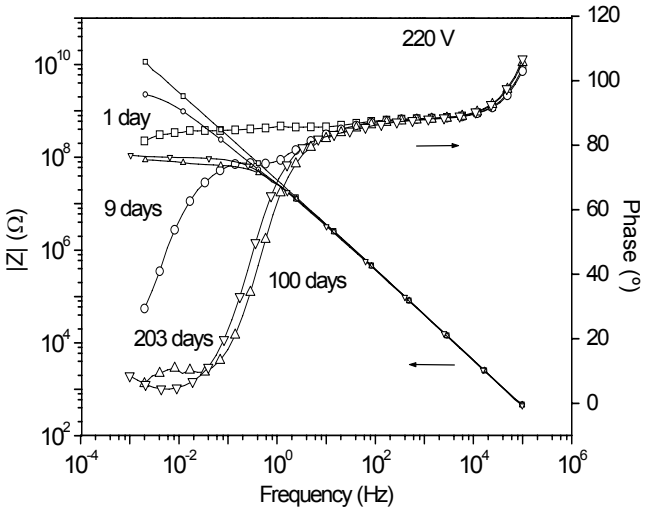

Fig. 8a. Bode plot (impedance modulus and phase angle versus frequency) for a primer applied at 220V over a metal substrate and after different exposure times: 1 (□), 9 (○), 100 (Δ) and 203 days (∇) to electrolyte (deionised water with 3.5% NaCl by weight). EIS test.

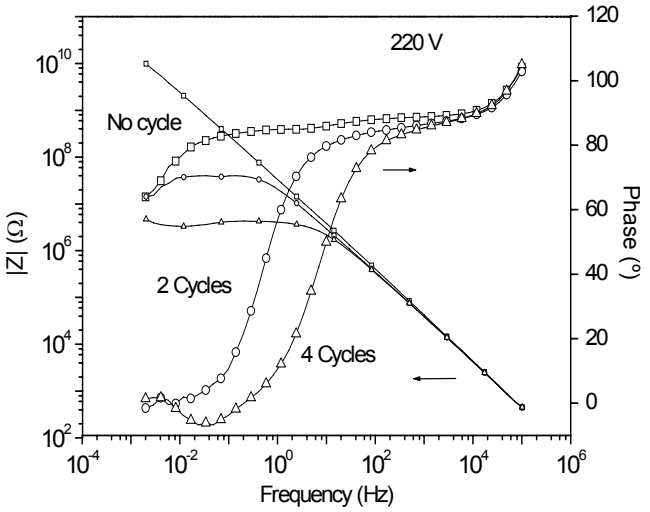

Fig. 8b. Bode plot (impedance modulus and phase angle versus frequency) for a primer applied at 220V over a metal substrate and after different cathodic polarisations: 0 (□), 2 (○) and 4(Δ). AC/DC/AC test.

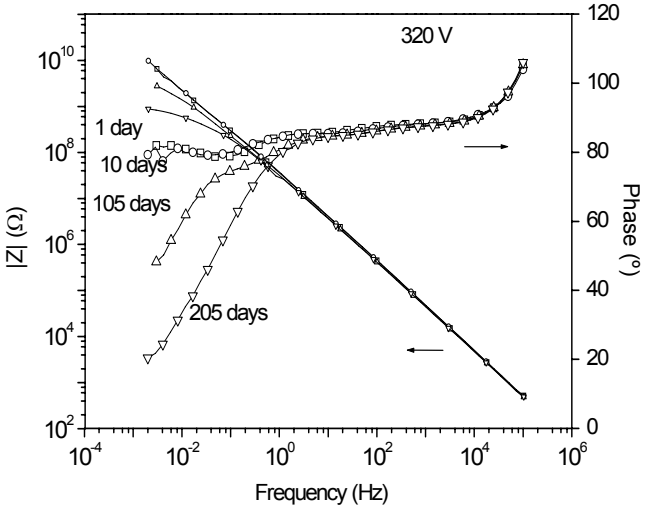

Fig. 9a. Bode plot (impedance modulus and phase angle versus frequency) for a primer applied at 320V over a metal substrate and after different exposure times: 1 (□), 10 (○), 105 (Δ) and 205 days (∇) to electrolyte (deionised water with 3.5% NaCl by weight). EIS test.

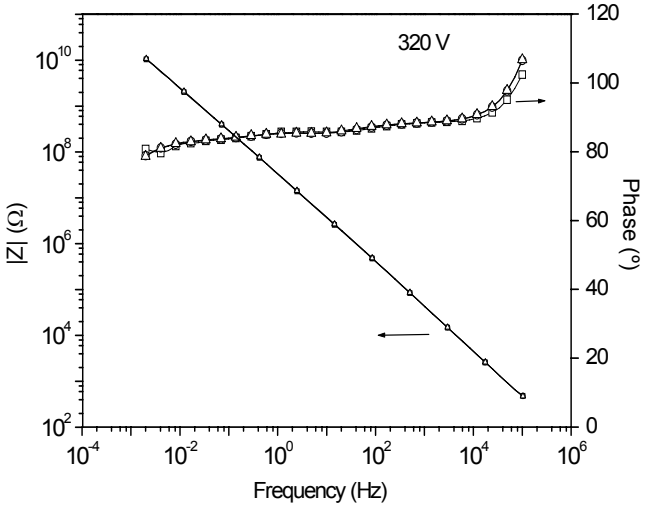

Fig. 9b. Bode plot (impedance modulus and phase angle versus frequency) for a primer applied at 320V over a metal substrate and after different cathodic polarisations: 0 (□), 2 (○) and 4(Δ). AC/DC/AC test

Figure 10 (a, b, c and d) shows the equivalent circuit modelled parameters for AC/DC/AC (4 cycles) and EIS (100 days) impedance results versus deposition voltage. It can clearly be seen that when the deposition voltage is in the 270-320V range, pores are less likely to be produced in the coating (high R_{po} values), the metallic surface is less active (higher R_p values and lower C_{dl}), and the cathodic polarisation gives rise to less primer delamination than when the voltage is below 270V or over 320V. When the deposition voltage is below 270V (220 and 245V), pore resistance decreases, the coating interphase is far more active and there is a strong increase in the coating delamination process. On the other hand, there is a strong correlation between results of AC/DC/AC and EIS tests obtaining the same conclusions with both techniques.

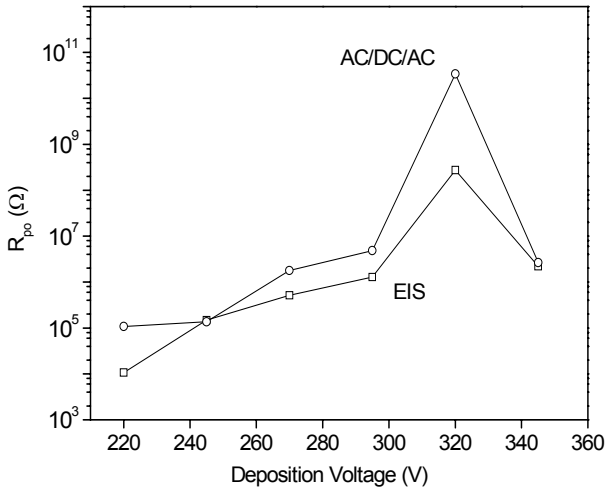

Fig. 10a. Evolution of pore resistance R_{po} versus the applied voltages. EIS (100 days) and AC/DC/AC test (4 cycles).

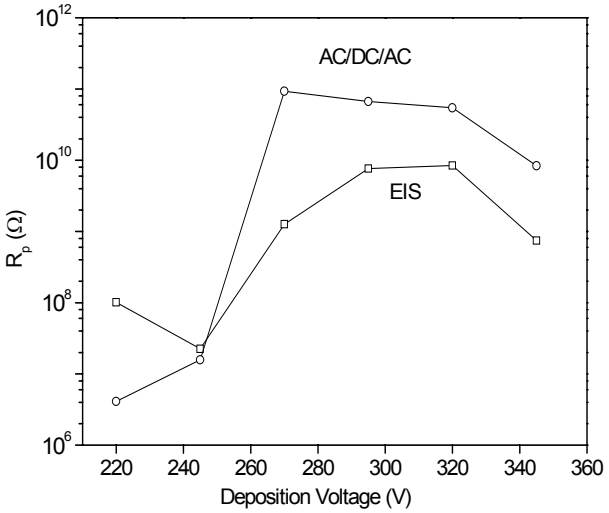

Fig. 10b. Evolution of polarisation resistance R_p versus the applied voltages. EIS (100 days) and AC/DC/AC test (4 cycles).

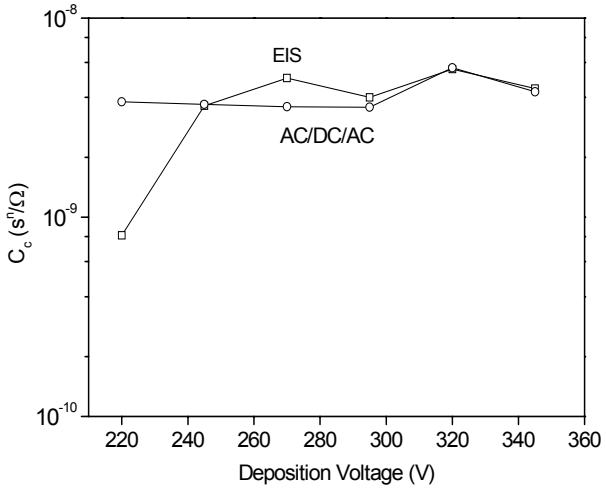

Fig. 10c. Evolution of coating capacitance C_c versus the applied voltages. EIS (100 days) and AC/DC/AC test (4 cycles).

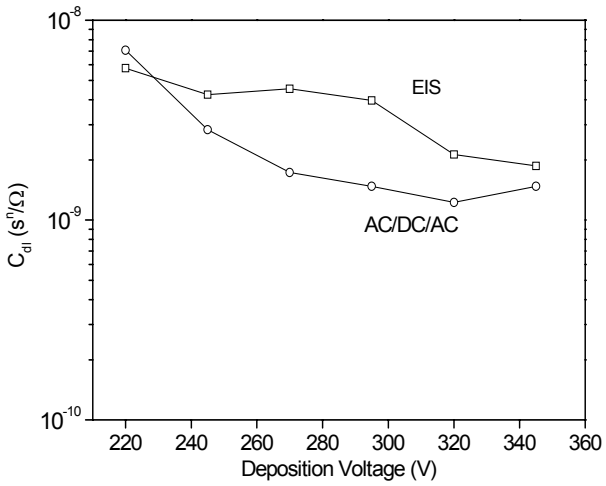

Fig. 10d. Evolution of double layer capacitance C_{dl} versus the applied voltages. EIS (100 days) and AC/DC/AC test (4 cycles).

In order to understand the AC/DC/AC technique, it is necessary to look at the theoretical basis underlying this method. The cathodic polarisation (DC) applied to the coated metal can cause the following to occur in the primer:

a. The introduction and passage of different cations (H^+, Na^+, and so on) from the electrolyte through the paint film due to the negative potential imposed in the metallic substrate. This can produce a concentration of positive charges in the primer that must be neutralised by balancing the entry of anions (like Cl^-). The passage of ions (which can also be hydrated) through the coating can cause its deterioration and the formation of pores.

b. The cathodic reaction that can take place in the metallic surface considering the level of negative polarisation and the type of electrolyte [40]:

$$2\ H_2O\ (l) + 2\ e^- \rightarrow H_2\ (g) + 2\ OH^-$$

The cathodic reaction will take place first if the electrolyte is able to pass through the coating and reaches the interface. This depends on the properties of the film (permeability to ions, adhesion to substrate, existence of areas of local film delamination, susceptibility of the coating to form cracks because of its high rigidity, and so on) and, of course, the applied voltage.

Obviously, the higher the quality of the primer is (impermeability and ductility of the film and high adhesion to the substrate) the lower the probability of the electrolyte reaching the interphase and of the cathodic reaction taking place will be.

The deterioration of the coating because of cathodic polarisations can be caused primarily by the film delamination process at the metallic interphase, if the cathodic reaction involving the production of H_2 (g) and OH^- finally takes place, although the passage of ions can also exert an effect.

If there are possibilities of detecting whether the cathodic reactions have taken place during polarisation, this information could be used to know a little more about the performance and quality of the primer. One possible way of detecting the existence of H_2 (g) and OH^- production (meaning more delamination) at the interphase, is to study the evolution of the open circuit potential after polarisation (during the relaxation time). When cathodic polarisation finishes, the coated metal potential will relax showing two possible spectra:

a. If cathodic reactions were taking place, the potential would have a quick relaxation around -1V [40] (with small variations depending on the coating), which corresponds to the ending of the reaction and, afterwards, a second relaxation that corresponds to ions and electrolyte leaving the coating. In any case, the cathodic reaction will produce the entry of electrolyte through the coating and the production of H_2 (g) and OH- in the metal/coating interface. The time needed for this electrolyte and the ions to leave the film will therefore be higher because they have to pass through the entire primer film.
b. If no cathodic reactions have taken place, there would be a single relaxation process that corresponds to ions and electrolyte leaving the primer. This relaxation will take place at longer times as ions and electrolyte penetrate deeper into the film, but they will probably need less time than in case “a” described above.

Figure 11 shows the potential relaxation versus time of the coatings deposited at different voltages (220, 245, 270, 295, 320 and 345V) after 6 cathodic polarisations. It can be clearly seen that there are two potential relaxation processes after polarisation: a fast one corresponding to the end of the cathodic reaction at short times, and a slower one at longer times, which corresponds to ions and electrolyte leaving the coating in primers deposited at 220, 245 and 345V. In the case of the curves corresponding to the lower voltages (220 and 245V), the second relaxation takes place at relatively long times. On the other hand, it can be seen how coatings deposited at the range of voltages 270-320V only present one very widely distributed relaxation.

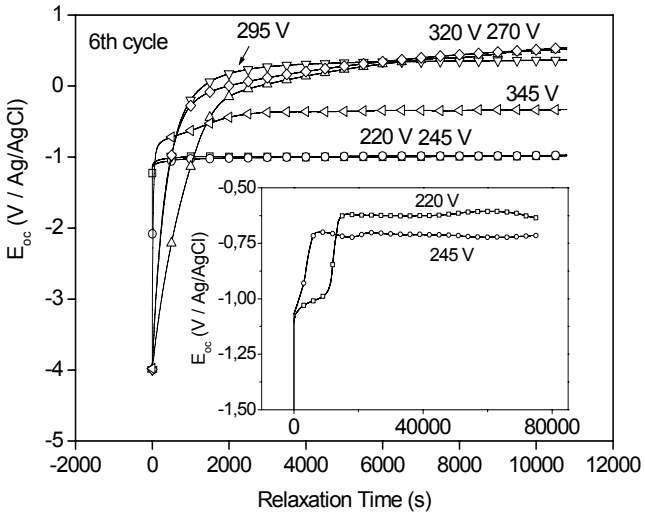

Fig. 11. Evolution of the open circuit potential (E_{OC}) versus relaxation time after exposure to 6 cathodic polarisations (AC/DC/AC test) for samples applied with different voltages: 220 (□), 245 (○), 270 (Δ), 295 (▽), 320 (◊) and 345V (☆).

Figure 12 represents the open circuit potential (E_{OC}) for a given time (10 000 seconds), where it is considered that the steady state has been attained versus different deposition voltages. In the optimum range of deposition voltage, the open circuit potential after stabilisation reaches its maximum value (especially at 270 and 320V) and decreases if any other voltage is used to deposit the coatings. Obviously, the E_{OC} must be higher as the coating film has fewer pores or cracks and is less delaminated (when it is more difficult for the electrolyte to reach the metallic substrate).

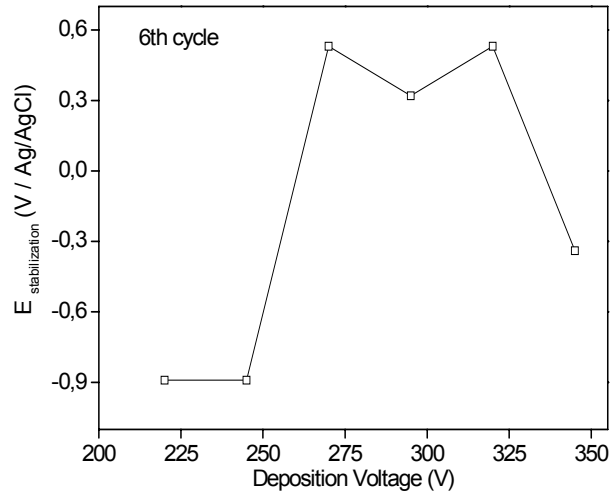

Fig. 12. Open circuit potential stabilisation value (at 10 000 seconds) after exposure to 6 cathodic polarisations (AC/DC/AC test) versus deposition voltage.

As can be seen, a coating with high anticorrosive properties will be that which only presents one relaxation process after cathodic polarisation (which means that the cathodic reaction of hydrogen and

OH^- production could not have taken place); very low potential relaxation times (ions can leave the coating very quickly because they have not penetrated very deeply into the film); high open circuit potential at the steady state; and, finally, with regard to the equivalent circuit parameters, high resistances and low capacitances. From this point of view, the optimum range of deposition voltages in the cathodic process that provided the maximum anticorrosive properties in the type of coatings that we have studied might be 270-320V.

3.5. Accelerated cyclic tests

Results of the accelerated test after 40 cycles are shown in figure 13. Blistering and oxidation are scaled from 0 to 10, where 0 is no blistering or delamination and 10 is great delamination and oxidation across the scribe. This type of test was not sensitive enough to be able to distinguish variations in these coatings. Some possible reasons are the high performance of the cataphoretic coatings and the fact that this kind of techniques is very subjective. No comparisons could be made with electrochemical tests due to the low sensitiveness of accelerated tests.

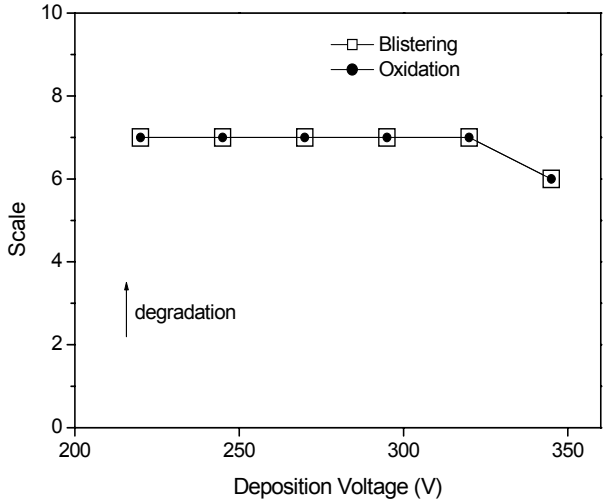

Fig. 13. Accelerated test graphic after 40 cycles exposure. Blistering and oxidation parameters. Scale 0-10, where 0 is minimum degradation and 10 maximum.

4. Conclusions

A cataphoretic epoxy primer was applied over a steel substrate at different voltages (220, 245, 270, 295, 320 and 345V) and studied by means of electrochemical methods (EIS and AC/DC/AC) as well as accelerated cyclic tests.

Results concerning the quality of primers obtained with the two electrochemical techniques were quite similar, although the AC/DC/AC test offered results in notably shorter times (1 day). Traditional accelerated tests were not sensitive enough to determine differences between the performances of the coatings and the influence of the deposition voltage.

The different results showed that, for this type of epoxy coating, the anticorrosive properties were enhanced when deposition voltage was in the 270-320V range, and decreased significantly when this voltage was under or over that range. The potential relaxation process after cathodic polarisation in the AC/DC/AC technique indicated that samples applied in the optimum range of deposition voltages did not degrade significantly with the test cycles and did not allow the cathodic reaction of H_2 (g) and OH^- production in the metal surface. On the other hand, coatings deposited at low voltages degraded with polarisation cycles and allowed H_2 (g) production cathodic reaction which produced delamination.

AC/DC/AC technique seems to be a good technique to characterise the anticorrosive performance of primers in short periods. It should therefore be highlighted that the test can be very useful as a method of industrial quality control and can be applied to complex procedures such as the formulation of anticorrosion primers. Nevertheless, more research in this field should be carried out in order to improve the technique and to have a better understanding of the different processes that take place during the test.

Acknowledgments

We would like to thank Ms Eva Romero, Miss Noelia Coll, Mr Eugeni Lozano, Mr Alfonso Pallares, Mr Ramón Novoa and Mr Juan Carlos Galvan for their help and collaboration in the development of this project. The authors are grateful for the economic support in this work of MAT 2000-0123-P4-03 project and to PPG Ibérica for supplying the samples.

---

1. J.J. Oravitz, Product Finishing Online, www.pfonline.com, February 1996
2. O. van der Biest, L.J. Vandeperre, *Annu. Rev. Mater. Sci.*, 29 (1999) 327
3. P.E. Pierce, *J. Coat. Tech.*, 53 (1981) 52
4. M. Ortner, *Plating*, 9 (1964) 885
5. K.M. Wernstahl, B. Carlsson, *J. Coat. Tech.*, 69, 865 (1997) 69
6. E. Almeida, I. Alves, C. Brites, L. Fedrizzi, *Prog. Org. Coat.*, 46 (2003) 8
7. J.J. Suay, M.T. Rodriguez, R. Izquierdo, A.H. Kudama, J.J. Saura, *J. Coat. Tech.*, 75, 945 (2003) 103
8. N. Vatistas, *Prog. Org. Coat.*, 33 (1998) 14
9. G.E.F. Brewer, R.F. Hines, *J. Paint Tech.*, 43 (1971) 71
10. W.B. Brown, *J. Paint Tech.*, 47 (1975) 43
11. F. Deflorian, L. Fedrizzi, S. Rossi, F. Buratti, P.L. Bonora, *Prog. Org. Coat.*, 39 (2000) 9
12. F. Mansfeld, *J. Applied Electrochem.*, 25 (1995) 187
13. G.P. Bierwagen, *J. Coat. Tech.*, 64 (1992) 71
14. B. Liu, Y. Li, H. Lin, C. Cao, *Acta Physico-Chimica Sinica.*, 17 (2001) 241
15. B.S. Skerry, C-T. Chen, C.J. Ray, *J. Coat. Tech.*, 64 (1992) 77
16. S. Gwori, K. Balakrishnan, *Prog. Org. Coat.*, 23 (1994) 363
17. M. Selvaraj, S. Guruviah, *Prog. Org. Coat.*, 28 (1996) 271
18. L.S. Hernández, B. del Amo, R. Romagnoli, *Anti-Corrosion Methods and Materials.*, 46 (1999) 198
19. X.Liu, H. Lu, J. Shao, P. Wan, S. Zhang, *Materials and Corrosion*, 46 (1995) 33
20. J. Hollaender, E. Ludwig, S. Hillebrand, *Proc. 5th International Tinplate Conference*, London, 300 (1992)
21. J. Hollaender, *Food additives and contaminants*, 14, 6-7 (1997) 617
22. J. Hollaender, C.A. Schiller, W. Strunz, *Proc. EIS 2001*, Marilleva-Italy (2001)
23. M.T. Rodriguez, J.J. Gracenea, J.J. Saura, J.J. Suay, *Prog. Org. Coat.*, 50 (2004) 68
24. J.J. Suay, M.T. Rodriguez, K.A. Razzaq, J.J. Carpio, J.J. Saura, *Prog. Org. Coat.*, 46 (2003) 121
25. M.T. Rodriguez, J.J. Gracenea, S.J. García, J.J. Saura, J.J. Suay, *Prog. Org. Coat.*, 50 (2004) 123
26. N.M. Acamovic, D.M. Drazic, V.B. Miskovic-Stankovic, *Prog. Org. Coat.*, 25 (1995) 293
27. P.E. Pierce, *J. Coat. Tech.*, 53 (1981) 32
28. P. Delahay, New Instrumental Methods in Electrochemistry, *Interscience Inc.*, New York (1954)

29. F. Mansfeld, *Electrochim. Acta*, 38 (1993)
30. A. Amirudin, D. Thierry, *Prog. Org. Coat.*, 26 (1995) 1
31. G.W. Walter, *J. Electroanal. Chem.*, 118 (1981) 259
32. G.W. Walter, *Corros. Sci.*, 26, 9 (1986) 681
33. N. Tang, W.J. Ooij, G. Górecki, *Prog. Org. Coat.*, 30 (1997) 255
34. J. Mijovic, *J. Appl. Polym. Sci.*, 3 (1986) 1177
35. D.J. Plazek, *J. Appl. Polym Sci.*, 24 (1986) 1303
36. G. Wisanrakkit, J.K. Gillham, J.B. Enns, *J. Appl. Polym. Sci.*, 4 (1990) 1895
37. M.F. Grenier-Loustatot, P Grenier, *Polymer,* 33 (1992) 6
38. J.J. Suay, M. Monleón, J.L. Gómez, *Polym. International*, 48 (1999) 1269
39. J.J. Suay, M. Monleón, J.L. Gómez, *Polym. Eng. & Sci.*, 40, 8 (2000) 1725
40. H. Leidheisser Jr., W. Wendy, L. Igefolt, *Prog. Org. Coat.*, 11 (1983) 19

Evaluation of cure temperature effects in cataphoretic automotive primers by electrochemical techniques

S. J. García[1], M. Rodríguez[1], R. Izquierdo[1], & J. Suay[2]

[1] Àrea de Ciència dels Materials i Enginyeria Metal·lúrgica, Departamento de Ingeniería de Sistemas Industriales y Diseño, Universitat Jaume I, Avda. Vicent Sos Baynat s/n, 12071 Castelló, Spain

[2] Centro de Biomateriales, Universitat Politècnica de València, Camino de Vera s/n, E-46071 Valencia, Spain

Corrosion Science XXX (2007) XXX
Enviado enero 2005. Bajo segunda revisión

Abstract

Companies producing organic coatings for the automotive industry frequently need to test newly formulated products or materials, habitually according to different production parameters, in order to determine their actual behaviour before large-scale production of the coating is implemented. Proper choice of the test for this characterization and the method of evaluation are critical. On the one hand, the choice is important because it is often necessary to distinguish coatings with very similar performance. On the other hand, results must be obtained in relatively short times, for it is impracticable for the manufacturers to wait for the completion of outdoor exposure tests. To reduce lead times in the development process, the use of accelerated aging tests to predict durability of the coating is essential (the time needed to perform them, however, is usually at least 500 hours). This article proposes the use of EIS and an electrochemical test, AC/DC/AC, which consists in a combination of impedance results and cathodic polarizations, in order to find out the performance of coatings with precision and in a very short time. These techniques have been used to determine the optimum range of curing temperatures of a primer in order to obtain the maximum anticorrosion properties. Results show very good degree of concordance between the two electrochemical tests, although the AC/DC/AC method is much faster.

1. Introduction

Protection against corrosion in automobiles is of great importance from the point of view of both the national economy and the private car owner. The automotive industry requires organic protective coatings with very high resistance to degradation. Coatings must protect the substrate against corrosion attack and keep it undamaged for a long time while at the same offering persistently good aesthetic properties, which means a high level of stability towards photo-oxidative degradation, mechanical abrasion and other harmful processes.

As is well known, the automotive sector has contributed on large scale to achieving compliance with increasingly restrictive environmental legislation in the field of surface treatments, above all in anticorrosive coatings. Today, it can be stated that the anticorrosive protection of almost all automobile bodywork includes a cataphoretic primer.

Although electrodeposition was introduced in the automotive industry in the 1960s, cathodic electrodeposition rapidly replaced anodic electrodeposition in the 1970s due to the greater anticorrosive protection that it conferred and to other film characteristics, which had never been attained with other techniques. At the beginning of the 1990s, cathodic systems were based on modified epoxy resins containing amino groups, systems which were described by Pierce [1]. These were dispersed in water by neutralizing the amino group with organic acids. The resins were cross-linked by blocked isocyanates. Pigmentation was based on titanium dioxide and extender pigments. Special lead-containing pigments, such as silicates, were used as anticorrosive agents, although lead was also used to catalyze the curing reactions. The first lead-free systems only came onto the market in the 1990s, coinciding with attempts to meet other challenges such as achieving reductions in the volatile organic solvent content and lowering the curing temperature [2-4].

The electrodeposition process is controlled by many parameters, such as mean applied voltage, rectified ripple voltage, anode-to-sample distance or temperature. All of these have an important effect on the final performance of primers. For example, it is well known that the ability of the cataphoretic process to deposit a film of paint in highly recessed areas increases with the deposition voltage, but the upper limit of the applicable deposition voltage is usually set by a phenomenon called film rupture, which causes blemishes [5-8].

It is also well known that the final properties of any thermoset resin depend on the curing process that is employed. In order to obtain good properties, cataphoretically deposited epoxy primers need to be cured at high temperatures but which, at the same time, are low enough not to damage any plastic components present in the bodywork to be painted. In predicting the interaction stability properties of the primer, the main problem arises from the complexity of the overall process itself. Due to this complexity, the main methods of interaction testing and material assessment were developed experimentally by using different exposure processes and techniques for the measurement of properties. The main types of exposure processes are the accelerated aging test and field exposure experiments (which must be planned for long times and are very expensive to run). Measurements of properties can be electrochemical, mechanical, chemical, and so on. Only if the exposure process and measurement test

are well defined and programmed will it be possible to obtain information about the coating deterioration process, reproducible results, and a time consumption that is not excessively long. Various electrochemical techniques have been used to evaluate the performance of organic coating/metal systems. The application of electrochemical impedance spectroscopy (EIS) to coated metals has proved to be a useful technique in the study of the corrosion performance of anticorrosive primers [9-16], although time is needed to perform this type of test because it takes days, weeks and sometimes months to obtain good results.

Therefore, there is still an explicit interest in rapid assessment methods for practical applications that provide a faster indication of corrosion processes in the surface of coated metallic substrates. Hollaender et al. [17-19] developed a rapid method for testing coated metals in food packaging consisting in a combination of DC and AC measurements (AC/DC/AC procedure) which has been successfully adapted and used by Suay, Rodríguez and García in liquid paints applied to steel substrates [20-22]. After a first AC measurement, the test sample is treated for a short time by a constant cathodic current (DC) and, following that, an AC spectrum is recorded again. The change in the characteristics of the impedance spectrum can be attributed to a coating deterioration (pore formation) and a delamination process in the metallic surface due to hydrogen and OH^- production (if a cathodic reaction takes place).

The present work focuses on: (I) the evaluation of the anticorrosive properties of an epoxide cathodic primer applied on steel substrates under the same conditions but cured in a given range of temperatures (145–195ºC) using different techniques; (II) the development of an electrochemical test procedure (AC/DC/AC) which can be applied to coated metals and offers results in a short time; and (III) comparing the different evaluation procedures applied to the coated metals in order to determine whether the conclusions offered by each of them coincide.

2. Experimental

2.1. Materials

A commercial anticorrosive epoxy coating (supplied by *Industrias PPG Ibérica* and with commercial reference “Lead Free Generation 6”) was cationically deposited on low-carbon steel substrates. Test panels (210 x 110 x 1 mm) were pre-treated by mechanical cleaning (polishing), degreased with a methyl-ethyl-ketone solution and rinsed with distilled water. Coatings were galvanostatically deposited for two minutes at the same deposition voltage (200V) in order to obtain 20 µm thick coatings. Anodes were placed parallel to the working electrode (steel panels) at a distance of 1.5 cm. The temperature of the electrolyte bath was kept at 30ºC throughout the whole cationic process. There was an anode/cathode area ratio of 1:4. The conditions of the cationic process, sample identification and curing conditions are summarised in Table 1. At least 5 samples were obtained under each condition. The composition of the cataphoretic bath was 47% of water, 45.3% of binder (adduct of cationic polyepoxydic resin (based on bisphenol-A) with polyamine cured with a polyurethane-based crosslinker) and 7.7% of pigments and charges.

When the painted samples were removed from the cationic bath, they were cured for 15 minutes at different temperatures, as shown in Table 1.

Table1. Identification and specifications (deposition potential, time of potential application, curing temperature and time) of the cataphoretically coated samples that were studied

Sample Identification	Deposition Voltage (V)	Time of voltage application (s)	Curing Temperature (ºC)	Curing time (min)
A	200V (needed to obtain primers 20μm thick)	120	145	15
B			155	
C			165	
D			175	
E			185	
F			195	

2.2. Testing Methods and Equipment

2.2.1. Differential Scanning Calorimetry (DSC)

A Perkin Elmer DSC7 differential scanning calorimeter was employed for dynamic scans in order to measure the vitreous transition temperature (T_g) of coatings cured at different temperatures. The DSC was calibrated with a high-purity indium sample. Test samples weighed from 6 to 8 mg. A flow of 20 $cm^3 \cdot min^{-1}$ of argon was used as a purge gas. DSC scans were performed at $10ºC \cdot min^{-1}$ on cured primers to determine the midpoint T_g.

2.2.2. Electrochemical impedance spectroscopy (EIS)

Electrochemical Impedance Spectroscopy (EIS) tests were carried out on coated samples exposed to 3.5% NaCl (by weight) in deionised water for periods up to three months. The three-electrode electrochemical cell was obtained by sticking a glass cylinder on the sample sheet and filling it with the test solution. The exposed surface area was 16.6 cm^2. A carbon sheet acted as the counter electrode and an Ag/AgCl electrode was used as the reference one.

The AC impedance data were obtained at the free corrosion potential using an AUTOLAB PGSTAT30 potentiostat and a frequency response analyser. The impedance tests were carried out over a frequency range of 100 kHz down to 1 mHz using a sinusoidal voltage of 10 mV as the amplitude inside a Faraday cage in order to minimise external interferences on the system. The impedance spectrum was analyzed using Z-view software.

The equivalent circuit model, shown in Figure 1, was employed to analyze the EIS spectra. The circuit consisted of a working electrode (steel substrate), a reference electrode (Ag/AgCl), electrolyte resistance R_s, pore resistance R_{po}, constant phase element of the coating capacitance CPE_c, polarisation resistance R_p and constant phase element of the double layer capacitance CPE_{dl}.

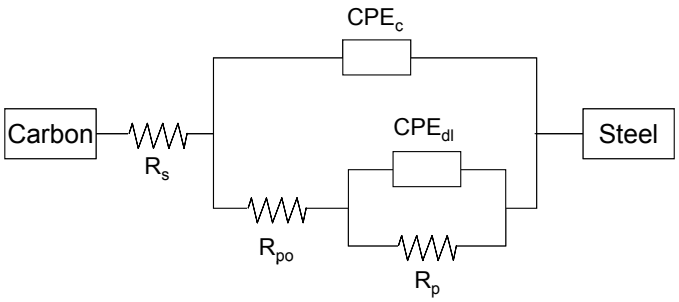

Fig. 1. Equivalent circuit used to model EIS and AC/DC/AC impedance data where passive parameters (R_s = electrolyte resistance, CPE_c = constant phase element of the coating capacitance, CPE_{dl} = constant phase element of the double layer capacitance, R_{po} = pore resistance, R_p = polarization resistance) can be defined.

Fitting the EIS data to the circuit determined the values of the equivalent circuit elements. The chi-squared parameter of the fit was usually below 0.1. When modelling the equivalent circuit with CPE, the software gives values of capacitance in units s^n/Ω together with a parameter known as "n". When n is close to 1 (ideal capacitor), it can be considered that the values of capacitances given by the software match with the effective capacitances (ideal). Thus, it is not necessary to calculate the effective capacitances, and results can be interpreted as capacitances but with units s^n/Ω instead of those for effective/real capacitances (s/Ω or F).

2.2.3. AC/DC/AC

The AC/DC/AC procedure consists in a combination of DC and AC measurements. First, an AC test is applied to the sample under the same conditions as described above in EIS. This measurement allows the present state of the test sample to be determined.

Following the first AC measurement, the test sample is treated for a short time with a constant cathodic voltage (–4V) for 20 minutes (DC) and, after that, it is registered the relaxation time of the sample until it reaches a new steady state and the potential is once more stabilised. In this case the relaxation time was of 3 hours. During that time, a registration of the system's potential variation with time was performed (relaxation time). Finally, a new EIS measurement (AC) is applied to the sample in order to determine the new present state. A schematic representation of the AC/DC/AC procedure is shown in Figure 2.

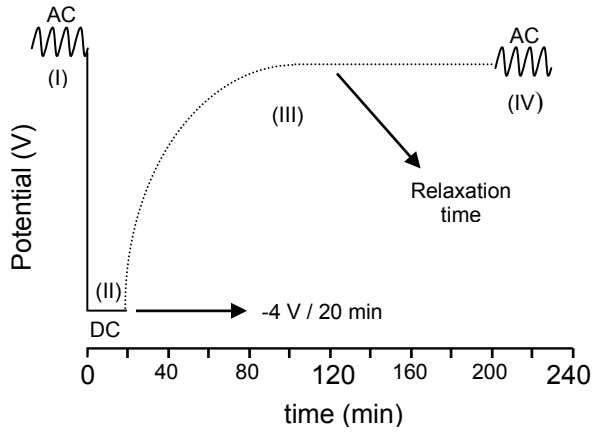

Fig. 2. AC/DC/AC test schematic figure versus time.

This test sequence is repeated at least 6 times, which means that almost 24 hours are needed for this purpose. The AC/DC/AC procedure is absolutely automated on PGSTAT 30 AUTOLAB equipment.

Experimental results obtained in EIS measurements are modeled using the equivalent circuit shown in Figure 1 and with the same procedure as described above.

2.2.4. Equivalent Circuit Interpretation

It is generally assumed that there is a correlation between the elements of the equivalent circuit and the corrosion properties of the system [23].

Pore resistance R_{po} is a measure of the porosity and deterioration of the coating. R_{po} values have usually been related to the number of pores or capillary channels perpendicular to the substrate surface through which the electrolyte reaches the interface [24]. Although R_{po} can also increase with immersion time, probably as a result of pore or defect blockage by corrosion products, it usually decreases.

Some authors, as Walter [25, 26], have found three regions in the time-dependent trend of R_{po}. It initially decreases rapidly, the slowly (displaying a plateau) and then rapidly again, coinciding with the appearance of the second semi-circle. The plateau is explained by making the assumption that the number of pathways formed is approximately constant with time.

C_c is the capacitance of the coating and this should be a measure of the permeation of water into the coating and is given by:

$$C_c = \varepsilon \cdot \varepsilon_0 \cdot A / d \quad (1)$$

where ε is the dielectric constant of the coating, ε_o is the vacuum permittivity, A is the area of the coating exposed to the electrolyte and d is the thickness. The coating capacitance will usually change during electrolyte absorption because the dielectric constant of water is approximately twenty times greater than that of a typical coating.

C_c usually increases at the initial stage of exposure and seems to be a measure of water absorption. When the coating has been exposed for a long time, it can be correlated to disbonding and deterioration.

The polarisation resistance R_p and double layer capacitance C_{dl} are two parameters used to specify the disbonding of the top coat and the onset of corrosion at the interface. The specific polarisation resistance is associated with the charge transfer behavior of the metal substrate. R_p, like C_{dl}, can only be calculated well when at least two time constants appear in the spectrum.

C_{dl}, the double layer capacitance, is a measure of the area over which the coating has disbonded. It can only be correctly measured at advanced stages of coating deterioration. The trend of C_{dl} is complex. A change in the C_{dl} value can be associated with the competition between disbonding and corrosion product accumulation at the interface. The C_{dl} value increases as water spreads at the interface and the delaminated area extends. On the other hand, the accumulation of corrosion products at the interface reduces the area of the double layer capacitor, which will lead to a decrease in the C_{dl} value. Therefore, the change of trend in C_{dl} may depend on which factor, disbonding or corrosion product accumulation, was more dominant during the corrosion process. However, it should be pointed out that both the

increase and the decrease in C_{dl} are the results of the development of corrosion at the metal surface, while a constant C_{dl} is an indication of a stable interface [27].

3. Results and Discussion

3.1. Thermal Analysis (DSC)

In Figure 3, the midpoint T_g trend with the curing temperature is shown. It can be observed that as the curing temperature increases, so does the T_g value.

It is well known that the T_g of an epoxy system increases with cross-linking density as the curing reaction progresses [28, 29], so T_g is a good indicator of the degree of curing reached by the system. This is especially true in the later stages of the reaction, when, in other thermal tests (like isothermal or dynamic scans), the heat flow signal is below the sensitivity of the apparatus [30].

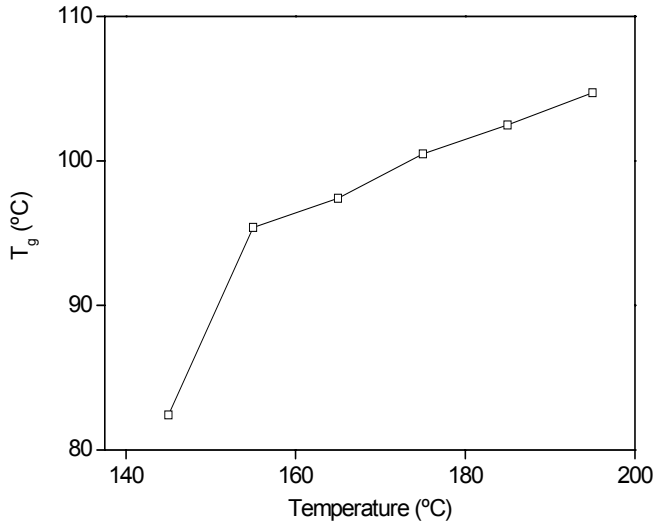

Fig. 3. Glass transition temperature (T_g) versus curing temperature.

It is also known that, as the curing temperature increases so does the cross-linking density and the T_g of the thermoset. This phenomenon is directly correlated with large changes in mechanical properties (as T_g becomes higher, the rigidity of the system and, as a consequence, also the brittleness increases). When the curing temperature is 145ºC, the T_g of the coating is especially low (82.4ºC). The cross-linking density will be much lower than in the other samples (cured at higher temperatures) and the free volume will be higher, thus increasing the molecular mobility of the polymer chains and making the film coating more permeable to ions and electrolyte.

3.2. Electrochemical impedance spectroscopy (EIS)

Figure 4 shows a Bode plot representing the impedance response (impedance modulus |Z| and phase angle) versus frequency for coatings cured at different temperatures and after 100 days' exposure to electrolyte.

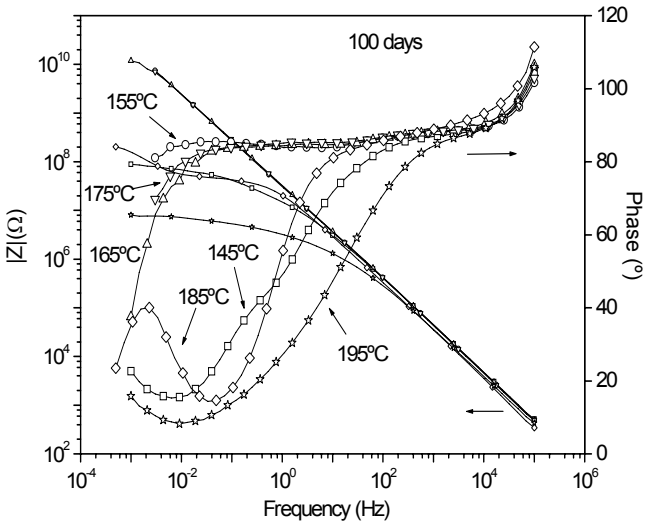

Fig. 4. Bode plot (impedance modulus and phase angle versus frequency) for samples of the primer cured at different temperatures (ºC): 145 (□), 155 (○), 165 (△), 175 (▽), 185 (◊) and 195 (☆) applied on metal substrates after 100 days' exposure to electrolyte (deionised water with 3.5% NaCl by weight). EIS test.

In this figure, two very clearly differentiated trends can be observed, one corresponding to the extreme temperatures (145, 185 and 195ºC) and the other one representing temperatures in the medium temperature range (155–175ºC). If we focus on the results obtained at low frequencies, we can see that samples cured in the medium range show a capacitive trend while the other three temperatures show a more resistive trend, meaning that they have poorer anticorrosive properties.

Figure 5 (a, b and c) shows the equivalent circuit parameters modelled for EIS results which correspond to pore resistance R_{po}, polarisation resistance R_p and double layer capacitance C_{dl}. Results of coating capacitance C_c are not shown because they present slight differences between samples and an almost constant value for the exposure time interval of $5 \cdot 10^{-9}$ s^n/Ω. These figures support the results shown in the Bode plot. Coatings cured in the range of temperatures 155–175ºC showed the best anticorrosion properties, with the maximum R_{po} and R_p, and minimum C_{dl}. If the curing temperature is under 155ºC (145ºC), the primer/metallic substrate interphase is more active (R_p is not stable and there is a significant increase in C_{dl}, which means a greater trend towards coating delamination). If curing temperatures over 175ºC are used, the anticorrosive properties decrease significantly, 195ºC being the curing condition that gives the poorest anticorrosive performance.

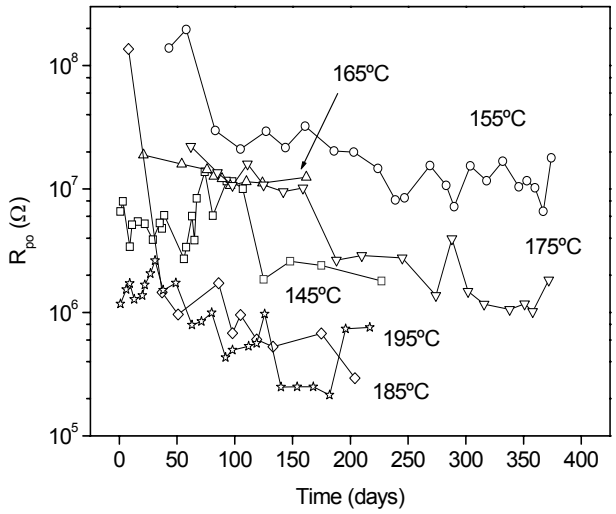

Fig. 5a. Evolution of pore resistance R_{po} versus time of exposure to electrolyte (deionised water with 3.5% NaCl by weight) for samples of the primer cured at different temperatures (ºC): 145 (□), 155 (O), 165 (Δ), 175 (∇), 185 (◊) and 195 (☆) applied on metal substrates. EIS test.

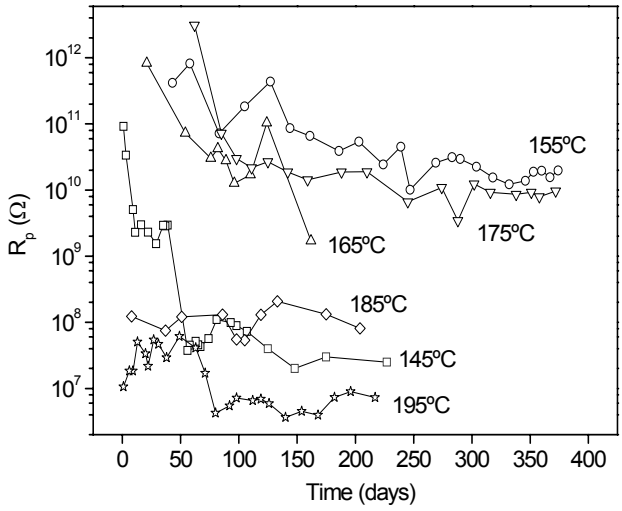

Fig. 5b. Evolution of polarisation resistance R_p versus time of exposure to electrolyte (deionised water with 3.5% NaCl by weight) for samples of the primer cured at different temperatures (ºC): 145 (□), 155 (O), 165 (Δ), 175 (∇), 185 (◊) and 195 (☆) applied on metal substrates. EIS test.

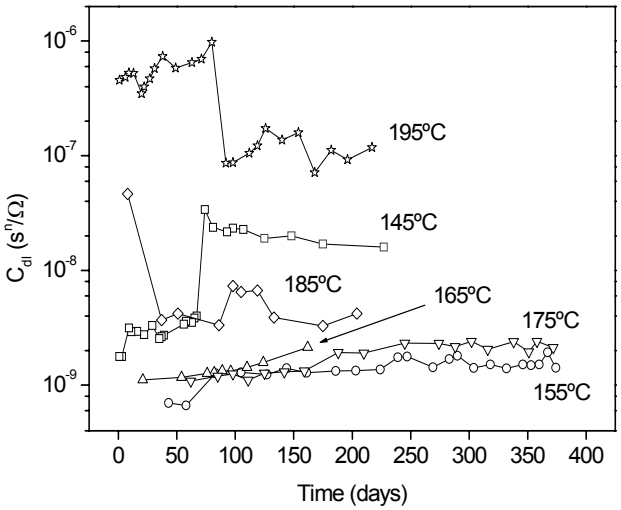

Fig. 5c. Evolution of double layer capacitance C_{dl} versus time of exposure to electrolyte (deionised water with 3.5% NaCl by weight) for samples of the primer cured at different temperatures (ºC): 145 (□), 155 (O), 165 (Δ), 175 (∇), 185 (◊) and 195 (☆) applied on metal substrates. EIS test.

When the curing temperature is very low (145ºC), the epoxy resin curing process is very slow, so the cross-linking density that is obtained is not high. The thermoset used as a binder will have a high free volume content that will allow the ions and reactive species to reach the interface, producing corrosion reactions in the metallic surface and, consequently, delaminating the coating. On the other hand, if the curing temperature is high (195ºC), the curing is very fast, thus giving higher cross-linking densities than those obtained for other temperatures, although the primer will be more brittle and fragile. Adherence to the metallic surface can be locally reduced because of the applied stress. Stress can be developed during the curing process because of the strong shrinkage of the film coating produced by a fast cross-linking process, the existence of thermal cycles suffered by the primer during the service conditions, water absorption, the presence of corrosion products in the metallic surface, and so on. If the primer is rigid and there are stresses applied to it, there will probably be coating delamination and the development of cracks in some areas of the interface. These are the reasons why the anticorrosive properties will be lower.

As has been shown, increasing the curing temperature will have benefits (less permeable coating film because of free volume reduction) and disadvantages (stresses can produce local delaminations and cracks because of the high rigidities) on the performance of anticorrosion primers. We can therefore expect there to be an optimum value (or an optimum range) of the curing temperature that will provide the best properties in the primer.

3.3. AC/DC/AC

Figure 6 shows a Bode graph (impedance modulus and phase angle versus frequency) for coatings cured at different temperatures and after 3 cathodic polarisations. It can be observed that results are very similar to those obtained by the EIS technique. Findings show that the maximum impedance modulus is obtained when the paint is cured in the range of temperatures 155 to 185ºC and that the impedance

decreases significantly when the primer is cured at a low temperature (145ºC) or a very high one (195ºC).

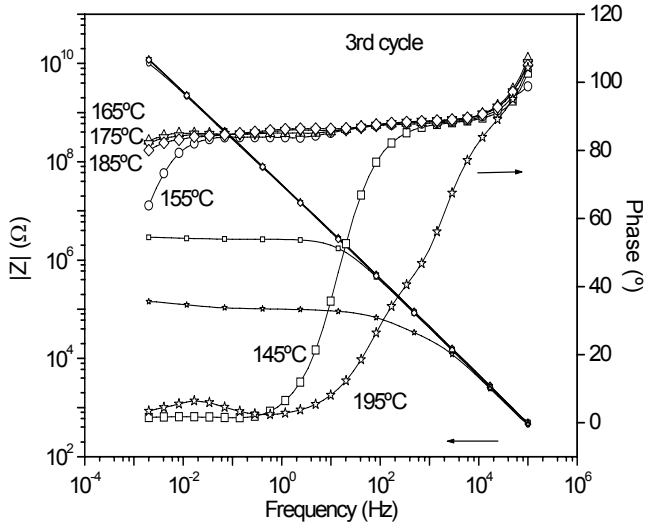

Fig. 6. Bode plot (impedance modulus and phase angle versus frequency) for samples of the primer cured at different temperatures (ºC): 145 (□), 155 (O), 165 (Δ), 175 (∇), 185 (◊) and 195 (☆) applied on metal substrates after three cathodic polarisations. AC/DC/AC test.

Figure 7 (a and b) shows the Bode plots for a coating cured at 165ºC, tested by EIS performed during 5, 54 and 110 days (Fig. 7a) and by AC/DC/AC test after three different cathodic polarisations (Fig. 7b). Figures 8 (a and b) show the same kind of Bode plots as those in Figure 7 but for a coating cured at 145ºC. As can be seen in these Bode plots, coatings cured at 145ºC do not have a very good anticorrosion performance and its impedance decreases with the time of exposure to electrolyte and also with the cathodic polarisations. In the case of the coating cured at 165ºC, it has a very good anticorrosion quality as can be seen in its impedance modulus, which remains almost unchanged with time or polarisations. Results of the two techniques for a coating with very good performance and another with not such good quality largely coincide.

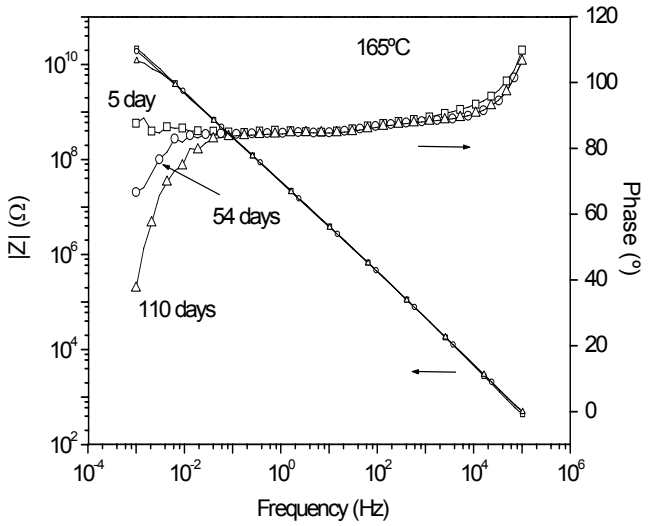

Fig. 7a. Bode plot (impedance modulus and phase angle versus frequency) for a primer cured at 165ºC and after different exposure times: 5 (□), 54 (O) and 110 days (Δ) to electrolyte (deionised water with 3.5% NaCl by weight). EIS test.

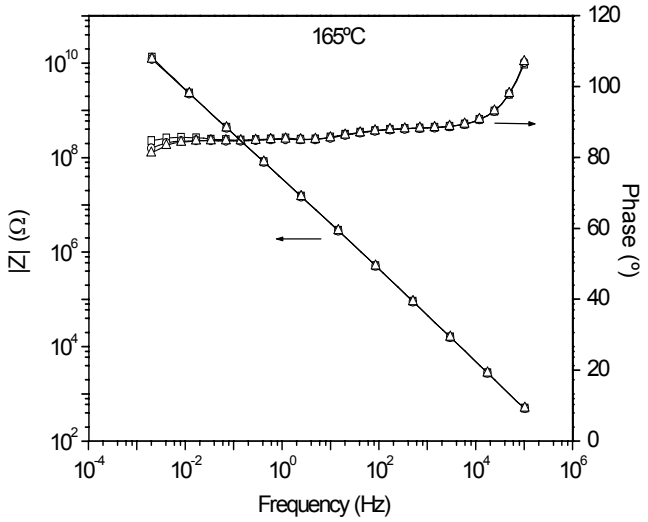

Fig. 7b. Bode plot (impedance modulus and phase angle versus frequency) for a primer cured at 165ºC and after different cathodic polarisations: 0 (□), 2 (O) and 4(Δ). A/DC/AC test.

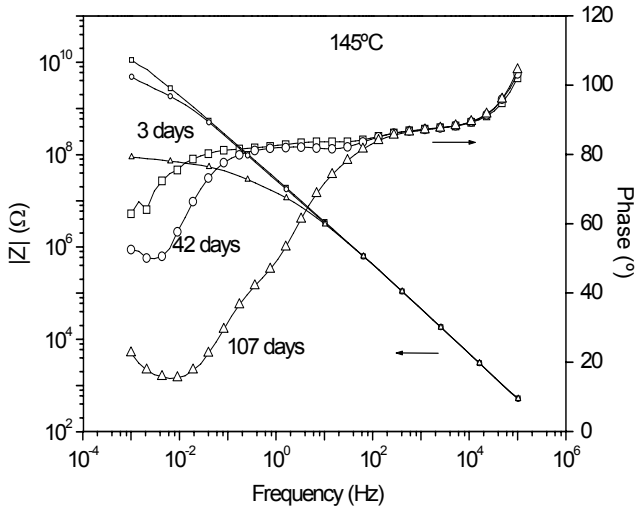

Fig. 8a. Bode plot (impedance modulus and phase angle versus frequency) for a primer cured at 145ºC and different exposure times: 3 (□), 42 (O) and 107 days (Δ) to electrolyte (deionised water with 3.5% NaCl by weight). EIS test.

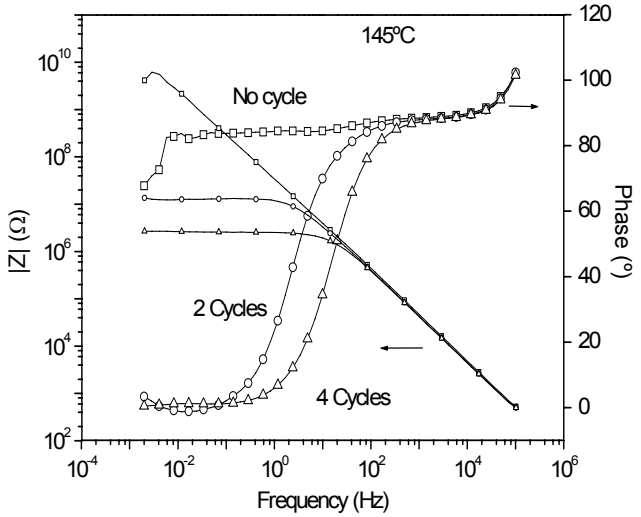

Fig. 8b. Bode plot (impedance modulus and phase angle versus frequency) for a primer cured at 145ºC and after different cathodic polarisations: 0 (□), 2 (O) and 4(Δ). A/DC/AC test.

Figure 9 (a, b, and c) shows the equivalent circuit modelled parameters for AC/DC/AC and EIS impedance results versus curing temperature. Results of coating capacitance C_c are not shown because they present slight differences between samples and an almost constant value for the exposure time interval of $5 \cdot 10^{-9}$ F/cm^2 and exactly the same shape for AC/DC/AC and EIS tests. It can clearly be seen that when the coating is cured in the 155–185ºC range, pores are less likely to be produced in the coating (high R_{po} values), the metallic surface is less active (higher R_p values and lower C_{dl}), and the cathodic polarisation gives rise to less primer delamination than when the temperature is below 155ºC or over 185ºC. With these extreme temperatures, pore resistance decreases, the coating interphase is far more active and there is a strong increase in the coating delamination process (there is a 5 orders of magnitude decrease in the double layer capacitance). On the other hand, there is a strong correlation

between results from the AC/DC/AC and EIS tests, the same conclusions being obtained with both techniques.

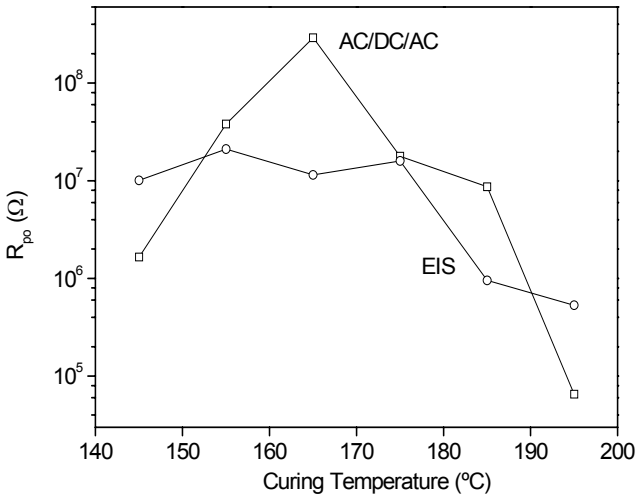

Fig. 9a. Evolution of pore resistance R_{po} versus the curing temperature (ºC): 145 (□), 155 (O), 165 (Δ), 175 (∇), 185 (◊) and 195 (☆). EIS (after 110 days of exposure to electrolyte) and AC/DC/AC test (after 5 cathodic polarisations).

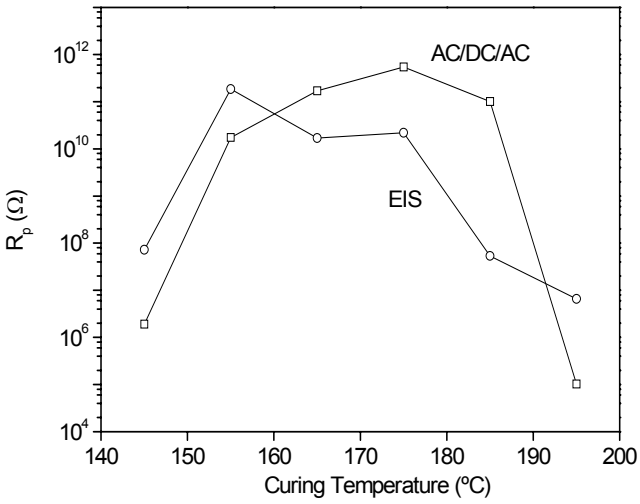

Fig. 9b. Evolution of polarisation resistance R_p versus the curing temperature (ºC): 145 (□), 155 (O), 165 (Δ), 175 (∇), 185 (◊) and 195 (☆). EIS (after 110 days of exposure to electrolyte) and AC/DC/AC test (after 5 cathodic polarisations).

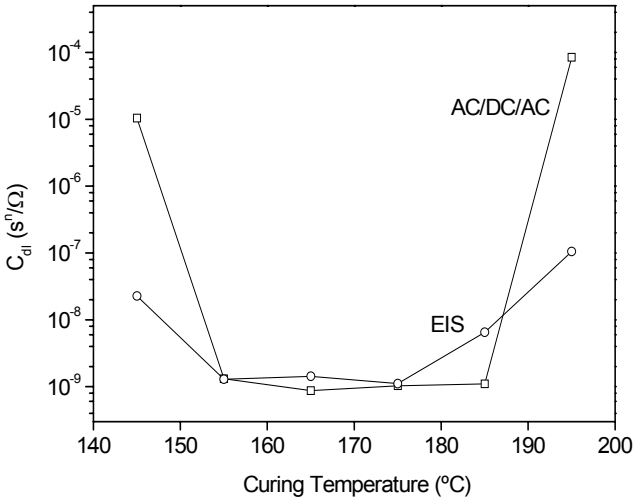

Fig. 9c. Evolution of double layer capacitance C_{dl} versus the curing temperature (ºC): 145 (□), 155 (O), 165 (Δ), 175 (▽), 185 (◊) and 195 (☆). EIS (after 110 days of exposure to electrolyte) and AC/DC/AC test (after 5 cathodic polarisations).

The main difference between the two electrochemical techniques (EIS and AC/DC/AC) is that in the second one a stress is applied to the coating before measuring the impedance of the system. In our case, the stress is a cathodic polarisation which can cause the following to occur in the system:

a. The introduction and passage of different cations (H^+, Na^+, and so on) from the electrolyte through the paint film due to the negative potential imposed in the metallic substrate. This can produce a concentration of positive charges in the primer that must be neutralised by balancing the entry of anions (like Cl^-). The passage of ions (which can also be hydrated) through the coating can cause its deterioration and the formation of pores.

b. The cathodic reaction that can take place in the metallic surface, considering the level of negative polarisation and the type of electrolyte [31]:

$$2\ H_2O\ (l) + 2\ e^- \rightarrow H_2\ (g) + 2\ OH^-$$

The cathodic reaction will take place first if the electrolyte is able to pass through the coating and reaches the interface. This depends on the properties of the film (permeability to ions, adhesion to substrate, existence of areas of local film delamination, susceptibility of the coating to form cracks because of its high rigidity, and so on) and, of course, the potential applied.

Obviously, the higher the quality of the primer is (impermeability and ductility of the film and high adhesion to the substrate) the lower the probability will be of the electrolyte reaching the interphase and of the cathodic reaction taking place.

The deterioration of the coating because of cathodic polarisations can be caused primarily by the film delamination process at the metallic interphase, if the cathodic reaction involving the production of H_2 (g) and OH^- finally takes place, although the passage of ions can also exert an effect.

If there are possibilities of detecting whether the cathodic reactions have taken place during polarisation, this information could be used to know a little more about the performance and quality of the primer. One possible way of detecting the existence of H_2 (g) and OH^- production at the interphase is to study the evolution of the open circuit potential after polarisation. When cathodic polarisation finishes, the coated metal potential will relax showing two possible spectra:

a. If cathodic reactions were taking place, the potential would have a quick relaxation around -1V [31] (with small variations depending on the coating), which corresponds to the end of the reaction and, afterwards, a second relaxation that corresponds to ions and electrolyte leaving the coating. In any case, the cathodic reaction will produce the entry of electrolyte through the coating and the production of H_2 (g) and OH- in the metal/coating interface. The time needed for this electrolyte and the ions to leave the film will therefore be higher because they have to pass through the entire primer film.
b. If no cathodic reactions have taken place, there would be a single relaxation process that corresponds to ions and electrolyte leaving the primer. This relaxation will take place at longer times as ions and electrolyte penetrate deeper into the film, but they will probably need less time than in case “a” described above.

Figure 10 shows the open circuit potential relaxation versus time of the coatings cured at the different curing temperatures. It can be clearly seen that there are two potential relaxation processes after polarisation: a fast one corresponding to the end of the cathodic reaction at short times and a slower one at longer times corresponding to ions and electrolyte leaving the coating in primers cured at 145, 155 and 195ºC. In the case of the curves corresponding to the extreme curing temperatures (145 and 195ºC), the second relaxation takes place at relatively long times. If the curing temperature is 145ºC, water and reactive species are able to reach the interphase because of its low cross-linking density, while, when a high curing temperature is used (195ºC), the species can reach the metal because of crack formation in the organic film due to high rigidity and stress applied by different phenomena (such as shrinkage during the curing process). On the other hand, coatings cured in the range between 165 and 185ºC just present one very distributed relaxation. The case of the sample cured at 155ºC falls between these two behaviours. It presents two relaxation processes but the second one appeared in relatively short times.

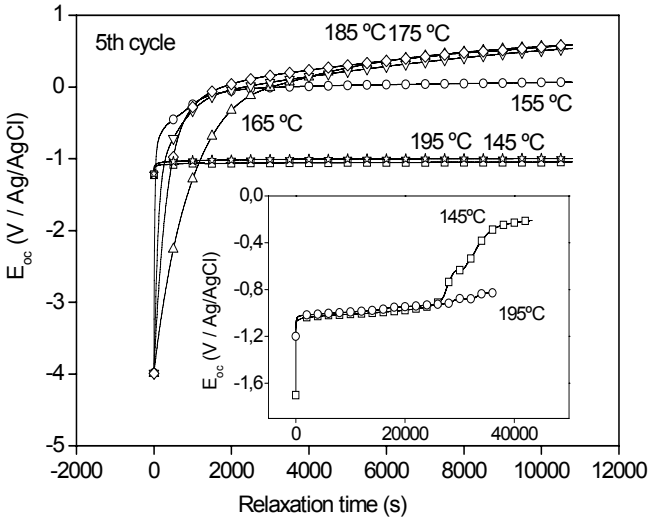

Fig. 10. Evolution of the open circuit potential (E_{OC}) versus relaxation time after exposure to 5 cathodic polarisations for samples cured at different temperatures (ºC): 145 (□), 155 (O), 165 (Δ), 175 (▽), 185 (◊) and 195 (☆). AC/DC/AC test.

Figure 11 shows the evolution of the stabilization potential with temperature after 5 AC/DC/AC cycles. The stabilization potential is defined as the open circuit potential the system has when the stabilization is reached after the cathodic polarization has been applied. In the optimum range of curing temperatures detected by EIS (165–185ºC), the stabilization potential ($E_{stabilisation}$) is maximum (especially at 175 and 185ºC) and decrease if any other temperature is used to cure the coatings. Obviously, the $E_{stabilization}$ must be higher as the coating film has fewer pores or cracks and is less delaminated (it being more difficult for the electrolyte to reach the metallic substrate).

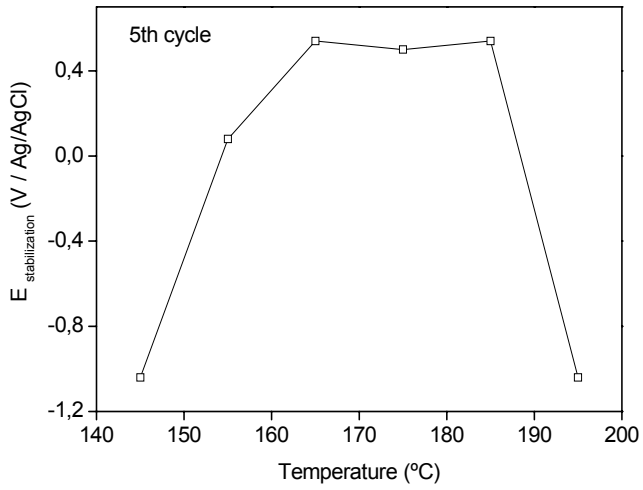

Fig. 11. Open circuit potential stabilization values (at 10 000 seconds) after exposure to 5 cathodic polarisations (AC/DC/AC test) versus curing temperature.

As can be seen, a coating with high anticorrosive properties will be that which only presents one relaxation process after cathodic polarization (this means that the cathodic reaction of hydrogen and OH^- production could not take place), high stabilization potentials and, finally, with regard to the equivalent circuit parameters, high resistances and low capacitances. From this point of view, the optimum curing temperature range in the cathodic process that provided the maximum anticorrosive properties in the kind of coatings that we studied is 165–185ºC.

4. Conclusions

A cataphoretic epoxy primer was applied on low-carbon steel substrate by cataphoretic deposition and cured in the range of temperatures 145–195ºC. The samples were studied by means of electrochemical methods (EIS and AC/DC/AC).

Results concerning the quality of primers obtained with the two electrochemical techniques were quite similar, although the AC/DC/AC test offered results in notably shorter times (1 day).

The different results showed that, for this type of epoxy coating, the anticorrosion properties were enhanced when the curing temperature was in the 165–185ºC range and decrease significantly when this cure temperature decreases or increases. The potential relaxation process after cathodic polarisation in the AC/DC/AC technique indicated that samples cured in the optimum range of curing temperatures did not degrade significantly with the test cycles and did not allow the cathodic reaction of H_2 (g) and OH^- production in the metal surface. On the other hand, coatings cured at lower or higher curing temperatures degraded with polarisation cycles and allowed the H_2 (g) production and cathodic reaction which produced delamination.

With this article, the AC/DC/AC technique has been proved to be an efficient technique in the evaluation of primer performance, showing results that it can be easily correlated to EIS ones but obtained in very short times (almost 1 day). Nevertheless more research in this field should be done in order to be sure that the good correlation here showed is always obtained.

Acknowledgments

We would like to thank Ms Eva Romero, Mss Noelia Coll, Mr Eugeni Lozano, Mr Alfonso Pallares, Mr Ramón Novoa and Mr Juan Carlos Galvan for their help and collaboration in the development of this project. The authors are grateful for the economic support in this work of the MAT 2000-0123-P4-03 project and to PPG Ibérica for supplying the samples.

1. P.E. Pierce, *J. Coat. Tech.*, 53 (1981) 52
2. K.M. Wernstahl, B. Carlsson, *J. Coat. Tech.*, 69, 865 (1997) 69
3. E. Almeida, I. Alves, C. Brites, L. Fedrizzi, *Prog. Org. Coat.*, 46 (2003) 8
4. J.J. Suay, M.T. Rodríguez, R. Izquierdo, A.H. Kudama, J.J. Saura, *J. Coat. Tech.*, 75, 946 (2003) 103
5. N. Vatistas, *Prog. Org. Coat.*, 33 (1998) 14

6. G.E.F. Brewer and R.F. Hines, *J. Paint Tech.*, 43 (1971) 71
7. W.B. Brown, *J. Paint Tech.*, 47 (1975) 43
8. Y-I. Suzuki, H. Fukui, K. Tsuchiya, S. Arita, Y.H. Ogata, *J. Electrochem. Soc.*, 150, 4 (2003) C-251
9. F. Mansfeld, *J. Applied Electrochem.*, 25 (1995) 187
10. G.P. Bierwagen, *J. Coat. Tech.*, 64 (1992) 71
11. B. Liu,Y. Li, H. Lin, C.Cao, *Acta Physico-Chimica Sinica.*, 17 (2001) 241
12. B.S. Skerry, C-T. Chen, C.J. Ray, *J. Coat. Tech.*, 64 (1992) 77
13. S. Gwori, K. Balakrishnan, *Prog. Org. Coat.*, 23 (1994) 363
14. M. Selvaraj, S. Guruviah, *Prog. Org. Coat.*, 28 (1996) 271
15. L.S. Hernández, B. del Amo, R. Romagnoli, *Anti-Corrosion Methods and Materials.*, 46 (1999) 198
16. J. Shao, P. Wan et al, *Materials and Corrosion.*, 46 (1995) 33
17. J. Hollaender, E. Ludwig, S. Hillebrand, Proc. 5th International Tinplate Conference, London, 300 (1992)
18. J. Hollaender, *Food additives and contaminants.*, 14, 6-7 (1997) 617
19. J. Hollaender, C.A. Schiller, W. Strunz, *Proc. EIS 2001*, Marilleva-Italy (2001)
20. M.T. Rodriguez, J.J. Gracenea, J.J. Saura, J.J. Suay, *Prog. Org. Coat.*, 50 (2004) 68
21. J.J. Suay, M.T. Rodriguez, K.A. Razzaq, J.J. Carpio, J.J. Saura, *Prog. Org. Coat.*, 46 (2003) 121
22. M.T. Rodriguez, J.J. Gracenea, S.J. García, J.J. Saura, J.J. Suay, *Prog. Org. Coat.*, 50 (2004) 123
23. F. Mansfeld, *Electrochem. Acta*, 38 (1993) 1891
24. A. Amirudin, D. Thierry, *Prog. Org. Coat.*, 26 (1995) 1
25. G.W. Walter, *J. Electroanal. Chem.*, 118 (1981) 259
26. G.W. Walter, *Corros. Sci.*, 26 (9) (1986) 681
27. N. Tang, W.J. Ooij, G. Górecki, *Prog. Org. Coat.,* 30 (1997) 255
28. J. Mijovic, *J. Appl. Polym. Sci.*, 3 (1986) 1177
29. D.J. Plazek, *J. Appl. Polym Sci.*, 24 (1986) 1303
30. G. Wisanrakkit, J.K. Gillham, J.B. Enns, *J. Appl. Polym. Sci.*, 4 (1990) 1895
31. H. Leidheisser Jr., W. Wendy, L. Igefolt, *Prog. Org. Coat.*, 11 (1983) 19

5.2. CINÉTICA DE CURADO DE PINTURAS EN POLVO

En este segundo apartado del capítulo de *resultados y discusión* se trata el estudio cinético de las diferentes pinturas en polvo formuladas a partir de triflatos de erbio e iterbio para comprobar su posibilidad de uso a nivel industrial. El objetivo principal desde el punto de vista cinético sería obtener sistemas capaces de curar a bajas temperaturas.

El apartado presenta un primer artículo donde se estudia la cinética de curado de sistemas epoxi en polvo formulados con distintas proporciones de triflato de erbio, un segundo artículo variando la proporción de triflato de iterbio y un tercero empleando el triflato de erbio y de iterbio como catalizadores para un sistema epoxi/orto-tolilbiguanida.

El estudio cinético se realizó por dos vías: en primer lugar empleando el software de Metler-Toledo STARe, y en segundo lugar empleando un estudio isoconversional por medio de hojas de cálculo para determinar el triplete cinético (incluido el modelo de reacción) y estudiar la posibilidad de emplear los métodos dinámicos para extrapolar resultados a ensayos isotermos, conociendo así las condiciones de curado de los sistemas a temperatura constante.

Por medio de estas dos vías se consiguió establecer un conocimiento de los procesos de reacción, parámetros característicos (E, lnA y g(α)), triplete de curado (temperatura/tiempo/conversión[1]) y del efecto de la introducción de los triflatos de lantánido en los sistemas epoxi como iniciadores y/o como catalizadores.

[1] Este tipo de gráficos tiempo-conversión-temperatura se muestran a partir del punto 5.3 de Resultados y discusión

Addition effect of Erbium (III) trifluoromethanesulfonate in the homopolymerization kinetics of a DGEBA resin

S.J. García[1], X. Ramis[2], A. Serra[3] & J. Suay[4]

[1] Àrea de Ciència dels Materials i Enginyeria Metal·lúrgica, Departament de Tecnologia. Universitat Jaume I. Avda. Vicent Sos Baynat s/n, 12071 Castelló, Spain

[2] Laboratori de Termodinàmica, Escola Tècnica Superior Enginyeria Industrial Barcelona, Universitat Politècnica de Catalunya, Diagonal 647, 08028 Barcelona, Spain

[3] Departament de Q. Analítica i Q. Orgànica. Facultat de Química. Universitat Rovira i Virgili. C/Marcel·lí Domingo s/n, 43007 Tarragona, Spain

[4] Centro de Biomateriales, Universitat Politècnica de València, Camino de Vera s/n, E-46071 Valencia, Spain

Thermochimica Acta
Vol. 441 (2006), 45-52

Abstract

Solid bisphenol-A epoxy resin of medium molecular weight was cured using a Lewis acid initiator (erbium (III) trifluoromethanesulfonate) in three different proportions (0.5, 1 and 2 phr). A kinetic study was performed in a differential scanning calorimeter. The complete kinetic triplet was determined (activation energy, pre-exponential factor, and integral function of the degree of conversion) for each system. A kinetic analysis was performed with an integral isoconversional procedure (model-free), and the kinetic model was determined both with the Coats–Redfern method (the obtained isoconversional value being accepted as the effective activation energy) and through the compensation effect (IKR). All the systems followed the same isothermal curing model simulated from non-isothermal ones. The growth-of-nuclei Avrami kinetic model $A_{3/2}$ has been proposed as the polymerization kinetic model. The addition of initiator accelerated the reaction having higher influence when low temperatures were applied.

1. Introduction

The formulation of low curing temperatures epoxy powder coatings (using new initiator and crosslinkers) has become one of the main lines of research in industries and related research centres. One of the main objectives of the research is to obtain epoxy systems with low curing temperatures so that they can be applied on different substrates sensitive to temperature (mainly different types of organic ones like plastics), and of course to reduce energetic costs. Properties of the paints (mechanical, thermal, anticorrosive and so on) are specially influenced by the kind of epoxy network-structure (which depends on the crosslinker and initiator employed in its formulation).

Powder coatings are currently the fastest growing section of industrial paints, because of their favourable environmental attributes and performance advantages. They are well-adapted for the main strategic goals of the paint industry, namely corrosion protection, improved durability, increased transfer efficiency, elimination of organic solvents, reduction of toxic waste, conservation of energy and reduction of costs. Since they are fully solid, and without volatile organic emissions, powder coatings are considered to be the best alternative for the reduction of the volatile organic contents (VOCs) of solvent-based paints, among the emerging coating technologies (powder coatings, high solid coatings and waterborne ones) [1,2].

Compared to liquid paints, the film formation process of powder coatings is different since it is occurring in the molten phase. Melting, flow, gel point and cure completion are the principal stages in film formation of powder coatings and determine both the aesthetic and protective properties of the paint. The duration of these stages is directly affected by the paint composition, e.g., type of binder and cross-linker, pigmentation (nature and particle size, packaging and distribution), initiator, and additives, curing and application conditions. These factors, in turn, determine important coating characteristics such as levelling, adhesion, gloss, chemical resistance and exterior durability [3-12].

Catalysts are important in polymerization processes because they decrease the activation energies and accelerate the reaction. They can be stimulated by heating or photoirradiation but, from the practical point of view, heating is the easier option; homogeneous heating of reaction mixtures can be achieved without difficulty [13]. In addition, elementary reactions are accelerated and the viscosity of the reaction mixture decreases. This shortens the reaction time, especially for systems in which the curing rate is diffusion-determined. Among the new thermal initiators, those having anions with low nucleophilicity, minimize or prevent the reaction of the growing chain with the anion, being more actives their cationic salts and more effective the polymerization [14].

The Lewis acid character and the great oxophilicity of lanthanide compounds is highly improved in the case of lanthanide triflates because of the electron-withdrawing capacity of the anionic group [15], which can coordinate to the epoxyde oxygens weakening the C-O bond. Lewis acids, such as $AlCl_3$, BF_3 or $TiCl_4$ are moisture sensitive and easily decomposed or deactivated in the presence of humidity. On the contrary, lanthanide triflates are stable and work as Lewis acids in water. This fact represents an enormous advantage in their technological application as initiators.

As usual in Lewis acid initiators, erbium (III) trifluoromethanesulfonate leads to chain growth polymerization of epoxy compounds, which mainly proceed by the cationic chain end mechanism depicted in Scheme 1, where oxirane group of DGEBA resin is opened by coordination of oxirane oxygen to the cation and nucleophylic attack of another oxirane group.

DGEBA resin:

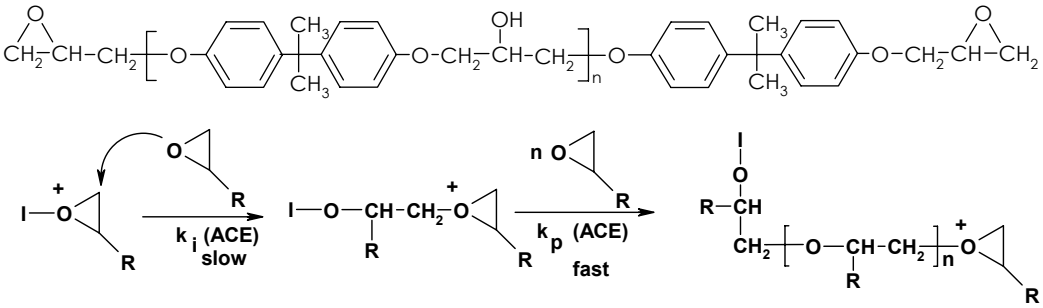

Scheme 1. Activated chain-end mechanism / ACE

Moreover, the presence of hydroxylic groups can lead to hydroxylic initiated polyetherification processes that can change both the kinetics of the reaction and the properties of the materials (scheme 2), although this kind of reaction is less important in extension than the first one and, because of the low proportion of hydroxyls.

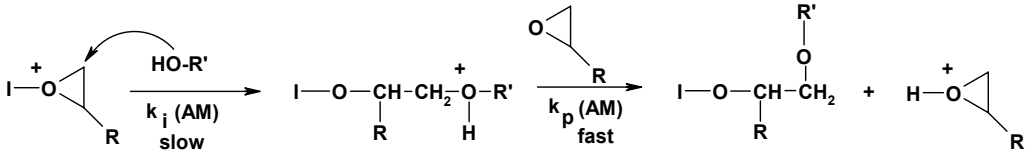

Scheme 2. Activated monomer mechanism / AM

Nevertheless, the proportion of hydroxilic groups can influence the global propagation rate. In addition to these competitive growth chain mechanisms, inter and intra molecular transfer processes can occur and also termination reactions. All these processes lead to changes in the network structure and difficult the study of the kinetics of each one by separate. Thus, the kinetics of a cationic cure should be studied taking the process as a whole [16, 17].

The usefulness of this type of initiator has been proved in other studies [14,18] with liquid epoxy resins, showing that the initiators highly accelerated the reactions of the system. Nevertheless, the behaviour of these initiators in powder coatings (using epoxy resins in the molten phase) has not yet been studied.

To predict the temperatures and times at which these polymerizations should be performed, one must know the kinetics. Preliminary kinetic studies have been performed using the method described by Kissinger [19]. This procedure, used by many authors because of its simplicity, assumes a reaction

mechanism of order *n*. However, this assumption is not correct in many cases and leads to incorrect values of the pre-exponential factor A. In addition, kinetic methods that only use the maximum of the velocity curve to determine the kinetic parameters do not allow an assessment of whether these parameters vary during polymerization or not. Here we attempt to establish a method for this type of polymerization that allows the complete kinetic triplet (kinetic model, E and A) to be determined throughout the entire reaction. To analyze exothermic polymerizations, we have adapted a method from earlier studies addressing the kinetics of curing and degradation [20].

Many exothermic polymerizations present difficulties for the determination of the heat of reaction through isothermal experiments and deduction of the kinetics from these values. When reactions are performed at high temperatures, some of the heat may be lost during the stabilization of the apparatus, whereas at low temperatures, the heat is released slowly and can fall below the sensitivity of the calorimeter. Another problem arises when a physical phenomenon (eg. fusion) overlaps with the polymerization. One alternative in both cases is to simulate isothermal polymerization with non isothermal data [21].

In this work a complete kinetic study of homo-polymerization of DGEBA resin with Erbium (III) trifluoromethanesulfonate as initiator has been developed. Isothermal polymerization was simulated with non isothermal data. The reaction model was established from non isothermal data with two different methods and proved with a posterior isothermal scan. The first method was the Coats-Redfern method [22], and the E value obtained isoconversionally was taken as the effective value (E_{ef}). The second method used the compensation effect existing between E and A at the change in the degree of conversion (α) [20, 23].

2. Experimental

2.1. Materials

Solid, bisphenol-A based epoxy resin of medium molecular weight, 733 gr/eq epoxy (from Huntsman), was homo-polymerized with Erbium (III) trifluoromethanesulfonate (from Aldrich) in three different amounts: 0.5, 1 and 2 phr (parts of initiator per hundred of resin, w/w).

Samples were premixed and hand-shacked until good mixing was afforded. After that, the material was extruded in a single screw extruder (Haake Rheomex 254), where operating conditions were 80 ºC along the extruder and 60rpm. After extruding, the material was grinded in an ultra-centrifugal mill ZM 100 and sieved at 100 micron.

2.2. Testing Methods and Equipment

2.2.1. Differential scanning calorimeter (DSC)

A Perkin Elmer DSC 7 differential scanning calorimeter was employed for dynamic scans in order to study the non isothermal curing process and to obtain the kinetic model parameters. The samples were analyzed in covered aluminium pans, using high purity indium sample for calibration. A flow of 20 $cm^3 \cdot min^{-1}$ of argon was used as purge gas. The weigh of the samples was between 8 and 9 mg. Non

isothermal tests were performed at rates of 2.5, 5, 10 and 15 $K \cdot min^{-1}$ to not-cured-samples of epoxy systems using three different erbium triflate initiator amounts. The scans were performed at the range of temperature from 25 to 300ºC.

Isothermal scans at 120ºC were also performed in order to obtain the experimental isothermal conversion degree. Different samples were maintained at the isothermal temperature for different given times. After each isothermal scan, the sample was cooled until ambient temperature inside the calorimeter and followed by a dynamic scan in order to obtain the residual enthalpy. With these data and the total enthalpy obtained from a dynamic scan to a non-cured sample, the conversion degree was calculated.

STARe Mettler Toledo software was used in order to calculate conversion degrees and kinetics of the process. Kinetic analysis, using Coats-Redfern and IKR methods, was used to calculate the kinetic triplet.

2.2.2. Kinetic analysis

If we accept that the dependence of the rate constant on the temperature follows the Arrhenius equation, the kinetics of the reaction is usually described as follows:

$$r = \frac{d\alpha}{dt} = A\exp\left(-\frac{E}{RT}\right)f(\alpha) = kf(\alpha) \quad (1)$$

where *t* is the time, *T* is the absolute temperature, *R* is the gas constant, and $f(\alpha)$ is the differential conversion function.

Kinetic analysis has generally been performed with an isoconversional method. The basic assumption of such method is that the reaction rate at a constant conversion is solely a function of temperature [24].

2.2.2.1. Isothermal Methods

By integrating the rate equation (eq 1) under isothermal conditions, we obtain

$$\ln t = \ln\left[\frac{g(\alpha)}{A}\right] + \frac{E}{RT} \quad (2)$$

where g(α) is the integral conversion function. It is defined as follows:

$$g(\alpha) = \int_0^{\alpha} \frac{d\alpha}{f(\alpha)} \quad (3)$$

According to eq 2, E and the constant ln[g(α)/A] can be obtained from the slope and the intercept, respectively, of the linear relationship $ln\ t = f(T^{-1})$ for a constant value of α.

2.2.2.2. Non-isothermal Methods

When non-isothermal methods are applied, the integration of rate equation (eq. 1) and its reordering, gives place to the so-called temperature integral:

$$g(\alpha) = \int_0^{\alpha} \frac{d\alpha}{f(\alpha)} = \frac{A}{\beta}\int_0^{T} e^{-(E/RT)}dT \quad (4)$$

where β is the heating rate.

By using the Coats-Redfern [22] approximation for the resolution of eq 4 and considering 2RT/E << 1, we can rewrite this equation as follows:

$$\ln\frac{g(\alpha)}{T^2} = \ln\left[\frac{AR}{\beta E}\right] - \frac{E}{RT} \quad (5)$$

For a given kinetic model, the linear representation of $\ln[g(\alpha)/T^2]$ versus T^{-1} makes it possible to determine E_{ap} (apparent E value) and A from the slope and the ordinate at the origin. In this work, the kinetic model that had the best linear correlation in the Coats-Redfern equation and that had an E value (E_{ap}) similar to that obtained isoconversionally (considered to be the effective E value, E_{ef}) was selected.

By reordering equation 5, we can rewrite:

$$\ln\frac{\beta}{T^2} = \ln\left[\frac{AR}{g(\alpha)E}\right] - \frac{E}{RT} \quad (6)$$

The linear representation of $\ln[\beta/T^2]$ versus 1/T makes it possible to determine E_{ef} and the kinetic parameter $\ln[AR/g(\alpha)E]$ for every value of α.

The constant $\ln[AR/g(\alpha)E]$ is directly related by the R/E to the constant $\ln[g(\alpha)/A]$ of the isothermal adjustment. Thus, taking the dynamic data $\ln[AR/g(\alpha)E]$ and E from equation 6, we can determine the isothermal parameters of eq 2 and simulate isothermal curing without knowing $g(\alpha)$ [25, 26].

The STARe Mettler Software uses equations 6 and 2 to determine the isonconversional activation energy and the isothermal times, respectively.

2.2.2.3. Compensation effect and isokinetic relationship (IKR)

Complex processes are characterized by the dependences of E on A and α. This generally reflects the existence of a compensation effect through the following equation:

$$\ln A_\alpha = aE_\alpha + b = \frac{E_\alpha}{RT} + \ln\left[\frac{(d\alpha/dt)_\alpha}{f(\alpha)}\right] \quad (7)$$

Where a and b are constants and subscript α represents the degree of conversion that produces a change in the Arrhenius parameters.

The slope $a = 1/RT_{iso}$ is related to the isokinetic temperature (T_{iso}), and the intercept $b = \ln k_{iso}$ is related to the isokinetic rate constant (k_{iso}). Equation 7 represents an IKR and can be deduced by the reordering of equation 2. The appearance of the IKR shows that only one mechanism is present,

whereas the existence of parameters that do not meet the IKR implies that there are multiple reaction mechanisms [27].

In this study, the kinetic model whose IKR had the best linear correlation between E_{ef} and A and in which the associated T_{iso} value was near the experimental temperature range was selected [28]. The influence of more addition of erbium triflate in the kinetics of the system has been studied.

3. Results and discussion

In Figure 1 it is shown the thermogram corresponding to the heating of three different samples with 0.5, 1 and 2 phr of erbium triflate, at a rate of 5ºC/min. The thermogram exhibits in the three cases a small endothermic peak at 60ºC (where the T_g should be detected) related with physical aging of the DGEBA and an exothermic one at higher temperatures (near 120ºC) related to the curing reaction of the epoxy resin. It can be seen that for the three different samples, similar curve thermograms were obtained. As the content in erbium trilfate increases, the thermogram shifts to minor temperatures. The reaction heat is almost constant at 105 KJ/mg for all the samples.

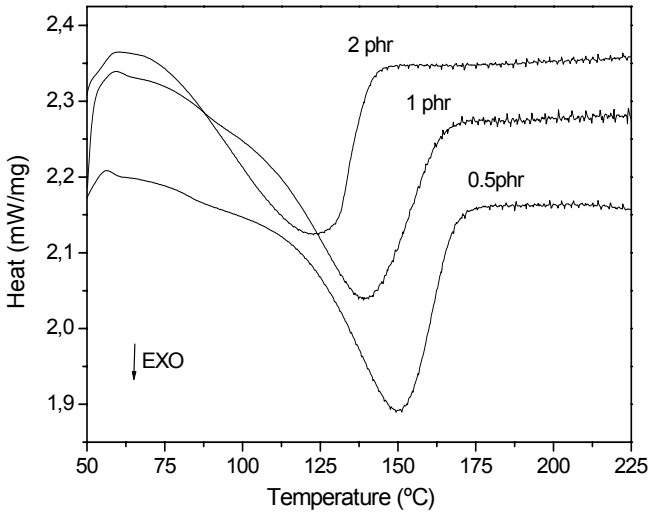

Fig. 1. Non-isothermal DSC thermograms at 5ºC/min of heating rate for three different epoxy systems containing 0.5, 1 and 2 phr of erbium triflate.

The results of the calorimetric scannings were employed to obtain the conversion degree with temperature, by means of the STARe software. Figure 2 shows α versus T plots for a constant rate of 5ºC/min for the three samples used. It can be seen that the higher the content in erbium triflate, the lower the temperature for a given conversion degree is.

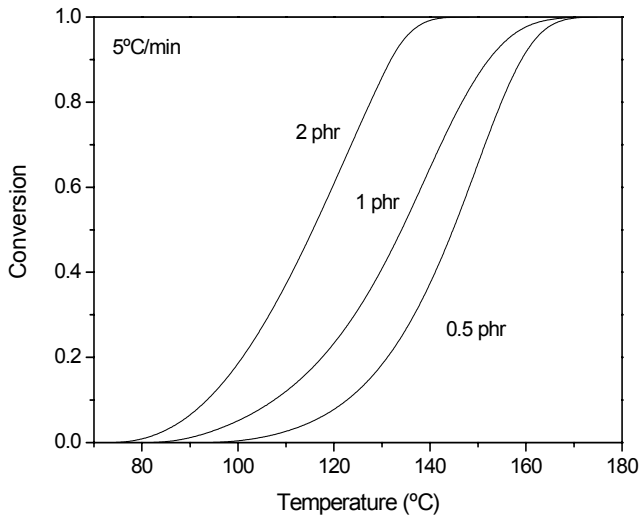

Fig. 2. Conversion degree (α) versus temperature plots for a heating rate of 5ºC/min for three different epoxy systems containing 0.5, 1 and 2 phr of erbium triflate as initiator.

In Figure 3, it is plotted the influence of the heating rate for a sample with 1phr of erbium triflate obtained with STARe software. It can be seen that as the rate of heating increases, the thermogram shifts to higher temperatures.

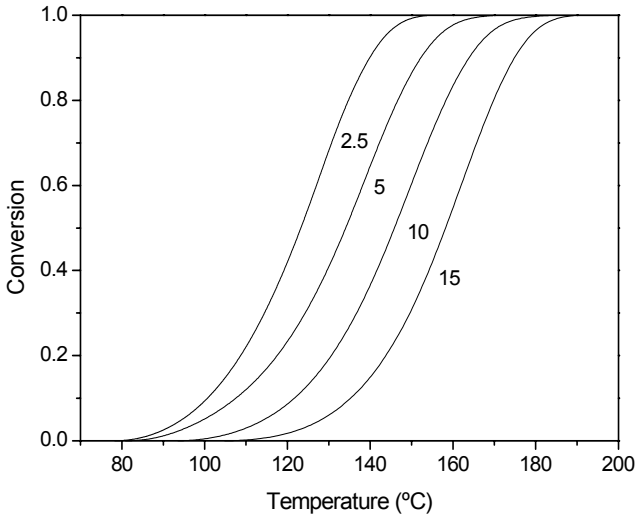

Fig. 3. Conversion degree (α) for an epoxy system with 1 phr of erbium triflate as initiator at different heating rates (2.5, 5, 10 and 15ºC/min).

The non-isothermal isoconversional kinetic parameters were calculated from the α-T curves by the application of equation 6 to different conversions, and from these, the isothermal parameter ln[g(α)/A] and E_{ef}, with which the studied curing process would subsequently be simulated. Table 1 shows the results obtained for the sample prepared at 1phr of erbium triflate. The process was repeated with the other proportions of triflate.

Table 1. Kinetic parameters of non-isothermal homopolymerization obtained by Eq (6), for a sample with 1phr of erbium triflate

α	E_{ef} (KJ/mol)[a]	ln[AR/g(α)E] ($K^{-1}min^{-1}$)[a]	ln[g(α)/A] (min)[b]	lnA (min^{-1})[c]	r
0.1	71.3	12.34	-21.39	19.89	0.968
0.2	74.6	12.80	-21.91	20.91	0.982
0.3	76.9	13.16	-22.29	21.60	0.987
0.4	79.0	13.48	-22.64	22.19	0.989
0.5	80.6	13.71	-22.89	22.64	0.990
0.6	81.8	13.82	-23.02	22.96	0.992
0.7	82.7	13.83	-23.04	23.16	0.993
0.8	83.7	13.89	-23.11	23.43	0.994
0.9	85.3	14.03	-23.27	23.82	0.996

a. ln[*AR/g*(α)*E*] and *E* were calculated on the basis of non-isothermal DSC experiments as the intercept and slope of the isoconversional relationship $\ln[\beta/T^2] = \ln[AR/g(\alpha)E] - E/RT$
b. ln[*g*(α)/*A*] was calculated on the basis of ln[*AR/g*(α)*E*] and *E*
c. ln *A* was calculated with kinetic model A3/2 and ln[*g*(α)/*A*]

Figure 4 shows the experimental relationship between $\ln[\beta/T^2]$ and the inverse of temperature, with the adjustment made with equation 6. Table 1 shows that E_{ef} is weakly modified during homopolymerization, rising with the advance of the reaction, probably due to the increased viscosity of the reaction medium as the molecular weight increases. The parameters ln[AR/g(α)E] and the associated A values exhibit the same trend as E_{ef}. The same results were obtained for the other two proportions.

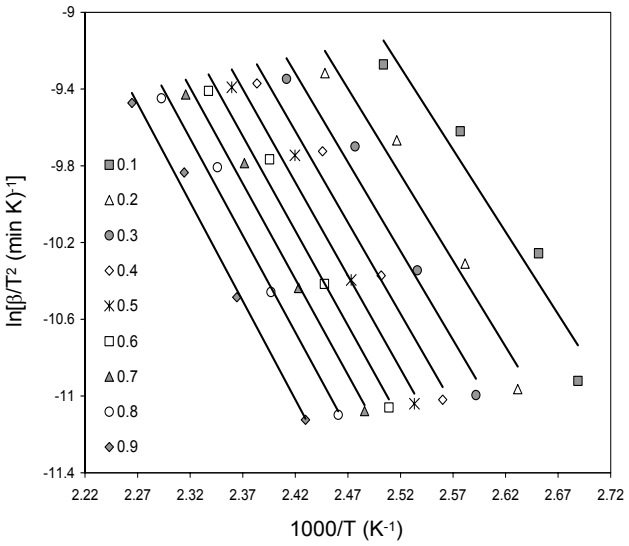

Fig. 4. Correlations between $\ln[\beta/T^2]$ and the inverse of the temperature (1000/T) for different values of α of an epoxy sample with 1 phr of erbium triflate.

To establish the kinetic model for the system with an initiator amount of 1phr, the isoconversional kinetic parameters (Table 1) and the equation 7 were used (the same process was done for the other two systems). From the parameters ln[AR/g(α)E] and E_{ef} shown in Table 1 and the g(α) functions, *A* values were calculated for all the different kinetic models used (see Table 2). Subsequently, by plotting E_{ef} against lnA, we determined the IKRs for all the models (eq 7).

Table 2. Algebraic expressions for $f(\alpha)$ and $g(\alpha)$ for the kinetic models used

Models	$f(\alpha)$	$g(\alpha)$
$A_{3/2}$	$(3/2)(1-\alpha)\left[-\ln(1-\alpha)\right]^{1/3}$	$\left[-\ln(1-\alpha)\right]^{2/3}$
A_2	$2(1-\alpha)\left[-\ln(1-\alpha)\right]^{1/2}$	$\left[-\ln(1-\alpha)\right]^{1/2}$
A_3	$3(1-\alpha)\left[-\ln(1-\alpha)\right]^{2/3}$	$\left[-\ln(1-\alpha)\right]^{1/3}$
A_4	$4(1-\alpha)\left[-\ln(1-\alpha)\right]^{3/4}$	$\left[-\ln(1-\alpha)\right]^{1/4}$
R_2	$2(1-\alpha)^{1/2}$	$1-(1-\alpha)^{1/2}$
R_3	$3(1-\alpha)^{2/3}$	$1-(1-\alpha)^{1/3}$
D_1	$(2\alpha)^{-1}$	α^2
D_2	$\left[-\ln(1-\alpha)\right]^{-1}$	$(1-\alpha)\ln(1-\alpha)+\alpha$
D_3	$3/2(1-\alpha)^{2/3}\left[1-(1-\alpha)^{1/3}\right]^{-1}$	$\left[1-(1-\alpha)^{1/3}\right]^2$
D_4	$3/2(1-\alpha)^{1/3}\left[1-(1-\alpha)^{1/3}\right]^{-1}$	$(1-2/3\alpha)(1-\alpha)^{2/3}$
F_1	$(1-\alpha)$	$-\ln(1-\alpha)$
power	$2\alpha^{1/2}$	$\alpha^{1/2}$
n+m=2; n=1.9	$\alpha^{0.1}(1-\alpha)^{1.9}$	$\left[(1-\alpha)\alpha^{-1}\right]^{-0.9}(0.9)^{-1}$
n+m=2; n=1.5	$\alpha^{0.5}(1-\alpha)^{1.5}$	$\left[(1-\alpha)\alpha^{-1}\right]^{-0.5}(0.5)^{-1}$
n=2	$(1-\alpha)^2$	$-1+(1-\alpha)^{-1}$
n=3	$(1-\alpha)^3$	$2^{-1}\left[-1+(1-\alpha)^{-2}\right]$

Table 3 shows the obtained results, as well as the T_{iso} values determined from slope *a* of the IKRs. Although some models exhibit IKRs, the model considered that the best one describing the homopolymerization is the nucleation growth type of Johnson, Male, Avrami, Kolmogorov and Yerofeev, $JMAKY_{3/2}$, (from here on, named as Avrami $A_{3/2}$ in order to simplify [29]) because this model shows the best regression and has a T_{iso} value close to the experimental temperatures. In agreement with Vyazovkin and Linert [28], a T_{iso} value close to the range of experimental temperatures indicates that the kinetic model accurately describes the reactive process. The same conclusion was obtained for the systems with 0.5 and 2phr of erbium triflate.

Table 3. Arrhenius parameters determined by the Coats–Redfern method and isokinetic parameters for a sample with 1phr of erbium triflate

Models	Coats-Redfern (1 phr)			IKR (1 phr)			
	E_{ap} (kJ/mol)	lnA (min^{-1})	r	a (mol/kJ)	b (min^{-1})	T_{iso} (ºC)	r
$A_{3/2}$	54.88	14.362	0.9999	0.2807	-0.039	155.55	0.9990
A_2	39.47	9.541	0.9999	0.2447	2.902	218.49	0.9983
A_3	24.07	4.555	0.9999	0.2088	5.843	303.09	0.9970
A_4	16.37	1.924	0.9998	0.1908	7.313	357.34	0.9959
R_2	71.34	18.484	0.9994	0.3304	-5.402	91.00	0.9982
R_3	75.89	19.549	0.9998	0.3204	-4.177	102.45	0.9971
D_1	124.69	34.596	0.9968	0.4507	-14.999	-6.12	0.9937
D_2	146.53	41.551	0.9989	0.4830	-18.034	-23.98	0.9966
D_3	158.52	43.113	0.9998	0.5240	-22.529	-43.45	0.9990
D_4	146.14	39.203	0.9993	0.4965	-20.521	-30.73	0.9976
F_1	85.68	23.790	0.9999	0.3525	-5.921	68.17	0.9996
power	26.12	4.999	0.9953	0.2154	5.044	285.53	0.9921
n+m=2; n=1.9	107.68	31.053	0.9955	0.4046	-9.467	24.28	0.9968
n+m=2; n=1.5	56.83	15.946	0.9951	0.2856	0.586	148.11	0.9994
n=2	120.40	34.824	0.9956	0.4343	-11.938	3.92	0.9961
n=3	162.46	48.051	0.9885	0.5356	-19.413	-48.41	0.9832

To confirm the methodology used, we determined E_{ap} and lnA for each of the tested models with the Coats-Redfern method (eq 5). The results obtained (using conversion and temperature from STARe for the rate of 5ºC/min) for the sample with 1phr of erbium triflate when eq 5 was applied to conversions between 0.2 and 0.8 are shown in table 3 (other tested rates showed similar results). The same process was applied to the other two samples. Some of the models exhibit very good regressions, and so from these data alone, it is not possible to establish the reaction mechanism. To determine the kinetic model, it was also used the mean value of E_{ef} obtained isoconversionally (79.9 KJ/mol; table 1). This value of E is considered the effective value because it was obtained without the necessity of determining the model. In addition to exhibiting a good regression, the correct kinetic model must also possess a value of E_{ap} similar to the effective value, E_{ef}. According to these criteria, model $A_{3/2}$ with r=0.9999 and E_{ap}= 54.88 KJ/mol, is considered the correct one even if the E_{ap} value is lower than that found with the isoconversional (table 5). Other models like R_3 and F_1 could also describe the process, but taking into account that the three systems using erbium triflate must show the same model, it was chosen that one representing all the systems and having good regression in all cases. In table 4 it can be seen the Coats-Redfern results for the other two samples and how the kinetic model chosen is valid for all the systems.

Table 4. Arrhenius parameters determined by the Coats–Redfern method for samples with 0.5phr and 2phr of $Er(TfO)_3$

Models	Coats-Redfern (0.5 phr)			Coats-Redfern (2 phr)		
	E_{ap} (kJ/mol)	lnA (min^{-1})	r	E_{ap} (kJ/mol)	lnA (min^{-1})	r
$A_{3/2}$	72.37	19.207	0.9998	53.69	14.830	0.9998
A_2	52.55	13.240	0.9998	38.66	9.913	0.9997
A_3	32.72	7.120	0.9998	23.63	4.827	0.9997
A_4	22.81	3.936	0.9998	16.49	2.171	0.9996
R_2	162.27	44.684	0.9995	69.56	18.994	0.9981
R_3	188.60	52.810	0.9994	74.07	20.108	0.9990
D_1	205.76	55.724	0.9971	121.14	35.297	0.9943
D_2	189.83	50.889	0.9990	142.49	42.314	0.9974
D_3	93.57	24.563	0.9999	154.58	44.166	0.9991
D_4	99.43	25.968	0.9994	142.32	40.122	0.9979
F_1	112.01	30.938	0.9998	83.76	24.457	0.9998
power	35.38	7.718	0.9960	25.46	5.223	0.9918
n+m=2; n=1.9	140.30	39.843	0.9952	105.73	32.021	0.9971
n+m=2; n=1.5	74.87	20.934	0.9948	55.88	16.516	0.9968
n=2	156.66	44.565	0.9952	118.19	35.891	0.9971
n=3	210.77	60.939	0.9878	159.98	49.618	0.9910

Table 5. Variation of the activation energy with the conversion of samples with 0.5, 1 and 2 phr of erbium triflate

Conversion	E_{ef} (KJ/mol)		
	0.5 phr	1 phr	2 phr
0.1	53.8	71.3	61.4
0.2	59.6	74.6	61.5
0.3	62.7	76.9	62.2
0.4	64.6	79.0	63.5
0.5	66.0	80.6	65.4
0.6	67.1	81.8	67.7
0.7	67.9	82.7	70.4
0.8	68.6	83.7	73.3
0.9	69.3	85.3	75.1

All the samples have shown that the two methodologies produce the same result, and in both cases, it is necessary to know the effective E (isoconversional) value to determine the complete kinetic triplet (E_{ef}, A and $f(\alpha)$).

If we compare the activation energies (Table 5), a simple analysis would conclude that the fastest system is that with the major E_{ef}, but this is not always true because it exist a compensation effect between E and lnA. Then, to know which system is the most efficient it should be compared the conversion rate *r*. Equation 8 shows the Arrhenius relation between *k* (rate constant), A and E.

$$k = A\exp\left(-\frac{E}{RT}\right) \rightarrow \ln k = \ln A - \frac{E}{RT} \tag{8}$$

From equation 1,

$$\ln r = \ln A - \frac{E}{RT} + \ln f(\alpha) \tag{9}$$

Introducing in this equation values of E, A and α with the chosen kinetic model $A_{3/2}$ and for a given conversion degree (α =0.5) we can obtain a graphic like Figure 5 (ln r = f (1/T)).

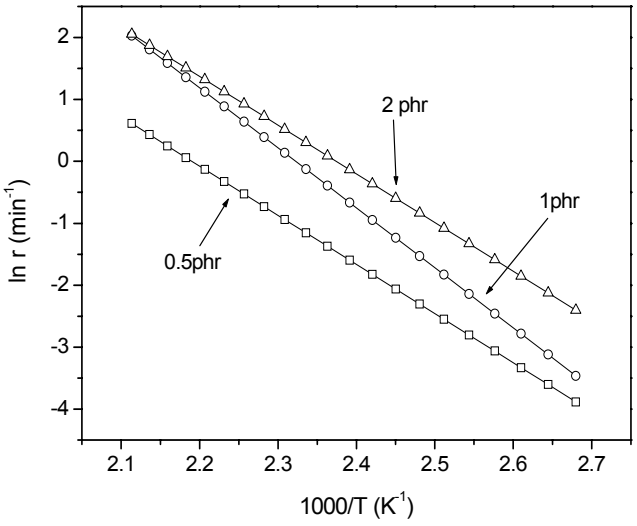

Fig. 5. Conversion rate (ln r) versus the inverse of the temperature (1000/T) for samples with 0.5, 1 and 2phr of erbium triflate.

In this figure it can be observed that, when introducing more initiator the faster the system is. As temperature raises, the conversion rate of the systems with 1phr and 2phr of erbium initiator get closer, meaning that the system is almost not accelerated when introducing initiator over 1phr when high temperatures are used (ex. 200ºC). But when low temperatures are used, significant acceleration of the system is shown (ex. 100ºC) when more initiator is added. These results corroborate that in order to know which system is the fastest; it is appropriate to consider not only E_{ef} but also the parameter lnA if the kinetic models are the same.

In order to know whether the kinetic model chosen and isoconversional data obtained by the STAR software fitted the experimental data or not, a comparison between conversion-time graphics for a given temperature was made. Because isothermal reactions of these systems were very fast, the DSC equipment was not able to detect the initial calorimetric signal because stabilization time is needed and the initial part of the cure was lost.

The experimental conversion degree (α) data were obtained doing a first isothermal test during a given time in a DSC, afterwards a scan from 25 to 300ºC at 5ºC/min was performed for each isothermal test. With equation 10 and the residual enthalpies obtained, the different conversion values where calculated.

$$\alpha_{\exp} = \frac{\Delta H_{total} - \Delta H_{residual}}{\Delta H_{total}} \qquad (10)$$

where, ΔH_{tot} = 73.3 KJ/eq epoxy obtained from non-isothermal data.

Figure 6, represents the three curves obtained: kinetic model data, isoconversional data obtained by the STAR software and finally experimental data, for a sample with 1phr of erbium triflate.

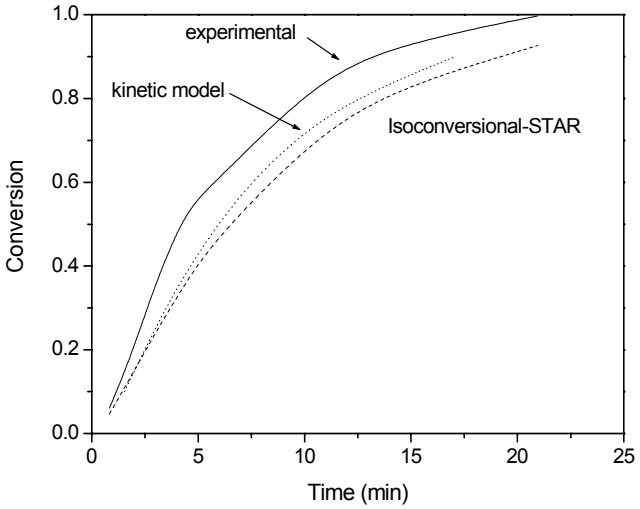

Fig. 6. Conversion versus time graphics of data obtained experimentally (isothermally at 120ºC), isoconversionally with the STAR software and from the chosen kinetic model for a sample with 1 phr of erbium triflate.

It can be observed that the three curves show the same trend, although experimental data present shorter times for the same conversion. These shorter experimental times at a given temperature compared to the modelled data can be due either to the fact that the epoxy curing process could not exactly be the same under isothermal or non-isothermal tests, or to some experimental problems in the calorimeter. Firstly, the DSC needs a short time to bring the sample to the isothermal curing temperature, meaning that the curing reaction begins before reaching the isothermal temperature. Secondly, when the isothermal test finishes the cooling of the sample in the calorimeter is not immediate, so again some time is needed to decrease the temperature and the reaction process continues until ambient temperature is reached, probably non-isothermal data give more accurate results than these isothermal experiments.

Nevertheless, as the curves are very similar it can be pointed out that the kinetic model chosen fits quite well the isoconversional data obtained with STAR software and experimental data.

4. Conclusions

To compare kinetic results, it is necessary to know the complete kinetic triplet (E, A, g(α)) because of the existence of a compensation effect between E and lnA. The use of E as a unique comparative parameter can introduce errors. Two methods that allow the determination of the complete kinetic triplet have been shown, as well as the simulation of the polymerization. Both methods require the effective E value to be known, which can be determined with an isoconversional procedure (model-free).

An epoxy system composed by a DGEBA resin and a Lewis acid initiator (Erbium (III) trifluoromethanesulfonate) with applications in the formulation of low curing powder coatings was studied. Three different amounts of initiator were prepared: 0.5, 1 and 2phr. A kinetic study by means of non-isothermal tests in a DSC was carried out and a posterior iso-kinetic study was developed. All systems showed that the reaction mechanism followed an $A_{3/2}$ grain growth model, showing no dependence on the initiator amount.

Reaction rates for all the systems were obtained. Results showed that the more the initiator is added, the faster the reaction rate is, but when high temperatures were used, the differences in the conversion degree decreased.

A simulation of the isothermal curing to a reasonably accurate degree has been obtained. In this way it has been possible to obtain the isothermal curing degree versus temperature and time without any isothermal tests (that in fast catalyzed curing systems are experimentally difficult to perform) but only with four DSC dynamic scans at different rates.

Acknowledgments

Authors would like to thank Ms Eva Romero, Mr. José Ortega and Ms. Raquel Oliver for their help in the development of this project. The authors from the Jaume I University are grateful for the economic support in this work of CICYT MAT 2000-0123-P4-03. The author from the Rovira i Virgili University would like to thank the CICYT-FEDER MAT2002-00291 and CIRIT SGR 00318 projects. Author from the Universitat Politécnica de Catalunya would like to thank CICYT and FEDER MAT2004-04165-C02-02 for their financial support.

1. E. Bodner, *Eur. Coat. Tech.,* 44 (1987)
2. S.S. Lee et al, *Prog. Org. Coat.,* 36 (1999) 79
3. E.G. Belder, H.J.J. Rutten, D.Y. Perera, *Prog. Org. Coat.,* 42 (2001) 142
4. J. Hess, Powder everywhere, *Coatings World*, Vol. 36. 1999
5. T.A. Misec (Ed.), *Powder Coatings Chemistry and technology*, Wiley, New York, 1991
6. R. van der Linde, B.J.R. Scholtens, E.G. Belder, Proceedings of the 11th International Conference on Organic Coatings in Science and Technology, pp. 147, Athens, Greece, 1985
7. F.M. Witte, C.D. Goemans, R. van der Linde, D.A. Stanssens, *Prog. Org. Coat.,* 32 (1997) 241
8. M. Osterhold, F. Niggemann, *Prog. Org. Coat.,* 33 (1998) 55
9. M. Johansson, H. Falken, A. Irestedt, A. Hult, *J. Coat. Tech.,* 70 (884) (1998) 57
10. S.S. Lee, H.Z.Y. Han, J.G. Hilborn, J.-A.E. Manson, *Prog. Org. Coat.,* 36 (1999) 79
11. R. van der Linde, E.G. Belder, D.Y. Perera, Proceedings of the 25th International Conference on Organic Coatings in Science and Technology, Vol. 15, Athens, Greece, 1999, *Prog. Org. Coat.,* 40 (2000) 215
12. D. Maetens, L. Moens, L. Boogaerts, k. Buysens, *Eur. Coat. J.,* 25, 1999
13. T. Endo, F. Sanda, *Macromol. Symp.,* 107 (1996) 237
14. C. Mas, A. Serra, A. Mantecón, J.M. Salla, X. Ramis, *Macromol. Chem. Phys.,* 202 (2001) 2554
15. S. Kobayashi, *Synlett,* (1996) 689
16. L. Matejka, P. Chabanne, L. Tighzert, J.P. Pascault*, J. Polym. Sci. Part A: Polym. Chem.*, 32 (1994) 1447-1458
17. P. Chabanne, L. Tighzert, J.P. Pascault, *J. Apply. Polym. Sci.*, 53 (1994) 769-785
18. P. Castell, M. Galià, A. Serra, J.M. Salla, X. Ramis, *Polymer,* 41 (2000) 8465
19. H.E., Kissinger, *Anal. Chem.,* 29 (1957) 1702
20. X. Ramis, J.M. Salla, C. Mas, A. Mantecón, A. Serra, *J. Appl. Polym. Sci.,* 92 (2004) 381
21. X. Ramis, J.M. Salla, J. Puiggalí, J. *Polym. Sci. Part A: Polym. Chem*, Vol. 43 (2005) 1166-1176
22. A.W. Coats, J. Redfern, *Nature,* 207 (1964) 290
23. S. Vyazovkin, W. Linert, *Int. Rev. Phys. Chem.,* 14 (1995) 355
24. S. Vyazovkin, C.A. Wight, *Annu. Rev. Phys. Chem.,* 48 (1997) 125
25. X. Ramis, A. Cadenato, J.M. Salla, J.M. Morancho, A. Vallés, L. Contat, A. Ribes, *Polym. Degrad. Stab.,* 86 (2004) 483
26. X. Ramis, J.M. Salla, A. Cadenato, J.M. Morancho, *J. Therm. Anal. Calorim.*, 72 (2003) 707
27. S. Vyazovkin, W. Linert, *J. Solid State Chem.,* 114 (1995) 392
28. S. Vyazovkin, W. Linert, *Chem. Phys.,* 193 (1995) 109
29. J. Sestak, Thermal Analysis in Thermophysical Properties of solids, Elsevier, Amsterdam 1984

Cationic crosslinking of solid DGEBA resins with ytterbium (III) trifluoromethanesulfonate as initiator

S.J. García[1], X. Ramis[2], A. Serra[3] & J. Suay[4]

[1] Àrea de Ciència dels Materials i Enginyeria Metal·lúrgica, Departamento de Ingeniería de Sistemas Industriales y Diseño. Universitat Jaume I. Avda. Vicent Sos Baynat s/n, 12071 Castelló, Spain

[2] Laboratori de Termodinàmica, Escola Tècnica Superior Enginyeria Industrial Barcelona, Universitat Politècnica de Catalunya, Diagonal 647, 08028 Barcelona, Spain

[3] Departament de Q. Analítica i Q. Orgànica. Facultat de Química. Universitat Rovira i Virgili. C/Marcel·lí Domingo s/n, 43007 Tarragona, Spain

[4] Centro de Biomateriales, Universitat Politècnica de València, Camino de Vera s/n, E-46071 Valencia, Spain

Journal of Thermal Analysis and Calorimetry
Vol. 83 (2006) 2, 429-438

Abstract

Solid bisphenol-A epoxy resin of medium molecular weight was cured using a Lewis acid initiator (ytterbium (III) trifluoromethanesulfonate) in three different proportions (0.5, 1 and 2 phr). A kinetic study was performed in a differential scanning calorimeter. The complete kinetic triplet was determined (activation energy, pre-exponential factor, and integral function of the degree of conversion) for each system. A kinetic analysis was performed with an integral isoconversional procedure (model-free), and the kinetic model was determined both with the Coats–Redfern method (the obtained isoconversional value being accepted as the effective activation energy) and through the compensation effect (IKR). All the systems followed the same isothermal curing model simulated from non-isothermal ones. The growth-of-nuclei Avrami kinetic model $A_{3/2}$ has been proposed as the polymerization kinetic model. The addition of initiator accelerated the reaction especially when 2phr was added. 0.5 and 1phr showed very few kinetic differences between them.

1. Introduction

The formulation of low curing temperatures epoxy powder coatings (using new initiators and crosslinkers) has become one of the main lines of research in industries and related research centres. One of the main objectives of this research is to obtain epoxy systems with low curing temperatures so that they can be applied on different substrates sensitive to temperature (mainly different types of organic ones like plastics), and of course to reduce energetic costs. Properties of the paints (mechanical, thermal, anticorrosive and so on) are specially influenced by the kind of epoxy network-structure (which depends on the crosslinker and initiator employed in its formulation).

Powder coatings are currently the fastest growing section of industrial paints, because of their favourable environmental attributes and performance advantages. They are well-adapted for the main strategic goals of the paint industry, namely corrosion protection, improved durability, increased transfer efficiency, elimination of organic solvents, reduction of toxic waste, conservation of energy and reduction of costs. Since they are fully solid, and without volatile organic emissions, powder coatings are considered to be the best alternative for the reduction of the volatile organic contents (VOCs) of solvent-based paints, among the emerging coating technologies (powder coatings, high solid coatings and waterborne ones) [1, 2].

Compared to liquid paints, the film formation process of powder coatings is different since it is occurring in the molten phase. Melting, flow, gel point and cure completion are the principal stages in film formation of powder coatings and determine both the aesthetic and protective properties of the paint. The duration of these stages is directly affected by the paint composition, e.g., type of binder and cross-linker, pigmentation (nature and particle size, packaging and distribution), catalyst, and additives, curing and application conditions. These factors, in turn, determine important coating characteristics such as levelling, adhesion, gloss, chemical resistance and exterior durability [3-12].

Catalysts are important in polymerization processes because they decrease the activation energies and accelerate the reaction. They can be stimulated by heating or photoirradiation but, from the practical point of view, heating is the easier option; because of homogeneous heating of reaction mixtures can be achieved without difficulty [13]. In addition, elementary reactions are accelerated and the viscosity of the reaction mixture decreases. This shortens the reaction time, especially for systems in which the curing rate is diffusion-determined. Among the new thermal initiators, those having anions with low nucleophilicity, minimize or prevent the reaction of the growing chain with the anion, being more actives their cationic salts and more effective the polymerization [14].

The Lewis acid character and the great oxophilicity of lanthanide compounds is highly improved in the case of lanthanide triflates because of the electron-withdrawing capacity of the anionic group [15]. Thus, the metal can coordinate to the epoxyde oxygens weakening the C-O bond. Lewis acids, such as $AlCl_3$, BF_3 or $TiCl_4$ are moisture sensitive and easily decompose in the presence of humidity. On the contrary, lanthanide triflates are stable and act as Lewis acids in water. This fact represents an enormous advantage in their technological application as initiators.

As usual in Lewis acid initiators, ytterbium (III) trifluoromethanesulfonate leads to chain growth polymerization of epoxy compounds, which mainly proceed by the cationic chain end mechanism depicted in Scheme 1, where oxirane group of DGEBA resin is opened by coordination of oxirane oxygen to the initiator and subsequent nucleophylic attack of another oxirane group.

DGEBA resin:

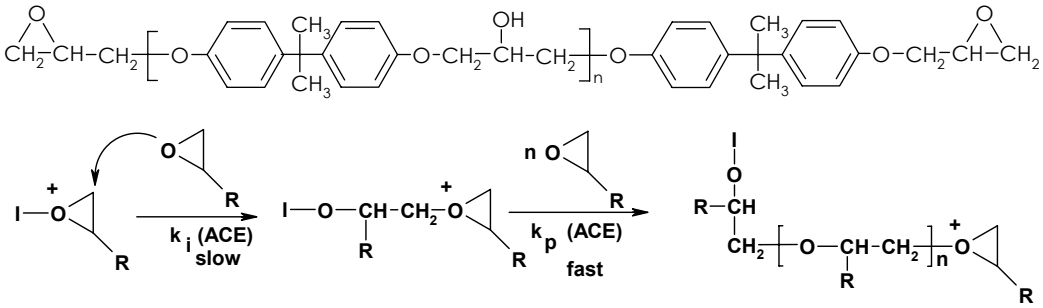

Scheme 1. Activated chain-end mechanism / ACE

Moreover, the presence of hydroxylic groups can lead to hydroxylic initiated polyetherification processes that can change both the kinetics of the reaction and the properties of the materials (scheme 2), although this kind of reaction should be less important in extension than the first one, because of the low proportion of hydroxyls. This mechanism is known as activated monomer mechanism.

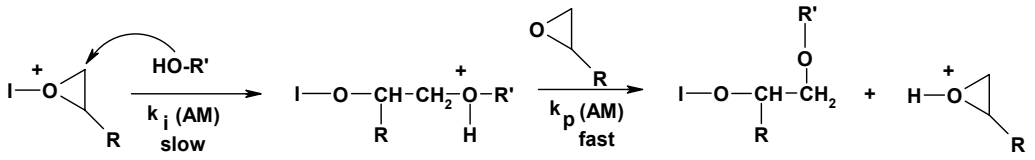

Scheme 2. Activated monomer mechanism / AM

Thus, the proportion of hydroxylic groups can influence the global propagation rate. In addition to these competitive chain growth mechanisms, inter and intra molecular transfer processes can occur and also termination reactions. All these processes lead to changes in the network structure and difficult the study of the kinetics of each separated process. Thus, the kinetics of a cationic cure should be studied taking the process as a whole [16, 17].

The usefulness of lanthanide triflates as initiators has been proved in other studies [14, 18] with liquid epoxy resins, showing that they highly accelerated the reactions of the system. Nevertheless, the behaviour of these initiators in powder coatings (using epoxy resins in the molten phase) has not been studied until now.

To predict the temperatures and times at which these polymerizations should be performed, one must know the kinetics. Preliminary kinetic studies have been performed using the method described by Kissinger [19]. This procedure, used by many authors because of its simplicity, assumes a reaction

mechanism of order *n*. However, this assumption is not correct in many cases and leads to incorrect values of pre-exponential factor A. In addition, kinetic methods that only use the maximum of the velocity curve to determine the kinetic parameters do not allow an assessment of whether these parameters vary during polymerization or not. Here we attempt to establish a method for this type of polymerization that allows the complete kinetic triplet (kinetic model, E and A) to be determined throughout the entire reaction. To analyze exothermic polymerizations, we have adapted a method from earlier studies addressing the kinetics of curing and degradation [20].

Many exothermic polymerizations present difficulties for the determination of the heat of reaction through isothermal experiments and the subsequent deduction of the kinetics from these values. When reactions are performed at high temperatures, some of the heat may be lost during the stabilization of the apparatus, whereas at low temperatures, the heat is released slowly and can fall below the sensitivity of the calorimeter. Another problem arises when a physical phenomenon (e.g. fusion) overlaps with the polymerization. One alternative in both cases is to simulate isothermal polymerization with non isothermal data [21]. Different works studying the curing kinetics of powder coatings and liquid ones using systems containing epoxy resins and diamines have been published [22-24].

In this work a complete kinetic study of homopolymerization of a medium molecular weight DGEBA resin with ytterbium (III) trifluoromethanesulfonate as initiator has been developed. Isothermal polymerization was simulated with non isothermal data. The reaction model was established from non isothermal data with two different methods and posterior isothermal scans during different times where performed in order to compare conversion-time-temperature data of the chosen kinetic model, experimental data and the isoconversional obtained data. The first method was the Coats-Redfern method [22-27], and the E value obtained isoconversionally was taken as the effective value, E_{ef}. The second method used the compensation effect existing between E and A at the change in the degree of conversion (α) [20,23].

2. Experimental

2.1. Materials

Solid bisphenol-A based epoxy resin of medium molecular weight, 733 gr/eq epoxy (from Huntsman), was homo-polymerized with Ytterbium (III) trifluoromethanesulfonate (from Aldrich) added in three different amounts: 0.5, 1 and 2 phr (parts of initiator per hundred of resin, w/w).

Samples were premixed and hand-shacked until good mixing was afforded. After that, the material was extruded in a single screw extruder (Haake Rheomex 254), where operating conditions were 80 ºC along the extruder and 60rpm. After extruding, the material was grinded in an ultra-centrifugal mill ZM 100 and sieved at 100 micron.

2.2. Testing Methods and Equipment

2.2.1. Differential scanning calorimeter (DSC)

A Perkin Elmer DSC 7 differential scanning calorimeter was employed for dynamic scans in order to study the non isothermal curing process and to obtain the kinetic model parameters. The samples were analyzed in covered aluminium pans, using high purity indium sample for calibration. A flow of 20 $cm^3 \cdot min^{-1}$ of argon was used as purge gas. The weigh of the samples was between 9 and 10 mg. Non isothermal tests were performed at rates of 2.5, 5, 10 and 15 $K \cdot min^{-1}$ to not-cured-samples of epoxy systems using three different ytterbium triflate initiator amounts. The scans were performed at the range of temperature from 25 to 300ºC.

Isothermal scans at 120ºC were also carried out in order to obtain the experimental isothermal conversion degree. Different samples were maintained at the isothermal temperature for different given times. After each isothermal scan, the sample was cooled until ambient temperature inside the calorimeter and a second dynamic scan was registered in order to obtain the residual enthalpy. With these data and the total enthalpy obtained from a dynamic scan to a non-cured sample, the conversion degree was calculated.

STARe Mettler Toledo software was used in order to calculate conversion degrees and kinetics of the process. Kinetic analysis, using Coats-Redfern and IKR methods, was used to calculate the kinetic triplet (*A* pre-exponential factor, *E* activation energy, and g(α) integral function of the degree of conversion).

2.2.2. Kinetic analysis

If we accept that the dependence of the rate constant on the temperature follows the Arrhenius equation, the kinetics of the reaction is usually described as follows:

$$r = \frac{d\alpha}{dt} = A\exp\left(-\frac{E}{RT}\right)f(\alpha) = kf(\alpha) \quad (1)$$

where *t* is the time, *T* is the absolute temperature, *R* is the gas constant, and *f(α)* is the differential conversion function. Kinetic analysis has generally been performed with an isoconversional method. The basic assumption of such method is that the reaction rate at a constant conversion is solely a function of temperature [29].

2.2.2.1. Isothermal Methods

By integrating the rate equation (eq 1) under isothermal conditions, we obtain

$$\ln t = \ln\left[\frac{g(\alpha)}{A}\right] + \frac{E}{RT} \quad (2)$$

where g(α) is the integral conversion function. It is defined as follows:

$$g(\alpha) = \int_0^{\alpha} \frac{d\alpha}{f(\alpha)} \quad (3)$$

According to eq 2, E and the constant ln[g(α)/A] can be obtained from the slope and the intercept, respectively, of the linear relationship *ln t = f(T $^{-1}$)* for a constant value of α.

2.2.2.2. Non-isothermal Methods

When non-isothermal methods are applied, the integration of rate equation (eq. 1) and its reordering, gives place to the so-called temperature integral:

$$g(\alpha) = \int_0^{\alpha} \frac{d\alpha}{f(\alpha)} = \frac{A}{\beta}\int_0^{T} e^{-(E/RT)}dT \qquad (4)$$

where β is the heating rate.

By using the Coats-Redfern [25] approximation for the resolution of eq 4 and considering 2RT/E << 1, we can rewrite this equation as follows:

$$\ln\frac{g(\alpha)}{T^2} = \ln\left[\frac{AR}{\beta E}\right] - \frac{E}{RT} \qquad (5)$$

For a given kinetic model, the linear representation of ln[g(α)/T^2] versus T^{-1} makes it possible to determine E_{ap} (apparent E value) and *A* from the slope and the ordinate at the origin. In this work, the kinetic model that had the best linear correlation in the Coats-Redfern equation and that had an E value (E_{ap}) similar to that obtained isoconversionally (considered to be the effective E value, E_{ef}) was selected. By reordering equation 5, we can rewrite:

$$\ln\frac{\beta}{T^2} = \ln\left[\frac{AR}{g(\alpha)E}\right] - \frac{E}{RT} \qquad (6)$$

The linear representation of ln[β/T^2] versus 1/T makes it possible to determine E_{ef} and the kinetic parameter ln[AR/g(α)E] for every value of α. The constant ln[AR/g(α)E] is directly related by the R/E to the constant ln[g(α)/A] of the isothermal adjustment. Thus, taking the dynamic data ln[AR/g(α)E] and E from equation 6, we can determine the isothermal parameters of eq 2 and simulate isothermal curing without knowing g(α) [24, 30]. The STARe Mettler Software uses equations 6 and 2 to determine the isonconversional activation energy and the isothermal times, respectively.

2.2.2.3. Compensation effect and isokinetic relationship (IKR)

Complex processes are characterized by the dependences of E on A and α. This generally reflects the existence of a compensation effect through the following equation:

$$\ln A_\alpha = aE_\alpha + b = \frac{E_\alpha}{RT} + \ln\left[\frac{(d\alpha/dt)_\alpha}{f(\alpha)}\right] \qquad (7)$$

where a and b are constants and subscript α represents the degree of conversion that produces a change in the Arrhenius parameters.

The slope $a = 1/RT_{iso}$ is related to the isokinetic temperature (T_{iso}), and the intercept $b = lnk_{iso}$ is related to the isokinetic rate constant (k_{iso}). Equation 7 represents an IKR and can be deduced by the reordering of equation 2. The appearance of the IKR shows that only one mechanism is present, whereas the existence of parameters that do not meet the IKR implies that there are multiple reaction mechanisms [31]. In this study, the kinetic model whose IKR had the best linear correlation between E_{ef} and A and in which the associated T_{iso} value was near the experimental temperature range was selected [32]. The influence of more addition of erbium triflate in the kinetics of the system has been studied.

3. Results and discussion

In Figure 1 we can see the thermograms corresponding to the heating of three different samples with 0.5, 1 and 2 phr of ytterbium, at a rate of 5ºC/min. The thermograms exhibit a small endothermic peak at 55ºC (where the T_g should be detected) related to the physical aging of the DGEBA and an exothermic one at higher temperatures (near 120ºC) related to the curing reaction of the epoxy resin. It can be seen that for the three different samples, a similar shape of the thermograms was obtained. As the content of ytterbium triflate increases, the thermogram shifts to minor temperatures.

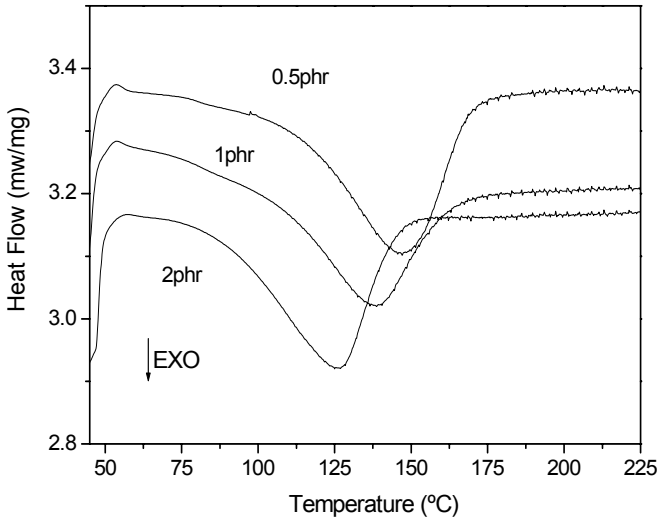

Fig. 1. Non-isothermal DSC thermograms at 5ºC/min of heating rate for three different epoxy systems containing 0.5, 1 and 2 phr of ytterbium triflate.

The results of the calorimetric scans were employed to obtain the conversion degree with the temperature, by means of the STARe software. Figure 2 shows α versus T plots for a constant rate of 5ºC/min for the three samples studied.

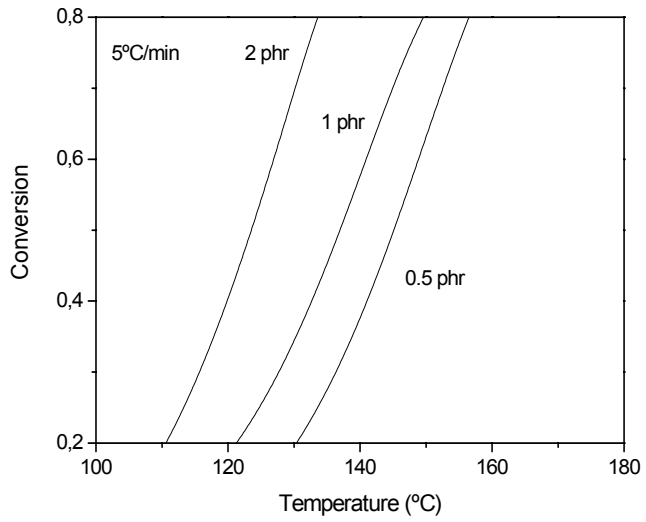

Fig. 2. Conversion degree (α) versus temperature plots for a heating rate of 5ºC/min for three different epoxy systems containing 0.5, 1 and 2 phr of ytterbium triflate as initiator.

It can be seen that the higher the content of ytterbium triflate, the lower the temperature for a given conversion degree is. It could be also pointed out, that for 0.5phr of initiator the reaction seems faster at high temperatures. On the other hand, when the amount of initiator is 2 phr, there are few differences with the other two samples but the curing was always faster.

The non-isothermal isoconversional kinetic parameters were calculated from the α-*T* curves by the application of equation 6 to different conversions, and from these, the isothermal parameter *ln[g(α)/A]*, with which the studied curing process would subsequently be simulated. Table 1 shows the kinetic parameters of non-isothermal curing obtained from equation 6 for the sample prepared at 1phr of ytterbium triflate. The process was repeated with the other proportions of triflate.

Table 1. Kinetic parameters of non-isothermal homopolymerization obtained by Eq (6), for a sample with 1phr of ytterbium triflate

α	E_{ef} (KJ/mol)[a]	ln[AR/g(α)E] ($K^{-1}min^{-1}$)[a]	ln[g(α)/A] (min)[b]	lnA (min^{-1})[c]	r
0.1	49.9	5.22	-13.91	12.41	0.9994
0.2	55.2	6.49	-15.29	14.29	0.9997
0.3	58.5	7.23	-16.09	15.40	0.9991
0.4	60.9	7.74	-16.64	16.19	0.9984
0.5	62.7	8.10	-17.03	16.78	0.9977
0.6	64.1	8.35	-17.30	17.25	0.9971
0.7	65.2	8.50	-17.46	17.59	0.9965
0.8	66.2	8.58	-17.56	17.88	0.9960
0.9	67.4	8.63	-17.63	18.19	0.9941

a. ln[*AR/g*(α)*E*] and *E* were calculated on the basis of non-isothermal DSC experiments as the intercept and slope of the isoconversional relationship $\ln[\beta/T^2] = \ln[AR/g(\alpha)E] - E/RT$
b. ln[*g*(α)/*A*] was calculated on the basis of ln[*AR/g*(α)*E*] and *E*
c. ln *A* was calculated with kinetic model A3/2 and ln[*g*(α)/*A*]

Figure 3 shows the experimental relationship between $ln[\beta/T^2]$ and the inverse of the temperature, with the adjustment made with equation 6. Table 1 shows that E_{ef} is weakly modified during curing, rising

with the advance of the reaction, probably due to the increased viscosity of the reaction medium as the molecular weight increases. The parameters *ln[AR/g(α)E]* and the associated *A* values exhibit the same trend as E_{ef}. Similar tendencies were obtained for the other two proportions.

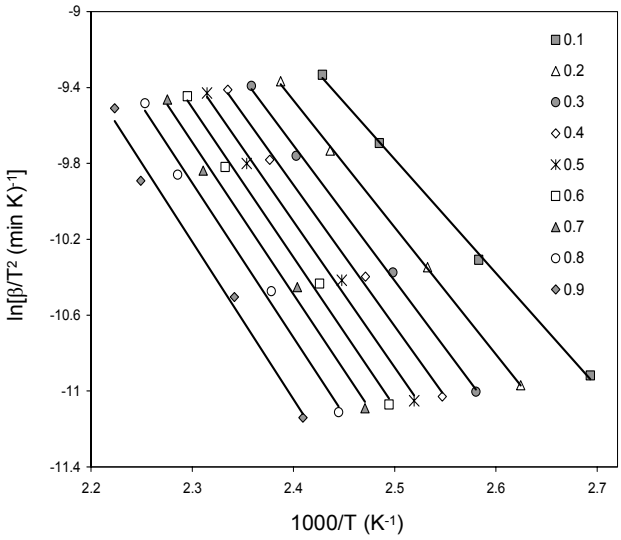

Fig. 3. Correlations between ln[β/T^2] and the inverse of the temperature (1000/T) for different values of α of an epoxy sample with 1 phr of ytterbium triflate.

To establish the kinetic model for the system with an initiator amount of 1phr, the isoconversional kinetic parameters (Table 1) and the equation 7 were used (the same process was done for the other two systems). From the parameters *ln[AR/g(α)E]* and E_{ef} shown in Table 1 and the *g(α)* functions, *A* values were calculated for all the different kinetic models used (see Table 2). Subsequently, by plotting E_{ef} against *lnA*, we determined the IKRs for all the models (eq 7).

Table 3 shows the obtained results, as well as the T_{iso} values determined from the slope of the IKRs. Although some models exhibit IKRs (specially $A_{3/2}$ and m=0.5/n=1.5 models), the model considered the best one describing the homopolymerization is the nucleation growth type $A_{3/2}$ because this model shows good regression and T_{iso} values closer to the experimental temperatures. In agreement with Vyazovkin and Linert [28], a T_{iso} value close to the range of experimental temperatures indicates that the kinetic model accurately describes the reactive process. The same conclusion was reached for the systems with 0.5 and 2 phr of ytterbium triflate.

Table 2. Algebraic expressions for $f(\alpha)$ and $g(\alpha)$ for the kinetic models used

Models	$f(\alpha)$	$g(\alpha)$
$A_{3/2}$	$(3/2)(1-\alpha)\left[-\ln(1-\alpha)\right]^{1/3}$	$\left[-\ln(1-\alpha)\right]^{2/3}$
A_2	$2(1-\alpha)\left[-\ln(1-\alpha)\right]^{1/2}$	$\left[-\ln(1-\alpha)\right]^{1/2}$
A_3	$3(1-\alpha)\left[-\ln(1-\alpha)\right]^{2/3}$	$\left[-\ln(1-\alpha)\right]^{1/3}$
A_4	$4(1-\alpha)\left[-\ln(1-\alpha)\right]^{3/4}$	$\left[-\ln(1-\alpha)\right]^{1/4}$
R_2	$2(1-\alpha)^{1/2}$	$1-(1-\alpha)^{1/2}$
R_3	$3(1-\alpha)^{2/3}$	$1-(1-\alpha)^{1/3}$
D_1	$(2\alpha)^{-1}$	α^2
D_2	$\left[-\ln(1-\alpha)\right]^{-1}$	$(1-\alpha)\ln(1-\alpha)+\alpha$
D_3	$3/2(1-\alpha)^{2/3}\left[1-(1-\alpha)^{1/3}\right]^{-1}$	$\left[1-(1-\alpha)^{1/3}\right]^2$
D_4	$3/2(1-\alpha)^{1/3}\left[1-(1-\alpha)^{1/3}\right]^{-1}$	$(1-2/3\alpha)(1-\alpha)^{2/3}$
F_1	$(1-\alpha)$	$-\ln(1-\alpha)$
power	$2\alpha^{1/2}$	$\alpha^{1/2}$
n+m=2; n=1.9	$\alpha^{0.1}(1-\alpha)^{1.9}$	$\left[(1-\alpha)\alpha^{-1}\right]^{-0.9}(0.9)^{-1}$
n+m=2; n=1.5	$\alpha^{0.5}(1-\alpha)^{1.5}$	$\left[(1-\alpha)\alpha^{-1}\right]^{-0.5}(0.5)^{-1}$
n=2	$(1-\alpha)^2$	$-1+(1-\alpha)^{-1}$
n=3	$(1-\alpha)^3$	$2^{-1}\left[-1+(1-\alpha)^{-2}\right]$

To confirm the methodology used, we determined E_{ap} and *ln A* for each tested model with the Coats-Redfern method (eq 5). The results obtained (using conversion and temperature obtained with the STARe) for the sample with 1 phr of ytterbium triflate when eq 5 was applied to conversions between 0.2 and 0.8 are shown in table 3 (other tested rates showed similar results). The same process was applied to the other two samples. Some of the models exhibit very good regressions, and so from these data alone, it is not possible to establish the reaction mechanism. To determine the kinetic model, it was also used the mean value of E_{ef} obtained isoconversionally (61.12 KJ/mol; table 1). This value of E is considered the effective value because it was obtained without the necessity of determining the model. In addition to exhibiting a good regression, the correct kinetic model must also possess a value of E_{ap} similar to the effective value E_{ef}. According to these criteria, model $A_{3/2}$ with r=0.9992 and E= 67.17 KJ/mol, is considered the correct one. The F_1 model also presents a good regression but its E_{ap} is too much higher than that obtained isoconversionally, so it is not considered an appropriate model.

Table 3. Arrhenius parameters determined by the Coats–Redfern method and isokinetic parameters for a sample with 1phr of ytterbium triflate

Models	Coats-Redfern (1 phr)			IKR (1 phr)			
	E_{ap} (kJ/mol)	lnA (min^{-1})	r	a (mol/kJ)	b (min^{-1})	T_{iso} (ºC)	r
$A_{3/2}$	67.17	17.966	0.9992	0.3300	-3.949	91.45	0.9994
A_2	48.67	12.288	0.9991	0.3017	-2.138	125.64	0.9988
A_3	30.17	6.464	0.9989	0.2734	-0.326	166.90	0.9976
A_4	21.01	3.429	0.9987	0.2593	0.579	190.91	0.9968
R_2	86.47	22.840	0.9944	0.3699	-7.791	52.14	0.9994
R_3	92.09	24.202	0.9966	0.3623	-2.287	58.99	0.9989
D_1	149.39	41.560	0.9854	0.4673	-13.773	-15.61	0.9982
D_2	174.73	49.486	0.9924	0.4920	-15.746	-28.53	0.9994
D_3	190.99	52.245	0.9968	0.5231	-18.879	-43.05	0.9999
D_4	175.71	47.527	0.9938	0.5022	-17.785	-33.51	0.9997
F_1	104.17	29.087	0.9993	0.3866	-7.572	38.09	0.9999
power	32.23	6.885	0.9802	0.2794	-0.971	157.43	0.9953
n+m=2; n=1.9	131.85	37.948	0.997	0.4249	-9.318	10.04	0.9970
n+m=2; n=1.5	70.22	19.863	0.9968	0.3324	-3.077	88.80	0.9997
n=2	147.26	42.463	0.9971	0.4481	-10.837	-4.56	0.9961
n=3	199.66	58.584	0.9874	0.5238	-14.887	-43.37	0.9838

In table 4 it can be seen the Coats-Redfern results for the other two samples and how the kinetic model chosen ($A_{3/2}$) is valid for all the systems. In both cases the model F_1 could be possible from the point of view of the regression but the obtained E_{ap} is much higher than the isoconversional one (table 5). Thus, the model $A_{3/2}$ was chosen and considered appropriate for all the systems. These results where also confirmed by the so called method of the Reduced Master Curves proposed by J.M. Criado [33, 34], and results showed that the kinetic model chosen ($A_{3/2}$) fitted very well with experimental data.

Table 4. Arrhenius parameters determined by the Coats–Redfern method for samples with 0.5phr and 2phr of $Yb(TfO)_3$

Models	Coats-Redfern (0.5 phr)			Coats-Redfern (2 phr)		
	E_{ap} (kJ/mol)	lnA (min^{-1})	r	E_{ap} (kJ/mol)	lnA (min^{-1})	r
$A_{3/2}$	59.17	15.242	0.9997	66.71	18.626	0.9999
A_2	42.65	10.210	0.9997	48.39	12.809	0.9999
A_3	26.14	5.016	0.9996	30.07	6.837	0.9999
A_4	17.88	2.284	0.9996	20.91	3.726	0.9999
R_2	76.93	19.621	0.9997	86.26	23.809	0.9989
R_3	81.78	20.739	0.9999	91.69	25.173	0.9995
D_1	134.40	36.543	0.9975	149.64	43.373	0.9957
D_2	157.40	43.729	0.9992	174.20	51.262	0.9982
D_3	170.46	45.465	0.9999	189.94	54.113	0.9995
D_4	157.26	41.408	0.9996	175.18	49.388	0.9987
F_1	92.20	25.094	0.9997	103.34	30.056	0.9999
power	28.43	5.516	0.9964	32.49	7.403	0.9943
n+m=2; n=1.9	115.54	32.583	0.9947	129.57	38.769	0.9965
n+m=2; n=1.5	61.12	16.808	0.9942	69.07	20.346	0.9962
n=2	129.14	36.521	0.9978	144.70	43.369	0.9965
n=3	173.87	50.216	0.9871	194.81	59.362	0.9899

Table 5. Variation of the activation energy with the conversion of samples with 0.5, 1 and 2 phr of ytterbium triflate

Conversion	E_{ef} (KJ/mol)		
	0.5 phr	1 phr	2 phr
0.1	47.9	59.5	59.0
0.2	60.0	60.9	62.2
0.3	62.0	61.9	61.3
0.4	62.9	62.4	61.0
0.5	63.5	63.0	61.1
0.6	63.9	63.4	61.5
0.7	64.2	64.0	61.7
0.8	64.6	64.7	61.7
0.9	64.9	66.0	61.3

All the samples have shown that the two methodologies (IKR and Coats-Redfern) produce the same result, and in both cases, it is necessary to know the effective *E* (isoconversional) value to determine the complete kinetic triplet (E_{ef}, *A* and $f(\alpha)$).

If we compare the activation energies (Table 5), a simple analysis would conclude that the fastest system is that with the minor E_{ef}, but this is not always true because it exist a compensation effect between *E* and *lnA*. Then, to know which system is the most efficient it should be compared the conversion rate *r*. Equation 8 shows the Arrhenius relation between *k* (rate constant), *A* and *E*.

$$k = A \cdot \exp\left(-\frac{E}{RT}\right) \rightarrow \ln k = \ln A - \frac{E}{R \cdot T} \tag{8}$$

From equation 1,

$$\ln r = \ln A - \frac{E}{RT} + \ln f(\alpha) \tag{9}$$

Introducing in this equation values of *E, A* and α with the chosen kinetic model $A_{3/2}$ and for a given conversion degree (α =0.5) we can obtain a graphic like Figure 4 (ln r = f (1/T)). In this figure it can be observed that, the higher the proportion of initiator the faster the system is. This graphic shows that when initiator is added in proportions of 0.5 and 1 phr there are almost no changes in the reaction rate, so the system is not too much accelerated when 1 phr is added. Nevertheless, when the initiator amount is 2 phr the curing gets faster than in the other two samples, especially at high temperatures. When 0.5 and 1 phr are used, straight lines are observed, it can be seen that at high temperatures there is almost a crossing between both reaction rate lines, meaning that some little differences in *E* where obtained. These results corroborate that in order to know which system is the fastest it is appropriate to consider not only E_{ef} but also the parameter *lnA* if they fit the same kinetic model.

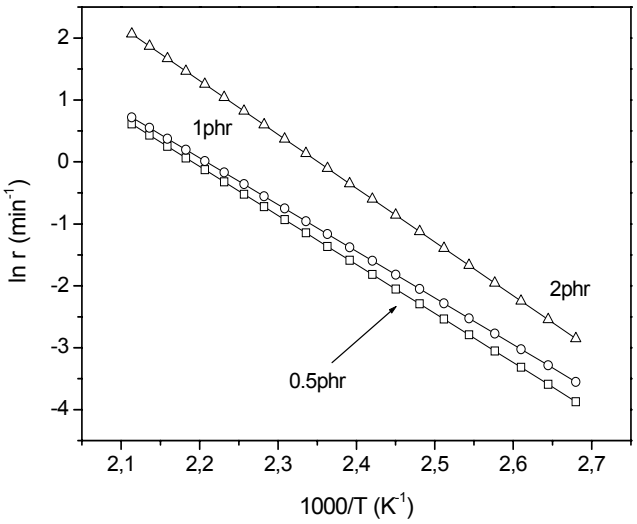

Fig. 4. Conversion rate (ln r) versus the inverse of the temperature (1000/T) for samples with 0.5, 1 and 2phr of ytterbium triflate.

In order to investigate whether the kinetic model chosen and isoconversional data obtained by the STAR software fitted the experimental data a comparison between conversion-time graphics for a given temperature was made. Because isothermal reactions of these systems took place very fast, the DSC equipment was not able to detect the initial calorimetric signal because stabilization time is needed and the initial part of the cure was lost.

The experimental conversion degree (α) data were obtained doing a first isothermal test during a given time in a DSC, and then a scan from 25 to 300ºC at 10ºC/min was performed for each isothermal test. With equation 10 and the residual enthalpies obtained, the different conversion values where calculated.

$$\alpha_{\exp} = \frac{\Delta H_{total} - \Delta H_{residual}}{\Delta H_{total}} \qquad (10)$$

where, ΔH_{tot} = 73.3 KJ/eq epoxy obtained from non-isothermal data.

Figure 5 represents the three curves obtained: kinetic model data, isoconversional data obtained by the STAR software and finally experimental data, for a sample with 0.5 phr of ytterbium triflate.

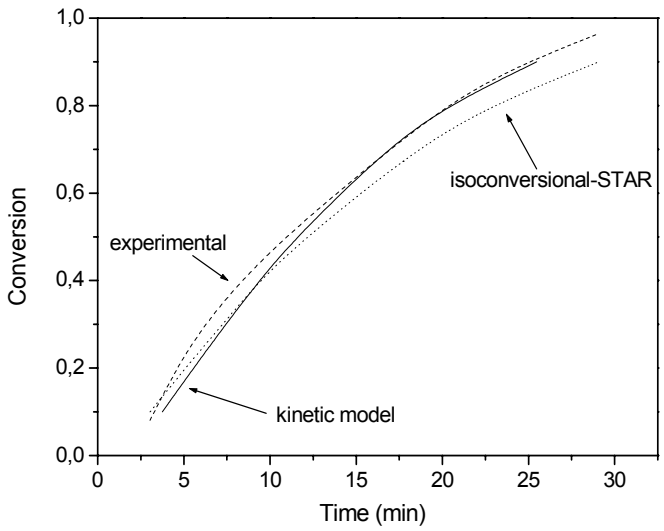

Fig. 5. Conversion versus time graphics of data obtained experimentally (isothermally at 120ºC), isoconversionally with the STAR software and from the chosen kinetic model for a sample with 0.5 phr of ytterbium triflate.

It can be observed that the three curves show a similar trend. The experimental data almost show the same conversion-time values than those obtained theoretically by the kinetic model. Only some few variations were found at low conversions.

The isoconversional data given by the STAR software were a bit different to those obtained by the kinetic model and experimentally.

Those little differences between the data could be due to the experimental limits of the DSC device.

Nevertheless, as the curves are very similar it can be pointed out that the kinetic model chosen fits quite well with the isoconversional data obtained with the STAR software and with the experimental data. So, with the appropriate kinetic model it has been possible to obtain easily the time-temperature-conversion triplet.

4. Conclusions

In order to reduce the curing temperature and time of powder coatings, and thus obtain production benefits, a Lewis acid as initiator has been proposed. The kinetics of reaction using Ytterbium (III) trifluoromethanesulfonate in three different proportions has been studied.

To compare kinetic results, it is necessary to know the complete kinetic triplet (*E*, *A*, $g(\alpha)$) because of the existence of a compensation effect between *E* and *lnA*. The use of *E* as a unique comparative parameter can introduce errors.

Two methods that allow the determination of the complete kinetic triplet have been shown, as well as the simulation of the curing. Both methods require the effective *E* value to be known, which can be determined with an isoconversional procedure (model-free).

An epoxy system composed by a DGEBA resin and a Lewis acid initiator (ytterbium (III) trifluoromethanesulfonate) with applications in the formulation of low curing powder coatings was studied. Three different amounts of initiator were studied: 0.5, 1 and 2phr. A kinetic study by means of non-

isothermal tests in a DSC was carried out and a posterior iso-kinetic study was developed. All systems showed that the reaction mechanism followed an $A_{3/2}$ grain growth model, showing no dependence on the initiator amount.

Reaction rates for all the systems were obtained. Results showed that the more the initiator is added the faster the reaction rate is, but adding 0.5 or 1 phr of initiator shows almost no differences in the reaction rate. An amount of 2 phr should be added in order to observe important changes in the acceleration of the system.

A simulation of the isothermal curing to a reasonably accurate degree has been obtained using a non-isothermal method. In this way it has been possible to obtain the isothermal curing degree versus temperature and time without any isothermal tests (that in fast catalyzed curing systems are experimentally difficult to perform) but only with four DSC dynamic scans at different rates.

Acknowledgments

Authors would like to thank Ms Eva Romero for her help in the development of this project. The authors from the Jaume I University are grateful for the economic support in this work of CICYT MAT 2000-0123-P4-03. The author from the Rovira i Virgili University would like to thank the CICYT-FEDER MAT2002-00291 and CIRIT SGR 00318 projects. Author from the Universitat Politécnica de Catalunya would like to thank CICYT and FEDER MAT2004-04165-C02-02 for their financial support.

1. R.A. Dickie, D.R. Bauer, S.M. Ward, D.A. Wagner, *Prog. Org. Coat.,* 31 (1997) 209
2. S.S. Lee, H.Z.Y. Han, J.G. Hilborn, J.-A.E. Manson, *Prog. Org. Coat.,* 36 (1999) 79
3. E.G. Belder, H.J.J. Rutten, D.Y. Perera, *Prog. Org. Coat.,* 42 (2001) 142
4. J. Hess, Powder everywhere, *Coatings World*, Vol. 36. 1999
5. T.A. Misec (Ed.), *Powder Coatings Chemistry and technology*, Wiley, New York, 1991
6. R. van der Linde, B.J.R. Scholtens, E.G. Belder, *Proceedings of the 11th International Conference on Organic Coatings in Science and Technology*, pp. 147, Athens, Greece, 1985
7. F.M. Witte, C.D. Goemans, R. van der Linde, D.A. Stanssens, *Prog. Org. Coat.,* 32 (1997) 241
8. M. Osterhold, F. Niggemann, *Prog. Org. Coat.,* 33 (1998) 55
9. M. Johansson, H. Falken, A. Irestedt, A. Hult, *J. Coat. Tech.,* 70 (884) (1998) 57
10. S.S. Lee, H.Z.Y. Han, J.G. Hilborn, J.-A.E. Manson, *Prog. Org. Coat.,* 36 (1999) 79
11. R. van der Linde, E.G. Belder, D.Y. Perera, *Proceedings of the 25th International Conference on Organic Coatings in Science and Technology*, Vol. 15, Athens, Greece, 1999, *Prog. Org. Coat.,* 40 (2000) 215
12. D. Maetens, L. Moens, L. Boogaerts, K. Buysens, *Eur. Coat. J.,* 5 (1999) 26
13. T. Endo, F. Sanda, *Macromol. Symp.,* 107 (1996) 237
14. C. Mas, A. Serra, A. Mantecón, J.M. Salla, X. Ramis, *Macromol. Chem. Phys.,* 202 (2001) 2554
15. S. Kobayashi, *Synlett,* (1996) 689
16. L. Matejka, P. Chabanne, L. Tighzert, J.P. Pascault, *J. Polym. Sci. Part A: Polym. Chem.,* 32 (1994) 1447
17. P. Chabanne, L. Tighzert, J.P. Pascault, *J. Apply. Polym. Sci.,* 53 (1994) 769
18. P. Castell, M. Galià, A. Serra, J.M. Salla, X. Ramis, *Polymer,* 41 (2000) 8465
19. H.E., Kissinger, *Anal. Chem.,* 29 (1957) 1702
20. X. Ramis, J.M. Salla, C. Mas, A. Mantecón, A. Serra, *J. Appl. Polym. Sci.,* 92 (2004) 381
21. X. Ramis, J.M. Salla, J. Puiggalí, J. *Polym. Sci. Part A: Polym. Chem*, Vol. 43 (2005) 1166
22. J. Macan, I. Brnardić, M. Ivanković, H.J. Mencer, *J. Therm. Anal. Calorim.,* 81-2 (2005) 369
23. X. Ramis, A. Cadenato, J.M. Morancho, J.M. Salla, *Polymer,* 44 (2003) 2067
24. X. Ramis, J.M. Salla, A. Cadenato, J.M. Morancho, *J. Therm. Anal. Calorim.,* 72 (2003) 707
25. A.W. Coats, J. Redfern, *Nature,* 207 (1964) 290
26. M.J. Starink, *Thermochim. Acta,* 404 (2003) 163

27. L.A. Pérez-Maqueda, P.E. Sánchez-Jiménez, J.M. Criado, *Polymer,* 46 (2005) 2950
28. S. Vyazovkin, W. Linert, *Int. Rev. Phys. Chem.,* 14 (1995) 355
29. S. Vyazovkin, C.A. Wight, *Annu. Rev. Phys. Chem.,* 48 (1997) 125
30. X. Ramis, A. Cadenato, J.M. Salla, J.M. Morancho, A. Vallés, L. Contat, A. Ribes, *Polym. Degrad. Stab.,* 86 (2004) 483
31. S. Vyazovkin, W. Linert, *J. Solid State Chem.,* 114 (1995) 392
32. S. Vyazovkin, W. Linert, *Chem. Phys.,* 193 (1995) 109
33. J.M. Criado, *Thermochim. Acta,* 24 (1978) 186
34. F.J. Gotor, J.M. Criado, J. Malek, N. Koga, *J. Phys. Chem. A,* 104 (2000) 10777

Influence of the Addition of Erbium and Ytterbium Triflates in the Curing Kinetics of a DGEBA/o-tolylbiguanide powder mixture

S.J. García[1], A. Serra[2], X. Ramis[3] & J. Suay[4]

[1] Àrea de Ciència dels Materials i Enginyeria Metal·lúrgica, Departamento de Ingeniería de Sistemas Industriales y Diseño. Universitat Jaume I. Avda. Vicent Sos Baynat s/n, 12071 Castelló, Spain

[2] Departament de Q. Analítica i Q. Orgànica. Facultat de Química. Universitat Rovira i Virgili. C/Marcel·lí Domingo s/n, 43007 Tarragona, Spain

[3] Laboratori de Termodinàmica, Escola Tècnica Superior Enginyeria Industrial Barcelona, Universitat Politècnica de Catalunya, Diagonal 647, 08028 Barcelona, Spain

[4] Centro de Biomateriales, Universitat Politècnica de València, Camino de Vera s/n, E-46071 Valencia, Spain

Journal of Thermal Analysis and Calorimetry

11 Agosto 2006. Versión online-first

Abstract

Solid bisphenol-A epoxy resin (DGEBA) of medium molecular weight was cured using o-tolylbiguanide (TBG) as crosslinking agent. In order to improve the kinetics of the reactive system, two Lewis acid catalysts (erbium (III) and ytterbium (III) trifluoromethanesulfonates) were added in proportions of 1 phr. The kinetic study was performed by dynamic scanning calorimetry (DSC) and the complete kinetic triplet (E, A, and g(α)) determined. The kinetic analysis was performed with an integral isoconversional procedure (model-free), and the kinetic model was determined by the Coats–Redfern method and through the compensation effect (IKR). All the systems followed the m=1.5/ n=0.5 isothermal curing model simulated from non-isothermal experiments. The addition of a little proportion of ytterbium or erbium triflates accelerated the curing process. In order to extract further information about the role of the lanthanide triflates added to epoxy/TBG systems, the kinetic results were compared with our previous kinetic studies made on DGEBA/lanthanide triflates initiated systems.

1. Introduction

Powder coatings are currently the fastest growing section of industrial paints, because of their favourable environmental attributes (less than 4% of volatile organic contents) and performance advantages [1]. Apart from their clear advantages, powder coatings, show some limitations, like the difficulty of application on thermo-sensible substrates like wood or plastic [2]. Nowadays, the most used powder coating systems are those based on epoxy resins cured with dicyandiamide (DICY) or its derivatives, which are used in proportions of 4 to 6 phr and the curing temperature is above 448K [3]. For this reason, the formulation of new epoxy powder coatings (using new catalysts and crosslinkers) capable to cross-link at lower temperatures has become one of the main lines of research in industries and related research centres.

In Scheme 1 it can be observed the structure of the cross-linker used in the present work. o-Tolylbiguanide (TBG) is structurally related to DICY, which is a typical latent curing agent. This curing agent was reported to be effective in the curing of DGEBA epoxy resins [4] and in liquid crystalline epoxy resins [5] but no studies were reported on the reaction mechanism.

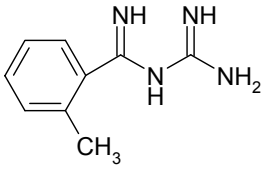

Scheme 1. Structure of the cross-linking agent, TBG

Barton [6] reported the mechanism followed by the curing of epoxy resins with DICY, in which the amine groups react with epoxides leading to the formation of four new C-N linkages. TBG should react similarly to DICY with epoxy groups, but from its structure, a functionality of five can be predicted (Scheme 2). Thus, one mol of TBG reacts with five equivalents of epoxy resin.

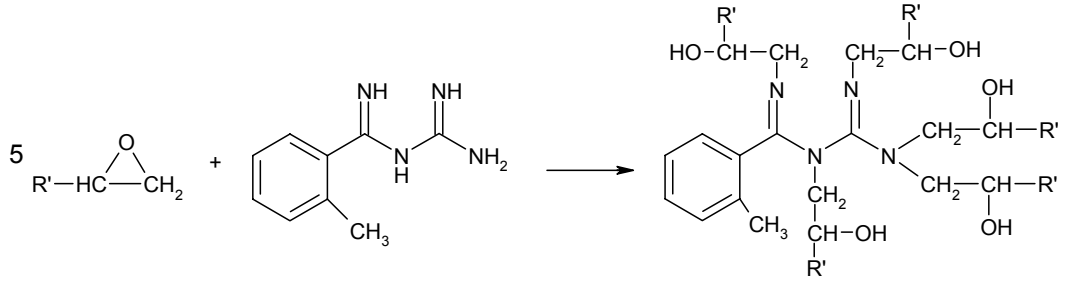

Scheme 2. Chemical structure of the network using TBG as cross-linking agent

One of the main objectives of this research was to obtain epoxy powder systems with low curing temperatures so that they can be applied on different substrates sensitive to temperature (mainly different types of organic ones, like plastics), and of course to reduce energetic costs in the curing process.

Catalysts are important in polymerization processes because they decrease the activation energies (when comparing systems with the same reaction mechanism process) and accelerate the reaction. They can be stimulated by heating or photoirradiation but, from the practical point of view, heating is the easier option, because homogeneous heating of reaction mixtures can be achieved without difficulty [7] and because the curing is not too much influenced by the pigments, like in UV paints happens [8]. Among the new cationic thermal initiators, those having anions with low nucleophilicity minimize or prevent the reaction of the growing chain with the anion, being more actives their cationic salts and more effective the polymerization [9].

Lewis acids used as initiators or catalysts, such as $AlCl_3$, BF_3 or $TiCl_4$ are moisture sensitive and easily decompose in the presence of humidity. On the contrary, lanthanide triflates are stable and act as Lewis acids in water or humid environments. This fact represents an enormous advantage in their technological applications as catalysts. The lanthanide cations (Ln(III)) have a very high coordination capacity and a great oxophilicity, thus, weakening the C-O bond [10], and favouring the cationic mechanisms of reaction. This process is improved by the electron-withdrawing capacity of the anionic group, TfO^- [10].

As usual in Lewis acid initiators, erbium (III) and ytterbium (III) trifluoromethanesulfonates (here on, $Er(TfO)_3$ and $Yb(TfO)_3$ respectively), lead to chain growth polymerization of epoxy compounds, which mainly proceed by the cationic chain end mechanism depicted in Scheme 3, where oxirane groups of DGEBA resin are opened by coordination of oxirane oxygen to the initiator and subsequent nucleophylic attack of another oxirane group. This mechanism is known as activated chain end mechanism (ACE).

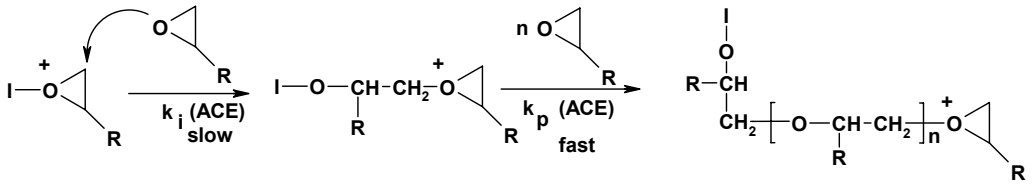

Scheme 3. Activated chain-end mechanism / ACE

Moreover, the presence of hydroxylic groups can lead to hydroxylic initiated polyetherification processes that can change both the kinetics of the reaction and the properties of the materials (Scheme 4), although this kind of reaction should be less important in extension than the first one, because of the low proportion of hydroxyls. This mechanism is known as activated monomer mechanism (AM).

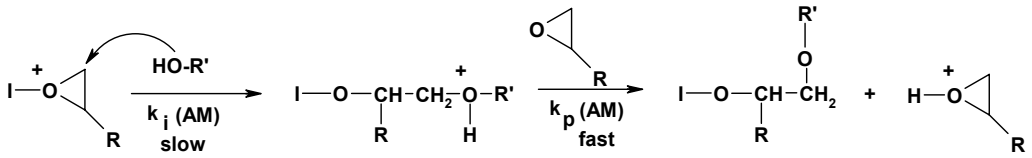

Scheme 4. Activated monomer mechanism / AM

Thus, the proportion of hydroxylic groups can influence the global propagation rate. In addition to these competitive chain growth mechanisms, inter and intra molecular transfer processes can occur and also termination reactions. All these processes lead to changes in the network structure and difficult the study of the kinetics of each separated process. Thus, the kinetics of a cationic cure should be studied taking the process as a whole [11,12].

The usefulness of lanthanide triflates as initiators has been proved in other studies [9, 13] with liquid epoxy resins, showing that they highly accelerated the reactions of the system. Their effect in powder coatings has also been studied for systems using DGEBA resin with lanthanide triflates as initiator [14, 15], proving that they offer very good improvements in curing kinetic processes. However, no research has been published about their effect in the curing kinetics of a powder system DGEBA resin-DICY derivative where a triflate is added as a catalyst.

Several authors described the ability of lanthanide triflates to catalyze the reaction of epoxides and nitrogen heterocycles [16] or amines [17,18] to give β-aminoalcohols. It seems that the coordination of oxirane oxygen to lanthanide facilitates the nucleophylic attack of the nitrogen to the oxirane ring by weakening the C-O bonds of the epoxide groups and making more electrophylic the carbon atoms of this group. Therefore, the use of lanthanide triflates could also catalyze the reaction of DGEBA with TBG facilitating the cure at lower temperatures.

Nevertheless, when using a Lewis acid catalyst we are promoting the homopolymerization where the nucleophylic agent is the oxirane oxygen instead of the amine, especially when hydroxylic groups are originated during curing. In this case, the Lewis acid acts as initiator, because it remains attached to the polymeric chain. However, nitrogen compounds are generally more nucleophylic than oxiranes or hydroxylic groups and therefore the competitive homopolymerization processes should be, in principle, less important. On the other hand, the reaction of TBG with the epoxy resin originates hydroxylic groups, which favours the homopolymerization of oxirane by an AM mechanism (Scheme 4). These facts prompted us to investigate the role of lanthanide triflates in the curing of DGEBA resins with TBG.

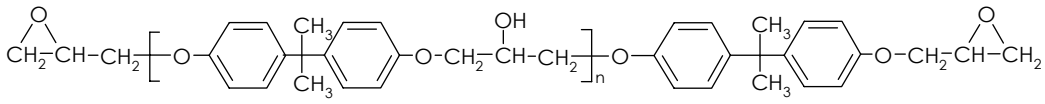

Scheme 5. DGEBA epoxy resin structure

The difference in the reaction mechanisms gives rise to differences in the structure of the network and in the reaction enthalpies. In order to know if the network formed is different or not we used infrared spectroscopy (FTIR) because it could give significant structural information. Moreover, some degradation tests (such as TGA measurements) were performed, because the stability of the network could be slightly affected by the chemical structure of the network.

To predict the temperatures and times at which these polymerizations should be performed, one must know the kinetics. Preliminary kinetic studies have been done using the method described by Kissinger [19]. This procedure, used by many authors because of its simplicity, assumes an *n* order mechanism. However, this assumption is not correct in many cases and leads to incorrect values of pre-

exponential factor A. In addition, kinetic methods that only use the maximum of the velocity curve to determine the kinetic parameters do not allow an assessment of whether these parameters vary during polymerization or not. In the present study we attempt to establish a method for this curing that allows the complete kinetic triplet (kinetic model, E and A) to be determined throughout the entire reaction. To analyze exothermic polymerizations, we have used a method from earlier studies addressing the kinetics of curing and degradation [20].

Many exothermic polymerizations have difficulties for the determination of the heat of reaction through isothermal experiments and the subsequent deduction of the kinetics from these values. When reactions are performed at high temperatures, some of the heat may be lost during the stabilization of the apparatus, whereas at low temperatures, the heat is released slowly and can fall below the sensitivity of the calorimeter. Another problem arises when a physical phenomenon (e.g. fusion) overlaps with the polymerization. One alternative in both cases is to simulate isothermal polymerization with non isothermal data [21]. Different studies on the curing kinetics of liquid [22-24] and powder coatings [14, 15] using systems containing epoxy resins and diamines have been published.

In this work, a complete kinetic study of polymerization of a medium molecular weight DGEBA resin cured with TBG and little proportions of erbium (III) or ytterbium (III) trifluoromethanesulfonates has been developed. The reaction model was established from non isothermal data by two different methods. The first was the Coats-Redfern method [25-27], where the E value obtained isoconversionally was taken as the effective value (E_{ef}) and used to obtain the correct kinetic model, g(α), by comparing E_{ef} with the E values obtained from Coats-Redfern method (E_{ap}). The second method used the compensation effect (IKR) existing between E and A at the change in the degree of conversion (α) [20, 28].

2. Experimental

2.1. Materials

Solid bisphenol-A based epoxy resin of medium molecular weight (Scheme 5), 733 gr/eq epoxy (from Huntsman), was polymerized in the ratio given by the producer with a Huntsman DICY derivative, TBG (with an H^+ active equivalent weight of 37g/eq), and adding 1 phr of Erbium (III) and Ytterbium (III) trifluoromethanesulfonates (from Aldrich) (one part of lanthanide triflate per hundred of resin, w/w). Two samples of epoxy resin were homopolymerized with 1 phr of Erbium (III) and Ytterbium (III) trifluoromethanesulfonates. The compositions of the samples are detailed in Table 1.

Table 1. Composition of the samples studied and glass transition temperature after curing

Sample	Epoxy resin	TBG (phr)	$Er(TfO)_3$ (phr)	$Yb(TfO)_3$ (phr)	T_g (K)
1	100	4.8	-	-	369
2	100	4.8	1	-	373
3	100	4.8	-	1	370
4	100	-	1	-	382
5	100	-	-	1	382

Samples were pre-mixed and hand-shacked until good pre-mixing was afforded. After that, the material was extruded in a single screw extruder (Haake Rheomex 254), where operating conditions were 352K along the extruder and 60 rpm. After extruding, the material was grinded in an ultra-centrifugal mill ZM 100 and sieved at 100 micron.

2.2. Testing Methods and Equipment

2.2.1. Differential scanning calorimeter (DSC)

A Perkin Elmer DSC 7 differential scanning calorimeter was employed for dynamic scans in order to study the non isothermal curing process and to obtain the kinetic model parameters. The samples were analyzed in covered aluminium pans, using high purity indium sample for calibration. A flow of 20 $cm^3 \cdot min^{-1}$ of argon was used as purge gas. The weight of the samples was between 9 and 10 mg. Non isothermal tests were performed at rates of 2.5, 5, 10 and 15 $K \cdot min^{-1}$ to the not-cured-samples showed in Table 1. The scans were performed in the temperature range from 298 to 573K.

DSC was also employed to measure the midpoint T_g of the samples after curing them at 423K for 25 minutes, reaching the total cure. DSC scans were performed at $10Kmin^{-1}$.

STARe Mettler-Toledo software was used in order to calculate conversion degrees and kinetics of the process. Kinetic analysis, using Coats-Redfern and IKR methods, were used to calculate the kinetic triplet (*A* pre-exponential factor, *E* effective activation energy, and *g(α)* integral function of the degree of conversion or kinetic model).

2.2.2. Kinetic Analysis

If we accept that the dependence of the rate constant (k) on the temperature follows the Arrhenius equation, then the kinetics of the reaction is usually described as follows:

$$r = \frac{d\alpha}{dt} = A \exp\left(-\frac{E}{RT}\right) f(\alpha) \qquad (1)$$

where *t* is the time, *T* is the absolute temperature, *R* is the gas constant, and *f(α)* is the differential conversion function. Kinetic analysis has generally been performed with an isoconversional method. The basic assumption of such method is that the reaction rate at a constant conversion is solely a function of temperature [29].

2.2.2.1. Isothermal Methods

By integrating the rate equation (eq 1) under isothermal conditions, we obtain:

$$\ln t = \ln\left[\frac{g(\alpha)}{A}\right] + \frac{E}{RT} \qquad (2)$$

where *g(α)* is the integral conversion function and is defined as follows:

$$g(\alpha) = \int_0^{\alpha} \frac{d\alpha}{f(\alpha)} \quad (3)$$

According to eq 2, *E* and the constant ln[g(α)/A] can be obtained from the slope and the intercept, respectively, of the linear relationship *ln t = f(T $^{-1}$)* for a constant value of α.

Isothermal methods require long times to be performed and give problems with the data acquisition. Firstly, as isothermal reactions of these systems took place very fast, the DSC equipment was not able to detect the initial calorimetric signal because stabilization time is needed and the initial part of the cure is lost (meaning that the curing reaction begins before reaching the isothermal temperature). Secondly, when the isothermal test finishes the cooling of the sample in the calorimeter is not immediate, so again some time is needed to decrease the temperature and the reaction process continues until ambient temperature is reached, probably non-isothermal data could give more accurate results than those given by isothermal experiments.

2.2.2.2. Non-isothermal Methods

When non-isothermal methods are applied, the integration of rate equation (eq. 1) and its reordering gives place to the so-called temperature integral:

$$g(\alpha) = \int_0^{\alpha} \frac{d\alpha}{f(\alpha)} = \frac{A}{\beta}\int_0^{T} e^{-(E/RT)}dT \quad (4)$$

where, β is the heating rate.

By using the Coats-Redfern [22] approximation for the resolution of eq. 4 and considering 2RT/E << 1, we can rewrite this equation as follows:

$$\ln\frac{g(\alpha)}{T^2} = \ln\left[\frac{AR}{\beta E}\right] - \frac{E}{RT} \quad (5)$$

For a given kinetic model, the linear representation of *ln[g(α)/T ^{2}]* versus *T $^{-1}$* makes it possible to determine E_{ap} and *A* from the slope and the ordinate at the origin.

In this work, the kinetic model that had the best linear correlation in the Coats-Redfern equation and that had an *E* value (E_{ap}) similar to that obtained isoconversionally (considered to be the effective *E* value, E_{ef}) was selected.

By reordering equation 5, we can write:

$$\ln\frac{\beta}{T^2} = \ln\left[\frac{AR}{g(\alpha)E}\right] - \frac{E}{RT} \quad (6)$$

The linear representation of *ln[β/T ^{2}]* versus *1/T* makes it possible to determine E_{ef} (effective E value) and the kinetic parameter *ln[AR/g(α)E]* for every value of *α*.

The constant *ln[AR/g(α)E]* is directly related by the *R/E* to the constant *ln[g(α)/A]* of the isothermal adjustment. Thus, taking the dynamic data *ln[AR/g(α)E]* and *E* from eq. 6, we can determine the isothermal parameters of eq. 2 and simulate isothermal curing without knowing *g(α)* [24, 30].

The STARe Mettler-Toledo Software uses eq. 6 and 2 to determine the isonconversional activation energy and the isothermal times, respectively.

2.2.2.3. Compensation Effect and Isokinetic Relationship (IKR)

Complex processes are characterized by the dependences of *E* on *A* and *α*. This generally reflects the existence of a compensation effect through the following equation:

$$\ln A_\alpha = aE_\alpha + b = \frac{E_\alpha}{RT} + \ln\left[\frac{(d\alpha/dt)_\alpha}{f(\alpha)}\right] \quad (7)$$

where, *a* and *b* are constants and the subscript α represents the degree of conversion that produces a change in the Arrhenius parameters.

The slope $a=1/RT_{iso}$ is related to the isokinetic temperature (T_{iso}), and the intercept $b=lnk_{iso}$ is related to the isokinetic rate constant (k_{iso}). Equation 7 represents an IKR and can be deduced by the reordering of eq. 2. The appearance of the IKR shows that there is only one model, whereas the existence of parameters that do not meet the IKR (meaning that for a given α the relation between A and E_{ef} changes) implies that there are several models [31], because f(α) is not constant in all the process.

In this study, the kinetic model whose IKR had the best linear correlation between E_{ef} and A and in which the associated T_{iso} value was near the experimental temperature range was selected [32]. The influence of the addition of erbium and ytterbium triflates in the kinetics of the epoxy/TBG system has been studied.

2.2.3. Infrared Spectroscopy (FTIR)

The FTIR spectra were taken using a 680Plus Jasco with a resolution of 4cm^{-1} in the absorbance mode. The samples were put on an attenuated reflection accessory with thermal control and diamond crystal (Golden Gate Heated Single Reflection Diamond ATR, Specac-Teknokroma) and were registered at room temperature.

2.2.4. Thermogravimetric Analysis (TGA)

A Setaram thermogravimetric analyzer (TGA) was used. Cured samples (25 minutes at 423K, so total curing was afforded) between 15 and 20 mg of weight were scanned up to 1173K at 10 $K \cdot min^{-1}$. All scans were performed with an argon flow of 50 cm^3min^{-1}.

3. Results and Discussion

Figure 1 shows the DSC-thermograms registered at a heating rate of 5K/min for the five different samples studied. The thermograms exhibit a small endothermic peak at 328K (where the T_g should be

detected) related to the physical aging of the DGEBA. All the thermograms show a big exothermic peak at high temperatures (with its minimum between 403 and 433K) related to the curing reaction of the epoxy resin. It can be seen, that when ytterbium and erbium triflate are used the exotherm shifts to minor temperatures compared to the reference sample DGEBA/TBG, demonstrating the acceleration effect of these Lewis acids. Moreover, when ytterbium and erbium triflates are used alone as initiators the exotherm appears at lower temperatures. Samples containing TBG and lanthanide triflates show a second exothermic peak at 498K in the curing, due to some secondary or residual reactions. This secondary peak has been observed in thermograms registered at different heating rates (figure 2) but when the rate is very low (2.5K/min) this peak has almost disappeared. The interpretation of this secondary peak is difficult because the complexity of the curing process [6].

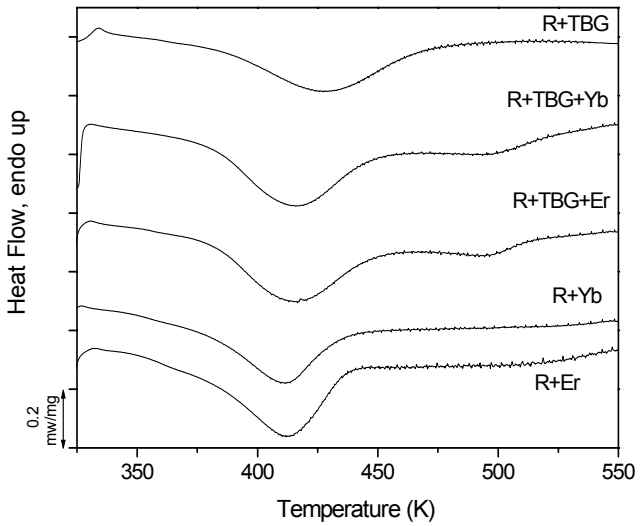

Fig. 1. Non-isothermal DSC thermograms at 5K/min of heating rate for mixtures epoxy resin/TBG, epoxy resin/TBG/erbium triflate, epoxy resin/TBG/ytterbium triflate, epoxy resin/erbium triflate, and epoxy resin/ytterbium triflate.

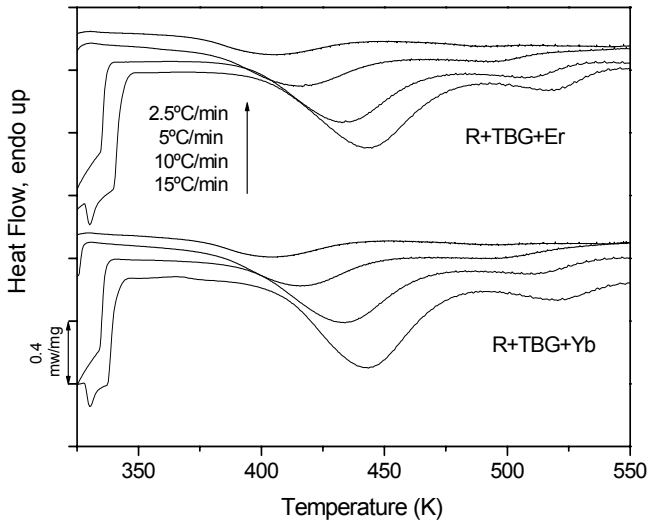

Fig. 2. Non-isothermal DSC thermograms at 2.5, 5, 10 and 15K/min of heating rate for mixtures epoxy resin/TBG/erbium triflate, and epoxy resin/TBG/ytterbium triflate.

The calorimetric scans at different heating rates were used to obtain the dependence of the conversion degree with the temperature, by means of the STARe software. Figure 3 shows *α* versus *T* plots for a heating rate of 5K/min for all the samples studied. Almost no differences are detected in systems cured with both TBG and ytterbium or erbium triflates. Nevertheless, larger differences are observed when lanthanide triflates are used alone as initiators. In this case, erbium triflate allows performing the curing at lower temperatures than with ytterbium. In all samples containing lanthanide triflates a displacement towards lower temperatures was observed.

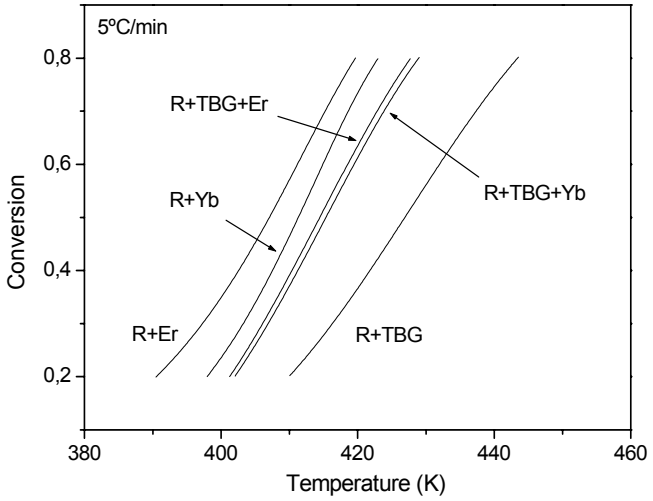

Fig. 3. Conversion degree (α) versus temperature plots for a heating rate of 5K/min for epoxy resin/TBG, epoxy resin/TBG/erbium triflate, epoxy resin/TBG/ytterbium triflate, epoxy resin/erbium triflate, and epoxy resin/ytterbium triflate mixtures.

The non-isothermal isoconversional kinetic parameters were calculated from the α-*T* curves (from the STARe) by the application of eq. 6 to different conversions, and from these, the isothermal parameter *ln[g(α)/A]*, with which the studied curing process would subsequently be simulated. Table 2 collects the E_{ef} values of non-isothermal curing obtained from eq. 6 for the samples prepared using TBG and TBG with lanthanide triflates. It can be seen that the introduction in the reactive mixture of an initiator, which can promote the cationic homopolymerization reaction, produces a rise of the E values of the system. This could be due to the fact that the homopolymerization of the epoxy resin has higher E values than those obtained for systems cured only with nitrogen compounds, as Barton observed previously [33]. In previous papers we reported the E_{ef} values obtained for DGEBA/lanthanide triflate mixtures, which are, in general, higher [14, 15]. Table 2 shows that E_{ef} is weakly modified during curing due to the complex reaction mechanism.

Table 2. Variation of the effective activation energy with the conversion of epoxy resin/TBG, epoxy resin/TBG/erbium triflate and epoxy resin/TBG/ytterbium triflate samples

Conversion	E_{ef} (KJ/mol)		
	R+TBG	R+TBG +Er(TfO)$_3$	R+TBG +Yb(TfO)$_3$
0.2	66,0	80,6	80,6
0.3	64,9	77,7	78,6
0.4	64,3	76,3	77,8
0.5	63,8	75,6	77,5
0.6	63,4	75,3	77,7
0.7	62,9	75,2	78,0
0.8	62,3	74,7	78,2
Average	63,9	76,5	78,3

Figure 4 shows the experimental relationship between $ln[\beta/T^2]$ and the inverse of the temperature, with the adjustment made with eq. 6 for the sample DGEBA/TBG/erbium triflate.

To establish the kinetic model for these systems, the isoconversional kinetic parameters obtained for each sample and the eq. 7 were used (IKR method). From the parameters $ln[AR/g(\alpha)E]$ and E_{ef}, and the $g(\alpha)$ functions (see reference [20]), *A* values were calculated for all the different kinetic models. Subsequently, by plotting E_{ef} against *lnA*, we determined the IKRs for all the models (eq. 7). Table 3 shows the obtained results for a sample epoxy resin/TBG, where T_{iso} values were determined from the slope of the IKRs. Although some models exhibit IKRs (especially $A_{3/2}$ and m=0.5/n=1.5), the best model, which describes the polymerization of the sample is the m=0.5/n=1.5 because it shows a good regression and T_{iso} values in the range of the experimental temperatures. In agreement with Vyazovkin and Linert [32], a T_{iso} value close to the range of experimental temperatures indicates that the kinetic model accurately describes the reactive process. The samples using triflates as catalysts showed similar results, and thus, similar conclusion, being the kinetic model the same.

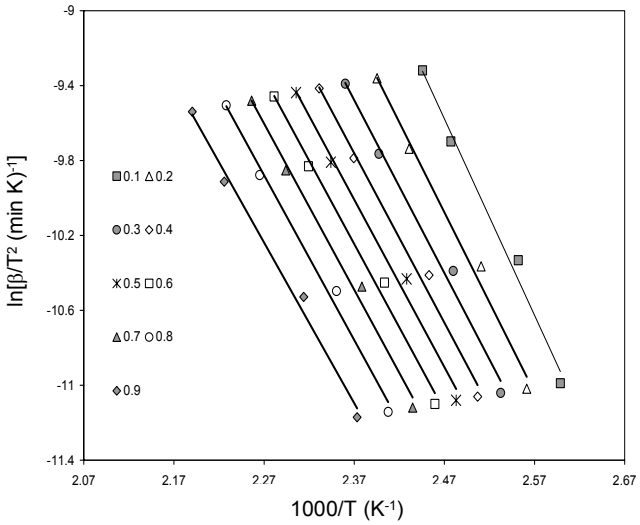

Fig. 4. Correlations between $\ln[\beta/T^2]$ and the inverse of the temperature (1000/T) for different values of α for a sample epoxy resin/TBG/erbium triflate.

Table 3. Arrhenius parameters determined by the Coats–Redfern method and isokinetic parameters for the curing of an epoxy resin/TBG mixture obtained at a heating rate of 5K/min

Models	Coats-Redfern			IKR			
	E_a (kJ/mol)	lnA (min^{-1})	r	a (mol/kJ)	b (min^{-1})	T_{iso} (K)	r
$A_{3/2}$	52.1	12.59	0.9981	0.318	-3.938	378.2	0.9980
A_2	37.3	8.17	0.9983	0.394	-8.685	305.8	0.9980
A_3	22.5	3.57	0.9977	0.469	-13.432	256.7	0.9976
A_4	15.1	1.13	0.9970	0.507	-15.806	237.6	0.9973
n+m=2; n=1.9	104.4	28.36	0.9995	0.051	13.587	2342.3	0.6632
n+m=2; n=1.5	54.8	14.38	0.9994	0.304	-2.007	395.9	0.9959
n=2	116.8	31.85	0.9995	-0.012	17.527	-10191.9	0.1717
n=3	159.5	44.64	0.9959	-0.235	32.391	-512.0	0.7953

To confirm the methodology used with the IKR, we determined E_{ap} and *ln A* for each tested model with the Coats-Redfern method (eq 5). The results obtained for the sample epoxy resin/TBG when eq. 5 was applied to conversions between 0.2 and 0.8, are shown in table 3 (similar results were obtained for the other two samples using TBG). Some of the models exhibit very good regressions, and so from these data alone, it is not possible to establish the reaction mechanism. To determine the kinetic model, it was also used the average value of E_{ef} obtained isoconversionally shown in Table 2. This value of *E* is considered the effective value because it was obtained without the necessity of determining the model. In addition to the good regression, the correct kinetic model must also possess a value of E_{ap} similar to the effective value (E_{ef}). According to these criteria model m=0.5/n=1.5, with good regression and E_{ap} value closer to the E_{ef} in the three samples, is considered the correct one for samples with TBG, although model $A_{3/2}$ could also be possible. Samples initiated by lanthanide triflate fit the kinetic model $A_{3/2}$ [14, 15]. The fact that samples with TBG and lanthanide triflate fit a kinetic model closer to that obtained for samples with TBG alone seems to suggest that the main reaction could be the nucleophylic attack of the

biguanide nitrogens to the oxirane rings catalyzed by the lanthanide salt and not the homopolymerization of epoxides initiated by lanthanide triflates.

In order to corroborate this hypothesis the FTIR spectra of all the samples containing TBG were registered. All these spectra showed an identical pattern, in which the most characteristic absorption is the associated hydroxylic bands between 3600 and 3300 cm^{-1}. This absorption confirms the total reaction of TBG with epoxides and the no homopolymerization of epoxides, because TBG and epoxides are mixed in stoichiometric proportions. Figure 5 shows, as an example, the spectrum of the DGEBA/TBG/$Yb(TfO)_3$ sample after curing.

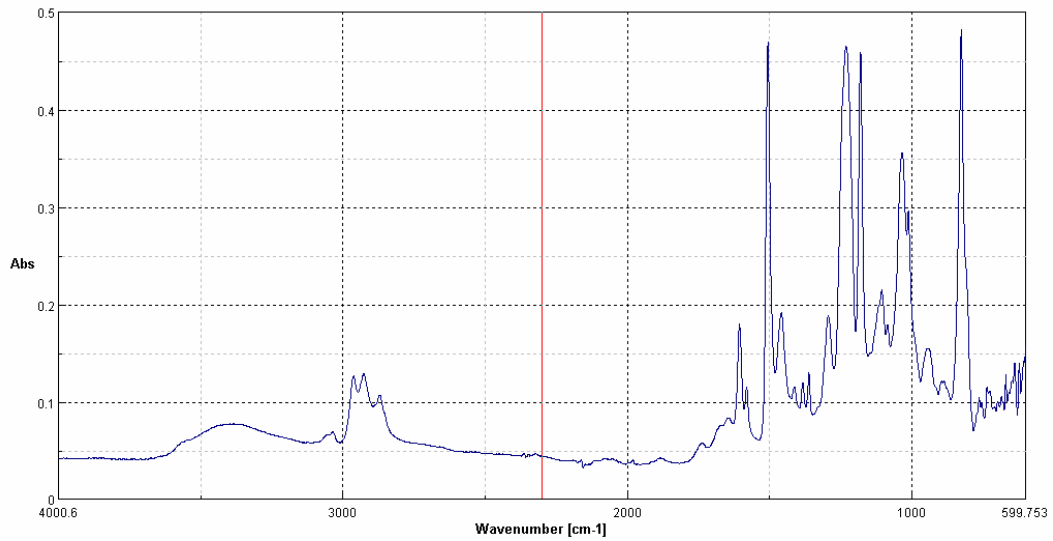

Fig. 5. FTIR spectrum of the cured material from a sample epoxy resin/TBG/ytterbium triflate.

Table 1 collects the glass transition temperature of the materials obtained from all the samples. First of all, it can be stated that there is only one T_g in all the materials, even in those containing TBG and lanthanide triflates together, which seems to indicate that the network is completely homogeneous for all the systems. Moreover, the T_g values obtained for the materials with TBG and lanthanide triflates are very close to those obtained for the system DGEBA/TBG. This fact indicates that the chemical structure of the network should be similar for the three systems using TBG, as well as the achieved curing degree.

Since the thermal stability is influenced by the chemical structure of the networks, some degradation tests were also carried out. In figure 6, we can see that the degradation curve of samples containing TBG and lanthanide triflate are closer to that obtained for the system using TBG alone. This fact again confirms that the network must have a similar chemical structure to that obtained for DGEBA/TBG mixtures.

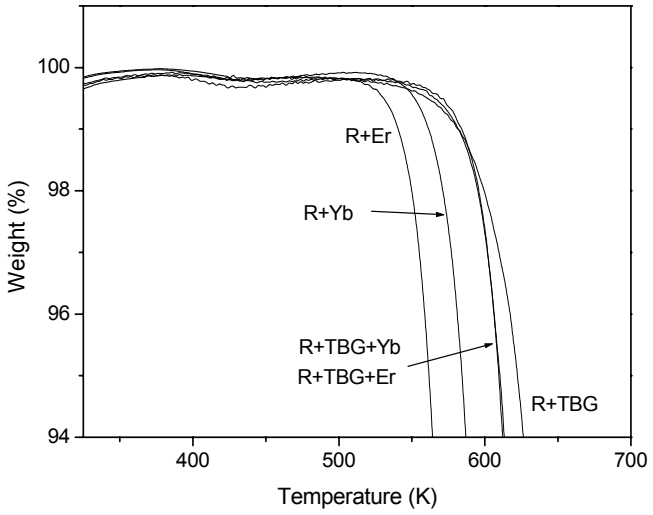

Fig. 6. TGA thermograms of epoxy resin/TBG, epoxy resin/TBG/erbium triflate, epoxy resin/TBG/ytterbium triflate, epoxy resin/erbium triflate, and epoxy resin/ytterbium triflate cured samples in argon atmosphere.

The obtained kinetic results were also confirmed by the so called method of the Reduced Master Curves proposed by J.M. Criado [34, 35] and showed that the kinetic model chosen (m=0.5/n=1.5) fitted very well with the experimental data.

All the samples investigated showed that the two methodologies (IKR and Coats-Redfern) lead to the same result, and in both cases, it is necessary to know the effective *E* (isoconversional) value to determine the complete kinetic triplet (E_{ap}, *A* and *f(α)*).

If we compare the activation energies (Table 2), a simple analysis would conclude that the fastest system is that with the minor E_{ef}, but this is not always true because a compensation effect between *E* and *lnA* exists. Then, to know which is the most efficient system it should be compared the conversion rate constant (because samples fit the same kinetic model g(*α*), if not, *r* should be compared instead of *k*). Eq. 8 shows the Arrhenius relation between *k* (rate constant), *A* and *E*.

$$k = A \cdot \exp\left(-\frac{E}{RT}\right) \rightarrow \ln k = \ln A - \frac{E}{R \cdot T} \tag{8}$$

From equation 1,

$$\ln r = \ln A - \frac{E}{RT} + \ln f(\alpha) \tag{9}$$

Introducing in equation (8) values of *E, A* and *α* with the chosen kinetic model (m=0.5/n=1.5) and for a given conversion degree (α =0.5) we can obtain a graphic like Figure 7 (ln k = f (1/T)). In this figure it can be observed that the addition of lanthanide triflate give rise to an acceleration of the reaction rate of systems cured with TBG. It can also be observed that there are no differences when using Yb or Er in systems with TBG. However, when ytterbium and erbium triflates were used alone as initiator differences in constant rates were observed between both lanthanide salts [14, 15]. These results corroborate that in

order to know which system could be cured at lower temperature it is appropriate to consider not only E_{ef} but also the parameter *lnA* if they fit the same kinetic model.

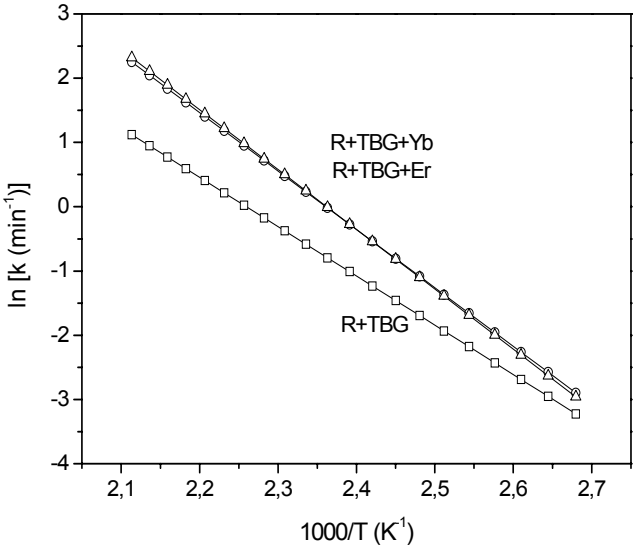

Fig. 7. Conversion rate (ln k) versus the inverse of the temperature (1000/T) for epoxy resin/TBG (□), epoxy resin/TBG/erbium triflate (o), and epoxy resin/TBG/ytterbium triflate (Δ).

Conclusions

In order to reduce the curing temperature and time of powder coatings based on DGEBA/TBG mixtures, and thus obtain production benefits, Erbium (III) and Ytterbium (III) trifluoromethanesulfonates have been proposed as catalysts. The kinetics of the curing processes has been studied.

Two methods that allow the determination of the complete kinetic triplet (*E*, *A*, *g(α)*) have been applied, as well as the simulation of the curing. Both methods require the effective *E* value to be known, which can be determined with an isoconversional procedure (model-free), for which STARe software has been used.

A kinetic study by means of non-isothermal tests in a DSC was carried out and a posterior iso-kinetic study was developed. All systems showed that the reaction mechanism followed an m=0.5/n=1.5 model, showing no dependence on the initiator used.

Reaction rates for all the systems were obtained. Results showed that adding lanthanide triflates accelerate the reaction of the system, but no differences were observed between ytterbium and erbium triflates.

Both FTIR and TGA studies confirm that the main reaction, which takes place in systems cured with TBG alone or TBG with 1phr of lanthanide triflate is the nucleophylic reaction between nitrogen and oxirane ring.

Acknowledgments

Authors would like to thank Ms Eva Romero for her help in the development of this project. The author from the Universitat Jaume I and Universitat Politècnica de València are grateful for the economic support in this work of CICYT MAT 2000-0123-P4-03. The author from the Universitat Rovira i Virgili would like to thank the MAT 2005-01806 project. Author from the Universitat Politècnica de Catalunya would like to thank CICYT and FEDER MAT2004-04165-C02-02 for their financial support.

---

1. S.S. Lee, H.Z.Y. Han, J.G. Hilborn, J.-A.E. Manson, *Prog. Org. Coat.*, 36 (1999) 79
2. U.S. Enviromental Protection Agency Center for Environmental Research Information, "*Technical Reference Manual on Techniques for reducing or eliminating releases of toxic chemicals in metal painting*",1995
3. R.S. Bauer, L.S. Corley, "*Epoxy Resins: Composites Technology*", Stuart M. Lee, Technomid Publishing Company. Inc., Pennsylvania 1989
4. M. Ochi, K. Mimura, H. Motobe, *J. Adhesion Sci. and Techn.*, 8 (1994) 223
5. B. Szczepaniak, K.C. Frisch, P. Penczek, J. Rejdych, A. Winiarska, *J. Polym. Sci: Part A: Polym. Chem.,* 35 (1997) 2739
6. J.M. Barton, K. Dusek, *Epoxy resins and composites, Adv. Polym. Sci.*, 72 (1985) 112
7. T. Endo, F. Sanda, *Macromol. Symp.*, 107 (1996) 237
8. The Powder Coating Institute, "*PCI Technical Brief No. 1*", *U.S.A.*
9. C. Mas, A. Serra, A. Mantecón, J.M. Salla, X. Ramis, *Macromol. Chem. Phys.*, 202 (2001) 2554
10. S. Kobayashi, *Synlett*, 689 (1996)
11. L. Matejka, P. Chabanne, L. Tighzert, J.P. Pascault, *J. Polym. Sci. Part A: Polym. Chem.*, 32 (1994) 1447
12. P. Chabanne, L. Tighzert, J.P. Pascault, *J. Apply. Polym. Sci.*, 53 (1994) 769
13. P. Castell, M. Galià, A. Serra, J.M. Salla, X. Ramis, *Polymer*, 41 (2000) 8465
14. S.J. García, X. Ramis, A. Serra, J. Suay, *J. Therm. Anal. Calorim.*, 83(2) (2006) 429
15. S.J. García, X. Ramis, A. Serra, J. Suay, *Thermochim. Acta*. 441 (2006) 45
16. S. Luo, B. Zhang, P.G. Wang, J. Cheng, *Synt. Commun.*, 33 (2003) 2989
17. M. Chini, P. Crotti, L. Favero, F. Macchia, M. Pineschi, *Tetrahedron Letters*, 35, (1994) 433
18. M. Meguro, N. Asao, Y. Yamamoto, *J. Chem. Soc. Perkin Trans. I,* 2597 (1994)
19. H.E., Kissinger, *Anal. Chem.*, 29 (1957) 1702
20. X. Ramis, J.M. Salla, C. Mas, A. Mantecón, A. Serra, *J. Appl. Polym. Sci.*, 92 (2004) 381
21. X. Ramis, J.M. Salla, J. Puiggalí, J. *Polym. Sci. Part A: Polym. Chem.*, 43 (2005) 1166
22. J. Macan, I. Brnardić, M. Ivanković, H.J. Mencer, *J. Therm. Anal. Calorim.*, 81 (2) (2005) 369
23. X. Ramis, A. Cadenato, J.M. Morancho, J.M. Salla, *Polymer*, 44 (2003) 2067
24. X. Ramis, J.M. Salla, A. Cadenato, J.M. Morancho, *J. Therm. Anal. Calorim.*, 72 (2003) 707
25. A.W. Coats, J. Redfern, *Nature*, 207 (1964) 290
26. M.J. Starink, *Thermochim. Acta*, 404 (2003) 163
27. L.A. Pérez-Maqueda, P.E. Sánchez-Jiménez, J.M. Criado, *Polymer*, 46 (2005) 2950
28. S. Vyazovkin, W. Linert, *Int. Rev. Phys. Chem.*, 14 (1995) 355
29. S. Vyazovkin, C.A. Wight, *Annu. Rev. Phys. Chem.*, 48 (1997) 125
30. X. Ramis, A. Cadenato, J.M. Salla, J.M. Morancho, A. Vallés, L. Contat, A. Ribes, *Polym. Degrad. Stab.*, 86 (2004) 483
31. S. Vyazovkin, W. Linert, *J. Solid State Chem.*, 114 (1995) 392
32. S. Vyazovkin, W. Linert, *Chem. Phys.*, 193 (1995) 109
33. J.M. Barton, W.W. Wright, *Thermochim. Acta*, 85 (1985) 411
34. J.M. Criado, *Thermochim. Acta*, 24 (1978) 186
35. F.J. Gotor, J.M. Criado, J. Malek, N. Koga, *J. Phys. Chem. A,* 104 (2000) 10777

5.3. PROPIEDADES MECÁNICAS Y TÉRMICAS DE PINTURAS EN POLVO

En este apartado se muestran las propiedades térmicas y mecánicas de sistemas epoxi homopolimerizados con triflato de erbio e iterbio en diferentes proporciones (0.5, 1 y 2 phr). A su vez los resultados se comparan con los obtenidos para sistemas polimerizados epoxi/o-tolilbiguanida (TBG) y sistemas polimerizados epoxi/o-tolilbiguanida catalizados con triflatos de erbio e iterbio en proporciones de 1phr.

En este capítulo también se muestran gráficos tiempo-temperatura-conversión obtenidos a partir del estudio presentado en el punto de propiedades cinéticas (punto 5.2.).

Se observa como el uso de triflatos de lantánido como iniciadores de la homopolimerización de resinas epoxi o catalizadores de sistemas epoxi/o-tolilbiguanida disminuye la temperatura y tiempo de curado con respecto al sistema polimerizado epoxi/o-tolilbiguanida, siendo este descenso más pronunciado a mayores proporciones de triflato. No obstante, las muestras con triflato presentaron peor estabilidad térmica (tanto peor cuanto más triflato) debido a que la presencia de triflatos de lantánido acelera la rotura de los grupos éter creados.

En este estudio se puso en evidencia que los sistemas formulados con triflatos de lantánido presentaron peores propiedades mecánicas que el sistema de referencia (epoxi/o-tolilbiguanida) especialmente a elevados contenidos en triflato. Las formulaciones con 1phr de triflato de iterbio (con y sin TBG) mostró una buena combinación de propiedades (cinética de curado, baja fragilidad, buena resistencia a impacto…).

Study of lanthanide triflates as curing initiators for solid DGEBA resin. Thermal and mechanical characterization

S. J. García[1,3], A. Serra[2] & J. Suay[3]

[1] Àrea de Ciència dels Materials i Enginyeria Metal·lúrgica, Departamento de Ingeniería de Sistemas Industriales y Diseño, Universitat Jaume I, Avda. Vicent Sos Baynat s/n, 12071 Castelló, Spain

[2] Departament de Q. Analítica i Q. Orgànica. Facultat de Química. Universitat Rovira i Virgili. C/Marcel·lí Domingo s/n. 43007 Tarragona, Spain

[3] Centro de Biomateriales, Universitat Politècnica de València, Camino de Vera s/n, E-46071 Valencia, Spain

XXXXXXXXXXXXXXXX

Pendiente de envío

Abstract

A new class of cationic initiators, lanthanide triflates, has been studied in the curing of diglycidyl ether of bisphenol-A (DGEBA). Two metal salts (Erbium and Ytterbium (III) trifluoromethanesulfonate) in various proportions (0.5, 1 and 2 parts per hundred of resin) have been used and the thermal and mechanical properties of the thermosets compared to a common solid epoxy system (crosslinked with o-tolylbiguanide). The kinetics of these processes has been evaluated by the isoconversional method that has been proved to be an excellent tool to predict the principal curing parameters (conversion/time/temperature). Their mechanical properties have been evaluated by dynamic mechanical thermal analysis (DMTA), stress-strain curves, impact resistances and adhesion to metallic substrates, and the thermal characteristics were measured by calorimetry (DSC) and thermogravimetry (TGA).

Keywords: Lanthanide triflates, DMTA, stress-strain, initiator, DGEBA

1. Introduction

Catalysts are important in polymerization processes because they decrease the activation energies and accelerate the reaction. They can be stimulated by heating or photoirradiation but, from the practical point of view, heating is the easiest option: homogeneous heating of reaction mixtures can be achieved without difficulty [1]. Moreover, elementary reactions are accelerated and the viscosity of the reaction mixture decreases in the first steps of the reaction.

Among the new thermal initiators, sulfonium, amonium, phosphonium and hydrazinium salts are described as latent initiators that can polymerize epoxide monomers by a cationic mechanism. The order of reactivity of the cationic salts also depends on the nature of the counter anions: Cl^-, BF_4^-, SbF_6^-, PF_6^- being more active the less nucleophilic. Low nucleophilicity minimizes or prevents the reaction of the growing chain with the anion, which stops the growing of the polymeric chain.

It is well documented [2] that the high acid character and great oxophilicity of lanthanide compounds is highly improved in the case of lanthanide triflates because of the electron-withdrawing capacity of the anionic group. Lanthanide cations can coordinate to the epoxide oxygens leading to a weak C-O bond. The lanthanide trifluoromethane –sulfonate salts studied in this paper contain an anion with an extremely poor nucleophilicity. Therefore, very low proportions of chain-end processes are expected.

The most widely used cationic polymerization catalyst in the field of epoxy technology has been the BF_3/amine compound. Epoxy formulations catalyzed by these compounds are relatively stable at room temperature and cure rapidly when exposed to high temperature. Unlike them, lanthanide triflates are stable even in aqueous media and have strong Lewis acid character. Lanthanide ions have low electronegativity and strong oxophilicity, which allows the metal to tightly coordinate to the oxiranic oxygen. They have large ionic radii and their coordination sphere can be modified leading to a different activity. All these characteristics allow the creation of template structures in the epoxide network [3].

In the present work, we have studied the possibility to use the lanthanide triflates in the thermal crosslinking process of medium molecular weight diglycidyl ether of bisphenol A resins as initiators and as catalysts of a conventional powder system epoxy/o-tolylbiguanide. The curing conditions, and the mechanical, morphological and adhesion to metal properties of the cured materials have been obtained in order to test their potential use in powder coating industrial applications.

2. Experimental

2.1. Materials

Nine different samples (see table 1) were prepared using a solid bisphenol-A based epoxy resin of medium molecular weight (scheme 1), and an average equivalent weight of 733 gr/eq. ep. A first sample, used as the reference one, was the epoxy resin polymerized in the ratio given by the producer with a Huntsman o-tolylbiguanide (TBG), with an H^+ active equivalent weight of 37g/Eq. The same system was catalyzed with two lanthanide triflates (erbium III and ytterbium III trifluoromethanesulfonate) in a proportion of 1 phr (parts of initiator per hundred of resin, w/w). Both triflates were also used to promote

the homopolymerization of the same epoxy resin. To do so, three different proportions of each triflate were prepared: 0.5, 1 and 2 phr of each one.

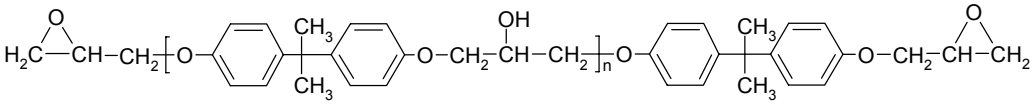

Scheme 1. DGEBA resin

Table 1. Composition of the studied samples

Sample	Epoxy resin	TBG (phr*)	Benzoine (phr*)	Flux Agent (phr*)	$Er(TfO)_3$ (phr*)	$Yb(TfO)_3$ (phr*)
TBG	100	4.8	0.18	1.27	-	-
TBG/$Er(TfO)_3$ 1phr	100	4.8	0.18	1.27	1	-
TBG/$Yb(TfO)_3$ 1phr	100	4.8	0.18	1.27	-	1
$Er(TfO)_3$ 0.5phr	100	-	0.18	1.27	0.5	-
$Er(TfO)_3$ 1phr	100	-	0.18	1.27	1	-
$Er(TfO)_3$ 2phr	100	-	0.18	1.27	2	-
$Yb(TfO)_3$ 0.5phr	100	-	0.18	1.27	-	0.5
$Yb(TfO)_3$ 1phr	100	-	0.18	1.27	-	1
$Yb(TfO)_3$ 2phr	100	-	0.18	1.27	-	2

*phr = parts per hundred resin (w/w)

Those materials, when applied on steel substrates for impact resistance tests, were formulated with benzoine (0.18phr) to avoid porosity, and flux agent (1.27phr) to allow the application by corona spray as powder coating.

Production of materials

Samples were pre-mixed and hand-shacked until good dispersion was afforded. After that, the materials were extruded in a single screw extruder (Haake Rheomex 254), where operating conditions were 80 ºC along the extruder and 60rpm. After extruding, the materials were grinded in an ultra-centrifugal mill ZM 100 and sieved at 100 micron, obtaining the different powder coatings ready to be applied on steel substrates or cured as free films for mechanical studies.

For the impact resistance tests the materials were applied on cold-rolled low-carbon steel normalized tests panels (15 x 7.5 x 0.1 cm). All test panels were degreased with acetone, and the powders were deposited by means of a corona electrostatic powder gun (powder coating equipment Easy 1-C). The epoxy formulations were totally cured for 15 minutes at 150ºC in an oven (25 minutes for the samples using TBG, reaching total cure). Curing conditions were established after the kinetic study and with the objective of fixing a general curing condition. Thicknesses determined were always within the range 60±5 µm.

For mechanical and thermal tests the materials were deposited manually on a polypropylene substrate and cured in an oven at 150ºC for one hour assuring that the samples reach the total cure. After curing, the samples were peeled and tested.

Reactions taking place

Depending on the formulation used, different chemical reactions during curing process can take place giving various networks with different structures and properties. Principal reactions are:

1. In epoxy systems using orto-tolylbiguanide (TBG) the reactions taking place are between amino and oxirane groups [4] (Scheme 2):

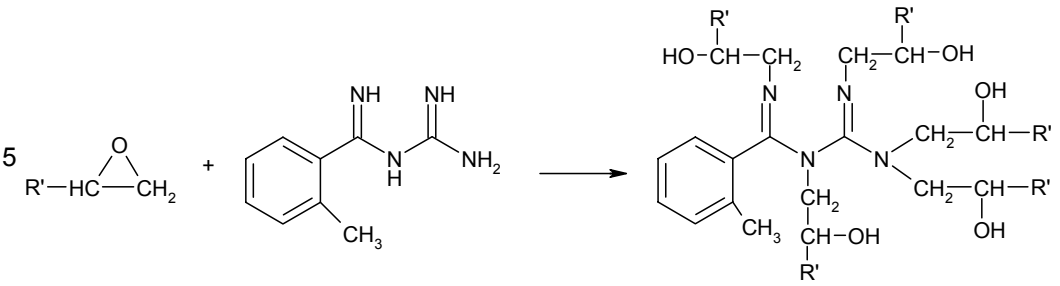

Scheme 2. Reaction o-tolylbiguanide (TBG) / oxirane ring

This kind of reaction (in the proportions used in this work) produces the total curing of the system in a range of temperature above 160ºC. This polycondensation process produces shrinkage of the system during the curing, and as scheme 2 shows a high number of hydroxylic groups are formed which can promote the adhesion to the metallic substrate [5].

2. When adding to this system (epoxy-TBG) a lanthanide triflate as catalyst, the reaction presented in scheme 2 becomes accelerated because of the creation of the oxiranic cation (scheme 3) which promotes a faster reaction between the epoxy and the amine group of the TBG due to the high nucleophilicity of the nitrogen (higher than the one of the oxirane ring) [6].

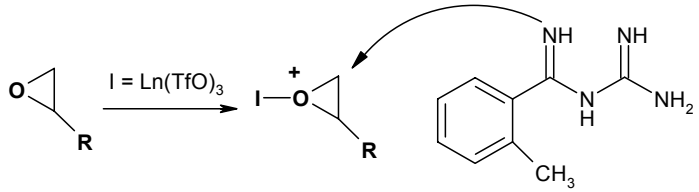

Scheme 3. Oxiranic cation produced by the presence of the triflate

3. In the case that we use lanthanide triflates to homopolymerize epoxy resins these compounds act as cationic ring-opening polymerization initiators and, therefore, two main mechanisms can be expected: the activated chain-end mechanism (ACE) which may be the most important one (scheme 3), and the activated monomer mechanism (AM) as the secondary one (scheme 4) which probably increases when more lanthanide triflate is added [7, 8].

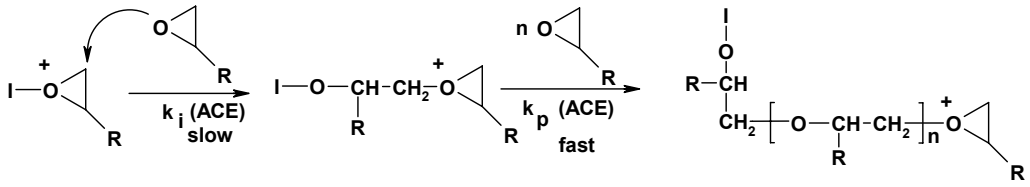

Scheme 3. Activated chain-end (ACE) mechanism

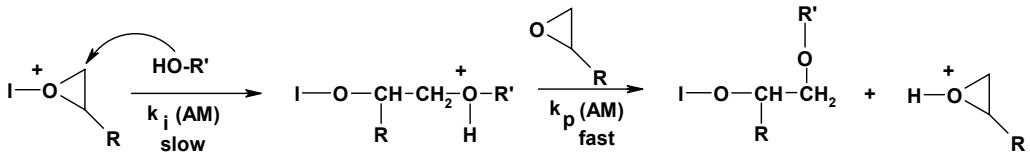

Scheme 4. Activated monomer (AM) mechanism

This kind of reactions also carries to a shrinkage which is usually lower than in case 1, because of the ring-opening polymerization mechanism. Moreover, these kind of reactions do not lead to the formation of hydroxyls, but lead to a highly crosslinked network and weakly plasticized (properties varying depending on the proportion of initiator used) [9].

2.2. Testing Methods and Equipment

2.2.1. Thermal characterization

A Perkin Elmer DSC 7 differential scanning calorimeter was employed for dynamic scans in order to study the non isothermal curing process and to apply the results to isothermal curing. The samples were analyzed in covered aluminium pans, using high purity indium sample for calibration. A flow of 20cm^3/min of argon was used as purge gas. The weight of the samples was between 8 and 9 mg. Non-isothermal scans were performed at rates of 2.5, 5, 10 and 15 ºC/min to not-cured-samples of the four prepared powder epoxy systems. The scans were done at the range of temperature from 25 to 300ºC.

Isoconversional STARe software from Mettler-Toledo was used in order to calculate conversion degrees and kinetics of the process.

Differential scanning calorimeter was also used to determine the vitreous transition temperature (T_g) of the different cured samples. Scans were performed under the same conditions of the kinetic study using cured samples of 8mg weight, at a scan rate of 10ºC/min in the range of 25-250ºC.

2.2.2. Thermogravimetric Analysis (TGA)

In order to determine the influence of triflate salts on the thermal stability of an epoxy network thermogravimetric tests were carried out in a Setaram thermogravimetric analyzer (Setaram TGA92). Samples between 15 and 20 mg were scanned up to 900ºC at 5 K·min^{-1}. All scans were performed with an argon flow of 50 cm^3/min.

2.2.3. Dynamic-mechanical thermal analysis (DMTA)

A dynamic mechanical Analyzer Seiko DMS210U was employed to perform mechanical measurements from 25ºC to 220ºC at 1ºC/min and a constant frequency of 1Hz in three point bending mode.

From the theory of rubber elasticity [11] and using the modulus of relaxed material (E'_r) obtained from the DMTA analysis (E' at T_g+50ºC), it can be calculated the average molecular weight between crosslinks ($\overline{M}_c$) by applying the simplified equation:

$$\overline{M}_c = \frac{3\nu\rho RT}{E'} \quad (1)$$

where ν is the front factor (ν =1, in this work), ρ is the density of the sample, T is the temperature in Kelvin (T=T_g+50ºC) and R the universal gas constant.

The apparent density of the samples was calculated by an apparatus of density measurement (from Mettler-Toledo) coupled to a weight balance and using equation 2.

$$\rho_{ap} = \frac{m_{air}}{m_{air} - m_{liq}}(\rho_0 - \rho_L) + \rho_L \quad (2)$$

where, ρ_0 is the density of the liquid (distilled water), ρ_L is the air density (0.0012g/cm^3), m_{air} is the weight of the sample in air, and m_{liq} is the weight of the sample immersed in the liquid.

2.2.4. Morphology study-SEM

The morphology of the samples was studied with a scanning electron microscopy (SEM). Samples were frozen with liquid N_2 and hand broken. The measurements were carried out on a Jeol-JSM 6300 at 10kV.

2.2.5. Mechanical tests (Stress–strain curves)

Tensile testing up to failure was performed with an Adamel-Lomargy DY34 using a fixed crosshead rate of 10mm/min with a 1kN cell. Five cured samples of each formulation were standardly cut and tested so the results were an average of five tests. Traction tests were performed according to ASTM D1708-96 and D638. Young's modulus was calculated in the region of deformation over 0.5%.

2.2.6. Impact resistance test

Samples were deposited and cured on steel substrates. A 1kg dart-mass was impacted at the back of each sample at different highs up to 1 meter. The effect of the impact was visually evaluated and compared.

2.2.7. Adhesion Test

Adhesion test was performed in accordance to ISO 4587 (1979). It consists on the deposition of the powder clearcoat between two rectangular and cleaned steel substrates, giving rise to a glued area of 13x25mm (figure 1). When the powder is deposited, the two rectangular substrates are fixed by means of

two pincers and cured for 150ºC one hour. After the curing process and three days of ambient exposure, the samples were tested with an Instron Universal Test Machine 4469-H1907 at a traction speed of 1mm/min. The data of tension and deformation were registered. With the break force (F) and the glued area, the shear stress is obtained (σ_{shear} (MPa) = F/area), giving the adhesion of the clearcoats to the substrates. Almost all the specimens showed an adhesive failure type. Five probes of each sample were prepared and tested.

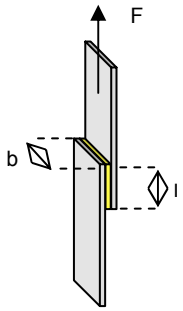

$\sigma_{shear} = F/b \cdot l$

Fig. 1. Scheme of an adhesion test. σ_{shear} calculus.

3. Results and Discussion

3.1. Thermal Properties

a. Curing kinetics and T_g.

It is known that initiators have a large influence on the processability, mechanical properties, adhesion, long-term stability, reactivity in different chemical/physical environments, and even in the total cost of the resulting crosslinking polymers. As has been mentioned above, Lewis acids induce cationic polymerizations leading to homopolymerization reactions.

Homopolymerization of epoxides by cationic mechanism has been recently kinetically studied in samples where DGEBA was solved in methanol and the triflate salt in dichloromethane [12]. It has been established that propagation occurs via nucleophilic attack of the monomer and with the production of a polyether.

The physical and mechanical properties of a thermosetting resin mainly depend on the degree of cure. On the other hand, the processability of a thermoset depends on the rate and extent of polymerization under process conditions. Thus, the kinetic characterization of the reactive resin is not only important for a better understanding of structure-properties relationships, but also to optimize the processing conditions. Among a great number of experimental techniques relating to the research on thermosetting curing reactions, differential scanning calorimetry (DSC) has been used by a number of researchers to study the kinetics and thermal characteristics.

In order to study the curing kinetics of all the systems, four DSC scans were performed from 25 to 300ºC at different heating rates for each formulation (2.5, 5, 10 and 15 ºC/min). With those scans and the use of the STARe software form Mettler-Toledo it can be obtained the curing enthalpies (table 2), the activation energy and the conversion as a function of the temperature. Using the isoconversional method of the software graphics of conversion in function of temperature and time can be plotted for systems

formulated with erbium triflate (figure 2), and for systems formulated with ytterbium triflate (figure 3) both for a conversion of 90%. The representation of time against curing temperature for each system at a given conversion gives a comparative idea of the curing kinetics.

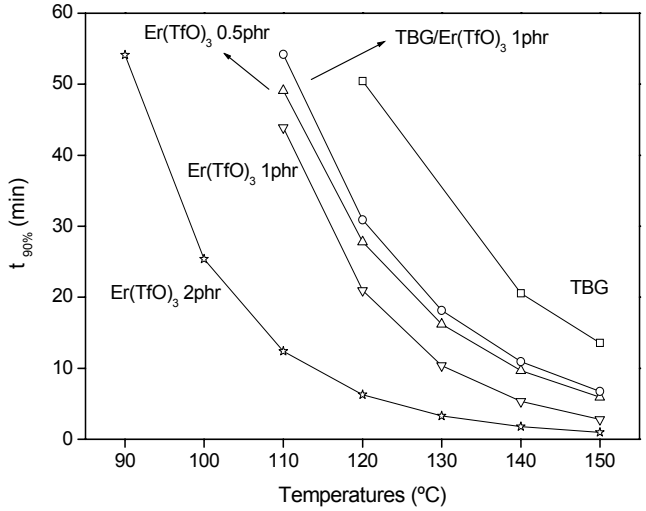

Fig. 2. Time-Temperature for a 90% conversion of the systems with erbium triflate: epoxy resin/TBG (□), epoxy resin/TBG/erbium triflate 1phr (○), epoxy resin/erbium triflate 0.5phr (△), epoxy resin/erbium triflate 1phr (▽), and epoxy resin/erbium triflate 2phr (☆).

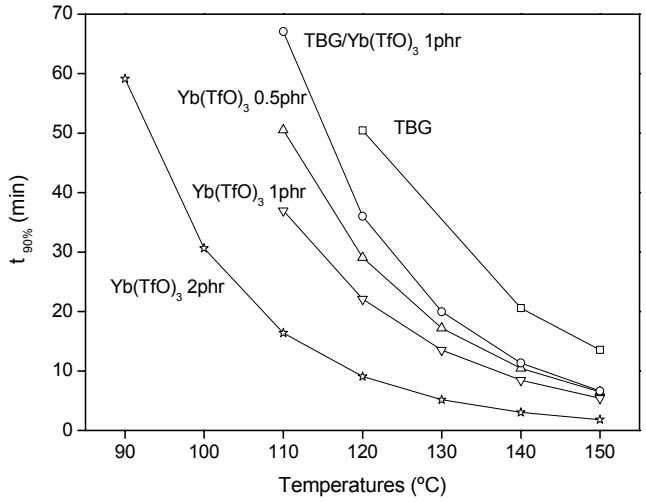

Fig. 3. Time-Temperature for a 90% conversion of the systems with ytterbium triflate: epoxy resin/TBG (□), epoxy resin/TBG/ytterbium triflate 1phr (○), epoxy resin/ytterbium triflate 0.5phr (△), epoxy resin/ytterbium triflate 1phr (▽), and epoxy resin/ytterbium triflate 2phr (☆).

As it can clearly be seen for systems initiated by lanthanide triflates (homopolymerization), when more triflate is added the curing reaction is catalyzed and the curing rates are faster (as lanthanide triflate content increases the mechanism AM becomes more important and faster the curing is). The curing enthalpies are almost the same independently on the proportion of triflate added, as expected. Moreover, the curing kinetics do not vary too much depending on the metal of the triflate (the coordinative abilities of the two lanthanide salts are similar and do not produce great variation in the reaction rate [9]) although systems with ytterbium present lower curing enthalpies values and slower curing rates.

When both lanthanide triflates are used in the presence of TBG there is a catalytic effect, although the curing rates are slower than for the cases where the lanthanide triflate is used to homopolymerize. The acceleration of the system using TBG, when triflate is added, is due to the activation of the epoxide ring as a cation by the metal. It could be expected that the first reaction should be the homopolymerization, nevertheless a complete kinetic study [6] showed that, due to the high nucleophilicity of TBG nitrogens, the reaction TBG/activated epoxide became accelerated and is the main process (scheme 3), although the homopolymerization reactions could also take place but in a lower extent.

From the practical point of view, in the powder coating industry the curing time is normally in the range of 20-25 minutes, which means a curing temperature for a conventional system (using TBG) of 150ºC minimum while for a system using 2phr of triflate the temperature can be reduced to nearly 100ºC if additives are introduced for reducing the vitrifying effect (when curing temperatures are below the vitreous transition temperature vitrification of the resin is produced). This fact can be a considerable advantage when using epoxy formulations as matrix of coatings especially if they have to be applied on thermosensible substrates (like wood or plastic).

In table 2 the different values of T_g can be seen. The use of lanthanide triflates increases the vitreous transition temperature in the homopolymerizing systems in a very similar way for erbium and ytterbium salts, being slightly higher when the proportion of initiator increases. The use of the lanthanide triflates as catalysts in systems epoxy-TBG slightly increases the T_g of the system, overall for the material obtained using erbium triflate. However, the values of T_g obtained in TBG systems do not reach the values obtained for homopolymerized thermosets.

Table 2. General properties

Sample	ΔH (kJ/eq. ep.)	T_g (ºC)	$T_{degradation}$ (5% mass loss) (ºC)	T_α (ºC)	T_α + 50 (ºC)	E'_{rubber} (Pa)	ρ_{ap} (g/cm^3)	$\overline{M_c}$ (g/mol)
TBG	64.3	95	349	109	159	3.97E6	1.1048	2998.5
TBG/Er(TfO)$_3$ 1phr	62.5	100	337	110	160	4.59E6	1.1451	2690.9
TBG/Yb(TfO)$_3$ 1phr	66.6	97	337	108	158	4.08E6	1.1445	3010.9
Er(TfO)$_3$ 0.5phr	75.9	109	296	121	171	15.45E6	1.1437	819.2
Er(TfO)$_3$ 1phr	73.9	109	289	119	169	15.16E6	1.1305	821.5
Er(TfO)$_3$ 2phr	75.3	118	276	124	174	10.23E6	1.062	1156.3
Yb(TfO)$_3$ 0.5phr	62.8	107	299	119	169	15.22E6	1.1525	833.9
Yb(TfO)$_3$ 1phr	57.8	109	312	119	169	16.54E6	1.1469	763.8
Yb(TfO)$_3$ 2phr	68.7	115	277	123	173	8.87E6	1.1133	1396.0

b. Degradation process.

Figure 4 and figure 5 shows the thermogravimetric curves of the thermosets obtained from systems formulated with erbium and ytterbium triflates respectively. When the content of lanthanide triflate is increased there is a decrease in the thermal stability (thermal stability is always lower than that of the reference system).

A possible explanation to this fact can be found in the Lewis acid characteristics of the lanthanide triflates, which can help to break the ether linkages of the material by coordination of the metal to the ether group. The higher the content of lanthanide triflate the lower the initial degradation temperature (see table 2, data calculated at 5% of mass loss), which is due to the increase of the proportion of metals breaking the bonds. On the other hand, systems cured with TBG have higher thermal stability due to the lower number of ether groups and more unreactive groups coming from the attack of the TBG nitrogen to the epoxy ring (C-N bonds).

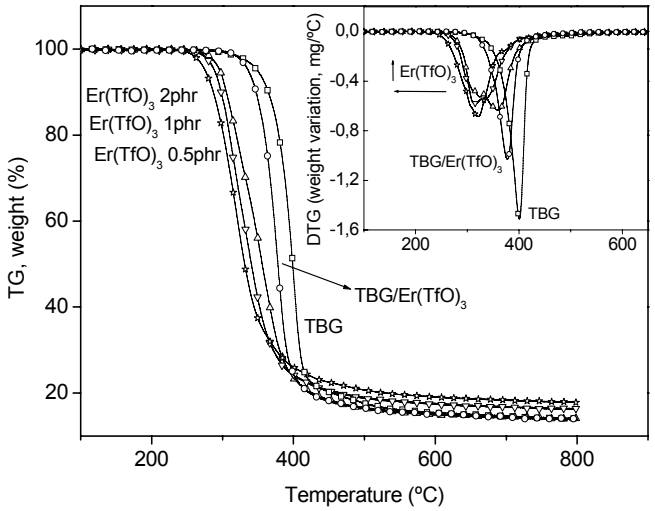

Fig. 4. Thermogravimetric graphics obtained at 5ºC/min for samples using erbium triflate: epoxy resin/TBG (□), epoxy resin/TBG/erbium triflate 1phr (O), epoxy resin/erbium triflate 0.5phr (Δ), epoxy resin/erbium triflate 1phr (∇), and epoxy resin/erbium triflate 2phr (☆).

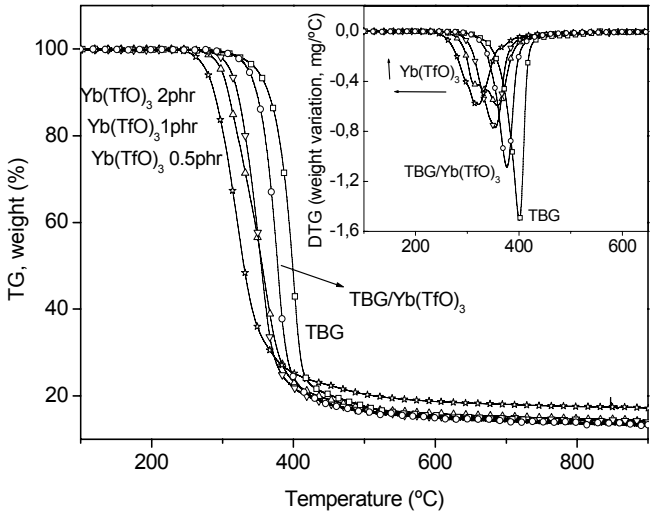

Fig. 5. Thermogravimetric graphics obtained at 5ºC/min for samples using ytterbium triflate: epoxy resin/TBG (□), epoxy resin/TBG/ytterbium triflate 1phr (O), epoxy resin/ytterbium triflate 0.5phr (Δ), epoxy resin/ytterbium triflate 1phr (∇), and epoxy resin/ytterbium triflate 2phr (☆).

3.2. Morphology study (SEM)

Figure 6 and 7 show the SEM-pictures at 75 magnifications of the thermosets obtained using erbium and ytterbium triflates respectively. The lowest porosity is obtained for the samples cured with TBG (with or without lanthanide triflates). When the system is homopolymerized with lanthanide triflates there is an increase in porosity, being higher when more initiator is added. This increase of the macroporosity is probably due to the fact that the higher the curing rate the higher the increase of viscosity with time and the higher the probability of occluding air in the material. Sample with 2 phr of triflate has a special morphology. Not only it is full of macropores but the resin particles are not sinterized at all, so the final structure is not homogeneous. The reason for this phenomenon can once more be the rapid curing kinetics for the 2 phr system that avoid the material to flow and to get sinterized.

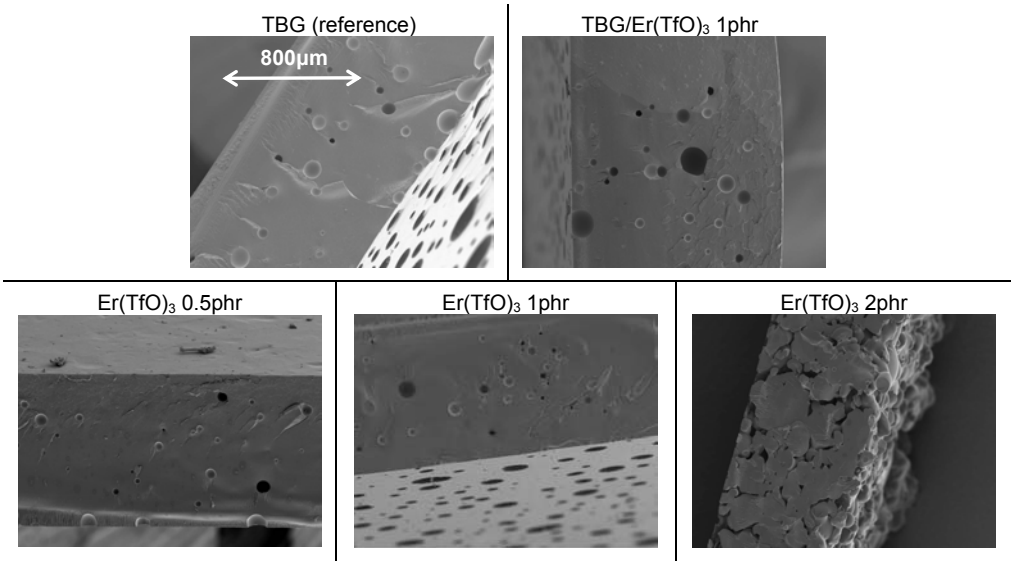

Fig. 6. SEM pictures at 75 magnifications for samples using erbium triflate.

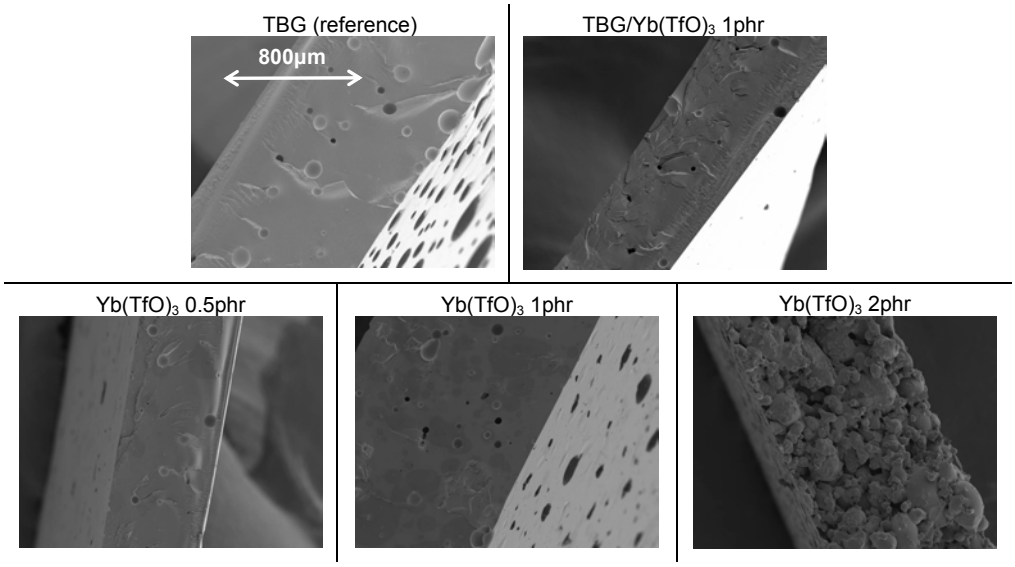

Fig. 7. SEM pictures at 75 magnifications for samples using ytterbium triflate.

3.3. DMTA

Dynamo-mechanical-thermal analysis of the cured samples were carried out in order to test the mechanical properties of these materials and to obtain more information of the extent of curing and morphology of the formed network. The results of the dynamic mechanical studies are presented in figures 8 and 9. The principal drop in the storage modulus, and the corresponding maximum in the loss factor curve are due to the principal transition associated with the increase in internal freedom, such as long range segmental motions at the primary (α) transition.

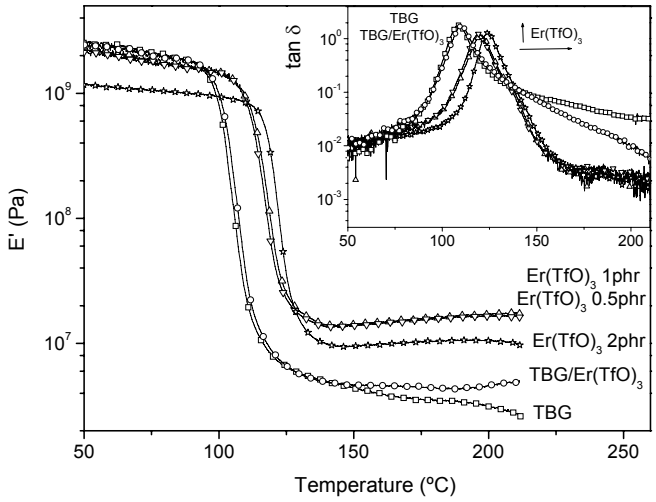

Fig. 8. Storage modulus (E') and loss tangent (tanδ) versus temperature obtained by DMTA for the formulations using erbium triflate epoxy resin/TBG (□), epoxy resin/TBG/erbium triflate 1phr (○), epoxy resin/erbium triflate 0.5phr (Δ), epoxy resin/erbium triflate 1phr (▽), and epoxy resin/erbium triflate 2phr (☆).

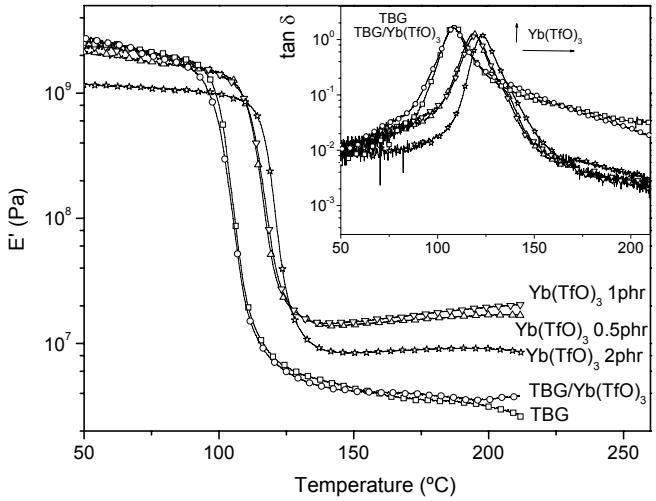

Fig. 9. Storage modulus (E') and loss tangent (tanδ) versus temperature obtained by DMTA for the formulations using ytterbium triflate: epoxy resin/TBG (□), epoxy resin/TBG/ytterbium triflate 1phr (○), epoxy resin/ytterbium triflate 0.5phr (△), epoxy resin/ytterbium triflate 1phr (▽), and epoxy resin/ytterbium triflate 2phr (☆).

The change of the mechanical relaxation as measured by the peak in the dynamic loss curve, and the change of the storage modulus, is often used to characterize the behaviour of polymeric plasticizers and plasticized polymers [13].

When lanthanide triflates are added to the epoxy system the peak of tanδ does not become broader, indicating no increase in the heterogeneity of the material. The peak also has a displacement towards higher temperatures as T_g does, indicating a possible higher crosslinking density with lower mobility of the chains and less free volume in the network. Moreover the addition of lanthanide triflates increases the rubber storage modulus (E'_{rubber} in table 2) which implies that the material is more rigid and in accordance to the results obtained with tanδ, due to the increase of the crosslinking density. It should be said, that the network of the homopolymerized materials is much more compact than that one obtained from TBG as curing agent.

3.4. Molecular weight between crosslinks ($\overline{M_c}$)

Apparent densities (ρ_{ap}) and values of $\overline{M_c}$ are presented in table 2. It can be observed as was expected from other studies with lanthanide triflates [9] that the use of these compounds as initiators in the homopolymerization of epoxy resins leads to low molecular weight between crosslinks and a bigger crosslinking density as can also be observed from the T_g and T_α values. On the other hand, the reference system, obtained from catalyzed and un-catalyzed TBG, presents much more $\overline{M_c}$ values than the samples homopolymerized with lanthanide triflates. This is due to the inclusion of the structure of the TBG in the network, which raises the value of $\overline{M_c}$.

Nevertheless samples with 2 phr of triflate present higher values of $\overline{M_c}$ and lower values of E'_{rubber}. This surprisingly result could be a consequence of the special morphologies of this type of materials, which are heterogeneous and full of macroscopic pores.

3.5. Stress-Strain

Figures 10 and 11 show the stress-strain curves corresponding to the traction tests performed to the formulated coatings using erbium triflate and ytterbium triflate respectively. Table 3 shows the parameters obtained from the mechanical tests: elastic modulus (E), elastic limit stress (σ_{el}), elastic limit strain (ε_{el}), maximum stress (σ_{max}), break stress (σ_{break}), break strain (ε_{break}), and toughness.

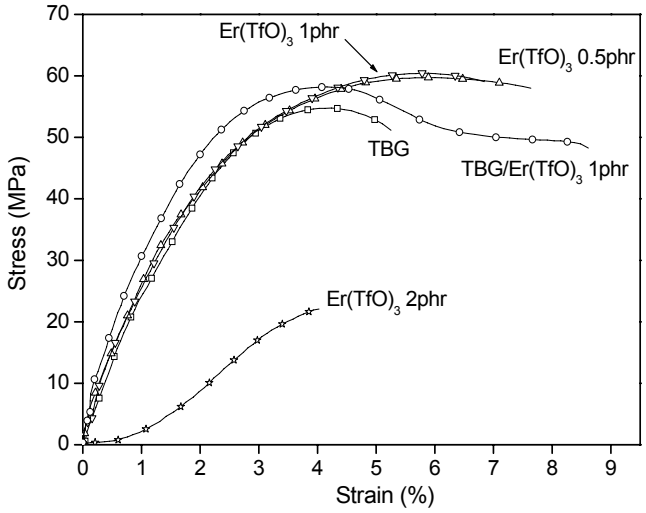

Fig. 10. Stress-strain curves of the samples using erbium triflate: epoxy resin/TBG (□), epoxy resin/TBG/erbium triflate 1phr (○), epoxy resin/erbium triflate 0.5phr (Δ), epoxy resin/erbium triflate 1phr (∇), and epoxy resin/erbium triflate 2phr (☆).

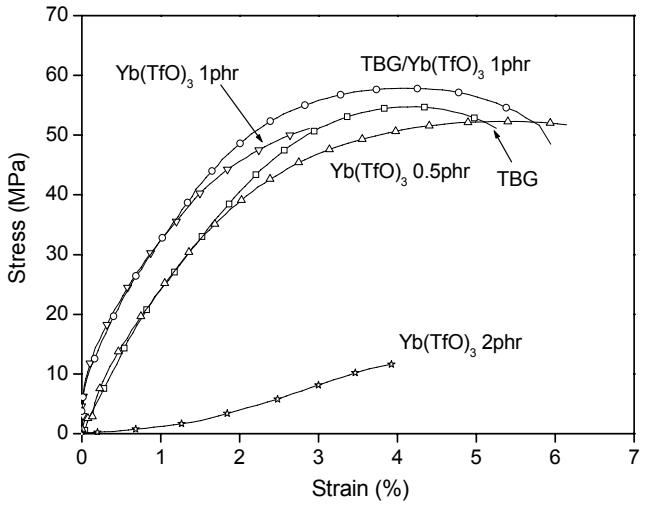

Fig. 11. Stress-strain curves of the samples using ytterbium triflate: epoxy resin/TBG (□), epoxy resin/TBG/ytterbium triflate 1phr (○), epoxy resin/ytterbium triflate 0.5phr (Δ), epoxy resin/ytterbium triflate 1phr (∇), and epoxy resin/ytterbium triflate 2phr (☆).

Table 3. Mechanical properties from stress-strain tests

Sample	E (MPa)	σ_{le} (MPa)	ε_{le} (%)	σ_{max} (kN)	σ_{break} (MPa)	ε_{break} (%)	Toughness (MPa)
TBG	1881.3 ± 205.6	46.7 ± 1.49	2.36 ± 0.13	56.01 ± 1.07	49.4 ± 0.77	5.55 ± 0.28	2.32 ± 0.114
TBG/$Er(TfO)_3$ 1phr	2479.9 ± 363.2	46.7 ±1.01	2.107 ± 0.26	55.20 ± 2.79	46.26 ± 2.34	7.75 ± 0.84	2.82 ± 0.51
TBG/$Yb(TfO)_3$ 1phr	2410.4 ± 223.7	45.2 ± 2.81	2.08 ± 0.14	59.63 ± 0.40	49.65 ± 3.27	6.85 ± 1.29	3.23 ± 0.062
$Er(TfO)_3$ 0.5phr	2328.1 ± 217.7	46.1 ± 2.82	2.40 ± 0.20	59.21 ± 0.54	57.50 ± 0.56	6.97 ± 1.26	3.35 ± 0.72
$Er(TfO)_3$ 1phr	1894.8 ± 139.0	52.12 ± 1.56	2.96 ± 0.12	59.05 ± 2.33	57.62 ± 1.45	6.66 ± 0.94	3.18 ± 0.63
$Er(TfO)_3$ 2phr	No linear behaviour			21.88 ± 1.17	21.88 ± 1.17	4.04 ± 0.43	0.38 ± 0.061
$Yb(TfO)_3$ 0.5phr	1901.6 ± 234.6	49.56 ± 2.39	3.35 ± 0.62	53.94 ± 1.65	53.40 ± 1.50	5.92 ± 0.37	2.50 ± 0.24
$Yb(TfO)_3$ 1phr	2464.9 ± 123.9	44.35 ± 3.46	2.01 ± 0.23	48.37 ± 2.88	48.37 ± 2.88	2.49 ± 0.37	0.73 ± 0.22
$Yb(TfO)_3$ 2phr	No linear behaviour			11.11 ± 0.54	11.11 ± 0.54	3.78 ± 0.16	0.16 ± 0.016

On comparing a homopolymerized system initiated by 0.5 or 1phr of erbium triflate to a system having TBG, it can be observed that the homopolymerized materials present higher break deformation and stress (which implies higher ductility), higher toughness (which implies that homopolymerized samples can absorb more energy before they break down), and a slight increase of the elastic modulus (rigidity) that can be correlated to an increase in the cross-linking density (lower $\overline{M_c}$). The increase in rigidity can also be detected in the increase of T_g and T_α.

For samples initiated by ytterbium triflates results are less clear and effects less positive compared to systems with erbium salt. Proportions of erbium and ytterbium salts of 2phr showed no linear correlation with the lower proportions and they presented lower mechanical properties probably due to the lower sintering. When lanthanide triflates are used as catalysts in systems with TBG, there is also an increase of rigidity (higher E), increase of ductility (higher break strain), and higher toughness (more energy absorption before break).

3.6. Impact resistance

Figure 12 shows the pictures of the nine impacted samples at a height of 100cm with a mass of 1kg. For homopolymerized systems, a formulation with 1phr of ytterbium triflate presents good impact resistance, while the other formulations with triflates did not. In any case, samples with ytterbium presented better results than those with erbium.

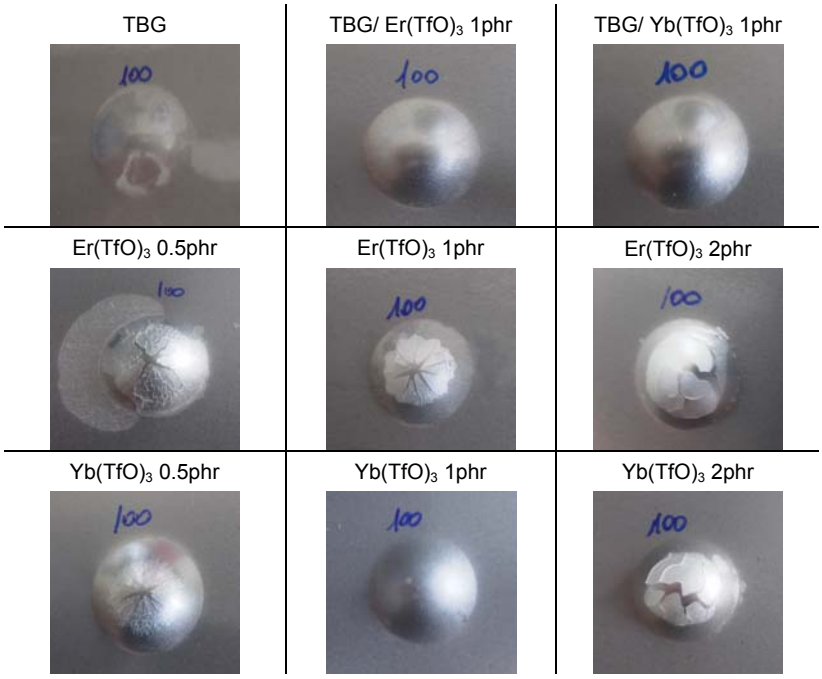

Fig. 12. Impact resistance pictures of the prepared samples tested at 100cm height with 1kg of mass dart.

When the lanthanide triflates were employed as catalysts of a system with TBG, impact results were very good independently of the lanthanide triflate used.

A possible explanation of the good impact properties of samples with TBG and the bad ones in the homopolymerized systems can be the more expanded structure of the network when using TBG, and the higher internal stresses produced by the fastest curing of homopolymerized materials [6-8, 14].

3.7. Adhesion

Figure 13 and 14 shows the shear stress for the materials obtained using erbium and ytterbium triflates respectively. A clear trend can be observed in both graphics. The system with TBG presents the best adhesion to the substrate (high σ_{shear}), probably due to the hydroxyl groups produced in the reaction. A higher proportion of hydroxylic groups promotes a higher adhesion [15-18] to the metallic substrate because of the increase in the possibility to establish hydrogen bonds between both materials. It can also be seen that the use of lanthanide triflates lowers the dry adhesion to the steel substrate, being the higher the decrease when the higher the triflate content is. This trend is probably due to the inexistence of hydroxylic groups, the less polar character of the network and the stress generated by the fast curing rate, and by a possible shrinkage which can lead to warping. Both ytterbium and erbium triflates showed similar results.

When lanthanide triflates were added as catalysts to TBG formulations there was also observed a decrease in adherence.

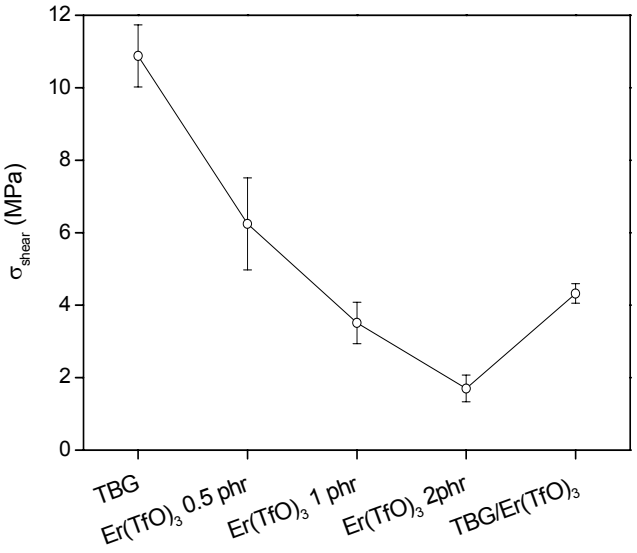

Fig. 13. Shear stress of the samples formulated with erbium triflate.

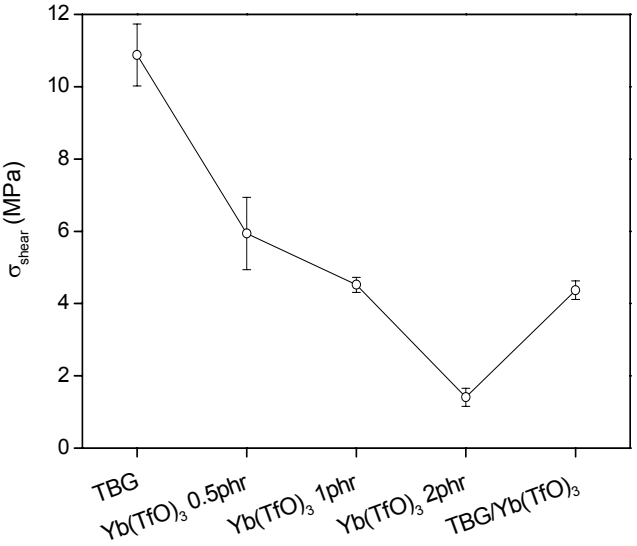

Fig. 14. Shear stress of the samples formulated with ytterbium triflate.

4. Conclusions

The results obtained show that the use of erbium and ytterbium triflates as initiators of the homopolymerization of DGEBA resins, and as catalysts of systems epoxy/o-tolylbiguanide (TBG) diminishes the curing temperature and time with respect to the reference system DGEBA/ TBG.

All samples using lanthanide triflates presented lower thermal stability compared to the reference system, being lower when a higher proportion of lanthanide triflate was added.

With respect to the influence on mechanical properties (including adhesion) and impact resistance, the homo-polymerization of the epoxy resin by means of lanthanide triflates did not lead to good results, especially when the proportion of lanthanide triflates increased until 2phr. Some possible explanations to this behaviour are based on the final composition of the epoxy network itself (non-existence of OH^- groups in homo-polymerized systems) and on the increase of internal stresses in these formulations due to the fast curing rate. Nevertheless, the system with 1phr of ytterbium salt (with and without TBG) presented a good combination of properties (mechanical properties were not too bad).

As these new systems have proved to increase some important properties needed in powder coatings (such as reducing curing rate and fragility decrease) they can be an alternative to actual systems, although further research has to be done in order to improve mechanical and impact resistance properties.

Acknowledgments

Authors would like to thank Ms Eva Romero and Ms Maite Rodríguez for their help in the development of this project. Authors are also grateful for the economic support in this work of CICYT (Comisión Internacional de Ciencia y Tecnología) and FEDER (Fondo Europeo de Desarrollo Regional) for the projects MAT 2000-0123-P4-03 and MAT 2005-01806.

1. T. Endo, F. Sanda, *Macromol. Symp.,* 107, (1996) 237
2. S. Kobayashi, *Synlett*, (1994) 689
3. H.C. Aspinall, J.L.M. Dwyer, N. Greeves, E.G. McIver, J.C. Woolley, *Organometallics,* 17 (1998) 1884
4. M. Ochi, K. Mimura, H. Motobe, *J. Adhesion Sci. and Tech.,* 8 (1994) 223
5. J.M. Martí-Martínez, M. Madrid-Vega, *Teoría de la adhesión, Tema 2: Propiedades de los adhesivos y los selladores antes del curado*, Loctite España
6. S.J. García, A. Serra, X. Ramis, J. Suay, *J. Them. Anal. Cal.*, August (2006) online-first
7. S.J. García, X. Ramis, A. Serra, J. Suay, *Thermochim. Acta.,* 441 (2006) 45
8. S.J. García, X. Ramis, A. Serra, J. Suay, *J. Therm. Anal. Calorim.,* 83 (2) (2006) 429
9. C.Mas, A. Serra, A. Mantecón, J.M. Salla, X. Ramis, *Macromol. Chem. Phys.,* 202 (2001) 2554
10. X. Ramis, A. Cadenato, J.M. Morancho, J.M. Salla, *Polymer,* 44 (2003) 2067
11. A.V. Tobolsky, D.W. Carlson, N. Indictor, *J. Polym. Sci.,* 54 (1960) 175
12. P. Castella, M. Galià, A. Serra, J.M. Salla, X. Ramis, *Polymer,* 41 (2000) 8465
13. M.T. Rodríguez, S.J. García, R. Cabello, J.J. Gracenea, J.J. Suay, *J. Coat. Tech.,* 2 (7) (2005) 557
14. C. Mas, X. Ramis, J.M. Salla, A. Mantecón, A. Serra, *J. Polym. Sci. Pol. Chem.,* 41 (2003) 2794
15. D. Greenfield, J.D. Scantleburry, *JCSE*, 3 (2000) paper5
16. E. Vaca-Cortés, M.A. Lorenzo, J.O. Jirsa, H.G. Wheat, R.L. Carrasquillo, *Adhesion testing of epoxy coating*, Centre for transportation research bureau of engineering research the university of Texas at Austin (1998)
17. N.I. Gaynes, *Testing of Organic Coatings*, Noyes Data Corp., Park Ridge, NJ (1977)
18. M.A. Lorenzo, *Experimental Methods for Evaluating Epoxy Coating Adhesion to Steel Reinforcement,* M.S. Thesis, The University of Texas at Austin (1997)

5.4. PROPIEDADES ANTICORROSIVAS DE PINTURAS EN POLVO

En este apartado del capítulo de *resultados y discusión* se trata el estudio de las propiedades anticorrosivas de las diferentes formulaciones preparadas y de las cuales se ha estudiado la cinética de curado y las propiedades térmicas y mecánicas. Hasta el momento se ha observado que los sistemas curados por medio de iniciadores lantánidos (triflatos de erbio e iterbio) han dado lugar a sistemas capaces de curar a bajas temperaturas y tiempos presentando buenas propiedades mecánicas en una formulación de 0.5 y 1phr, suponiendo de esta forma una gran ventaja respecto a otros sistemas en polvo tradicionales.

Este apartado se divide en tres artículos. Uno dedicado al triflato de erbio como iniciador, otro al triflato de iterbio también como iniciador, y uno final referente a la influencia de la introducción de los triflatos como catalizadores de un sistema convencional epoxi/orto-tolilbiguanida.

Cuando los triflatos se emplean como catalizadores (en sistemas convencionales) se observó que el erbio parece no ser apropiado por presentar bajas propiedades anticorrosivas y mecánicas. Sin embargo, el triflato de iterbio hidratado empleado como catalizador ofrece una disminución de temperatura y tiempo de curado frente al sistema convencional, así como unas buenas propiedades anticorrosivas.

En términos generales, en el estudio se ha encontrado que independientemente del triflato empleado, cuando éstos actúan como iniciadores o como catalizadores, las formulaciones con contenido entorno a 1phr de triflato de lantánido consiguen propiedades anticorrosivas óptimas con reducciones importantes en temperatura y tiempo de curado.

Influence on the anticorrosive properties of the use of Erbium III Trifluoromethanesulfonate as initiator in an epoxy powder clearcoat

S. J. García[1,2] & J. Suay[2]

[1] Àrea de Ciència dels Materials i Enginyeria Metal·lúrgica, Departamento de Ingeniería de Sistemas Industriales y Diseño, Universitat Jaume I, Avda. Vicent Sos Baynat s/n, 12071 Castelló, Spain

[2] Centro de Biomateriales, Universitat Politècnica de València, Camino de Vera s/n, E-46071 Valencia, Spain

Corrosion Science

Enviado en mayo de 2006. Bajo primera revisión

Abstract

New low curing temperature epoxy powder coatings cured cationically by the use of erbium (III) trifluoromethanesulfonate as initiator have been formulated. Their curing kinetics and anticorrosive properties have been studied and compared with a system commonly used in industry (o-tolylbiguanide / epoxy resin). Three different tests of anticorrosive properties (EIS, AC/DC/AC, and salt fog spray) have been used together with an adherence test, in order to establish the optimal system. Results show that a system employing 1phr of erbium triflate presents good anticorrosive properties. The technique AC/DC/AC has shown its ability to evaluate properly, much faster, and in accordance to anticorrosive properties results of powder coatings obtained by other techniques.

Keywords: EIS (B), organic coatings (A), polarization (B), rare earth elements (A)

1. Introduction

Powder coatings are currently the fastest growing section of industrial paints, because of their favourable environmental attributes and performance advantages. They are well-adapted for the main strategic goals of the paint industry, namely corrosion protection, improved durability, increased transfer efficiency, elimination of organic solvents, reduction of toxic waste, conservation of energy and reduction of costs. Since they are fully solid, and without volatile organic emissions (less than a 4%), powder coatings are considered to be the best alternative for the reduction of the volatile organic contents (VOCs) of solvent-based paints (>60% of VOCs), among the emerging coating technologies (powder coatings, high solid coatings and waterborne ones) [1,2]. Moreover, from the point of view of the cost per square meter of painted surface, powder coatings seem to be the best option [3].

Compared to liquid paints, the film formation process of powder coatings is different since it takes place in the molten phase. Melting, flow, gel point and cure completion are the principal stages in film formation of powder coatings and determine both the aesthetic and protective properties of the paint. The duration of these stages is directly affected by the paint composition, e.g., type of binder and cross-linker, pigmentation (nature and particle size, packaging and distribution), catalyst, and additives, curing and application conditions. These factors, in turn, determine important coating characteristics such as levelling, adhesion, gloss, chemical resistance and exterior durability [4-7].

Apart from their clear advantages, powder coatings, show some limitations, like the difficulty to apply on thermo-sensible substrates like wood or plastic. Nowadays, the most used powder coating systems are those based on epoxy resins cured with dicyandiamide (DICY) or its derivatives like o-tolylbiguanide (TBG), which are used in proportions of 4 to 6 phr and the curing temperature is usually above 175ºC [8]. For this reason, the formulation of new epoxy powder coatings (using new catalysts and crosslinkers) capable to cross-link at lower temperatures has become one of the main lines of research in industries and related research centres.

In predicting the anticorrosive properties of the primer, the main problem arises from the complexity of the overall process itself. Due to this complexity, the main routines of interaction testing and material assessment were developed experimentally by using different exposure processes and techniques for the measurement of properties. The main types of exposure processes are the accelerated aging test and field exposure experiments (which must be planned for long times and are very expensive to run). Measurements of properties can be electrochemical, mechanical, chemical, and so on. Only if the exposure process and measurement test are well defined and programmed will it be possible to obtain information about the coating deterioration process, reproducible results and a time consumption that is not excessively long. Various electrochemical techniques have been used to evaluate the performance of organic coating/metal systems. The application of electrochemical impedance spectroscopy (EIS) to coated metals has been proved to be a useful technique in the study of the corrosion performance of anticorrosive primers [9-16], although time is needed to perform this type of test because it takes days, weeks and sometimes months to obtain good results.

Therefore, it still exist an explicit interest in rapid assessment methods for practical applications that provide a faster indication of corrosion processes in the surface of coated metallic substrates. Hollaender et al. [17-19] developed a rapid method for testing coated metals in food packaging consisting in a combination of DC and AC measurements (AC/DC/AC procedure) which has been successfully adapted and used by Suay et al. in liquid paints applied to steel substrates [20-22]. After a first AC measurement, the test sample is treated for a short time by a constant cathodic voltage (DC) producing a stress to the sample and, following that, an AC spectrum is recorded again. The change in the characteristics of the impedance spectrum can be attributed to a coating deterioration (pore formation) and a delamination process in the metallic surface due to hydrogen and OH^- production (if a cathodic reaction takes place).

This work has three main goals which are: presenting erbium (III) trifluoromethanesulfonate as a good initiator for powder epoxy systems having acceptable anticorrosive properties while highly reducing the curing temperature and time compared to a typical epoxy system based in TBG; studying the effect of the crosslinking network on the anticorrosive properties; and finally presenting the technique AC/DC/AC as a useful method on the determination of anticorrosive properties of powder paints in very short times, and compare it with the different evaluation procedures of anticorrosive properties (EIS and Salt Fog Spray).

Theoretical bases of reaction mechanisms

In Scheme 1 it can be observed the curing reaction between an oxirane ring and o- tolylbiguanide (TBG), which is a typical latent curing agent. This curing agent was reported to be effective in the curing of DGEBA epoxy resins [23] and very extended in the industry. For this reason the system epoxy resin/TBG was used on this study as the reference one.

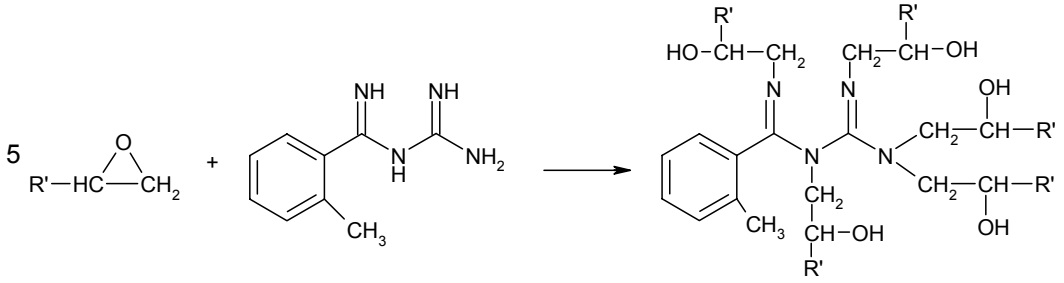

Scheme 1. Chemical structure of the network using TBG as cross-linking agent

In order to improve the reaction kinetics some new thermal initiators have been used during last years. Between them, those having anions with low nucleophilicity are commonly applied, being more actives their cationic salts and more effective the polymerization [24]. Lewis acids used as catalysts, such as $AlCl_3$, BF_3 or $TiCl_4$ are moisture sensitive and easily decompose in the presence of humidity. On the contrary, lanthanide triflates are stable and act as Lewis acids in water which represents an enormous advantage in their technological application as catalysts or initiators. The lanthanide cations (Ln(III)) have a very high coordination capacity due to their great oxophilicity, thus, weakening the C-O bond [25], and

favouring the cationic mechanism of reaction. This process is improved by the electron-withdrawing capacity of the anionic group, TfO^- [25].

As usual in Lewis acid initiators, erbium (III) trifluoromethanesulfonates (here on, erbium triflate, $Er(TfO)_3$, or ErTfO) lead to chain growth homo-polymerization of epoxy compounds, which mainly proceed by the cationic chain end mechanism depicted in Scheme 2, where oxirane group of DGEBA resin is opened by coordination of oxirane oxygen to the initiator and subsequent nucleophylic attack of another oxirane group [26,27] (reaction ACE).

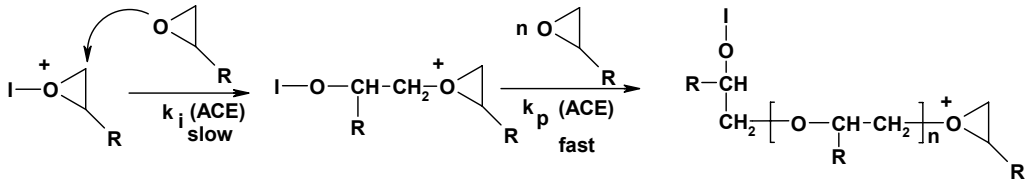

Scheme 2. Activated chain-end mechanism / ACE

Moreover, the presence of hydroxylic groups can lead to hydroxylic initiated polyetherification processes that can change both the kinetics of the reaction and the properties of the materials (Scheme 3), although this kind of reaction should be less important in extension than the first one, because of the low proportion of hydroxyls. This mechanism is known as activated monomer mechanism (reaction AM).

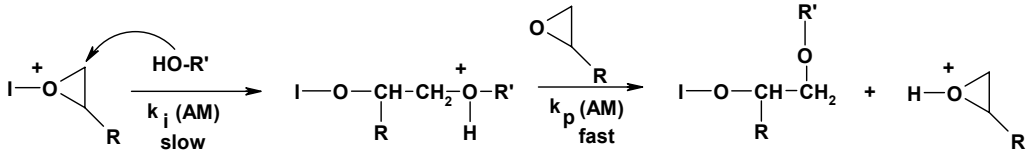

Scheme 3. Activated monomer mechanism / AM

Thus, the proportion of hydroxylic groups can influence the global propagation rate. In addition to these competitive chain growth mechanisms, inter and intra molecular transfer processes can occur and also termination reactions. All these processes lead to changes in the network structure and difficult the study of the kinetics of each separated process. Then, the kinetics of a cationic cure should be studied taking the process as a whole [28,29].

The reaction type AM can be promoted by more addition of erbium triflate. A higher Lewis acid initiator content will give rise to a higher number of oxirane cations which means a reduction of the non-active oxirane groups to continue the reaction ACE, giving as a result a higher possibility to the OH^- to react by the mechanism AM, and thus, reducing the number of hydroxyls and the adherence of the system to the substrate.

The usefulness of lanthanide triflates as initiators has been proved in other studies [24,30] with liquid epoxy resins, showing that they highly accelerated the reactions of the system. Their effect in powder coatings has also been studied for systems using DGEBA resin with triflate as initiator, proving that they

offer very good improvements in curing kinetic processes, reducing significantly the curing temperature and time [26, 27].

Nevertheless, the different reaction process of systems using triflates as initiators (cationic homo-polymerization, schemes 2 and 3) compared to the polymerization in presence of TBG (scheme 1) gives rise to different crosslinking networks [31], and these different networks may produce variations on the anticorrosive properties which might be studied.

2. Experimental

2.1. Materials

Solid bisphenol-A based epoxy resin of medium molecular weight (scheme 4), 733 gr/eq epoxy (from Huntsman), was homo-polymerized with Erbium (III) trifluoromethanesulfonate (from Aldrich) added in three different amounts: 0.5, 1 and 2 phr (parts of initiator per hundred of resin, w/w). A fourth sample used as the reference system was the same resin polymerized in the ratio given by the producer with a Huntsman DICY derivative (TBG), with an H^+ active equivalent weight of 37g/Eq. In order to perform the application of the samples on steel substrates 0.18phr of benzoine and 1.27phr of flux agent were added to the mixtures (table 1).

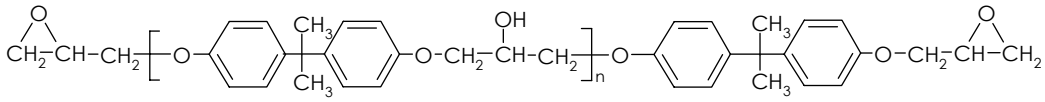

Scheme 4. DGEBA resin

Table1. Samples studied: epoxy resin/$Er(TfO)_3$ 0.5phr, epoxy resin/$Er(TfO)_3$ 1phr, epoxy resin/ $Er(TfO)_3$ 2phr, and epoxy resin/TBG

Sample	Epoxy resin	TBG (phr)	$Er(TfO)_3$ (phr)	Benzoine (phr)	Flux Agent (phr)	T_g (ºC)
1	100	-	0.5	0.18	1.27	109
2	100	-	1	0.18	1.27	109
3	100	-	2	0.18	1.27	118
reference	100	4.8	-	0.18	1.27	95

Samples were pre-mixed and hand-shacked until good pre-mixing was afforded. After that, the material was extruded in a single screw extruder (Haake Rheomex 254), where operating conditions were 80 ºC along the extruder and 60rpm. After extruding, the material was grinded in an ultra-centrifugal mill ZM 100 and sieved at 100 micron, obtaining then the different powder coatings ready to be applied on steel substrates. In order to know the curing conditions, a complete kinetic study was performed [26].

The different clearcoats were applied on cold-rolled low-carbon steel normalized tests panels (15 x 7.5 x 0.1 cm). All test panels were degreased with acetone, and paints were deposited by means of a corona electrostatic powder gun (powder coating equipment Easy 1-C), obtaining 10 panels of each sample. The clearcoats were totally cured for 15 minutes at 150ºC in an oven (25 minutes for the sample using TBG). Thicknesses, determined by an Elcometer, were always within the range 60±5 µm.

2.2. Testing Methods and Equipment

2.2.1. Electrochemical impedance spectroscopy (EIS)

Electrochemical Impedance Spectroscopy (EIS) tests were carried out on coated samples exposed to 3.5% NaCl (by weight) in deionised water for periods up to ten months. The three-electrode electrochemical cell was obtained by sticking a glass cylinder on the sample sheet and filling it with the test solution. The exposed surface area was 16.6 cm^2. A carbon sheet acted as the counter electrode and an Ag/AgCl electrode was used as the reference one.

The AC impedance data were obtained at the free corrosion potential using an AUTOLAB PGSTAT30 potentiostat and a frequency response analyser. The impedance tests were carried out over a frequency range of 10^5 Hz down to $2 \cdot 10^{-3}$ Hz using a sinusoidal voltage of 10 mV as amplitude inside a Faraday cage in order to minimise external interferences on the system.

The equivalent circuit model, shown in Figure 1, was employed to analyze the EIS spectra. The circuit consisted on a working electrode (metal substrate), a reference electrode (Ag/AgCl), electrolyte resistance R_s, pore resistance R_{po}, constant phase element of the coating capacitance CPE_c (here on C_c), polarisation resistance R_p, and constant phase element of the double layer capacitance CPE_{dl} (here on C_{dl}). The two CPE were used because the fitting was better than using capacitances in the equivalent circuit. The "n" value used to be between 0.7 and 1.

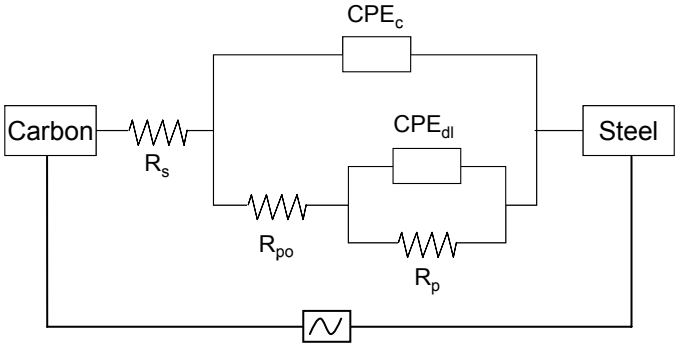

Fig. 1. Equivalent circuit used to model EIS and AC/DC/AC impedance data where passive parameters (R_s = electrolyte resistance, CPE_c = constant phase element of the coating capacitance, CPE_{dl} = constant phase element of the double layer capacitance, R_{po} = pore resistance, R_p = polarization resistance) can be defined.

Fitting the EIS data to the circuit by means of the Z-view software determined the values of the equivalent circuit elements. The chi-squared parameter of the fit was always below 0.1.

2.2.2. Equivalent circuit interpretation

It is generally assumed that there is a correlation between the elements of the equivalent circuit and the corrosion properties of the system [32].

Pore resistance R_{po} is a measure of the porosity and deterioration of the coating. R_{po} values have been usually related to the number of pores or capillary channels perpendicular to the substrate surface through which the electrolyte reaches the interface [33]. Although R_{po} can also increase with immersion time, probably as a result of pore or defect blockage by corrosion products, it usually decreases.

Some authors, as Walter [34,35], have found three regions in the time-dependent trend of R_{po}. It initially decreases rapidly, then slowly (displaying a plateau) and then rapidly again, coinciding with the appearance of the second semi-circle. The plateau is explained by making the assumption that the number of pathways formed is approximately constant with time.

In order to calculate de capacitances of the systems it was used the Constant Phase Elements (CPE). Ideally a capacitor is formed by two conducting plates separated by a non-conducting media (dielectric), nevertheless capacitors in EIS experiments do not behave ideally (e.g. dielectric is not ideal). Instead, they act like constant phase elements becoming the impedance of the capacitor:

$$Z_{CPE} = A(j\omega)^{-n} \quad (1)$$

where,

A= the inverse of the capacitance given by a software

n = an exponent which equals 1 for a capacitor

For a CPE the exponent n is less than 1. In practice, it is better to treat n as an empirical constant with no real physical basis [36].

Having this into account, the results are presented as capacitances but with units $s^n/\Omega cm^2$ instead of those for effective/real capacitances ($s/\Omega cm^2$ or F/cm^2).

C_c is the capacitance of the coating and this should be a measure of water permeation into the coating and is given by:

$$C_c = \varepsilon\varepsilon_0 A/d \quad (2)$$

where ε is the dielectric constant of the coating, ε_o is the vacuum permittivity, *A* is the area of the coating exposed to the electrolyte and *d* is the thickness. The coating capacitance will usually change during electrolyte absorption because the dielectric constant of water is approximately twenty times greater than that of a typical coating.

C_c usually increases at the initial stage of exposure, and seems to be a measure of water absorption. When the coating has been exposed for a long time, it can be correlated to disbonding and deterioration.

The polarisation resistance R_p and double layer capacitance C_{dl} are two parameters used to specify the disbonding of the top coat and the onset of corrosion at the interface. The specific polarisation resistance is associated with the charge transfer behaviour of the metal substrate. R_p, like C_{dl}, can only be calculated well when at least two time constants are evident in the spectrum.

C_{dl}, the double layer capacitance, is a measure of the area over which the coating has disbonded. It can only be correctly measured at advanced stages of coating deterioration. The trend of C_{dl} is complex. A change in the C_{dl} value can be associated with the competition between disbonding and corrosion product accumulation at the interface. As water spreads at the interface and the delaminated area extends, there is an increase of the C_{dl} value. On the other hand, the accumulation of corrosion products at the interface reduces the area of the double layer capacitor, which will lead to a decrease in the C_{dl} value. Therefore, the change of trend in C_{dl} may depend on which factor, disbonding or corrosion product

accumulation was more dominant during the corrosion process. However, it should be pointed out that both the increase and the decrease in C_{dl} are the results of the development of corrosion at the metal surface, while a constant C_{dl} is an indication of a stable interface [37].

2.2.3. AC/DC/AC test

The AC/DC/AC procedure consists in a combination of DC and AC measurements. First, an AC test is applied to the sample under the same conditions as described above in EIS. This measurement also allows knowing the impedance modulus of the tested sample and its characteristic parameters from the equivalent circuit of figure 1.

After the first AC measurement, the test sample is treated for a short time with a constant cathodic voltage (–2V for 20 minutes) which are the necessary conditions to force the production of H_2 and produce the delamination of the coating. This potential was established experimentally but must always be more negative than -1.0 V (vs SCE) which is the potential for the water hydrolysis and H_2 production [38], directly related to the degradation of the system. After applying the direct current of -2V, a registration of the system's open circuit potential variation with time was performed (relaxation time) until the sample reached a new steady state and the potential is once more stabilised. In this case, the relaxation time was of 3 hours, considered enough to obtain good results. When the relaxation time has end, a new EIS measurement (AC) is made to the sample in order to determine the new impedance modulus and characteristic parameters of the system. A schematic representation of the AC/DC/AC procedure is shown in Figure 2.

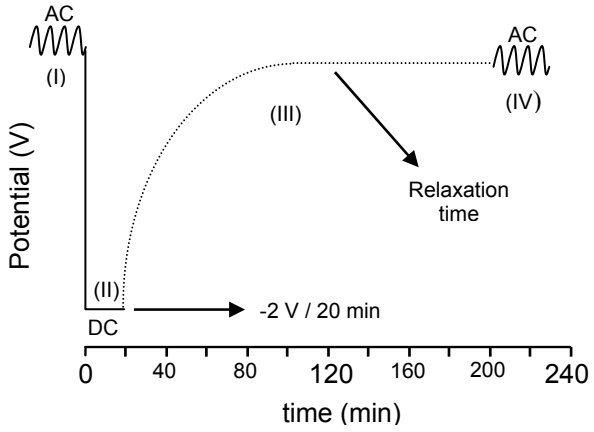

Fig. 2. AC/DC/AC test schematic figure versus time.

This test sequence is repeated at least 6 times, which means that about 24 hours are needed for performing this test. The AC/DC/AC procedure was absolutely automated in PGSTAT 30 AUTOLAB equipment.

2.2.4. Accelerated cyclic test (salt fog spray)

The accelerated salt fog spray test was performed in accordance to ASTM B 117-85 [39]. In this test a cross is performed along the coating until the bare metal is reached. The samples are then introduced

in a salt fog spray chamber were an alkaline fog is created with a 5% (in weight) NaCl water solution. The samples are collected at different periods of time and evaluated until a maximum of 300 hours of exposure. After each collection, the samples were dried, and blistering, corrosion and delamination were measured after 24h of ambient exposure. Delamination was evaluated after applying a tape of 40mm thick to one arm of the cross and peeling the clearcoat. Maximum value of delamination was 40mm.

2.2.5. Adhesion Test

Adhesion test was performed in accordance to ISO 4587 (1979). It consists on the deposition of the powder clearcoat between two rectangular and cleaned steel substrates, giving rise to a glued area of 13x25mm. When the powder is deposited, the two rectangular substrates are fixed by means of two pincers and cured for 150ºC one hour. After the curing process and three days of ambient exposure, the samples were tested on an Instron Universal Test Machine 4469-H1907 (figure 3) at a traction speed of 1mm/min. The data of tension and deformation were registered. With the break force (F) and the glued area, the shear stress is obtained (σ_{shear} (MPa) = F/area), giving the adhesion of the clearcoats to the substrates. Almost all the specimens showed an adhesive failure type. Five probes of each sample were prepared and tested.

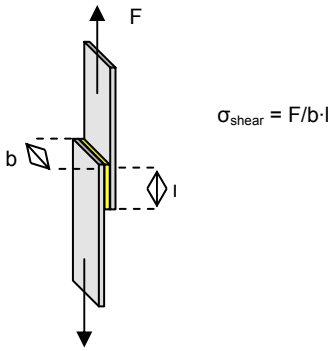

Fig. 3. Scheme of an adhesion test. σ_{shear} calculus.

2.2.6. Morphology study

The morphology of the samples was studied with a scanning electron microscopy (SEM). Samples were frozen with liquid N_2 and hand broken. The measurements were carried out on a Jeol-JSM 6300 at 10kV.

3. Results and Discussion

3.1. Thermal characterization

The curing kinetic process of an epoxy resin/erbium triflate system varying the triflate content, and a system epoxy resin/TBG have been previously studied [26,31], where a complete kinetic analysis of the systems were presented. From those data and the use of a STARe software from Mettler-Toledo, a graphic like figure 4 can be plotted, where for a given conversion (in this case α=0.98) it is represented the curing time needed for total cure in front of the curing temperature.

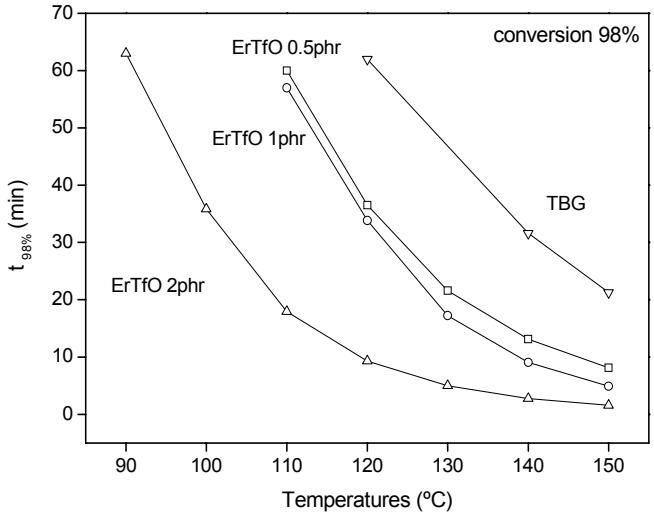

Fig. 4. Time-Temperature for a 98% conversion of the four different clearcoats: epoxy resin/$Er(TfO)_3$ 0.5phr (□), epoxy resin/$Er(TfO)_3$ 1phr (○), epoxy resin/$Er(TfO)_3$ 2phr (△), and epoxy resin/TBG (▽).

It can be clearly observed that systems with erbium triflate decrease meaningfully the curing temperature and time with respect a system cured with TBG (e.g. at 150ºC it is needed near 25 minutes to cure a system with TBG, while for a 0.5phr of triflate system the curing time was 8 minutes, which means a time reduction of about 70%). In systems varying the triflate content between 0.5 and 1phr there are not too big changes, nevertheless, introducing 2phr gives rise to a much more accelerated curing reaction. This shows that, from the point of view of the kinetics, the curing reaction is clearly accelerated when using erbium triflate than when using TBG. The use of erbium triflate also affects the formed network and its crosslinking. The different vitreous transition temperatures measured with DSC equipment at 10ºC/min can be seen in table 1. It is observed that when using erbium triflate the T_g is much higher than with TBG, which means that the network is more crosslinked.

3.2. Adherence

As it can be seen in figure 5, the higher the erbium triflate content the lower the σ_{shear} of the system (σ_{shear} is a measure of the adherence of a coating to a substrate when the failure of this union is not cohesive). On the other hand, the sample with TBG had the best adherence properties. The number of hydroxyl groups is correlated with the coating's adherence to the metallic substrate (because the adherence to it is due to hydrogen bonds formation in the metallic surface), thus, an increase of the number of hydroxyls will give as a result an increase of the adherence [40-43].

When using erbium triflate the crosslinking is produced by two reaction mechanisms (schemes 2 and 3). As stated in the introduction, a system with more erbium triflate will promote the reaction type AM (scheme 3), and the content of hydroxyl groups will decrease and thus the adherence.

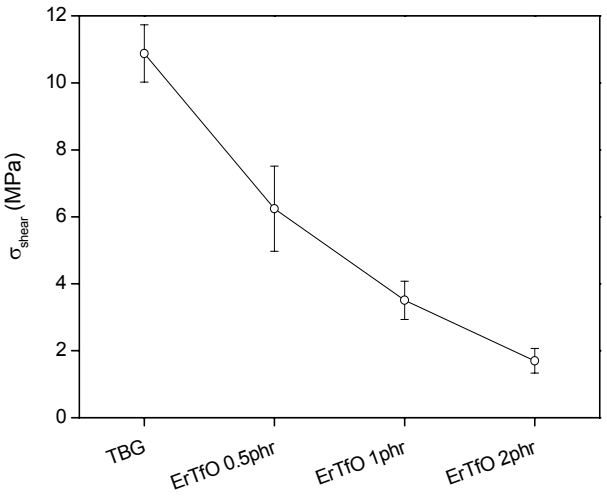

Fig. 5. Shear stress of the studied clearcoats: epoxy resin/$Er(TfO)_3$ 0.5phr, epoxy resin/$Er(TfO)_3$ 1phr, epoxy resin/$Er(TfO)_3$ 2phr, and epoxy resin/TBG.

In the case of the reference system, where the crosslinking is done by TBG (scheme 1), the number of hydroxyls is higher than when curing with triflate, because OH^- are formed in the reaction and maximum adherence is observed.

3.3. SEM

Figure 6 shows the SEM-pictures of the four systems at 75 magnifications. It can be seen a change in morphology when varying the content of erbium triflate as well as differences with the system using TBG. When more triflate is added there is a higher content of porosity probably due to a very fast curing reaction that prevents the exit of occluded air when more initiator is added. The biggest difference between the samples is for that one using 2phr erbium triflate, which presents a non-sinterized structure due to a too rapid curing kinetics, giving as a result a very high porosity.

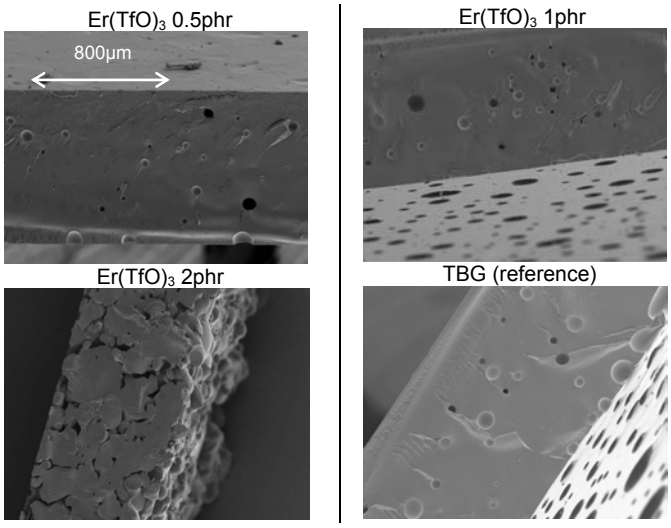

Fig. 6. SEM pictures at 75 magnifications.

3.4. EIS (electrochemical impedance spectroscopy)

Figure 7 shows a Bode graphic of the impedance response (impedance modulus versus frequency) for a coating with TBG and with erbium triflate in three different proportions (0.5, 1 and 2 phr) after 100 days of exposure to electrolyte. The higher modulus and phase angle is obtained for the reference system (TBG) followed by the samples with 1 and 0.5 phr of $Er(TfO)_3$. The sample with 2phr $Er(TfO)_3$ shows the lowest modulus and phase angle.

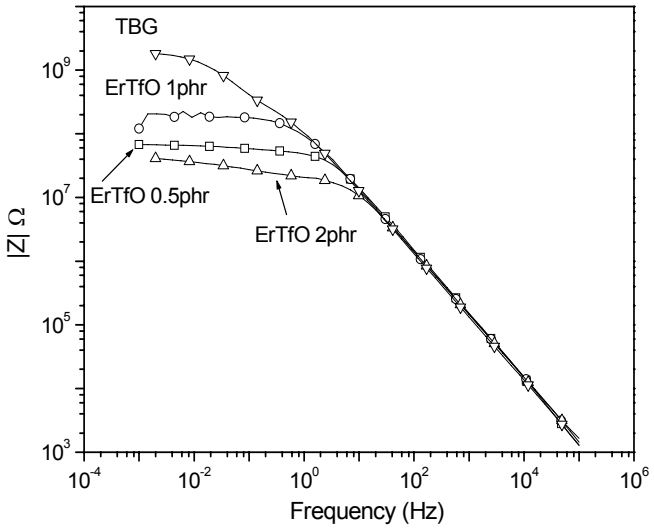

Fig. 7. Bode plot (impedance modulus versus frequency) for different clearcoats: epoxy resin/$Er(TfO)_3$ 0.5phr (□), epoxy resin/$Er(TfO)_3$ 1phr (○), epoxy resin/$Er(TfO)_3$ 2phr (△), and epoxy resin/TBG (▽) applied on metal substrates after 100 days' exposure to electrolyte (deionised water with 3.5% NaCl by weight). EIS test.

Figure 8a, 8b and 8c show the equivalent circuit parameters modelled for EIS results and corresponding to pore resistance R_{po}, polarization resistance R_p and double layer capacitance C_{dl} respectively. Results of coating capacitance C_c are not shown because they present slight differences between samples and an almost constant value over the exposure time interval of $7 \cdot 10^{-11}$ $s^n/\Omega cm^2$.

It could be stated with the EIS results that the best system from the point of view of the anticorrosive properties would be that one using TBG which presents the maximum resistance to pore formation (maximum R_{po}), more stable interface (maximum R_p), and minimum tendency to delamination (minimum C_{dl}). Worst results were found for 2phr erbium triflate system while the one with 1phr seems to be slightly better than that formulated with 0.5phr of $Er(TfO)_3$.

As it has been shown with thermal characterization, samples with higher content of erbium triflate had much higher transition temperature (T_g) and higher crosslinking density (meaning lower permeability) and, thus, a possible increase of anticorrosive properties. On the other hand, increasing erbium triflate increases the macro-porosity (because fast curing) and decreases coating's adherence to the substrate, leading to a decrease of anticorrosive properties.

As both effects caused by erbium triflate addition are opposite, there must be an optimum content of initiator that promotes good barrier properties (high crosslinking density) without decreasing too much the adherence to the substrate, like coatings with 0.5 and 1phr of erbium triflate. Adherence property seems

to have much more importance than barrier property, as it can be seen with TBG system where its anticorrosive performance is much higher than that of the coating with 2phr of erbium triflate even if the latter had higher T_g. Finally 2phr coating anticorrosive properties are the worst not only because bad adherence either to a non-sinterized structure because of too fast curing.

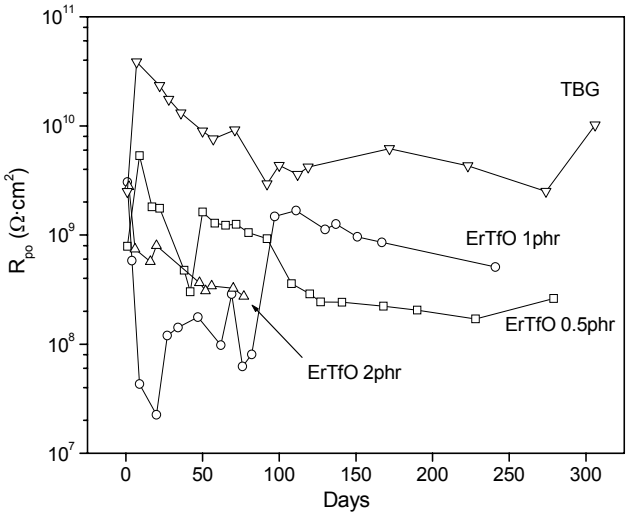

Fig. 8a. Evolution of pore resistance, R_{po} versus time of exposure to electrolyte (deionised water with 3.5% NaCl by weight) for different clearcoats: epoxy resin/$Er(TfO)_3$ 0.5phr (□), epoxy resin/$Er(TfO)_3$ 1phr (○), epoxy resin/$Er(TfO)_3$ 2phr (△), and epoxy resin/TBG (▽) applied on metal substrates. EIS test.

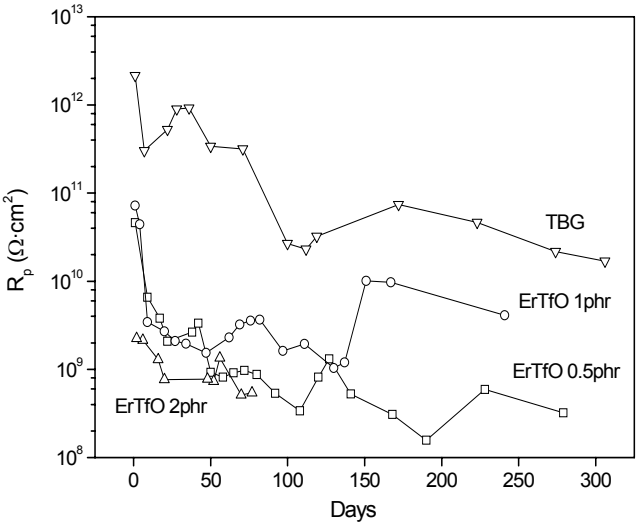

Fig. 8b. Evolution of polarization resistance, R_p versus time of exposure to electrolyte (deionised water with 3.5% NaCl by weight) for different clearcoats: epoxy resin/$Er(TfO)_3$ 0.5phr (□), epoxy resin/$Er(TfO)_3$ 1phr (○), epoxy resin/$Er(TfO)_3$ 2phr (△), and epoxy resin/TBG (▽) applied on metal substrates. EIS test.

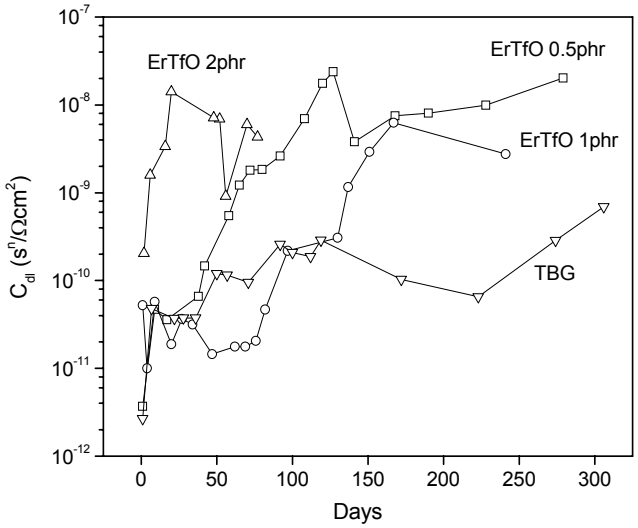

Fig. 8c. Evolution of double layer capacitance, C_{dl} versus time of exposure to electrolyte (deionised water with 3.5% NaCl by weight) for different clearcoats: epoxy resin/$Er(TfO)_3$ 0.5phr (□), epoxy resin/$Er(TfO)_3$ 1phr (○), epoxy resin/$Er(TfO)_3$ 2phr (△), and epoxy resin/TBG (▽) applied on metal substrates. EIS test.

3.5. AC/DC/AC test

Figure 9 shows a Bode graph (impedance modulus versus frequency) after 5 polarizations (DC) for the four different samples prepared. It can be observed that the reference one (with TBG) presents the best modulus, although the sample with 1phr of $Er(TfO)_3$ presents very close results. Sample with 2phr is still having the worst properties but much more accentuated than in EIS test (the displacement of the decrease of the modulus towards lower frequencies indicates a higher area of reaction).

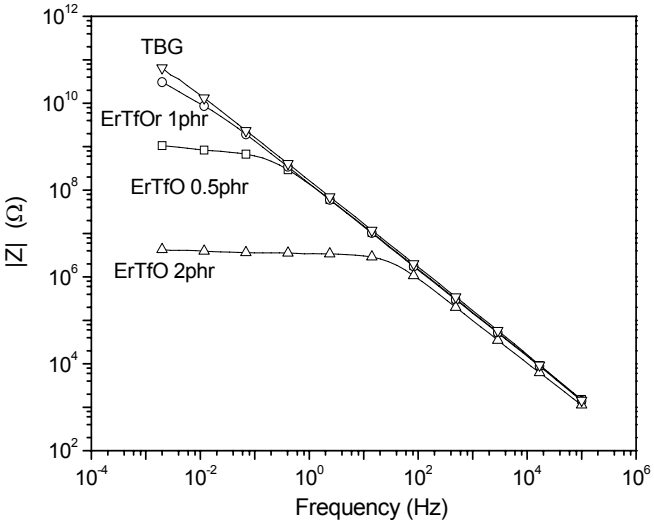

Fig. 9. Bode plot (impedance modulus versus frequency) for different clearcoats: epoxy resin/$Er(TfO)_3$ 0.5phr (□), epoxy resin/$Er(TfO)_3$ 1phr (○), epoxy resin/$Er(TfO)_3$ 2phr (△), and epoxy resin/TBG (▽) applied on metal substrates after 5 cathodic polarisations. AC/DC/AC test.

Figure 10a and 10b show the evolution of the equivalent circuit modelled parameters, R_p and C_{dl} respectively, with the number of cycles (polarizations) for the different systems. C_c is not plotted because there was almost no difference between the samples, while R_{po} is not plotted because it showed similar trend as R_p.

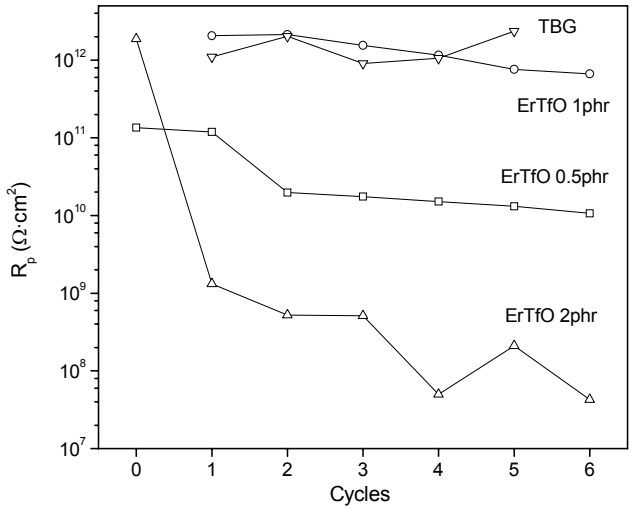

Fig. 10a. Evolution of polarization resistance, R_p versus cathodic polarizations for different clearcoats: epoxy resin/$Er(TfO)_3$ 0.5phr (□), epoxy resin/$Er(TfO)_3$ 1phr (○), epoxy resin/$Er(TfO)_3$ 2phr (Δ), and epoxy resin/TBG (∇) applied on metal substrates. AC/DC/AC test.

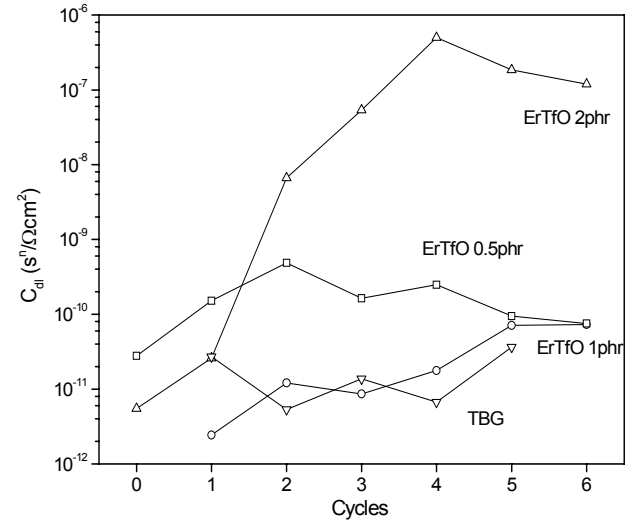

Fig. 10b. Evolution of double layer capacitance, C_{dl} versus cathodic polarizations for different clearcoats: epoxy resin/$Er(TfO)_3$ 0.5phr (□), epoxy resin/$Er(TfO)_3$ 1phr (○), epoxy resin/$Er(TfO)_3$ 2phr (Δ), and epoxy resin/TBG (∇) applied on metal substrates. AC/DC/AC test.

Results showed by AC/DC/AC technique were very similar to those showed by EIS. Maximum anticorrosive properties were obtained using TBG and 1phr erbium triflate, while the worst correspond to the system with 2phr of erbium triflate initiator.

In order to understand the AC/DC/AC technique, it is necessary to look at the theoretical basis underlying this method. The cathodic polarization (DC) applied to the coated metal can cause the following to occur in the coating:

a. The introduction and passage of different cations (H^+, Na^+, and so on) from the electrolyte through the clearcoat due to the negative potential imposed in the metallic substrate. This can produce a concentration of positive charges in the primer that must be neutralised by

balancing the entry of anions (like Cl^-). The passage of ions (which can also be hydrated) through the coating can cause its deterioration and the formation of pores.

b. The cathodic reaction that can take place in the metallic surface considering the level of negative polarisation and the type of electrolyte [41] is:

$$2\ H_2O\ (l) + 2\ e^- \rightarrow H_2\ (g) + 2\ OH^-$$

The cathodic reaction will take place first if the electrolyte is able to pass through the coating and reaches the interface. This depends on the properties of the film (permeability to ions, adhesion to substrate, existence of local film delamination, susceptibility of the coating to form cracks because of its high rigidity, etc.) and, of course, the applied cathodic voltage.

Obviously, the higher the quality of the primer is (impermeability and ductility of the film and high adhesion to the substrate), the lower will be the probability of the electrolyte to reach the interphase, and to the cathodic reaction to take place.

The deterioration of the coating because of cathodic polarisations can be caused primarily by the film delamination process at the metallic interphase produced by the cathodic reaction (H_2 evolving), although the passage of ions can also exert a degrading effect.

If there are possibilities of detecting whether the cathodic reactions have taken place during polarisation or not, this information could be used to know a little more about the performance and quality of the primer. One possible way of detecting the existence of H_2 (g) and OH^- production (meaning more delamination) at the interphase, is to study the evolution of the open circuit potential after polarisation, during the relaxation time. When cathodic polarisation finishes, the coated metal potential will relax showing two possible spectra:

a. If cathodic reactions were taking place (H_2 production), the potential would have a quick relaxation around -1V [41] (with small variations depending on the coating), which corresponds to the ending of the reaction and, afterwards, a second relaxation that corresponds to ions and electrolyte leaving the coating, and possibly the formation of a new double layer in the metallic surface. In any case, the cathodic reaction will produce the entry of electrolyte through the coating and the production of H_2 (g) and OH^- at the metal/coating interface. The time needed for this electrolyte and the ions to leave the film will therefore be higher because they have to pass through the entire primer film.
b. If no cathodic reactions have taken place, there would be a single relaxation process that corresponds to ions and electrolyte leaving the primer or to the polymer dipoles new configuration. This relaxation will take place at longer times as ions and electrolyte penetrate deeper into the film, but they will probably need less time than in case “a” described above.

Figure 11 shows the potential relaxation versus time of the different coatings after 5 cathodic polarizations. In the case of the sample with 2phr and 0.5phr there is observed two or more relaxations. For a sample with 2phr, and probably due to not being a sinterized structure and its low adhesion, after one cathodic polarization the coatings film breaks down because hydrogen production (fact that can be seen in the R_p decrease and C_{dl} increase).

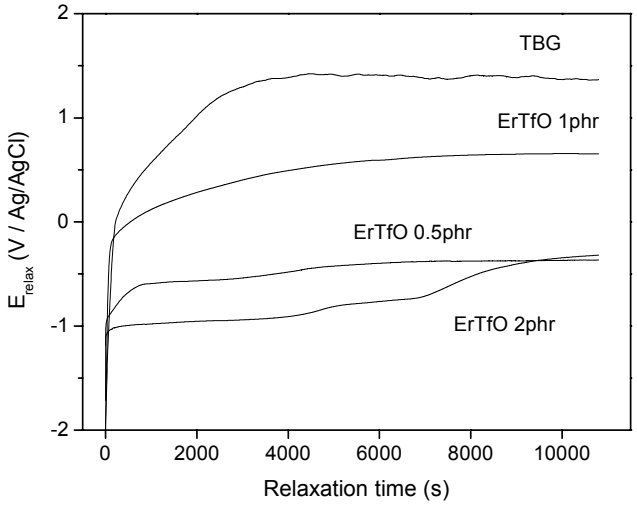

Fig. 11. Evolution of the open circuit potential (E_{OC}) versus relaxation time after exposure to 5 cathodic polarisations (AC/DC/AC test) for different clearcoats: epoxy resin/$Er(TfO)_3$ 0.5phr (□), epoxy resin/$Er(TfO)_3$ 1phr (○), epoxy resin/$Er(TfO)_3$ 2phr (Δ), and epoxy resin/TBG (▽) applied on metal substrates.

Samples with TBG and 1phr of erbium triflate, present only one relaxation and higher relaxation potentials (figure 11), being higher the relaxation potential of the sample with TBG, both showing the better anticorrosive properties. These results are due to a combination of good adhesion and not to high porosity.

As all the results obtained from the AC/DC/AC test show, a coating with high anticorrosive performance will be that which presents only one relaxation process after the cathodic polarization (which means that the cathodic reaction of hydrogen and OH^- production could not have taken place); high open circuit potential at the steady state (which means that the coating has high dielectric properties because low porosity and permeability); and, finally, with regard to the equivalent circuit parameters, high resistances and low capacitances. Thus, from this point of view the best coating is the one cured with TBG (reference system) followed by the one cured with 1phr of erbium triflate. An excess of erbium triflate gives rise probably to a lower permeability (because higher crosslinking density) but also much lower adherence and, consequently, worst anticorrosive performance.

3.6. Salt fog spray

Figure 12 presents some pictures of the samples after 214h of salt fog spray chamber exposure. In figure 13 it is plotted the evolution of delamination with time of exposure. It is clearly seen that the sample with 0.5phr of erbium triflate is less delaminated but with higher corrosion (pickling) than the others. The samples with 1phr and with TBG (reference one) show similar results between them, having less

corrosion and delamination than the sample with 0.5phr. The sample with 2phr had a catastrophic failure after only 100hours of exposure with total delamination and corrosion under the film. Sample with 0.5phr of $Er(TfO)_3$ started showing some points of corrosion after only 50hours of exposure, which is probably due to the higher porosity compared to the other samples with triflate.

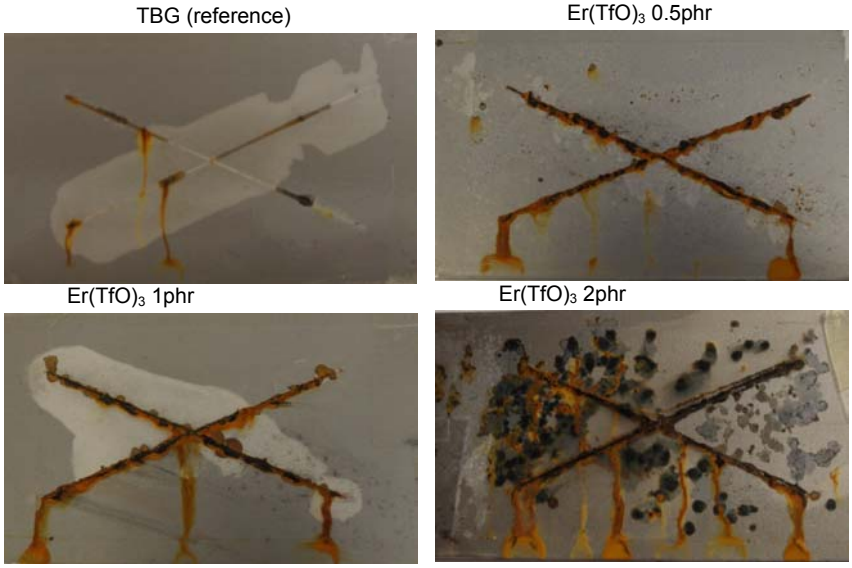

Fig. 12. Pictures of clearcoats epoxy resin/$Er(TfO)_3$ 0.5phr, epoxy resin/$Er(TfO)_3$ 1phr, epoxy resin/$Er(TfO)_3$ 2phr, and epoxy resin/TBG after 214hours of exposure to salt fog spray and after evaluation.

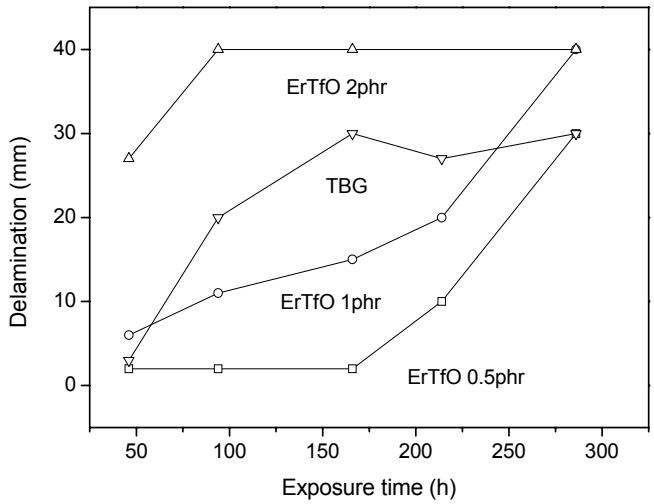

Fig. 13. Evolution of delamination with time of exposure of the different clearcoats, epoxy resin/$Er(TfO)_3$ 0.5phr (□), epoxy resin/$Er(TfO)_3$ 1phr (O), epoxy resin/$Er(TfO)_3$ 2phr (Δ), and epoxy resin/TBG (∇).

These results are partially in accordance to those found for some samples when tested with electrochemical tests (EIS and AC/DC/AC) because of the differences with TBG system.

4. Conclusions

Four different formulations of epoxy powder resin have been prepared, one sample cured with o-tolylbiguanide (used as the reference system), and the other three having different proportions of erbium triflate (0.5, 1 and 2 phr), a proposed initiator where the curing of the resin is done by homo-polymerization.

The use of the erbium triflate clearly reduced the curing temperature and time compared to the reference system. When increasing the content of $Er(TfO)_3$ there was a reduction of the adherence and an augmentation of the crosslinking (higher T_g).

When initiator content reaches 2phr it was observed an increase in porosity because there was no sinterization.

Three different evaluation tests of the anticorrosive properties have been applied: EIS, salt fog spray, and a new electrochemical test named AC/DC/AC. The results showed that the reference sample had the best anticorrosive properties together with the sample using 1phr of erbium triflate. The new clearcoats, using erbium triflate as initiator presented different results depending on their proportions. The sample with 2phr showed very bad anticorrosive properties due to its low adhesion and high macro-porosity.

The AC/DC/AC test has shown good correlation with EIS and salt fog spray test but giving results in very short times (less than 24hours) and giving objective information about the corrosive and degradation processes taking place in the coating. Nevertheless, future research in this direction should be done.

In spite of the relatively good results found for the new epoxy clear-coat system using 1phr of erbium (III) trifluoromethanesulfonate as crosslinker agent (reduction of curing temperature and/or time and good anticorrosive properties) more improvement with Lewis acids should be done in future research in order to obtain low curing powder coatings with very good anticorrosive properties.

Acknowledgements

Authors would like to thank Ms Eva Romero, Ms Àngels Serra, Mr Carlos Bonet and Ms Maite Rodríguez for their help in the development of this project. Authors are also grateful for the economic support in this work of CICYT MAT 2000-0123-P4-03.

1. R.A. Dickie, D.R. Bauer, S.M. Ward, D.A. Wagner, *Prog. Org. Coat.,* 31 (1997) 209
2. S.S. Lee, H.Z.Y. Han, J.G. Hilborn, J.-A.E. Manson, *Prog. Org. Coat.,* 36 (1999) 79
3. Powder coating – A Pollution Prevention Alternative from The Powder Coating Institute, *The Powder Coating Institute, U.S.A.* (1999)
4. E.G. Belder, H.J.J. Rutten, D.Y. Perera, *Prog. Org. Coat.,* 42 (2001) 142
5. F.M. Witte, C.D. Goemans, R. van der Linde, D.A. Stanssens, *Prog. Org. Coat.,* 32 (1997) 241
6. M. Johansson, H. Falken, A. Irestedt, A. Hult, *J. Coat. Tech.,* 70 (884) (1998) 57
7. R. van der Linde, E.G. Belder, D.Y. Perera, *Prog. Org. Coat.,* 40 (2000) 215
8. R.S. Bauer, L.S. Corley, "*Epoxy Resins: Composites Technology"* Ed. Stuart M. Lee, Technomid Publishing Company. Inc. Pennsylvania (1989)
9. F. Mansfeld, *J. Applied Electrochem.,* 25 (1995) 187

10. G.P. Bierwagen, *J. Coat. Tech.,* 64 (1992) 71
11. B. Liu, Y. Li, H. Lin, C. Cao, *Acta Physico-Chimica Sinica.,* 17 (2001) 241
12. B.S. Skerry, C-T. Chen, C.J. Ray, *J. Coat. Tech.,* 64 (1992) 77
13. S. Gwori, K. Balakrishnan, *Prog. Org. Coat.,* 23 (1994) 363
14. M. Selvaraj, S. Guruviah, *Prog. Org. Coat.,* 28 (1996) 271
15. L.S. Hernández, B. del Amo, R. Romagnoli, *Anti-Corrosion Methods and Materials,* 46 (1999) 198
16. X.Liu, H. Lu, J. Shao, P. Wan, S. Zhang, *Materials and Corrosion,* 46 (1995) 33
17. J. Hollaender, E. Ludwig, S. Hillebrand, *Proc. 5th International Tinplate Conference*, London, 300 (1992)
18. J. Hollaender, C.A. Schiller, W. Strunz*, Food additives and contaminants,* 14, 6-7 (1999) 617
19. J. Hollaender, C.A. Schiller, W. Strunz, *Proc. EIS 2001*, Marilleva-Italy (2001)
20. M.T. Rodriguez, J.J. Gracenea, J.J. Saura, J.J. Suay, *Prog. Org. Coat.,* 50 (2004) 68
21. J.J. Suay, M.T. Rodriguez, K.A. Razzaq, J.J. Carpio, J.J. Saura, *Prog. Org. Coat.,* 46 (2003) 121
22. M.T. Rodriguez, J.J. Gracenea, S.J. García, J.J. Saura, J.J. Suay, *Prog. Org. Coat.,* 50 (2004) 123
23. M. Ochi, K. Mimura, H. Motobe, *J. Adhesion Sci. and Techn.,* 8 (1994) 223
24. C. Mas, A. Serra, A. Mantecón, J.M. Salla, X. Ramis, *Macromol. Chem. Phys.,* 202 (2001) 2554
25. S. Kobayashi, *Synlett,* (1996) 689
26. S.J. García, X. Ramis, A. Serra, J. Suay, *Thermochim. Acta.,* 441 (2006) 45
27. S.J. García, X. Ramis, A. Serra, J. Suay, *J. Therm. Anal. Calorim.,* 83 (2) (2006) 429
28. L. Matejka, P. Chabanne, L. Tighzert, J.P. Pascault, *J. Polym. Sci. Part A: Polym. Chem.,* 32 (1994) 1447
29. P. Chabanne, L. Tighzert, J.P. Pascault, *J. Apply. Polym. Sci.,* 53 (1994) 769
30. P. Castell, M. Galià, A. Serra, J.M. Salla, X. Ramis, *Polymer,* 41 (2000) 8465
31. S.J. García, A. Serra, X. Ramis, J. Suay, *J. Therm. Anal. Cal.*, August (2006) online-first
32. F. Mansfeld, *Electrochim. Acta*, 38 (1993)
33. A. Amirudin, D. Thierry, *Prog. Org. Coat.,* 26 (1995) 1
34. G.W. Walter, *J. Electroanal. Chem.,* 118 (1981) 259
35. G.W. Walter, *Corros. Sci.,* 26, 9 (1986) 681
36. Gamry Instruments, "*Electrochemical Impedance Spectroscopy Primer*"
37. N. Tang, W.J. Ooij, G. Górecki, *Prog. Org. Coat.,* 30 (1997) 255
38. H. Leidheiser, *J. Adhesion Sci. Tech.,* 1 (1987) 79
39. Annual Book of ASTM Standards, Vol 03.02, ASTM, Philadelphia, PA (1985)
40. D. Greenfield, J.D. Scantleburry, *JCSE*, 3 (2000) paper5
41. E. Vaca-Cortés, M.A. Lorenzo, J.O. Jirsa, H.G. Wheat, R.L. Carrasquillo, *Adhesion testing of epoxy coating*, Centre for transportation research bureau of engineering research the university of Texas at Austin (1998)
42. N.I. Gaynes, *Testing of Organic Coatings*, Noyes Data Corp., Park Ridge, NJ (1977)
43. M.A. Lorenzo, *Experimental Methods for Evaluating Epoxy Coating Adhesion to Steel Reinforcement,* M.S. Thesis, The University of Texas at Austin (1997)
44. H. Leidheisser Jr., W. Wendy, L. Igefolt, *Prog. Org. Coat.,* 11 (1983) 19

Epoxy powder clearcoats used for anticorrosive purposes cured with Ytterbium III Trifluoromethanesulfonate

S. J. García[1,2] & J. Suay[2]

[1] Àrea de Ciència dels Materials i Enginyeria Metal·lúrgica, Departamento de Ingeniería de Sistemas Industriales y Diseño, Universitat Jaume I, Avda. Vicent Sos Baynat s/n, 12071 Castelló, Spain

[2] Centro de Biomateriales, Universitat Politècnica de València, Camino de Vera s/n, E-46071 Valencia, Spain

Corrosion (The Journal of Science and Engineering)

Enviado mayo 2006. Aceptado septiembre 2006. In press

Abstract

New low curing temperature epoxy powder coatings cured cationically by the use of ytterbium III trifluoromethanesulfonate as initiator have been formulated. Their curing kinetics and anticorrosive properties have been studied and compared with a system commonly used in industry (o-tolylbiguanide / epoxy resin). Three different tests of anticorrosive properties (EIS, AC/DC/AC, and salt fog spray) have been used together with an adherence test, in order to establish the optimal system. Results show that a system employing 1phr of ytterbium triflate presents good anticorrosive properties. The technique AC/DC/AC has shown its ability to evaluate properly, much faster, and in accordance to anticorrosive properties results of powder coatings obtained by other techniques.

Keywords: EIS, AC/DC/AC, Ytterbium triflate, powder coating, salt fog spray

1. Introduction

The prediction of the anticorrosive properties of a primer is one of the most important lines of research in the filed of organic coatings. Due to the difficulty of the corrosion and degradation processes in organic-metal systems, the main routines of interaction testing and material assessment were developed experimentally by using different exposure processes and techniques for the measurement of properties. The main types of exposure processes are the accelerated aging test (e.g. salt fog spray) and field exposure experiments (which must be planned for long times and are very expensive to run).

Salt fog spray, is one of the most extended evaluation techniques for which different International Standards have been proposed. Nevertheless, this technique is very subjective and does not give quantitative information about the corrosion processes and an interpretation of the overall process itself. It is still necessary to develop techniques to measure the anticorrosive properties, thus various electrochemical techniques have been used to evaluate the protection performance of organic coating/metal systems. The application of electrochemical impedance spectroscopy (EIS) to coated metals has proved to be a useful technique in the study of the anticorrosive primers behaviour [1-8], although to perform this type of test long times are needed (days, weeks and sometimes months) to obtain good results.

There is an explicit interest in creating rapid assessment methods for practical applications that provide a faster indication of corrosion processes at the interface of coated metallic substrates. Hollaender et al. [9-11] developed a rapid method for testing coated metals in food packaging consisting of a combination of DC and AC measurements (AC/DC/AC procedure) which has been successfully adapted and used by Suay et al. in liquid paints applied to steel substrates [12-14]. After a first EIS AC measurement, the test sample is treated for a short time by a constant cathodic voltage (DC) producing a stress to the sample and, following that, an AC spectrum is recorded again. The change in the characteristics of the impedance spectrum can be attributed to coating deterioration (pore formation) and a delamination process at the metallic surface due to hydrogen and OH^- production (if a cathodic reaction takes place).

Among the emerging coating technologies (powder coatings, high solid coatings and waterborne ones), powder coatings is considered to be the best alternative for the reduction of the volatile organic contents (VOCs) of solvent-based paints (>60% of VOCs), because their emissions are less than a 4% [15, 16]. Apart from its clear environmental and economic advantages [17], powder coatings present limitations, such as the difficulty associated with the application on thermo-sensible substrates as wood or plastic. For this reasons there exists an interest on creating systems with low curing temperatures. In a previous work [18] we presented the use of ytterbium (III) trifluoromethanesulfonate as initiator of the reaction of an epoxy powder coating. A complete kinetic study was performed and results showed the fast curing rate of these new systems, e.g. for a sample using 0.5phr of $Yb(TfO)_3$ a conversion of 0.98 was afforded after 25 minutes at a curing temperature of 120ºC. Nevertheless, their application as protective coatings and the anticorrosive properties have not yet been studied.

In this work, the EIS, AC/DC/AC, and salt fog spray techniques have been used to study the anticorrosive properties of an epoxy powder clearcoat using ytterbium (III) trifluoromethanesulfonate in three different proportions as the curing agent. Results have been compared to those given for a frequently used system where o-tolylbiguanide (derivative of the dicyanamide, DICY) is used as the crosslinking agent. Also, the validity of the AC/DC/AC technique as a useful method on the determination of anticorrosive properties of powder paints in very short times, comparing it with other different evaluation procedures (EIS and Salt Fog Spray).

2. Experimental

2.1. Materials

Solid bisphenol-A based epoxy resin of medium molecular weight, 733gr/eq epoxy (from Huntsman), was homo-polymerized with ytterbium (III) trifluoromethanesulfonate (from Aldrich) added in three different amounts: 0.5, 1 and 2 phr. A fourth sample used as the reference system was the same resin polymerized in the ratio given by the producer (4.8phr) with a Huntsman DICY derivative (TBG), with an H^+ active equivalent weight of 37g/Eq. In order to apply the samples on steel substrates 0.18phr of benzoine and 1.27phr of flux agent were added to the mixtures (Table 1).

Table1. Samples studied: epoxy resin/$Yb(TfO)_3$ 0.5phr, epoxy resin/$Yb(TfO)_3$ 1phr, epoxy resin/$Yb(TfO)_3$ 2phr, and epoxy resin/TBG

Sample	Epoxy resin	TBG (phr)	$Yb(TfO)_3$ (phr)	Benzoine (phr)	Flux Agent (phr)	T_g (ºC)
1	100	-	0.5	0.18	1.27	107
2	100	-	1	0.18	1.27	109
3	100	-	2	0.18	1.27	115
reference	100	4.8	-	0.18	1.27	95

Samples were pre-mixed and hand-shacked until good pre-mixing was obtained. After that, the material was extruded in a single screw extruder (Haake Rheomex 254). The operating conditions were 80 ºC and 60rpm. The material produced was grinded in an ultra-centrifugal mill ZM 100 and sieved at 100 micron to give the different powder coatings ready to be applied on steel substrates. In order to know the curing conditions, a complete kinetic study has been reported where the curing conditions were outlined [18, 19].

When using TBG, the principal reaction is that given by scheme 1 [19]:

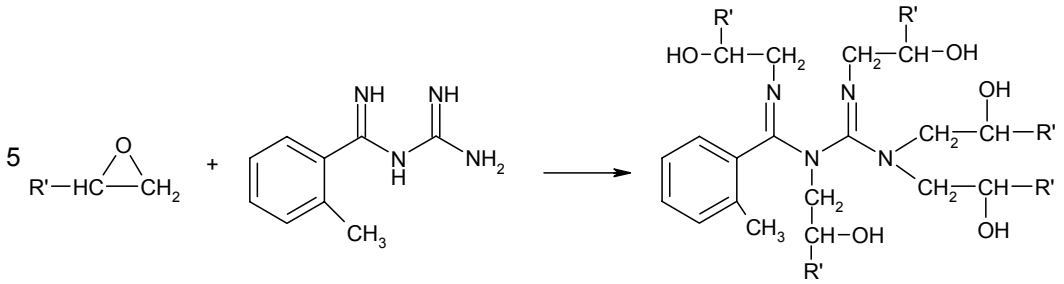

Scheme 1. Chemical structure of the network using TBG as cross-linking agent

Nevertheless, when using ytterbium triflate, the crosslinking is done by the Activated Chain-End Mechanism, ACE (scheme 2), although reactions by the Activated Monomer Mechanism, AM (scheme 3) can also take place but with less importance [18].

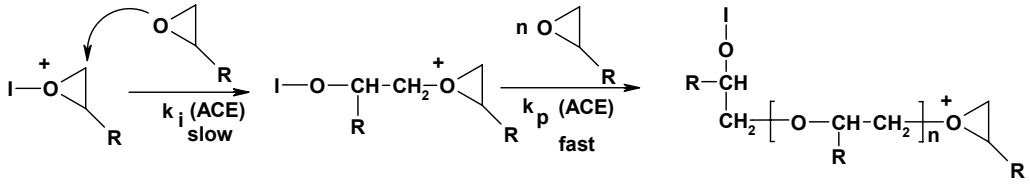

Scheme 2. Activated chain-end mechanism / ACE

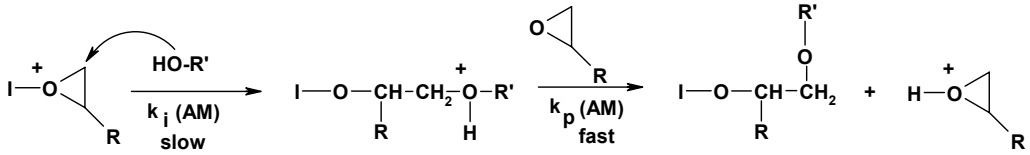

Scheme 3. Activated monomer mechanism / AM

The different clearcoats were applied on cold-rolled low-carbon steel normalized tests panels (15 x 7.5 x 0.1 cm). All test panels were degreased with acetone, and paints were deposited by means of a corona electrostatic powder gun (powder coating equipment Easy 1-C), obtaining 10 panels of each sample. The clearcoats were totally cured for 15 minutes at 150ºC in an oven (25 minutes for the sample using TBG). Thicknesses, determined by an Elcometer, were always within the range 60±5 µm [18, 19].

2.2. Testing Methods and Equipment

2.2.1. Electrochemical impedance spectroscopy (EIS)

Electrochemical Impedance Spectroscopy (EIS) tests were carried out on coated samples exposed to 3.5% NaCl (by weight) in deionised water for periods up to ten months. A three-electrode electrochemical cell was obtained by sticking a glass cylinder on the sample sheet and filling it with the test solution. The exposed surface area was 16.6 cm^2. A carbon sheet acted as the counter electrode and an Ag/AgCl electrode was used as the reference electrode.

The AC impedance data were obtained at the free corrosion potential using an AUTOLAB PGSTAT30 potentiostat and a frequency response analyser. The impedance tests were carried out over a frequency range of 10^5 Hz down to $2 \cdot 10^{-3}$ Hz using a sinusoidal voltage of 10 mV as amplitude inside a Faraday cage in order to minimise external interferences on the system.

The equivalent circuit model, shown in figure 1, was employed to analyze the EIS spectra. The circuit consisted on a working electrode (metal substrate), a reference electrode (Ag/AgCl), electrolyte resistance R_s, pore resistance R_{po}, constant phase element of the coating capacitance CPE_c, polarization resistance R_p, and constant phase element of the double layer capacitance CPE_{dl}. The two constant phase elements were used because the fitting was better than using pure capacitances in the equivalent circuit.

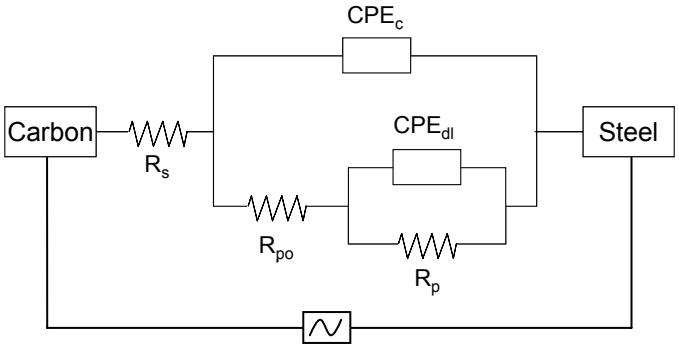

Fig. 1. Equivalent circuit used to model EIS and AC/DC/AC impedance data where passive parameters (R_s = electrolyte resistance, CPE_c = constant phase element of the coating capacitance, CPE_{dl} = constant phase element of the double layer capacitance, R_{po} = pore resistance, R_p = polarization resistance) can be defined.

Fitting the EIS data to the circuit by means of the Z-view software determined the values of the equivalent circuit elements. The chi-squared parameter of the fit was always below 0.1.

2.2.2. Equivalent circuit interpretation

It is generally assumed that there is a correlation between the elements of the equivalent circuit and the corrosion properties of the system [20].

Pore resistance R_{po} is a measure of the porosity and deterioration of the coating. R_{po} values have been usually related to the number of pores or capillary channels perpendicular to the substrate surface through which the electrolyte reaches the interface [21]. Although R_{po} can also increase with immersion time, probably as a result of pore or defect blockage by corrosion products, it usually decreases.

Some authors, as Walter [22, 23], have found three regions in the time-dependent trend of R_{po}. It initially decreases rapidly, then slowly (displaying a plateau) and then rapidly again, coinciding with the appearance of the second semi-circle. The plateau is explained by making the assumption that the number of pathways formed is approximately constant with time.

C_c is the capacitance of the coating and this should be a measure of water permeation into the coating.

The polarization resistance R_p and double layer capacitance C_{dl} are two parameters used to specify the disbonding of the top coat and the onset of corrosion at the interface. The specific polarization

resistance is associated with the charge transfer behaviour of the metal substrate. R_p, like C_{dl}, can only be calculated well when at least two time constants are evident in the spectrum.

C_{dl}, the double layer capacitance, is a measure of the area over which the coating has disbonded. It can only be correctly measured at advanced stages of coating deterioration. The trend of C_{dl} is complex. A change in the C_{dl} value can be associated with the competition between disbonding and corrosion product accumulation at the interface. As water spreads at the interface and the delaminated area extends, there is an increase of the C_{dl} value. On the other hand, the accumulation of corrosion products at the interface reduces the area of the double layer capacitor, which will lead to a decrease in the C_{dl} value. Therefore, the trend in C_{dl} may depend on which factor, disbonding or corrosion product accumulation was more dominant during the corrosion process. However, it should be pointed out that both the increase and the decrease in C_{dl} are the results of the development of corrosion at the metal surface, while a constant C_{dl} is an indication of a stable interface [24].

In order to model the impedance of the system, constant phase elements (CPEs) were used in the equivalent circuit instead of capacitances. Ideally, a capacitor is formed by two conducting plates separated by a non-conducting media (dielectric), nevertheless capacitors in EIS experiments do not behave ideally (e.g. dielectric is not ideal, due to inhomogeneities). Instead, they act like constant phase elements, which are associated with a distribution of the impedance. Thus, CPEs are used in order to offer a better fitting of the impedance.

The distribution of capacitance has been discussed on the literature and its origin related to different sources like [25] surface roughness and heterogeneities, electrode porosity (pore distribution…), variation of coating composition (inhomogeneities of layer properties…), slow adsorption reactions (within the substrate or coating) and non-uniform potential and current distribution. Thus the origin of CPE behaviour must be a distribution of time constants [25].

Normally, the fitting of the impedance parameters with a CPE introduces errors because the capacitance obtained from the fitting with commercial software (Y_0) is not exactly the capacitance (named effective, C_{dl}). When fitting the circuit with a CPE, the given capacitance value is accompanied by a value named as *n* which is the exponent of the equation given by Brug et al. [26].

$$Z_{CPE} = Y_0^{-1}(j\omega)^{-n} \quad (1)$$

Where, Z_{CPE} is the impedance of the CPE, Y_0 is a parameter with units s^n/Ω (the obtained capacitance by means of conventional software), *j* is the *j* the imaginary number ($j = (-1)^{1/2}$) and, ω is the angular frequency ($\omega=2\pi f$, f being the frequency). The parameter n gives then an idea of the deviation of the CPE with respect an ideal capacitance (where n=1), thus when n is 1, the CPE behaves like a capacitance, while when it is 0 it does as a resistor (more capacitance distribution).

Because the deviation in values of the fitted capacitances with respect to the effective capacitances, some researches have proposed equations that allow to calculate the effective capacitance (C_{dl}) by

means of the fitted one (Y_0) and the n values. This relation was first given by E. Van Westing [27] (equation 2).

$$C_{dl} = Y_0(\omega)^{n-1} / \sin(n\pi/2) \quad (2)$$

Despite this equation, Mansfeld and Hsu [28] proposed a new equation, equation 3, which they intend to be the appropriate one for a parallel connection of CPE and R (as this case of study).

$$C_{dl} = Y_0(\omega''_{\max})^{n-1} \quad (3)$$

Where ω''_{max} is the frequency of the maximum on the –Z'' (imaginary impedance) vs ω (angular frequency).

Jovic [29] studied the use of different equations for calculating the relation between C_{dl} and Y_0 arriving to the conclusion that the best equation was that given by Mansfeld and Hsu (equation 3). Moreover, the differences between Y_0 and C_{dl} can be significant depending on the values of R and n [29].

The use of the equations that correlate Y_0 with C_{dl} is recommended when values of n are well below 1. In this study the effective values of C_{dl} were calculated using equation 3 because the n values vary in a wide range. The values used in C_c were those given by the fitting because the n values were always very close to 1, so no differences are detected.

2.2.3. AC/DC/AC test

The AC/DC/AC procedure consists in a combination of DC and AC measurements. First, an AC test is applied to the sample under the same conditions as described above in EIS. This measurement also allows knowing the impedance modulus of the tested sample and its characteristic parameters from the equivalent circuit of figure 1.

After the first AC measurement, the test sample is treated for a short time with a constant cathodic voltage (–2V for 20 minutes) which are the necessary conditions to force the production of H_2 and produce the failure of the coating. This potential was established experimentally but must always be more negative than -1.0 V (vs SCE) which is the potential for the water hydrolysis and H_2 production [30], directly related to the degradation of the system. After applying the direct current of -2V, a registration of the system's open circuit potential variation with time was performed (relaxation time) until the sample reached a new steady state and the potential is once more stabilised. In this case, the relaxation time was of 3 hours, considered enough to obtain good results. When the relaxation time has end, a new EIS measurement (AC) is made to the sample in order to determine the new impedance modulus and characteristic parameters of the system. A schematic representation of the AC/DC/AC procedure is shown in figure 2.

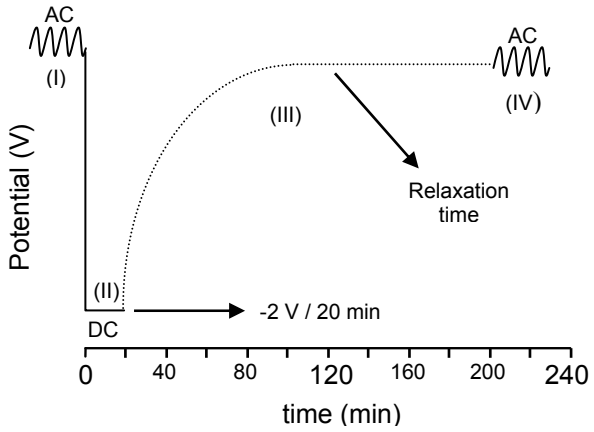

Fig. 2. AC/DC/AC test schematic figure versus time.

This test sequence is repeated at least 6 times, which means that about 24 hours are needed for performing this test. The AC/DC/AC procedure was absolutely automated in PGSTAT 30 AUTOLAB equipment.

2.2.4. Accelerated cyclic test (salt fog spray)

The accelerated salt fog spray test was performed in accordance to ASTM B 117-85 [31]. In this test a cross is performed along the coating until the bare metal is reached. After this, the samples are introduced in a salt fog spray chamber were an alkaline fog is created with a 5% (in weight) NaCl water solution. The samples are collected at different periods of time and evaluated until a maximum of 300 hours of exposure. After each collection, the samples were dried, and blistering and delamination were measured after 24h of ambient exposure. Delamination was evaluated after applying an adhesive tape to one arm of the cross and peeling the clearcoat. The maximum delamination was established in 40mm.

2.2.5. Adhesion Test

Adhesion test was performed in accordance to ISO 4587 (1979). It consists on the deposition of the powder clearcoat between two rectangular and cleaned steel substrates, giving rise to a glued area of 13x25mm. When the powder is deposited, the two rectangular substrates are fixed by means of two pincers and cured for 150ºC one hour. After the curing process and three days of ambient exposure, the samples were tested on an Instron Universal Test Machine 4469-H1907 (figure 3) at a traction speed of 1mm/min. The data of tension and deformation were registered. With the break force (F) and the glued area, the shear stress is obtained (σ_{shear} (MPa) = F/area), giving the adhesion of the clearcoats to the substrates. Almost all the specimens showed an adhesive failure type. Five probes of each sample were prepared and tested.

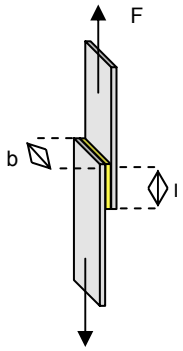

Fig. 3. Scheme of an adhesion test. σ_{shear} calculus.

2.2.6. Morphology study

The morphology of the samples was studied with a scanning electron microscopy (SEM). Samples were frozen with liquid N_2 and hand broken. The measurements were carried out on a Jeol-JSM 6300 at 10kV.

3. Results and Discussion

3.1. Thermal characterization

The curing kinetic process of an epoxy resin/ytterbium triflate system with varying triflate content and an epoxy resin/TBG systems has been previously studied [18, 19], where a complete kinetic analysis of the systems were presented. From those data and the use of a STARe software from Mettler-Toledo, a graphic like figure 4 can be plotted, where for a given conversion (in this case α=0.98) it is represented the curing time needed in front of the curing temperature.

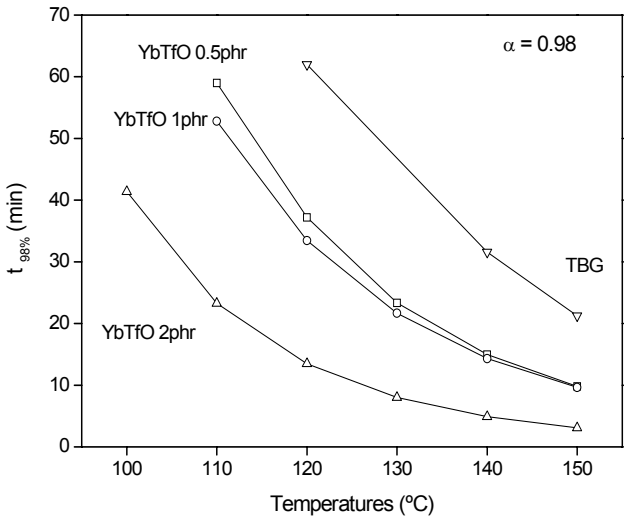

Fig. 4. Time-Temperature for a conversion of α=0.98 of the four different clearcoats: epoxy resin/$Yb(TfO)_3$ 0.5phr (□),epoxy resin/$Yb(TfO)_3$ 1phr (○),epoxy resin/$Yb(TfO)_3$ 2phr (△), and epoxy resin/TBG (▽).

It can be clearly observed that systems with ytterbium triflate decrease the curing temperature and time with respect to a system cured with TBG, e.g. at 150ºC it is needed near 25 minutes for a system with TBG, while for a system with 0.5phr of triflate curing time was 10 minutes, which means a time reduction of about 60% in time. When the triflate content varies between 0.5 and 1phr there are not too big differences in the curing rates, being lower the difference when higher temperatures are used (lines are closer). Nevertheless, when 2phr of ytterbium triflate is added, the system is highly accelerated. Thus, from the point of view of the kinetic study, the systems cured with ytterbium triflate present much higher curing rates than the traditional system using TBG.

The use of ytterbium triflate also affects the formed network and its crosslinking. The different vitreous transition temperatures (T_g) measured with DSC (dynamic scanning calorimeter) at 10ºC/min can be seen in Table 1. It is observed that when using ytterbium triflate the crosslinking is higher (higher T_g) than for a system with TBG, with little changes in reactivity and crosslinking between samples with 0.5 and 1phr and bigger ones when using 2phr of ytterbium triflate.

3.2. Adherence

As it can be seen in figure 5, the higher the ytterbium triflate content the lower the adherence of the system (lower σ_{shear} values). On the other hand, the sample with TBG had the best adherence properties.

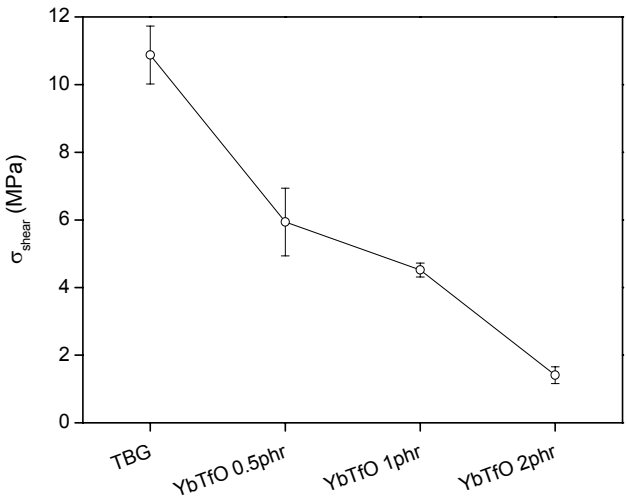

Fig. 5. Shear stress of the studied clearcoats: epoxy resin/$Yb(TfO)_3$ 0.5phr, epoxy resin/$Yb(TfO)_3$ 1phr, epoxy resin/$Yb(TfO)_3$ 2phr, and epoxy resin/TBG.

The number of hydroxyl groups has been correlated with the coating adherence to the metallic substrate (because of hydrogen bonds formation between the organic layer and the metal surface), thus, an increase of the hydroxyls is associated with an increase of the adherence [32-35].

In a system using ytterbium triflate the crosslinking is produced by two reaction mechanisms (schemes 2 and 3). A system with more ytterbium triflate will promote the reaction type AM [18], and the hydroxyl non-reacted groups present in the network will decrease giving rise to a lower adherence as ytterbium triflate content increases.

In the case of the reference system, where the crosslinking is done by TBG (scheme 1), the number of hydroxyls is higher than when curing with triflate, because OH^- are formed in the reaction and maximum adherence is then observed.

3.3. SEM

Figure 6 shows the SEM-pictures of the four systems at 75 magnifications. It can be seen a change in morphology when varying the content of ytterbium triflate as well as differences with the system using TBG. When more triflate is added there is a higher content of porosity probably due to a very fast curing reaction that prevents the exit of occluded air when more initiator is added. The biggest difference between the samples is for that one using 2phr ytterbium triflate, which presents a non-sinterized structure due to a rapid curing kinetics, giving as a result a very high porosity.

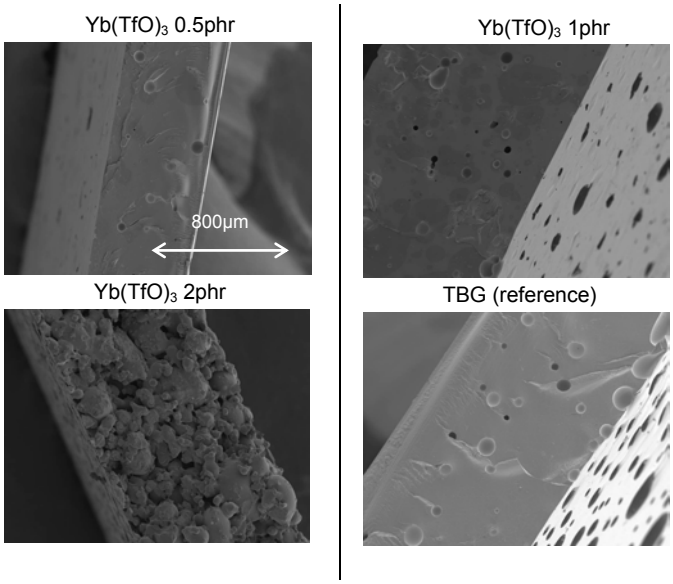

Fig. 6. SEM pictures at 75 magnifications.

3.4. EIS (electrochemical impedance spectroscopy)

Figure 7 shows a Bode graphic of the impedance response (impedance modulus versus frequency) for a coating with TBG, and with ytterbium triflate in three different proportions (0.5, 1 and 2phr) after 250 days of exposure to electrolyte. The higher modulus is obtained for the reference system (with TBG) and system with 1phr of $Yb(TfO)_3$. The sample with 2phr $Yb(TfO)_3$ shows the worst modulus.

Figure 8a, 8b and 8c show the equivalent circuit parameters modelled for EIS results and corresponding to pore resistance R_{po}, polarization resistance R_p, and double layer capacitance C_{dl} respectively. Results of coating capacitance C_c are not shown because they present slight differences between samples and an almost constant value over the exposure time interval of $7 \cdot 10^{-11}$ F/cm^2.

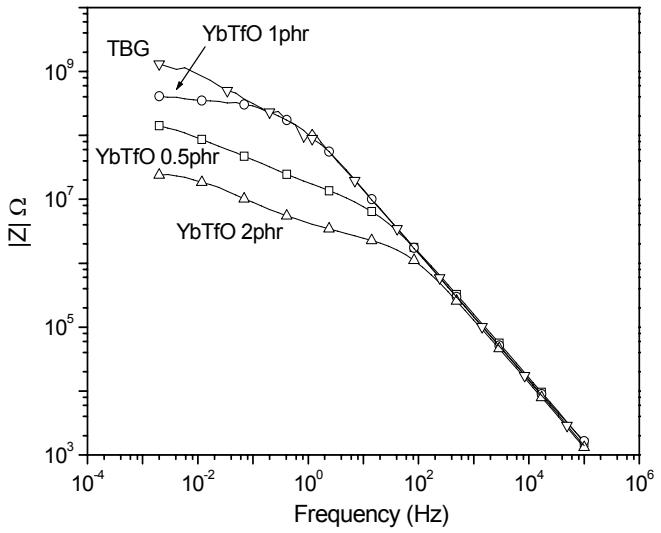

Fig. 7. Bode plot (impedance modulus and phase angle versus frequency) for different clearcoats: epoxy resin/$Yb(TfO)_3$ 0.5phr (□),epoxy resin/$Yb(TfO)_3$ 1phr (○),epoxy resin/$Yb(TfO)_3$ 2phr (Δ), and epoxy resin/TBG (∇) applied on metal substrates after 250 days' exposure to electrolyte (deionised water with 3.5% NaCl by weight). EIS test.

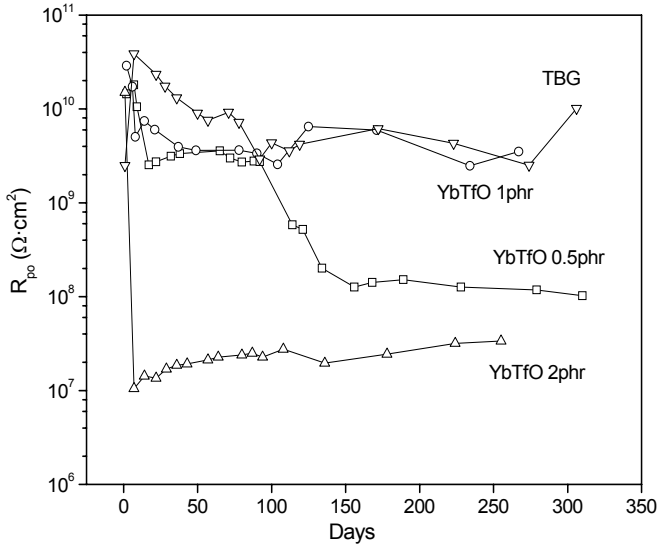

Fig. 8a. Evolution of pore resistance, R_{po} versus time of exposure to electrolyte (deionised water with 3.5% NaCl by weight) for different clearcoats: epoxy resin/$Yb(TfO)_3$ 0.5phr (□),epoxy resin/$Yb(TfO)_3$ 1phr (○),epoxy resin/$Yb(TfO)_3$ 2phr (Δ), and epoxy resin/TBG (∇) applied on metal substrates. EIS test.

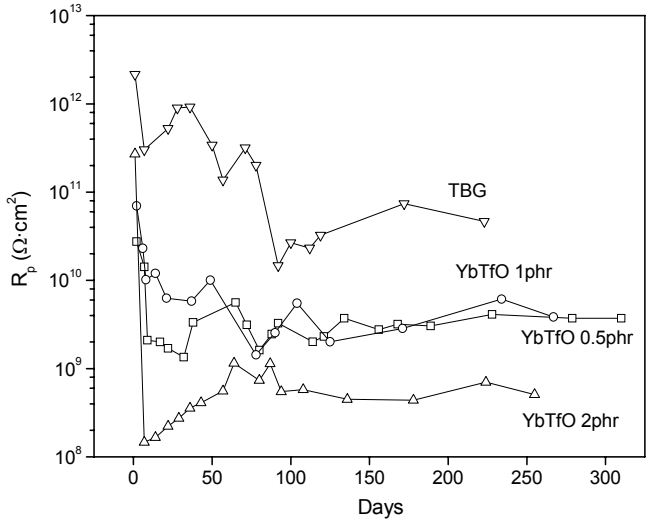

Fig. 8b. Evolution of polarization resistance, R_p versus time of exposure to electrolyte (deionised water with 3.5% NaCl by weight) for different clearcoats: epoxy resin/Yb(TfO)$_3$ 0.5phr (□),epoxy resin/Yb(TfO)$_3$ 1phr (○),epoxy resin/Yb(TfO)$_3$ 2phr (△), and epoxy resin/TBG (▽) applied on metal substrates. EIS test.

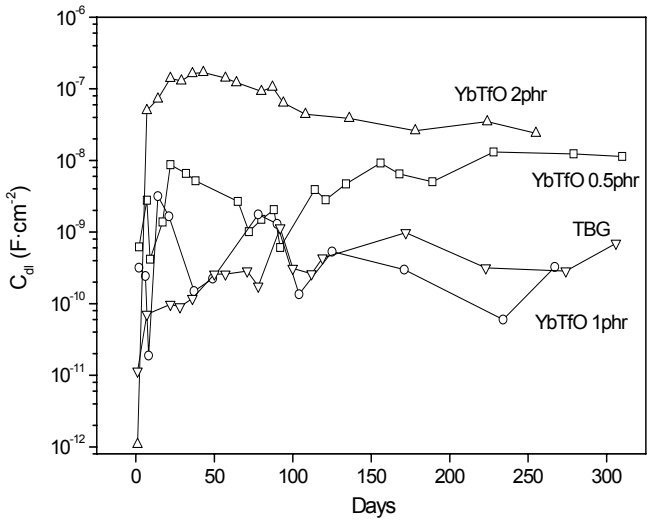

Fig. 8c. Evolution of double layer capacitance, C_{dl} versus time of exposure to electrolyte (deionised water with 3.5% NaCl by weight) for different clearcoats: epoxy resin/Yb(TfO)$_3$ 0.5phr (□),epoxy resin/Yb(TfO)$_3$ 1phr (○),epoxy resin/Yb(TfO)$_3$ 2phr (△), and epoxy resin/TBG (▽) applied on metal substrates. EIS test.

It could be stated with the EIS results that the best system from the point of view of the anticorrosive properties would be that one using TBG which presents the maximum resistance to pore formation (maximum R_{po}), more stable interface (maximum R_p), and minimum tendency to delamination (minimum C_{dl}). Nevertheless, the sample with 1phr of ytterbium triflate presents very similar anticorrosive properties. Worst results were found for 2phr ytterbium triflate system.

As it has been shown with thermal characterization, samples with higher content of ytterbium triflate had much higher transition temperature (T_g) and higher crosslinking density (meaning lower permeability) and, thus, a possible increase of anticorrosive properties. On the other hand, increasing ytterbium triflate increases the macro-porosity (because of fast curing) and decreases coating's adherence to the substrate, leading to a decrease of anticorrosive properties.

As both effects caused by ytterbium triflate addition are opposite, there must be an optimum content of initiator that promotes good barrier properties (high crosslinking density) without decreasing too much the adherence to the substrate, like the coating with 1phr of ytterbium triflate. Finally 2phr coating anticorrosive properties are the worst not only because bad adherence either to a non-sinterized structure because of too fast curing.

3.4. AC/DC/AC test

Figure 9 shows a Bode graph (impedance modulus versus frequency) after 6 polarizations (DC) for the four different samples prepared. It can be observed that in this case, the system with 1phr of ytterbium triflate presents the higher modulus (best behaviour) together with the reference one at low frequencies. Sample with 2phr is still having the worst properties, followed by the sample with 0.5phr, which nevertheless shows not too bad results.

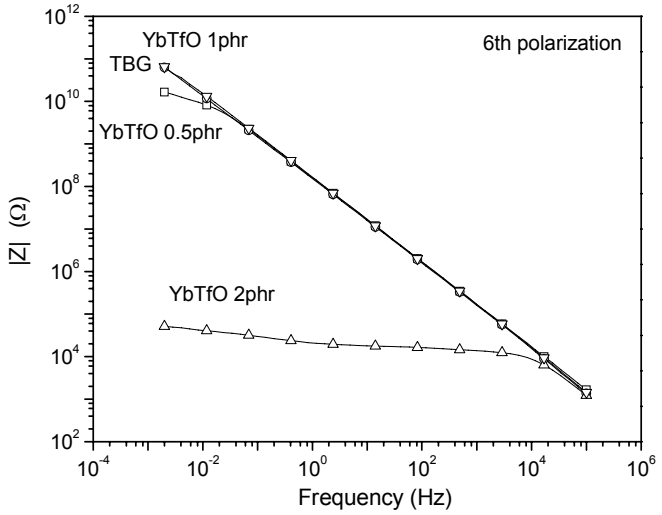

Fig. 9. Bode plot (impedance modulus and phase angle versus frequency) for different clearcoats: epoxy resin/$Yb(TfO)_3$ 0.5phr (□),epoxy resin/$Yb(TfO)_3$ 1phr (○),epoxy resin/$Yb(TfO)_3$ 2phr (Δ), and epoxy resin/TBG (∇) applied on metal substrates after 6 cathodic polarisations. AC/DC/AC test.

Figure 10a, 10b and 10c show the evolution of the equivalent circuit modelled parameters, R_{po}, R_p and C_{dl} respectively, with the number of cycles (polarizations) for the different systems. C_c is not plotted because there was almost no difference between the samples.

Results obtained by AC/DC/AC technique were very similar to those obtained by EIS. Maximum anticorrosive properties (higher resistances and lower capacitance) were obtained using TBG and 1phr ytterbium triflate, while the worst correspond to the system with 2phr of ytterbium triflate initiator. Nevertheless, the sample with 0.5phr of ytterbium triflate showed a better behaviour than in the EIS test, having its anticorrosive properties very close to those of the samples with 1phr and TBG.

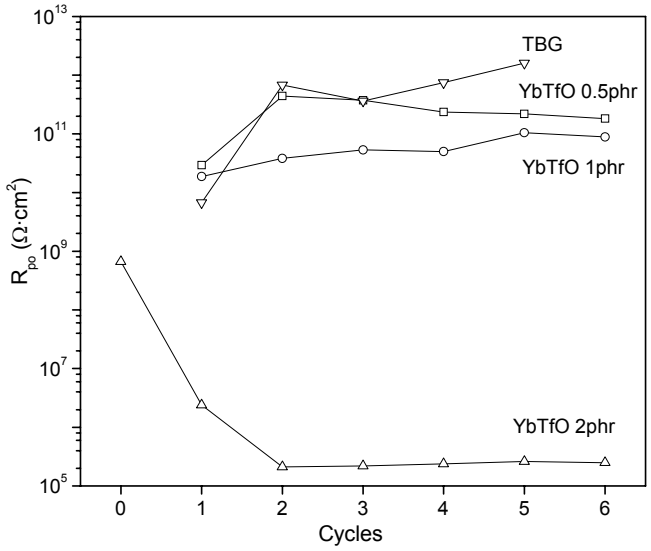

Fig. 10a. Evolution of pore resistance, R_{po} versus cathodic polarizations for different clearcoats: epoxy resin/$Yb(TfO)_3$ 0.5phr (□),epoxy resin/$Yb(TfO)_3$ 1phr (O),epoxy resin/$Yb(TfO)_3$ 2phr (Δ), and epoxy resin/TBG (∇) applied on metal substrates. AC/DC/AC test.

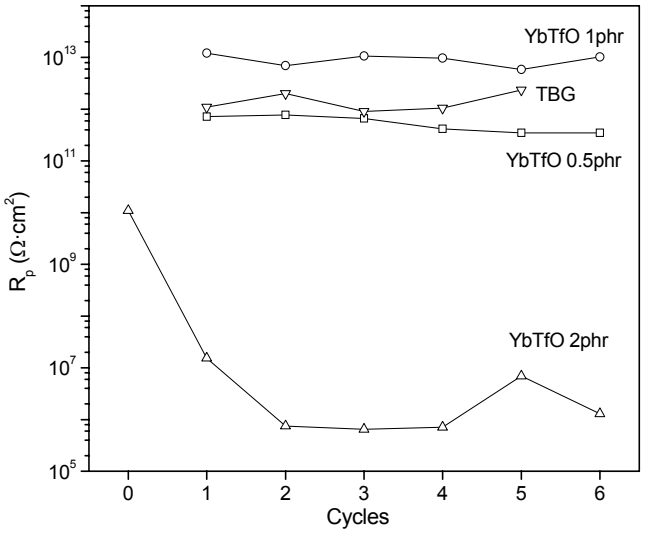

Fig. 10b. Evolution of polarization resistance, R_p versus cathodic polarizations for different clearcoats: epoxy resin/$Yb(TfO)_3$ 0.5phr (□),epoxy resin/$Yb(TfO)_3$ 1phr (O),epoxy resin/$Yb(TfO)_3$ 2phr (Δ), and epoxy resin/TBG (∇) applied on metal substrates. AC/DC/AC test.

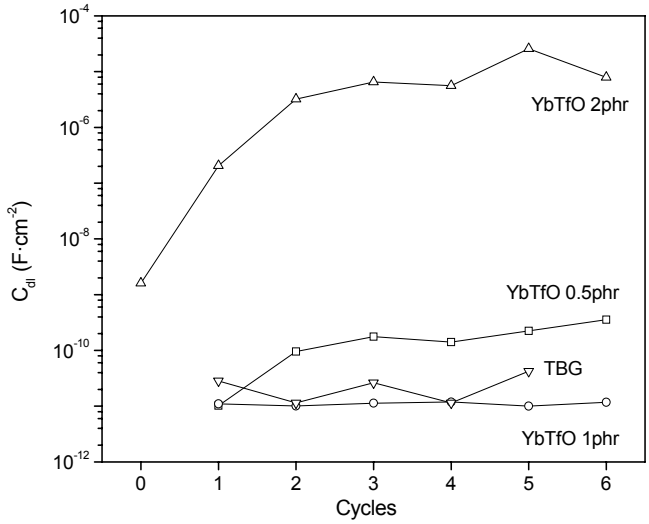

Fig. 10c. Evolution of double layer capacitance, C_{dl} versus cathodic polarizations for different clearcoats: epoxy resin/$Yb(TfO)_3$ 0.5phr (□),epoxy resin/$Yb(TfO)_3$ 1phr (O),epoxy resin/$Yb(TfO)_3$ 2phr (Δ), and epoxy resin/TBG (∇) applied on metal substrates. AC/DC/AC test.

In order to understand the AC/DC/AC technique, it is necessary to look at the theoretical basis underlying this method. The cathodic polarization (DC) applied to the coated metal can cause the following to occur in the coating:

a. The introduction and passage of different cations (H^+, Na^+, and so on) from the electrolyte through the clearcoat due to the negative potential imposed in the metallic substrate. This can produce a concentration of positive charges in the primer that must be neutralised by balancing the entry of anions (like Cl^-). The passage of ions (which can also be hydrated) through the coating can cause its deterioration and the formation of pores.

b. The cathodic reaction that can take place on the metallic surface considering the level of negative polarization and the type of electrolyte is [36]:

$$2\ H_2O\ (l) + 2\ e^- \rightarrow H_2\ (g) + 2\ OH^-$$

The cathodic reaction will take place first if the electrolyte is able to pass through the coating and reach the interface. This depends on the properties of the film (permeability to ions, adhesion to substrate, existence of local film delamination, susceptibility of the coating to form cracks because of its high rigidity, etc.) and, of course, the applied cathodic voltage [14].

Obviously, the higher the quality of the primer is (impermeability and ductility of the film, and high adhesion to the substrate) the lower will be the probability of the electrolyte to reach the interface, and for the cathodic reaction to take place.

The deterioration of the coating because of cathodic polarizations can be caused primarily by the film delamination process at the metallic interface produced by the cathodic reaction (H_2 evolving), although the passage of ions can also exert a degrading effect.

If there are possibilities of detecting whether the cathodic reactions have taken place during polarization or not, this information could be used to know a little more about the performance and quality of the primer. One possible way of detecting the existence of H_2 (g) and OH^- production (meaning more delamination) at the interface, is to study the evolution of the open circuit potential after polarization, during the relaxation time. When cathodic polarization finishes, the coated metal potential will relax showing two possible profiles:

a. If cathodic reactions were taking place (H_2 production), the potential would have a quick relaxation around -1V (with small variations depending on the coating) [36], which corresponds to the ending of the reaction and, afterwards, a second relaxation that corresponds to ions and electrolyte leaving the coating and possibly the formation of a new double layer in the metallic surface. In any case, the cathodic reaction will produce the entry of electrolyte through the coating and the production of H_2 (g) and OH^- at the metal/coating interface. The time needed for this electrolyte and the ions to leave the film will therefore be higher because they have to pass through the entire primer film.

b. If no cathodic reactions have taken place, there would be a single relaxation process that corresponds to ions and electrolyte leaving the primer or to the polymer dipoles new configuration. This relaxation will take place at longer times as ions and electrolyte penetrate deeper into the film, but they will probably need less time than in case “a” described above.

Figure 11 shows the potential relaxation versus time of the different clearcoats after six cathodic polarizations. In the case of the sample with 2phr two relaxation processes can be observed. For a sample with 2phr, and probably due to not being a sinterized structure and its low adhesion, after two cathodic polarizations the coating film breaks down because of hydrogen production (fact that can also be seen in the R_p decrease and C_{dl} increase).

As all the results obtained from the AC/DC/AC test show, a coating with high anticorrosive performance will be that which presents only one relaxation process after the cathodic polarization (which means that the cathodic reaction of hydrogen and OH^- production could not have taken place); high open circuit potential at the steady state (which means that the coating has high dielectric properties because low porosity and permeability); and, finally, with regard to the equivalent circuit parameters, high resistances and low capacitances. Thus, from this point of view the best coating is the one cured TBG together with the one cured with 1phr of ytterbium triflate. An excess of ytterbium triflate gives rise probably to a lower permeability (because higher crosslinking density) but also much lower adherence, and consequently worst anticorrosive properties.

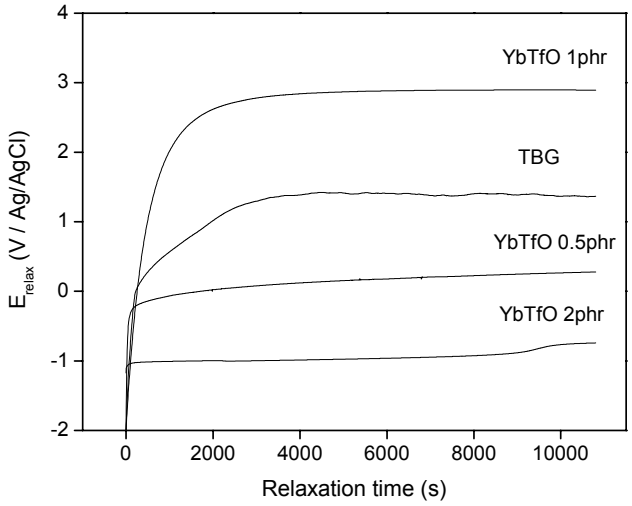

Fig. 11. Evolution of the open circuit potential (E_{OC}) versus relaxation time after exposure to 6 cathodic polarisations (AC/DC/AC test) for different clearcoats: epoxy resin/$Yb(TfO)_3$ 0.5phr (□),epoxy resin/$Yb(TfO)_3$ 1phr (O),epoxy resin/$Yb(TfO)_3$ 2phr (Δ), and epoxy resin/TBG (∇) applied on metal substrates.

3.5. Salt fog spray

Figure 12 presents some pictures of the samples after 214h of salt fog spray chamber exposure and figure 13 the evolution of the delamination with the exposure time. It is clearly seen that the sample with 0.5phr of ytterbium triflate is less delaminated but with higher corrosion (pickling) than the others which means higher adhesion but also higher porosity. Samples with 1phr and TBG show similar results between them, having less corrosion than the sample with 0.5phr, overall the sample with TBG. The sample with 2phr had a catastrophic failure with total delamination. None of the samples showed blistering along the time, although the sample with 0.5phr of $Yb(TfO)_3$ showed some points of corrosion, which are probably due to the higher porosity compared to the other samples with triflate. The sample with 1phr of $Yb(TfO)_3$ showed corrosion under the delaminated areas.

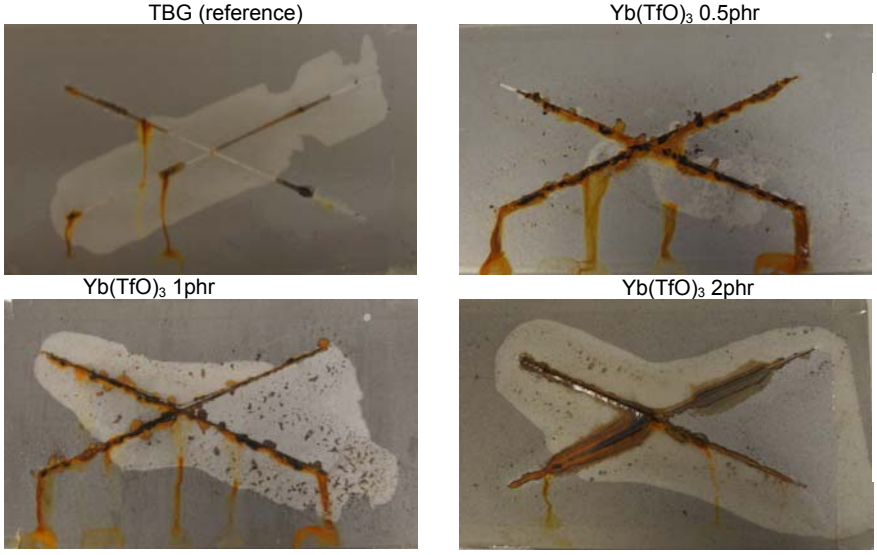

Fig. 12. Pictures of clearcoats epoxy resin/$Yb(TfO)_3$ 0.5phr, epoxy resin/$Yb(TfO)_3$ 1phr, epoxy resin/$Yb(TfO)_3$ 2phr, and epoxy resin/TBG after 214hours of exposure to salt fog spray and after evaluation.

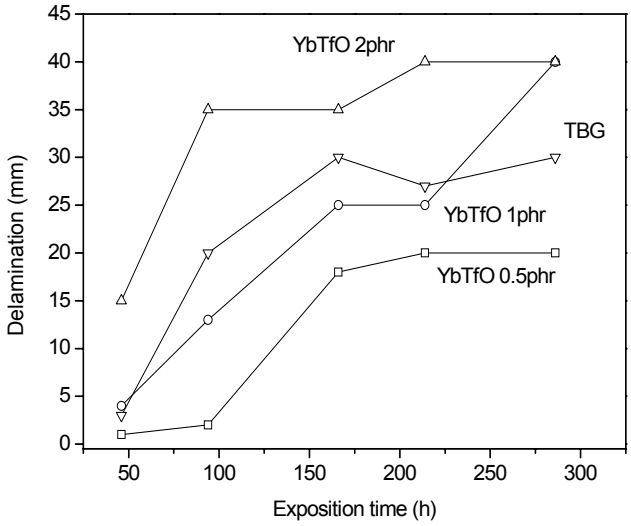

Fig. 13. Evolution of delamination with time of exposure of the different clearcoats, epoxy resin/$Yb(TfO)_3$ 0.5phr (□), epoxy resin/$Yb(TfO)_3$ 1phr (O), epoxy resin/$Yb(TfO)_3$ 2phr (Δ), and epoxy resin/TBG (∇).

4. Conclusions

Four different formulations of epoxy powder resin have been prepared and studied their anticorrosive properties. Three of the formulations were homo-polymerized using different proportions of ytterbium triflate (0.5, 1 and 2phr). A third formulation, used as the reference system, was cured with o-tolylbiguanide. Ytterbium triflate has been here proposed as a possible initiator of the homo-polymerization of epoxy powder resins.

The use of the ytterbium triflate clearly reduced the curing temperature and time compared to the reference system.

When initiator content reaches 2phr it was observed an increase in porosity because there was no sinterization.

Three different evaluation tests for anticorrosive properties were applied: EIS, salt fog spray, and a new electrochemical test named AC/DC/AC. The results showed that the reference sample and samples using 0.5 and 1phr of ytterbium triflate had very good anticorrosive properties while the sample with 2phr showed very bad anticorrosive properties due to its low adhesion. Despite the good correlation between the results given by the three different evaluation methods, the results offered by the electrochemical techniques (EIS and AC/DC/AC) were different to those given by the salt fog spray test for the system using 0.5phr of ytterbium triflate.

In this article it is proposed a new powder-epoxy coating using 1phr of ytterbium triflate as initiator of homo-polymerization reaction. These systems present a high reduction in curing temperature and time compared to a conventional system using o-tolylbiguanide (almost 60% reduction in curing time), while at the same time maintaining good anticorrosive properties.

The AC/DC/AC test has shown good correlation with EIS and salt fog spray test but giving results in very short times (less than 24hours) and at the same time by giving more objective information about the

corrosive and degradation processes taking place. Nevertheless, future research in this direction should be done.

Acknowledgments

Authors would like to thank Ms Eva Romero, Ms Àngels Serra, Mr Carlos Bonet and Ms Maite Rodríguez for their help in the development of this project. Authors are also grateful for the economic support in this work of CICYT MAT 2000-0123-P4-03.

1. F. Mansfeld, *J. Applied Electrochem.,* 25 (1995) 187
2. G.P. Bierwagen, *J. Coat. Tech.,* 64 (1992) 71
3. B. Liu, Y. Li, H. Lin, C. Cao, *Acta Physico-Chimica Sinica.,* 17 (2001) 241
4. B.S. Skerry, C-T. Chen, C.J. Ray, *J. Coat. Tech.,* 64 (1992) 77
5. S. Gwori, K. Balakrishnan, *Prog. Org. Coat.,* 23 (1994) 363
6. M. Selvaraj, S. Guruviah, *Prog. Org. Coat.,* 28 (1996) 271
7. L.S. Hernández, B. del Amo, R. Romagnoli, *Anti-Corrosion Methods and Materials,* 46 (1999) 198
8. X.Liu, H. Lu, J. Shao, P. Wan, S. Zhang, *Materials and Corrosion,* 46 (1995) 33
9. J. Hollaender, E. Ludwig, S. Hillebrand, *Proc. 5th International Tinplate Conference*, London, 300 (1992)
10. J. Hollaender, C.A. Schiller, W. Strunz, *Food additives and contaminants,* 14 (6-7) (1999) 617
11. J. Hollaender, C.A. Schiller, W. Strunz, *Proc. EIS 2001*, Marilleva-Italy (2001)
12. M.T. Rodriguez, J.J. Gracenea, J.J. Saura, J.J. Suay, *Prog. Org. Coat.,* 50 (2004) 68
13. J.J. Suay, M.T. Rodriguez, K.A. Razzaq, J.J. Carpio, J.J. Saura, *Prog. Org. Coat.,* 46 (2003) 121
14. M.T. Rodriguez, J.J. Gracenea, S.J. García, J.J. Saura, J.J. Suay, *Prog. Org. Coat.,* 50 (2004) 123
15. R.A. Dickie, D.R. Bauer, S.M. Ward, D.A. Wagner, *Prog. Org. Coat.,* 31 (1997) 209
16. S.S. Lee, H.Z.Y. Han, J.G. Hilborn, J.-A.E. Manson, *Prog. Org. Coat.,* 36 (1999) 79
17. Powder coating – A Pollution Prevention Alternative from The Powder Coating Institute, *The Powder Coating Institute, U.S.A*. 1999.
18. S.J. García, X. Ramis, A. Serra, J. Suay, *J. Therm. Anal. Calorim.,* 83 (2) (2006) 429
19. S.J. García, A. Serra, X. Ramis, J. Suay, *J. Therm. Anal. Calorim.*, August (2006) online-first
20. F. Mansfeld, *Electrochim. Acta*, 38 (1993)
21. A. Amirudin, D. Thierry, *Prog. Org. Coat.,* 26 (1995) 1
22. G.W. Walter, *J. Electroanal. Chem.,* 118 (1981) 259
23. G.W. Walter, *Corros. Sci.*, 26 (9) (1986) 681
24. N. Tang, W.J. Ooij, G. Górecki, *Prog. Org. Coat.,* 30 (1997) 255
25. J.-B. Jorcin, M.E. Orazem, N. Pébère, B. Tribollet, *Electrochim. Acta*, 51 (2006) 1473
26. G.J. Brug, A.L.G. van Eeden, M. Sluyters-Rehbach, J. Sluyters, *J. Electroanal. Chem.*, 176 (1984) 275
27. E. Van Westing, *Determination of coating performance with impedance measurement*s, PhD thesis, Technical University of Delft, (1992)
28. C.H. Hsu, F. Mansfeld, *Corrosion*, 57 (2001) 747
29. V.D. Jovic, "*Determination of the correct value of C_{dl} from the impedance results fitted by the commercially available software*", Gamry Instruments Inc. (2003)
30. H. Leidheiser, *J. Adhesion Sci. Tech.,* 1 (1987) 79
31. Annual Book of ASTM Standards, Vol 03.02, ASTM, Philadelphia, PA, (1985)
32. D. Greenfield, J.D. Scantleburry, *JCSE*, 3 (2000) paper5
33. E. Vaca-Cortés, M.A. Lorenzo, J.O. Jirsa, H.G. Wheat, R.L. Carrasquillo, *Adhesion testing of epoxy coating*, Centre for transportation research bureau of engineering research the university of Texas at Austin (1998)
34. N.I. Gaynes, *Testing of Organic Coatings*, Noyes Data Corp., Park Ridge, NJ (1977)
35. M.A. Lorenzo, *Experimental Methods for Evaluating Epoxy Coating Adhesion to Steel Reinforcement,* M.S. Thesis, The University of Texas at Austin (1997)
36. H. Leidheisser Jr., W. Wendy, L. Igefolt, *Prog. Org. Coat.,* 11 (1983) 19

Application of electrochemical techniques to study the effect on the anticorrosive properties of the addition of ytterbium and erbium triflates as catalysts on a powder epoxy network

S. J. García[1,2] & J. Suay[2]

[1] Àrea de Ciència dels Materials i Enginyeria Metal·lúrgica, Departamento de Ingeniería de Sistemas Industriales y Diseño, Universitat Jaume I, Avda. Vicent Sos Baynat s/n, 12071 Castelló, Spain

[2] Centro de Biomateriales, Universitat Politècnica de València, Camino de Vera s/n, E-46071 Valencia, Spain

Progress in Organic Coatings

Enviado mayo 2006. Aceptado septiembre 2006. In press

Abstract

New low curing temperature epoxy powder coatings cured with o-tolylbiguanide and catalyzed by the use of erbium III and ytterbium III trifluoromethanesulfonates have been formulated. Their curing kinetics and anticorrosive properties have been studied and compared with a system commonly used in industry (o-tolylbiguanide / epoxy resin). Three different tests for measuring anticorrosive properties (EIS, AC/DC/AC, and salt fog spray) have been used together with an adherence test, in order to establish the ideal system. Results show that a system using 1phr of ytterbium triflate presents good anticorrosive properties. The technique AC/DC/AC has shown its ability to evaluate properly and much faster than other techniques the anticorrosive properties of powder coatings with similar results.

Keywords: EIS, AC/DC/AC, biguanide, lanthanide, powder coating, salt fog spray

1. Introduction

In the prediction of the anticorrosive properties of an organic coating, the most spread technique is Salt Fog Spray test and its variants. Nevertheless, this kind of techniques is not able to give quantitative information related to the degradation of the organic/metal system. Moreover, they give very subjective information, in some occasions difficult to interpret, they require long times of exposure (one week to one month), and they are expensive to carry out [1]. Thus, in the 80's, some new evaluation techniques based on electrochemistry were developed to resolve all these problems, being the most used the EIS technique (electrochemical impedance spectroscopy), which has a wide acceptance in the scientific world [2-5]. Despite the good results of this technique, a big problem is still not resolved: the time needed to obtain good results with this technique can be very long depending on the quality of the film (sometimes several months).

Therefore, there is still an explicit interest in rapid assessment methods for practical applications that provide a faster indication of the coating's quality. This technique was initially developed by Hollaender et al. [6] for testing coated metals in food packaging, and successfully adapted by Suay, Rodríguez and García in the field of liquid and cataforetic paints [7-11] applied to steel substrates, receiving the name of "AC/DC/AC procedure".

Powder coatings are currently the fastest growing section of industrial paints, because of their favourable environmental attributes (less than 4% of volatile organic contents) and performance advantages [12]. Apart from their clear advantages, powder coatings, show some limitations, like the difficulty of application on thermo-sensible substrates like wood or plastic [13]. Nowadays, the most used powder coating systems are those based on epoxy resins cured with dicyandiamide (DICY) or its derivatives like o-tolylbiguanide (TBG) with curing temperatures above 175ºC [14]. For this reason, the formulation of new epoxy powder coatings (using new catalysts and crosslinkers) capable to cross-link at lower temperatures has become one of the main lines of research in industries and related research centres.

The use of Lewis Acid (Ytterbium and Erbium (III) trifluoromethanesulfonates) as catalysts has given very good results in accelerating the curing reaction between epoxy and o-tolylbiguanide (TBG) by the promotion of the polymerization oxirane/NH of the TBG [15]. The question now remains on the influence of the addition of these catalysts on the anticorrosive properties of the system.

In this article it is proposed to study the influence on the anticorrosive properties of the addition of $Yb(TfO)_3$ and $Er(TfO)_3$ on a typical epoxy/o-tolylbiguanide system by means of electrochemical techniques and salt fog spray. At the same time, it is studied the validity of the AC/DC/AC procedure on the evaluation of anticorrosive properties of organic/metal systems.

2. Experimental

2.1. Materials

Three powder epoxy clearcoats were formulated using a solid bisphenol-A based epoxy resin of medium molecular weight, 733gr/eq epoxy (from Huntsman), polymerized with 4.8phr TBG (with an H^+

active equivalent weight of 37g/eq). One of the samples was catalyzed using 1phr of Erbium (III) triflate, and another one using 1phr of Ytterbium (III) triflate, both from Aldrich. The compositions of the samples are detailed in Table 1.

Table1. Composition of the samples studied and glass transition temperature after curing

Sample	Epoxy resin	TBG (phr*)	Benzoine (phr*)	Flux Agent (phr*)	$Er(TfO)_3$ (phr*)	$Yb(TfO)_3$ (phr*)	T_g (ºC)
TBG	100	4.8	0.18	1.27	-	-	95
TBG+Er	100	4.8	0.18	1.27	1	-	101
TBG+Yb	100	4.8	0.18	1.27	-	1	97

Samples were pre-mixed and hand-shacked until good pre-mixing was afforded. After that, the material was extruded in a single screw extruder (Haake Rheomex 254), with the operating conditions: 80 ºC of temperature along the extruder and 60 rpm. The material produced was grinded in an ultra-centrifugal mill ZM 100 and sieved at 100 micron, obtaining then the different powder coatings ready to be applied on steel substrates. In order to know the curing conditions, a complete kinetic study was performed [15].

The different clearcoats were applied on cold-rolled low-carbon steel normalized tests panels (15 x 7.5 x 0.1 cm). All test panels were degreased with acetone, and paints were deposited by means of a corona electrostatic powder gun (powder coating equipment Easy 1-C), obtaining 10 panels of each sample. The clearcoats were totally cured in an oven for 25 minutes at 150ºC. Thicknesses, determined by an Elcometer, were always within the range 60±5 µm.

When using TBG, the principal reaction is that given by scheme 1 [16].

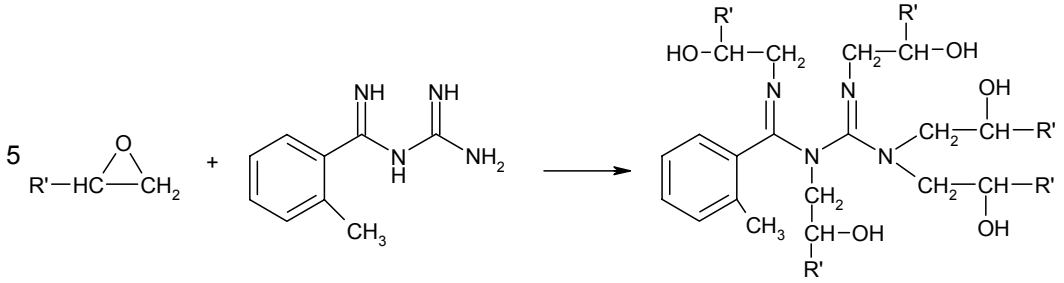

Scheme 1. Chemical structure of the network using TBG as cross-linking agent

But when adding a triflate as catalyst, the reaction presented in scheme 1 becomes accelerated because of the creation of the cation oxirane (scheme 2) which promotes a higher reaction between the epoxy and the amine group of the TBG due to the high nucleophility of the nitrogen (higher than the one of the oxirane ring), avoiding (or reducing) thus the homopolimerizations of the epoxy resin [15].

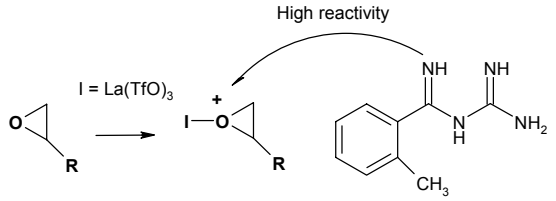

Scheme 2. Cation oxirane produced by the presence of the triflate

2.2. Testing methods and equipment

2.2.1. Accelerated cyclic test (salt fog spray)

The accelerated salt fog spray test was performed in accordance to ASTM B 117-85 [17]. In this test a cross is performed along the coating until the bare metal is reached. The samples are then introduced in a salt fog spray chamber were an alkaline fog is created with a 5% (in weight) NaCl water solution. The samples are collected at different periods of time and evaluated until a maximum of 300 hours of exposure. After each collection, the samples were dried, and blistering, corrosion and delamination were measured after 24h of ambient exposure. Delamination was evaluated after applying a tape of 40mm thick to one arm of the cross and peeling the clearcoat. Maximum value of delamination was 40mm.

2.2.2. Electrochemical impedance spectroscopy (EIS)

Electrochemical Impedance Spectroscopy (EIS) tests were carried out on coated samples exposed to 3.5% NaCl (by weight) in deionised water for periods up to ten months. The three-electrode electrochemical cell was obtained by sticking a glass cylinder on the sample sheet and filling it with the test solution. The exposed surface area was 16.6 cm^2. A carbon sheet acted as the counter electrode and an Ag/AgCl electrode was used as the reference one.

The AC impedance data were obtained at the free corrosion potential using an AUTOLAB PGSTAT30 potentiostat and a frequency response analyser. The impedance tests were carried out over a frequency range of 10^5 Hz down to $2 \cdot 10^{-3}$ Hz using a sinusoidal voltage of 10 mV as amplitude inside a Faraday cage in order to minimise external interferences on the system.

The equivalent circuit model, shown in Figure 1, was employed to analyze the EIS spectra. The circuit consisted on a working electrode (metal substrate), a reference electrode (Ag/AgCl), electrolyte resistance R_s, pore resistance R_{po}, constant phase element of the coating capacitance CPE_c, polarisation resistance R_p, and constant phase element of the double layer capacitance CPE_{dl}. The two CPE were used instead of ideal capacitances because the fitting was more. The “n” value used to be between 0.7 and 1.

Fitting the EIS data to the circuit by means of the Z-view software determined the values of the equivalent circuit elements. The chi-squared parameter of the fit was always below 0.1.

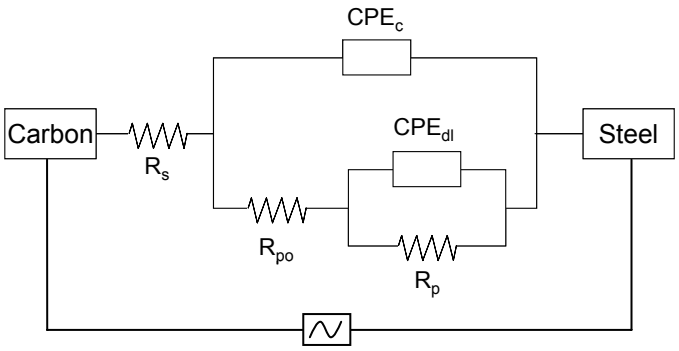

Fig. 1. Equivalent circuit used to model EIS and AC/DC/AC impedance data where passive parameters (R_s = electrolyte resistance, CPE_c = constant phase element of the coating capacitance, CPE_{dl} = constant phase element of the double layer capacitance, R_{po} = pore resistance, R_p = polarization resistance) can be defined.

2.2.3. Equivalent circuit interpretation

It is generally assumed that there is a correlation between the elements of the equivalent circuit and the corrosion properties of the system [18].

Pore resistance R_{po} is a measure of the porosity and deterioration of the coating. R_{po} values have been usually related to the number of pores or capillary channels perpendicular to the substrate surface through which the electrolyte reaches the interface [19]. Although R_{po} can also increase with immersion time, probably as a result of pore or defect blockage by corrosion products, it usually decreases.

Some authors, as Walter [20,21], have found three regions in the time-dependent trend of R_{po}. It initially decreases rapidly, then slowly (displaying a plateau) and then rapidly again, coinciding with the appearance of the second semi-circle. The plateau is explained by making the assumption that the number of pathways formed is approximately constant with time.

In order to calculate de capacitances of the systems it was used the Constant Phase Elements (CPE). Ideally a capacitor is formed by two conducting plates separated by a non-conducting media (dielectric), nevertheless capacitors in EIS experiments do not behave ideally (e.g. dielectric is not ideal). Instead, they act like constant phase elements becoming the impedance of the capacitor:

$$Z_{CPE} = A(j\omega)^{-n} \quad (1)$$

where,

A = the inverse of the capacitance given by a software

n = an exponent which equals 1 for a capacitor

For a CPE the exponent n is less than 1. In practice, it is better to treat n as an empirical constant with no real physical basis [22].

Having this into account, the results are presented as capacitances but with units $s^n/\Omega cm^2$ instead of those for effective/real capacitances ($s/\Omega cm^2$ or F/cm^2).

C_c is the capacitance of the coating and this should be a measure of water permeation into the coating. The polarisation resistance R_p and double layer capacitance C_{dl} are two parameters used to specify the disbonding of the top coat and the onset of corrosion at the interface. The specific polarisation

resistance is associated with the charge transfer behaviour of the metal substrate. R_p, like C_{dl}, can only be calculated well when at least two time constants are evident in the spectrum.

C_{dl}, the double layer capacitance, is a measure of the area over which the coating has disbonded. It can only be correctly measured at advanced stages of coating deterioration. The trend of C_{dl} is complex. A change in the C_{dl} value can be associated with the competition between disbonding and corrosion product accumulation at the interface. As water spreads at the interface and the delaminated area extends, there is an increase of the C_{dl} value. On the other hand, the accumulation of corrosion products at the interface reduces the area of the double layer capacitor, which will lead to a decrease in the C_{dl} value. Therefore, the change of trend in C_{dl} may depend on which factor, disbonding or corrosion product accumulation was more dominant during the corrosion process. However, it should be pointed out that both the increase and the decrease in C_{dl} are the results of the development of corrosion at the metal surface, while a constant C_{dl} is an indication of a stable interface [23].

2.2.4. AC/DC/AC test

The AC/DC/AC procedure (figure 2) is based on the application of a stress (DC) to a coated sample measuring the impedance (AC) of the system after it. This sequence stress/impedance is repeated several times until the system is totally damaged. In order to obtain more information about the coating itself and the whole system, a step of depolarization can be included for a given period (relaxation time). A first AC carried out as a normal EIS measurement gives an idea of the impedance of the system (Bode plots, and modelled characteristic parameters using Z-View and figure1). The relaxation time will give an idea of the evolution with time of the system after the applied stress, until it reaches again the steady state (graphics E_{oc} = f(time)).

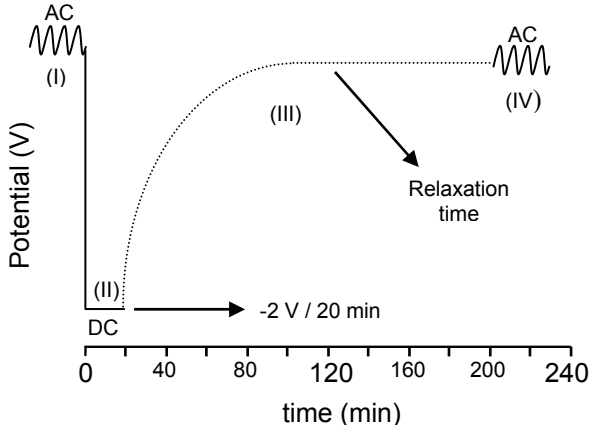

Fig. 2. AC/DC/AC test schematic figure versus time.

This technique has its fundaments on the influence that the cathodic reaction of water hydrolysis (produced when the potential is more negative than -1.0 V (vs SCE) [24]) has on the adhesion because of the formation of H_2 (gas) and OH^-. The evolving of H_2 will increase local delaminations (figure 3) giving rise to the failure of the coating system (reflected on the variation of the impedance). When the cathodic reaction stops and the H_2 production has taken place, the normal electrochemical corrosion of the system

happens in presence of electrolyte with production of iron oxides and hydroxides. On the other hand, the forced polarization makes that the double layer in the interface gets disturbed and needs reorganization, which is reflected on the variation of the potential at the relaxation process. At the same time, the different ions inside the coating will leave it producing charges equilibration and polymeric molecule dipoles reorganization producing also a variation on the potential. Thus the system is degraded by the loose of adherence (formation of H_2), the pore opening by the incoming of the different species from the electrolyte, and the formation of corrosion products by electrochemical processes.

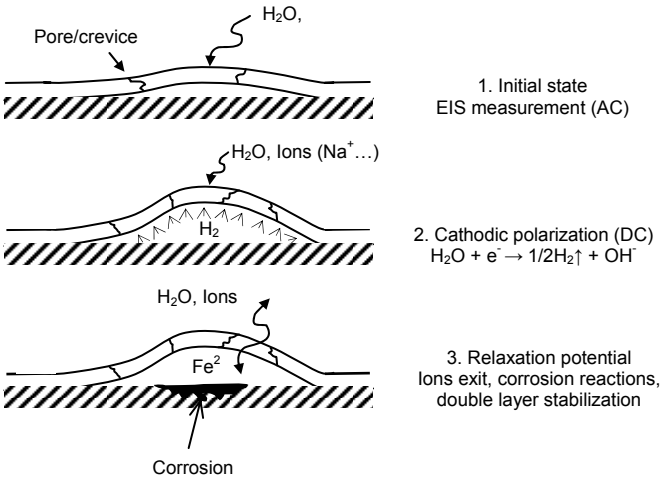

Fig. 3. Physic effect of AC/DC/AC test on a coated metallic substrate. Failure of an anticorrosive coating.

The AC/DC/AC procedure measures the quality of the coating and its adhesion by the study of the resistance that the system offers to its degradation with the cathodic polarizations. In this case of study the cathodic polarization (DC) was carried out for 20minutes at a constant voltage of -2V. Following that, the relaxation time was of 3 hours, and finally an EIS was applied under the conditions above mentioned. The test sequence was repeated six times (around 24hours of test) and was absolutely automated in PGSTAT 30 AUTOLAB equipment.

2.2.5. Adhesion Test

In order to have an overall idea of the influence of the triflates on the adhesion of the epoxy system, an adhesion test was carried out. Adhesion test was performed in accordance to ISO 4587 (1979). It consists on the deposition of the powder clearcoat between two rectangular and cleaned steel substrates, giving rise to a glued area of 13x25mm. When the powder is deposited, the two rectangular substrates are fixed by means of two pincers and cured for 150ºC one hour. After the curing process and three days of ambient exposure, the samples were tested on an Instron Universal Test Machine 4469-H1907 (figure 4) at a traction speed of 1mm/min. The data of tension and deformation were registered. With the break force (F) and the glued area, the shear stress is obtained (σ_{shear} (MPa) = F/area), giving the adhesion of the clearcoats to the substrates. Almost all the specimens showed an adhesive failure type. Five probes of each sample were prepared and tested.

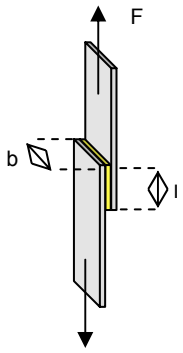

$\sigma_{shear} = F/b \cdot l$

Fig. 3. Scheme of an adhesion test. σ_{shear} calculus.

3. Results and Discussion

3.1. Thermal characterization

Figure 5 shows the curing time in function of the curing temperature for a conversion of 0.98 for the three studied samples. This graphic being obtained in a previous study [15] and using the software STARe from Mettler-Toledo. It can be seen that the addition of Lewis Acids to the epoxy system cured with TBG accelerates the curing reaction, being the faster when erbium triflate is used. Higher differences are observed at lower temperatures, e.g. for a curing time of 130ºC, about 45% reduction in curing time is obtained with respect to a system without catalyst.

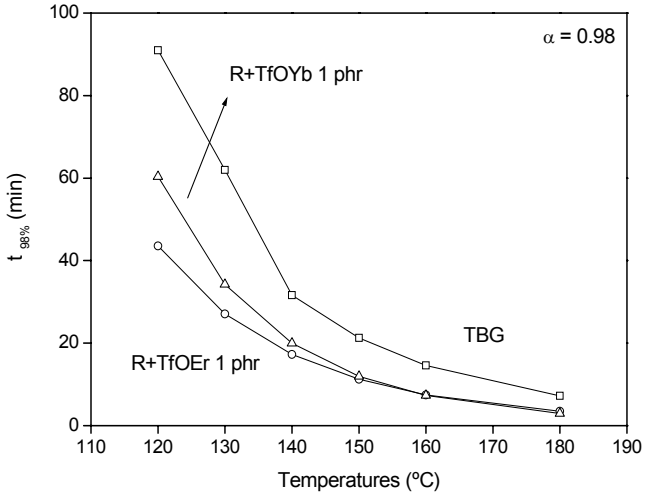

Fig. 5. Time-Temperature for a 98% conversion of the four different clearcoats: epoxy resin/TBG, epoxy resin/TBG/$Er(TfO)_3$ 1phr, and epoxy resin/TBG/$Yb(TfO)_3$ 1phr.

On the other hand, for samples totally cured (1hour at 150ºC) the addition of erbium and ytterbium triflates increases the vitreous transition temperature, T_g, of the system (table 1), specially the sample with erbium, giving a higher crosslinked system. The fact that the sample with erbium shows the higher T_g (more crosslinked) could be strange because the higher reactivity should be expected for the sample with ytterbium for being more acid (more reactivity) [25,26], nevertheless the results are justified because the ytterbium triflate employed was a hydrated one, giving as a result a lower number of reacted groups than expected.

3.2. Adhesion test

Figure 6 presents the adhesion properties of epoxy resin cured with TBG, and systems epoxy resin/TBG catalyzed by erbium and ytterbium triflates.

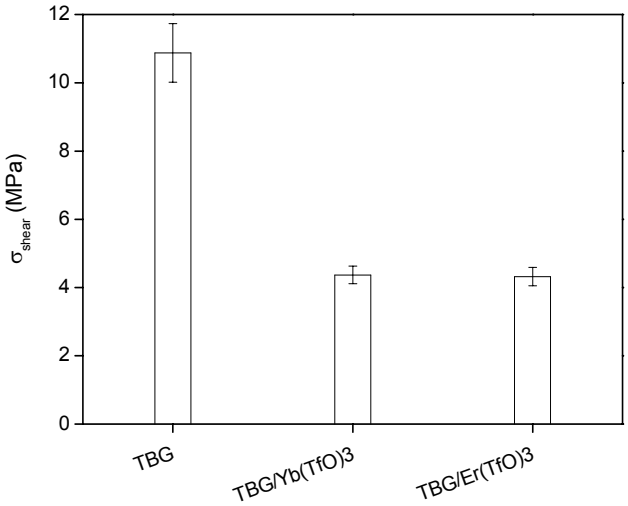

Fig. 6. Shear stress of the studied clearcoats: epoxy resin/TBG, epoxy resin/TBG/$Er(TfO)_3$ 1phr, and epoxy resin/TBG/$Yb(TfO)_3$ 1phr.

It can be seen that the addition of triflate reduces the adhesion to the steel, probably due to a combination of two effects: the reduction of the OH^- content due to secondary reactions, like oxirane/OH^- (coating adhesion to metallic substrate is based on the hydrogen bond formation), and a possible increase of the stress after curing process because of material shrinkage due to a faster curing [26].

3.3. Salt Fog Spray

Figure 7 shows some pictures of the epoxy studied samples (TBG, TBG/$Er(TfO)_3$ and TBG/$Yb(TfO)_3$) after 214h salt fog spray exposure. Figure 8 shows the delamination evolution with time of the same samples after exposure to salt fog spray test.

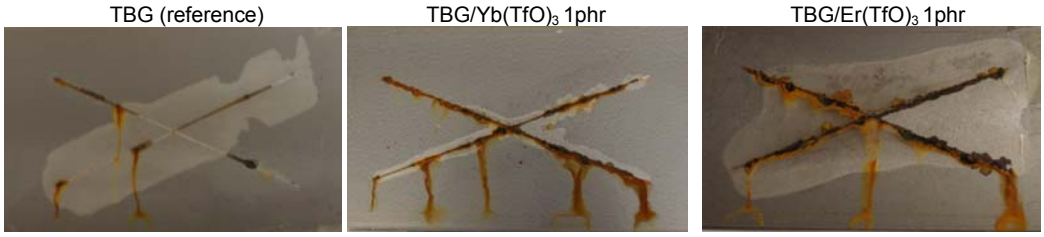

Fig. 7. Pictures of clearcoats: epoxy resin/TBG, epoxy resin/TBG/$Er(TfO)_3$ 1phr, and epoxy resin/TBG/$Yb(TfO)_3$ 1phr after 214 hours of exposure to salt fog spray and after evaluation.

It is clear that the epoxy coating cured with TBG/$Yb(TfO)_3$ showed very good results with low delamination and corrosion. On the other hand coatings with TBG and TBG/$Er(TfO)_3$ showed similar and not good anticorrosive resistance. Results of the system with erbium triflate were very bad probably due to its very low adhesion to the substrate.

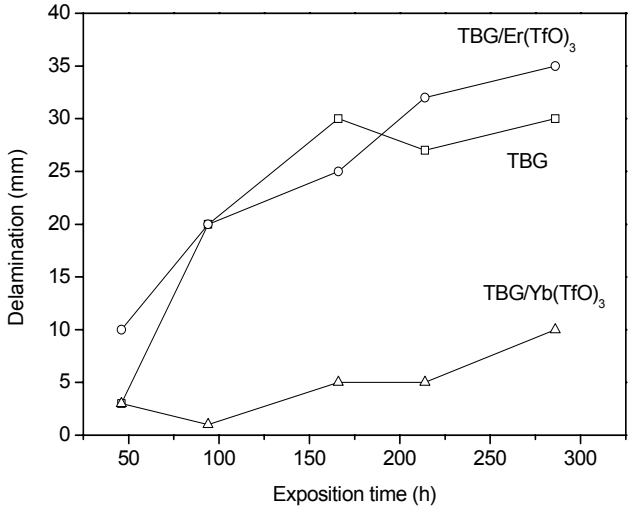

Fig. 8. Evolution of delamination with time of exposure of the different clearcoats, epoxy resin/TBG (□), epoxy resin/TBG/Er(TfO)$_3$ 1phr (O), and epoxy resin/TBG/Yb(TfO)$_3$ 1phr (Δ).

3.3. Electrochemical Impedance Spectroscopy

Figure 9 shows a Bode plot (impedance modulus versus frequency) for 300 days' exposure of the three studied samples. The EIS test gives an idea of the processes taking place at the coating (high frequencies) and also those taking place at the interface (low frequencies). Nevertheless, for samples with low porosity this technique can require long times to offer good results because it is necessary that the electrolyte, and the different species present in the solution, pass through the coating and reach the interface to make the corrosion processes to occur. If the impedance is observed, it can be concluded that the sample with Ytterbium offers the best results, while TBG and TBG/Er(TfO)$_3$ are very similar.

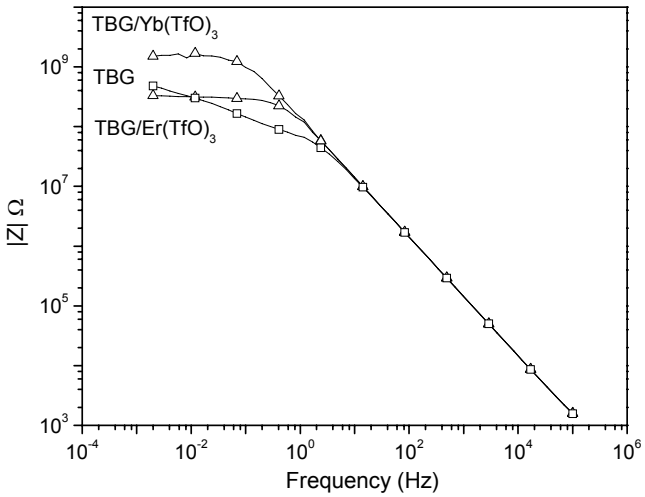

Fig. 9. Bode plot (impedance modulus versus frequency) for different clearcoats: epoxy resin/TBG (□), epoxy resin/TBG/Er(TfO)$_3$ 1phr (O), and epoxy resin/TBG/Yb(TfO)$_3$ 1phr (Δ) applied on metal substrates after 300 days' exposure to electrolyte (deionised water with 3.5% NaCl by weight). EIS test.

Results from EIS test have been modelized with an electric equivalent circuit (figure 1) and its characteristic parameters determined. The evolution with time of the different parameters gave information about the anticorrosive coating properties and its evolution.

Figures 10a, 10b and 10c show the evolution of the pore resistance R_{po}, polarization resistance R_p, and double layer capacitance C_{dl} respectively.

Results of coating capacitance C_c are not presented because they present slight differences between samples and almost constant values along the exposure time interval of approximately $7 \cdot 10^{-11}$ $s^n/\Omega cm^2$.

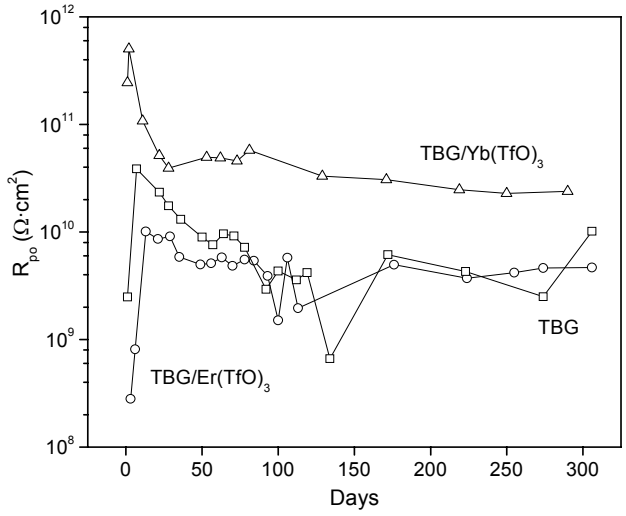

Fig. 10a. Evolution of pore resistance, R_{po}, versus time of exposure to electrolyte (deionised water with 3.5% NaCl by weight) for different clearcoats applied on metal substrates: epoxy resin/TBG (□), epoxy resin/TBG/Er(TfO)$_3$ 1phr (O), and epoxy resin/TBG/Yb(TfO)$_3$ 1phr (Δ). EIS test.

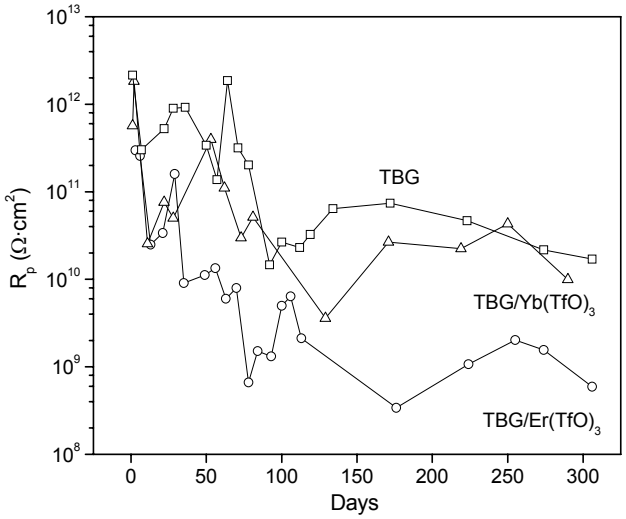

Fig. 10b. Evolution of polarization resistance, R_p, versus time of exposure to electrolyte (deionised water with 3.5% NaCl by weight) for different clearcoats applied on metal substrates: epoxy resin/TBG (□), epoxy resin/TBG/Er(TfO)$_3$ 1phr (O), and epoxy resin/TBG/Yb(TfO)$_3$ 1phr (Δ). EIS test.

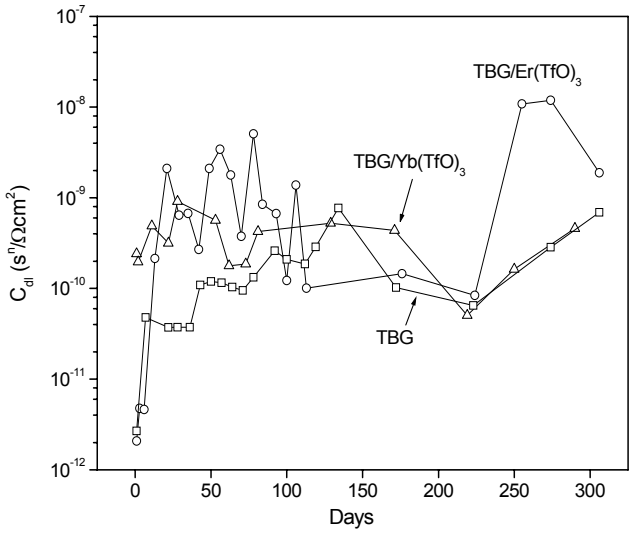

Fig. 10c. Evolution of double layer capacitance, C_{dl}, versus time of exposure to electrolyte (deionised water with 3.5% NaCl by weight) for different clearcoats applied on metal substrates: epoxy resin/TBG (□), epoxy resin/TBG/$Er(TfO)_3$ 1phr (O), and epoxy resin/TBG/$Yb(TfO)_3$ 1phr (Δ). EIS test.

It could be stated with EIS results that the best system from the point of view of the anticorrosive properties will be that one using TBG catalyzed with $Yb(TfO)_3$ which presents the higher resistance to pore formation (higher R_{po}), the most stable interface (higher R_p), and little delamination (low C_{dl}).

Worse results were found for samples cured with TBG and TBG/$Er(TfO)_3$ showing the latter the maximum activity in the interface (minimum R_p) and bigger trend to delamination (higher C_{dl}).

3.4. AC/DC/AC test

Figure 11 shows the Bode plot (impedance versus frequency) for the three tested samples after the 5th polarization in AC/DC/AC test. It can be seen that the system TBG/$Er(TfO)_3$ shows the worst properties, and how the samples TBG and TBG/$Yb(TfO)_3$ do not present big differences between them (although TBG system is slightly better).

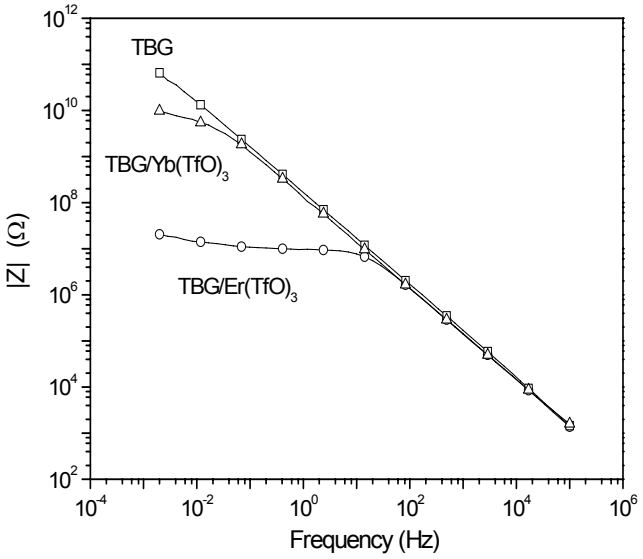

Fig. 11. Bode plot (impedance modulus versus frequency) for different clearcoats applied on metal substrates after 5 cathodic polarisations: epoxy resin/TBG (□), epoxy resin/TBG/Er(TfO)$_3$ 1phr (○), and epoxy resin/TBG/Yb(TfO)$_3$ 1phr (Δ). AC/DC/AC test.

In order to have a general idea of the evolution of the systems with the polarizations, the modelization of the data can be done, and the characteristic parameters obtained (figures 12a, 12b and 12c).

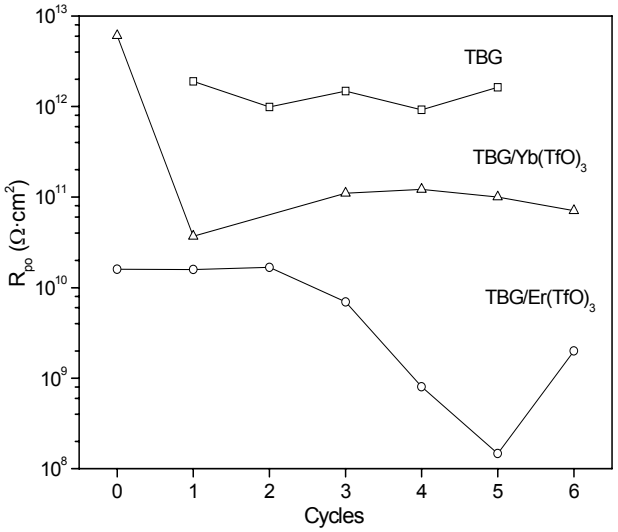

Fig. 12a. Evolution of pore resistance, R_{po}, versus cathodic polarizations for different clearcoats applied on metal substrates: epoxy resin/TBG (□), epoxy resin/TBG/Er(TfO)$_3$ 1phr (○), and epoxy resin/TBG/Yb(TfO)$_3$ 1phr (Δ). AC/DC/AC test.

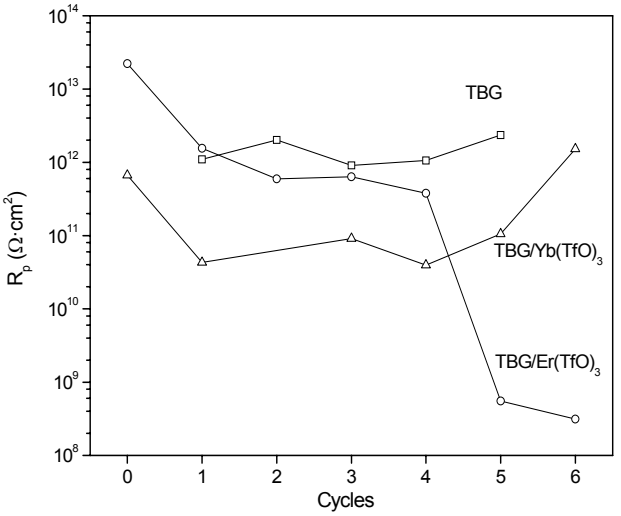

Fig. 12b. Evolution of polarization resistance, R_p, versus cathodic polarizations for different clearcoats applied on metal substrates: epoxy resin/TBG (□), epoxy resin/TBG/Er(TfO)$_3$ 1phr (○), and epoxy resin/TBG/Yb(TfO)$_3$ 1phr (Δ). AC/DC/AC test.

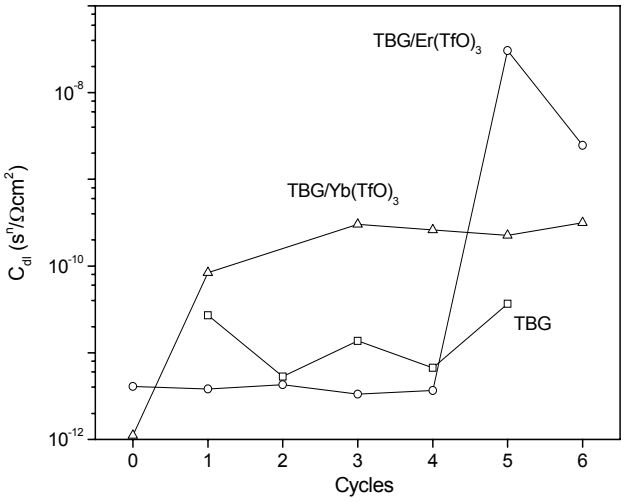

Fig. 12c. Evolution of double layer capacitance, C_{dl}, versus cathodic polarizations for different clearcoats applied on metal substrates: epoxy resin/TBG (□), epoxy resin/TBG/Er(TfO)$_3$ 1phr (○), and epoxy resin/TBG/Yb(TfO)$_3$ 1phr (Δ). AC/DC/AC test.

In this kind of test the different species are forced to pass through the coating degrading it, and at the same time, the reaction of H_2 production is forced if the electrolyte reaches the metallic surface. The effect of the polarizations on the systems depends on the pores and microcracking of the coating, and at the same time on the local delaminations (figure 3). The coating using TBG/Er(TfO)$_3$ had initially good R_{po} and R_p (figures 12a and 12b respectively), but with the number of polarizations (cycles) these resistances felt down. This effect is probably produced by the low adhesion of the coating to the substrate (see data after the 5th polarization) and possible local delamination due to the fast curing kinetics of the system. Systems with Yb(TfO)$_3$ and TBG present high resistances and low capacitances even when the number of cycles (polarizations) increase. High anticorrosion performance of TBG system can be due to its high

adherence to the substrate, while for the system with $Yb(TfO)_3$ it can be due to low porosity and possible low microcracking due to a little bit lower curing speed compared to the sample using erbium triflate.

Figure 13 clearly shows the relaxation potential after the 5th polarization. It can be seen two relaxations in the samples with catalysts. The first relaxation (low times) indicates that the H_2 production reaction has taken place, while the second one indicates the exit of ions and reordering of the double layer at the interface. With this graphic a classification can also be done, being the sample with erbium the worst and the sample without catalyst the best one (higher potential).

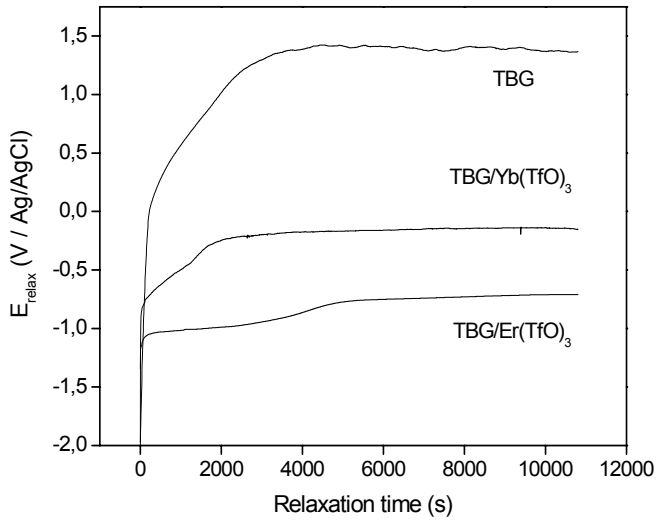

Fig. 13. Evolution of the open circuit potential (E_{OC}) versus relaxation time after exposure to 5 cathodic polarisations (AC/DC/AC test) for different clearcoats, epoxy resin/TBG, epoxy resin/TBG/$Er(TfO)_3$ 1phr, and epoxy resin/TBG/$Yb(TfO)_3$ 1phr, applied on metal substrates.

4. Conclusions

Erbium and ytterbium triflates showed its viability as catalysts for a system epoxy/TBG, reducing the curing time and/or temperature. Nevertheless, less adhesion was afforded for catalyzed systems, probably due to the decrease of the number of hydroxyl groups and higher shrinkage produced by the curing mechanism.

The EIS test gave the same results as the salt fog spray about the anticorrosion performance of the different systems, while the AC/DC/AC showed better results for TBG than the other techniques.

Acknowledgments

Authors would like to thank Ms Eva Romero, Ms Àngels Serra, Mr Carlos Bonet and Ms Maite Rodríguez for their help in the development of this project. Authors are also grateful for the economic support in this work of CICYT MAT 2000-0123-P4-03.

1. G. Bierwagen, D. Tallman, J.P. Li, L.Y. He, C. Jeffcoate, *Prog. Org. Coat.,* 46 (2) (2003) 148
2. G. Adrian, A. Bittner, *J. Coat. Tech.*, 58 (740) (1986) 59
3. F. Deflorian, V.B. Miskovic-Stankovic, P.L. Bonora, L. Fedrizzi*, Corros. Sci.*, 50 (1994) 438

4. L.S. Hernández, G. García, C. López, B. del Amo, R. Romagnoli*, Surf. Coat. Intern.*, 1 (1998) 19
5. I. Sekine, *Prog. Org. Coat.*, 31 (1997) 73
6. J. Hollaender, C.A. Schiller, W. Strunz, *Food additives and contaminants,* 14 (6-7) (1999) 617
7. M.T. Rodriguez, J.J. Gracenea, J.J. Saura, J.J. Suay, *Prog. Org. Coat.,* 50 (2004) 68
8. J.J. Suay, M.T. Rodriguez, K.A. Razzaq, J.J. Carpio, J.J. Saura, *Prog. Org. Coat.,* 46 (2003) 121
9. M.T. Rodriguez, J.J. Gracenea, S.J. García, J.J. Saura, J.J. Suay, *Prog. Org. Coat.,* 50 (2004) 123
10. S.J. García, M. Rodríguez, R. Izquierdo, F. Romero, J. Suay, "Validity of an electrochemical accelerated technique (ac/dc/ac) for rapid assessment of automotive primers", *Corr. Sci.,* (2006), in press
11. S.J. García, M.T. Rodríguez, R. Izquierdo, J. Suay, "Evaluation of cure temperature effects in cataphoretic automotive primers by electrochemical techniques", *Corr. Sci.,* (2006), in press
12. S.S. Lee, H.Z.Y. Han, J.G. Hilborn, J.-A.E. Manson, *Prog. Org. Coat.*, 36 (1999) 79
13. U.S. Enviromental Protection Agency Center for Environmental Research Information, "*Technical Reference Manual on Techniques for reducing or eliminating releases of toxic chemicals in metal painting*", 1995
14. R.S. Bauer, L.S. Corley, "*Epoxy Resins: Composites Technology*", Stuart M. Lee, Technomid Publishing Company. Inc., Pennsylvania 1989
15. S.J. García, A.Serra, X. Ramis, J. Suay, *J. Them. Anal. Cal.*, August (2006) online-first
16. M. Ochi, K. Mimura, H. Motobe, *J. Adhesion Sci. and Techn.,* 8 (1994) 223
17. *Annual Book of ASTM Standards*, Vol 03.02, ASTM, Philadelphia, PA, (1985)
18. F. Mansfeld, *Electrochim. Acta*, 38 (1993)
19. A. Amirudin, D. Thierry, *Prog. Org. Coat.,* 26 (1995) 1
20. G.W. Walter, *J. Electroanal. Chem.,* 118 (1981) 259
21. G.W. Walter, *Corros. Sci.,* 26 (9) (1986) 681
22. Gamry Instruments, "*Electrochemical Impedance Spectroscopy Primer*"
23. N. Tang, W.J. Ooij, G. Górecki, *Prog. Org. Coat.,* 30 (1997) 255
24. H. Leidheiser, *J. Adhesion Sci. Tech.,* 1 (1987) 79
25. P. Castell, M. Galià, A. Serra, J.M. Salla, X. Ramis, *Polymer,* 41 (2000) 8465
26. C. Mas, A. Serra, A. Mantecón, J.M. Salla, X. Ramis, *Macromol. Chem. Phys.,* 202 (2001) 2554

5.5. MEJORA DE PRODUCTO: SISTEMA EPOXI / ÁCIDO DE MELDRUM / $Er(TfO)_3$

Del análisis general de los anteriores capítulos se pude extraer como conclusión parcial que el empleo de ácidos de Lewis fuertes como los triflatos de lantánido acelera en gran medida el proceso de curado, obteniendo así recubrimientos capaces de alcanzar curado total a 110-130ºC en cortos periodos de tiempo. Sin embargo, el principal inconveniente que presentan los sistemas formulados es su falta de adherencia.

De los apartados anteriores se puede sacar como conclusión que existe una proporción óptima de triflato de lantánido a incluir en un sistema epoxi. El valor que se consideró más adecuado de las tres formulaciones fue empleando 1phr de triflato de lantánido como iniciador en los sistemas homopolimerizados.

A pesar de los resultados aceptables de estos sistemas homopolimerizados, se consideró que podrían ser mejorados con la introducción de más componentes. De esta forma partiendo del sistema que presentó mejor adherencia y propiedades anticorrosivas aceptables (sistemas con 0.5phr de triflato) se reformuló la mezcla.

Así, en este último apartado del capítulo de Resultados y Discusión se presenta un recubrimiento con una formulación que mejora propiedades (térmicas, cinéticas, mecánicas y anticorrosivas) en comparación con los recubrimientos homopolimerizados con triflatos de lantánido o sistemas tradicionales catalizados con los mismos triflatos.

El capítulo está estructurado en dos artículos en los que se muestra el estudio cinético, térmico y mecánico por una parte, y el estudio anticorrosivo por otra.

La nueva formulación muestra el ácido de Meldrum como una solución a los problemas de falta de adherencia y falta de plasticidad. A su vez, la introducción de este componente acelera enormemente el proceso de curado obteniendo de esta forma recubrimientos capaces de alcanzar curado total a 110ºC en 20-25 minutos.

New powder coatings with low curing temperature and enhanced mechanical properties obtained from DGEBA epoxy resins and Meldrum acid using erbium triflate as curing agent

S. J. García[1,3], A. Serra[2] & J. Suay[3]

[1] Àrea de Ciència dels Materials i Enginyeria Metal·lúrgica, Departamento de Ingeniería de Sistemas Industriales y Diseño, Universitat Jaume I, Avda. Vicent Sos Baynat s/n, 12071 Castelló, Spain

[2] Departament de Q. Analítica i Q. Orgànica. Facultat de Química. Universitat Rovira i Virgili. C/Marcel·lí Domingo s/n. 43007 Tarragona, Spain

[3] Centro de Biomateriales, Universitat Politècnica de València, Camino de Vera s/n, E-46071 Valencia, Spain

XXXXXXXXXXXXXXXX

Pendiente de envío (2006)

Abstract

New low curing temperature powder coatings obtained by copolymerization of epoxy resins with Meldrum acid initiated by erbium (III) trifluoromethanesulfonate have been formulated. Their mechanical and thermomechanical properties have been studied and compared with a commonly used industrial system (o-tolylbiguanide/epoxy resin) and with an already formulated epoxy powder coating homopolymerized by erbium trifluoromethanesulfonate. Systems containing low proportions of Meldrum acid and initiated by erbium trifluoromethanesulfonate lead to a great reduction of curing conditions (temperature/time). Moreover, the new formulated systems present very good mechanical properties, adhesion and impact resistance.

Keywords: Meldrum acid, epoxy, lanthanide triflate, thermal properties, mechanical properties

1. Introduction

The polymerization of epoxy monomers by Lewis acids follows a ring-opening mechanism, which is based on the strain of the oxirane group and the Lewis basic character of the oxygen, which can interact with cationic curing agents [1]. The networks formed have a polyether structure.

Cationic polymerization of epoxides is often carried out using conventional Lewis acids [2-4], such as BF_3 complexes. However, they have to be used under controlled humidity conditions because Lewis acids decompose in water. The first report on lanthanide triflates, which are water-compatible Lewis acids, in synthetic organic applications appeared in 1991 [5]. They are stable in water, act as Lewis acids in catalytic processes, and can also be recovered [6]. Thus, lanthanide triflates are regarded as environmentally friendly catalysts [7]. The strong electron-withdrawing capacity of the trifluoromethanesulfonate anion enhances the Lewis acid character of the initiator and its stability can help to reduce the termination processes in ring-opening polymerization mechanisms.

In many industrial applications such as industrial coatings, thermal and mechanical properties of the epoxy systems determine the quality of the final product. Moreover, in thermosetting coatings, the curing at lower temperatures and/or shorter times and the strong adhesion to the metallic substrates are the main objectives to obtain good products to be used in the industry with energy saving.

It has been reported that volume shrinkage during curing leads to poor adhesion to the substrate, warping, delamination and the apparition of microvoids and microcraks, which reduce the durability of the paint [8], thus, coatings obtained without shrinkage can be expected to have enhanced mechanical properties and longer service lives. Nevertheless, the main difficulty on developing new coatings is to combine a fast curing with no shrinkage and maintaining their good mechanical properties.

In previous studies we proposed the use of lanthanide triflates as initiators, thus promoting the homopolymerization of the resin [9, 10], as well as their use as catalysts for conventional powder epoxy resins [11]. Moreover, copolymerization of epoxy resins with other cyclic monomers as lactones could reduce the shrinkage, and improve the mechanical properties [12].

Bailey and co-workers [13, 14] introduced the term “expanding monomers”, which refers to monomers that lead to zero shrinkage or even positive expansion during polymerization. These monomers are generally bicyclics that open with the conversion of covalent bonds to Van der Waals distances. The three principal requirements of expandable bicyclic monomers are that (1) they must have at least one common atom, which must, therefore, be fused or spiranic; (2) each ring must contain at least one heteroatom; and (3) the rings must not open symmetrically. Of the bicyclic compounds that fulfil these requirements, spiroorthoesters (SOEs) are some of the most commonly used. SOEs are quite stable under alkaline conditions but undergo, in the presence of a Lewis acid initiator (such as lanthanide triflates), cationic ring-opening polymerization, which is the most suitable mechanism of polymerization for reducing shrinkage [15].

Despite of the polymerization of SOEs, which leads to thermosetting materials with no volume change [16], their synthesizing cost is very high and then they can not be used directly. As SOEs can be obtained “in situ” when reacting lactones and epoxides [17], it has been proposed the formation of epoxy

networks by copolymerization of lactones with epoxy resins which can form an intermediate SOE. As SOEs polymerize at the end of the curing process they can reduce the shrinkage after gelation [15]. It should be mentioned, that the internal stress is mainly originated after gelation, when the material has no mobility.

To form and open an intermediate SOE compound, Lewis acids are needed and, therefore the use of lanthanide triflates has been proposed to copolymerize these monomers [15]. The reaction epoxy resin-lactone is very fast when catalyzed by lanthanide triflates, leading to an increase of the curing rate when more catalyst is added [15, 18].

One option of relatively low cost lactone is the Meldrum acid (MA). This compound in presence of a lanthanide triflate should react quickly with the oxirane group of the epoxy resin giving as a result a SOE.

Until now no epoxy systems copolymerized by Meldrum acid have been reported in the literature, neither from its mechanical, kinetic or thermal point of view nor from its anticorrosive properties. In this work we present the big advantages that these systems have with respect to their mechanical properties combined to a very fast curing (thus improving the quality of the film and reducing curing costs). In addition, to prove the quality of the new systems, we compare the results to those obtained for a homopolymerized system with erbium triflate and another conventional epoxy formulation cured with o-tolybiguanide (TBG) very used in the coating's industry.

2. Experimental

2.1. Materials

Four different formulations (see table 1) were prepared using a solid bisphenol-A based epoxy resin of medium molecular weight (scheme 1), 733 gr/eq. ep. (Araldite GT 7004 from Huntsman). A first system, used as the reference one, was the epoxy resin polymerized in the ratio given by the producer with a Huntsman o-tolylbiguanide (TBG), with an H^+ active equivalent weight of 37g/eq. A second system was homopolymerized with 0.5 phr (parts of initiator per hundred of resin, w/w) of Erbium (III) trifluoromethanesulfonate from Aldrich. Other two samples containing Meldrum acid (from Aldrich) in two different proportions (3.3 and 5 phr) were cross-linked using erbium triflate as initiator.

Table1. Composition of studied samples

Sample	Epoxy resin	TBG (phr*)	$Er(TfO)_3$ (phr*)	Meldrum Acid (phr*)	Benzoine (phr*)	Flux Agent (phr*)
TBG	100	4.8	-	-	0.18	1.27
ErTfO 0.5phr	100	-	0.5	-	0.18	1.27
M.A.1	100	-	0.5	3.3	0.18	1.27
M.A.2	100	-	0.5	5	0.18	1.27

*phr = parts per hundred resin (w/w)

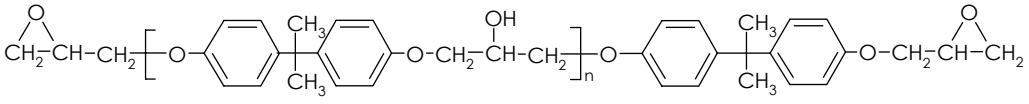

Scheme 1. DGEBA resin

Samples were pre-mixed and hand-shacked until good dispersion was afforded. After that, the material was extruded in a single screw extruder (Haake Rheomex 254), where operating conditions were 80 ºC along the extruder and 60rpm. After extruding, the material was grinded in an ultra-centrifugal mill ZM 100 and sieved at 100 micron, obtaining the different powder coatings ready to be applied on steel substrates or cured as free films for mechanical studies.

In order to study the impact resistance of the systems it was necessary to add to the mixture benzoine to avoid porosity (0.18 phr) and flux agent to allow the application by corona spray (1.27 phr). Clearcoats were then applied on cold-rolled low-carbon steel normalized tests panels (15 x 7.5 x 0.1 cm). All test panels were degreased with acetone, and paints were deposited by means of a corona electrostatic powder gun (powder coating equipment Easy 1-C). The clearcoats were totally cured for 15 minutes at 150ºC in an oven (25 minutes for the sample using TBG, reaching total cure). Curing conditions were established after the kinetic study and to fix a general condition. Thicknesses determined by an Elcometer were always within the range 60±5 µm.

For the mechanical tests, epoxy systems were deposited manually on a polypropylene substrate and cured in an oven at 150ºC for one hour assuring that the samples reach the total cure. After the curing, the systems were peeled off the substrate and tested.

2.2. Testing Methods and Equipment

2.2.1. Thermal characterization

A Perkin Elmer DSC 7 differential scanning calorimeter was employed for dynamic scans in order to study the non isothermal curing process and apply results to isothermal curing. The samples were analyzed in covered aluminium pans, using high purity indium sample for calibration. A flow of 20 $cm^3 \cdot min^{-1}$ of argon was used as purge gas. The weight of the samples was between 8 and 9 mg. Non-isothermal scans were performed at rates of 2.5, 5, 10 and 15 $K \cdot min^{-1}$ to not-cured-samples of the four prepared epoxy systems. The scans were done at the range of temperature from 25 to 300ºC.

Isoconversional STARe software from Mettler-Toledo was used in order to calculate conversion degrees and kinetics of the processes.

Differential scanning calorimeter was also used to find the vitreous transition temperature (T_g) of the different cured samples. Scans at a rate of 10ºC/min in the range of 25-250ºC were performed under the same conditions of the kinetic study using cured samples of 8 mg weight.

2.2.2. Dynamic-mechanical thermal analysis (DMTA)

A dynamic mechanical Analyzer Seiko DMS210U was employed to perform mechanical measurements from 25ºC to 220ºC at 1ºC/min and a constant frequency of 1Hz in three point bending mode.

From the theory of rubber elasticity [19] and using the rubber modulus of the material (E'_{rubber}) obtained from the DMTA analysis (E' at T_g+50ºC), it can be calculated the average molecular weight between cross-links ($\overline{M_c}$) by applying the simplified equation:

$$\overline{M}_c = \frac{3\nu\rho RT}{E'} \quad (1)$$

where ν is the front factor (ν =1, in this work), ρ is the density of the sample, T is the temperature in Kelvin ($T=T_g+50ºC$) and R the universal gas constant.

The apparent density of the samples was calculated by an apparatus of density measurement coupled to a weight balance and using equation 2.

$$\rho_{ap} = \frac{m_{air}}{m_{air} - m_{liq}}(\rho_0 - \rho_L) + \rho_L \quad (2)$$

where, ρ_0 is the liquid density (distilled water), ρ_L is the air density ($0.0012 g/cm^3$), m_{air} is the weight of the sample in air, and m_{liq} is the weight of the sample immersed in the liquid.

2.2.3. Morphology study-SEM

The morphology of the samples was studied with a scanning electron microscopy (SEM). Samples were frozen with liquid N_2 and hand broken. The measurements were carried out on a Jeol-JSM 6300 at 10kV.

2.2.4. Mechanical tests (Stress–strain curves)

Tensile testing up to failure was performed with an Adamel-Lomargy DY34 using a fixed crosshead rate of 10mm/min with a 1kN cell. Five cured samples of each formulation were standardly cut and tested so results were an average of five tests. Traction tests were performed according to ASTM D1708-96 and D638. Young's modulus was calculated in the region of deformation over 0.5%.

2.2.5. Impact resistance test

Samples were deposited and cured on steel substrates. A 1kg dart-mass was impacted at the back of each sample at different highs up to 1 meter. The effect of the impact was visually evaluated and compared.

2.2.6. Adhesion Test

Adhesion test was performed in accordance to ISO 4587 (1979). It consists on the deposition of the epoxy system (with benzoine and flux agent) between two rectangular and cleaned steel substrates, giving rise to a glued area of 13x25mm (figure 1). When the epoxy is deposited, the two rectangular substrates are fixed by means of two pincers and cured for 150ºC one hour. After the curing process and three days of ambient exposure, the samples were tested with an Instron Universal Test Machine 4469-H1907 at a traction speed of 1mm/min. The data of tension and deformation were registered. With the break force (F) and the glued area, the shear stress is obtained (σ_{shear} (MPa) = F/area), giving the adhesion of the clearcoats to the substrates. Almost all the specimens showed an adhesive failure type. Five probes of each sample were prepared and tested.

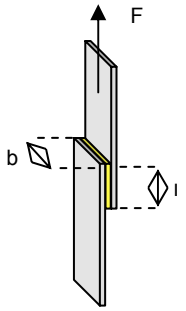

$\sigma_{shear} = F/b \cdot l$

Fig. 1. Scheme of an adhesion test. σ_{shear} calculus.

3. Results and Discussion

3.1. Reactive processes

The reaction of epoxides with Meldrum acid in the presence of Lewis acids takes place by the formation of a SOE intermediate (scheme 2).

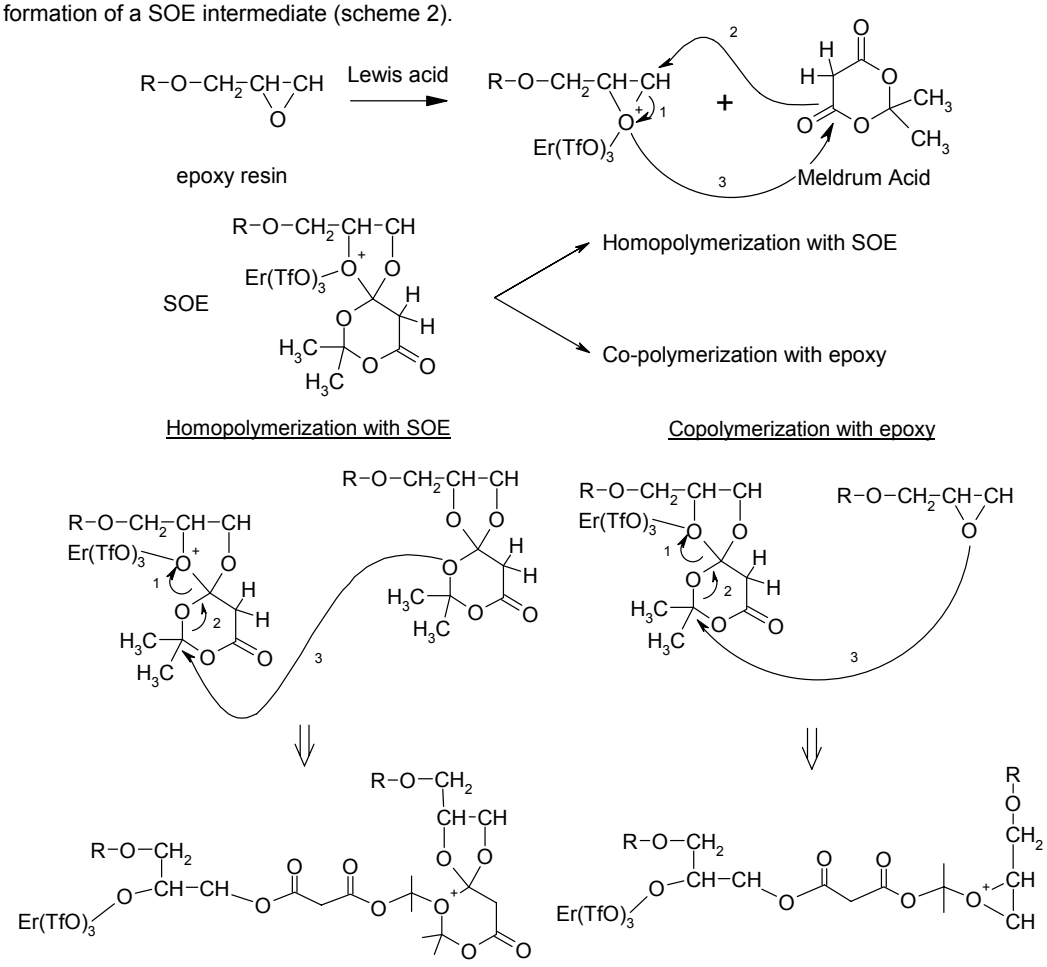

Scheme 2. Chemical processes which occurs in the co-polymerization of DGEBA epoxy resin with Meldrum acid in the presence of erbium triflate

The formed SOE can homopolymerize or copolymerize with epoxides leading to poly(ether-ester) structures. Moreover, epoxides can homopolymerize as well giving poly(ether) chains. Once some SOE is formed, all the chemical processes occur simultaneously, but SOE tends to homopolymerize at the end of the curing process [15]. Thus, the formation of SOE from epoxides and lactones occurs with a high shrinkage and its homo and copolymerization leads to an expansion which partially compensates the shrinkage on curing. Thus, the shrinkage is higher in the initial steps of the reaction and is reduced in the last steps when the internal stress is originated. It should be said that, in this system, DGEBA and Meldrum acid have a functionality of four and two respectively. Thus the addition of MA leads to a more expanded network than the homopolymerization of DGEBA alone and increases the distance between cross-links. This fact, should improve the mechanical properties of the thermosetting material.

In contrast, when the curing mixture is formed by equimolecular proportions of DGEBA resin and o-tolylbiguanide (TBG) the following chemical process occurs [20].

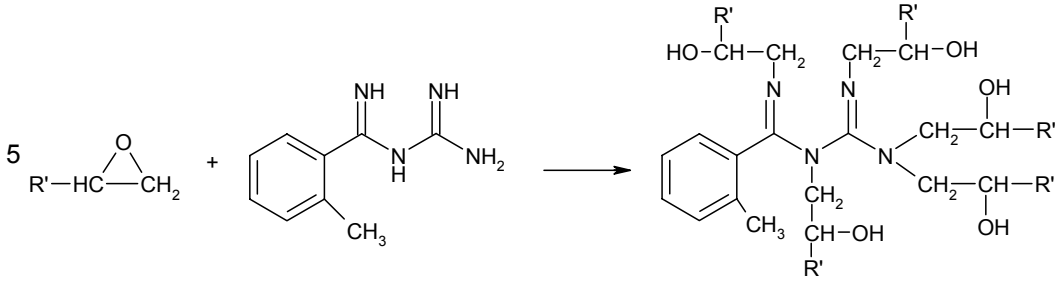

Scheme 3. Reaction between o-tolylbiguanide and oxirane groups

This reaction follows a typical condensation mechanism of nucleophilic attack of the nitrogen to the oxirane group. In this reactive system the DGEBA acts as a bifunctional monomer and TBG as a pentafunctional cross-linking agent. This kind of reaction gives as a result some shrinkage in the material, nevertheless at the same time, a big number of hydroxide groups are formed which can promote the adhesion to the metallic substrate [21]. Thus, the conventional TBG epoxy coatings and the erbium triflate initiated copolymerization leads to structurally very different materials that should have different mechanical and adhesion characteristics.

3.2. Thermal properties

In order to study the kinetics of these systems, four DSC experiments were performed from 25 to 300ºC at different heating rates for each sample. With those scans and the use of the STARe software from Mettler-Toledo it can be obtained the curing enthalpies (table 2) [9-11], the activation energy and the conversion as a function of the temperature. Using the isoconversional method of the software it can be plotted graphics of conversion in function of temperature and time.

Table 2. Table of general properties of the cured samples

Sample	ΔH_{cur} (kJ/eq ep)	T_g (ºC)	T_α (ºC)	E'_{rubber} (Pa)	ρ_{ap} (g/cm^3)	$\overline{M_c}$
TBG	65	95	109	4,46E6	1.1048	2998.5
ErTfO 0.5	76	109	121	1,43E7	1.1437	819.2
MA1	71	92	114	1,20E7	1.1106	913.9
MA2	67	83	112	9,87E6	1.1113	1101.2

Figure 2 represents for a given conversion (in this case α=0.98) the curing time versus the curing temperature for all the samples. Thus, a comparative idea of the curing kinetics can be obtained. It can be seen that the addition of Meldrum Acid to the system catalyzed by erbium triflate leads to a very high reduction of the curing conditions (time/temperature). At the curing temperature of 120ºC the reduction of time is about 80% with respect to the conventional reference system (TBG with resin), and around 60% with respect to a homopolymerized system ($Er(TfO)_3$ with resin). This shows that from the point of view of the kinetics, an epoxy system containing Meldrum acid and catalyzed by 0.5phr of erbium triflate represents a very good alternative to conventional epoxy systems used to produce powder coatings, being a possible solution for the coating application to thermosensible substrates, because of the possibility of curing at quite low temperatures.

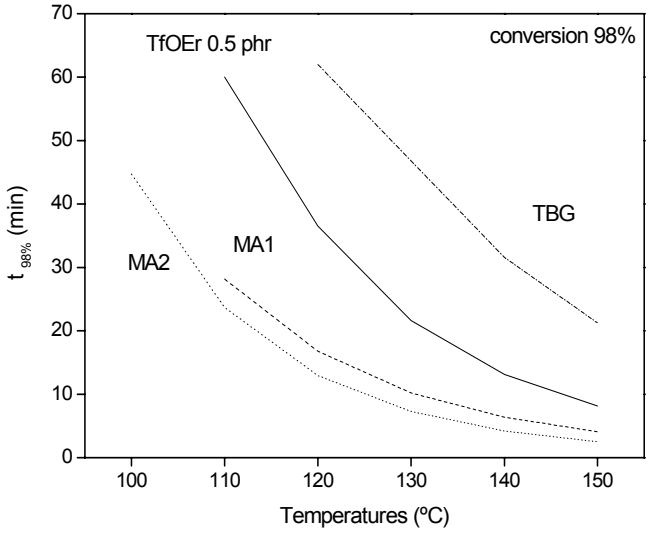

Fig. 2. Time-Temperature plot for a 98% conversion of the four different clearcoats: epoxy resin/erbium triflate 0.5phr (—), epoxy resin/erbium triflate 0.5phr/Meldrum acid 3.3phr (---), epoxy resin/erbium triflate 0.5phr/Meldrum acid 5phr (···), and epoxy resin/TBG (-·-).

One possible explanation to the acceleration observed by the addition of Meldrum acid can be found in the acid characteristics of these monomers. It has been reported that Lewis acids, such as BF_3 needed a co-catalyst such as water (which acts as proton donor) and that the rate of polymerization was proportional to the amount of water added [1, 22]. This can be true also in our case, because the higher the proportion of Meldrum acid in the reactive mixture the higher the curing rate. However, it has been demonstrated that the presence of a lactone in an epoxide-lanthanide triflate curing system is

accelerated by the formation of a more reactive initiating specie in which the lactone coordinates to the initiator [15], but this point has not been experimentally demonstrated in the present case.

In table 2 the different values of T_g are collected. The use of Meldrum acid gives rise to lower T_g values than homopolymerizing the system with erbium triflate, due to the inclusion of the Meldrum acid on the network giving as a result longer chains between crosslinks, and increasing in this way the mobility of the network. The Meldrum acid has a plasticizing effect on the system.

3.3. Morphological study

Figure 3 shows the SEM-pictures of the four systems at 75 magnifications. The lowest porosity is obtained for a sample cured with TBG and that one cured with $Er(TfO)_3$ at 0.5phr. When Meldrum acid is added to a system homopolymerized with erbium triflate there is an increase in porosity, being higher when more MA is added. This increase is probably due to the fact that the higher the reaction rate the higher the increase of viscosity with time and the higher the probability of occluding air in the material. It should be said, that the porosity observed by SEM make the measurement of densities only approximated.

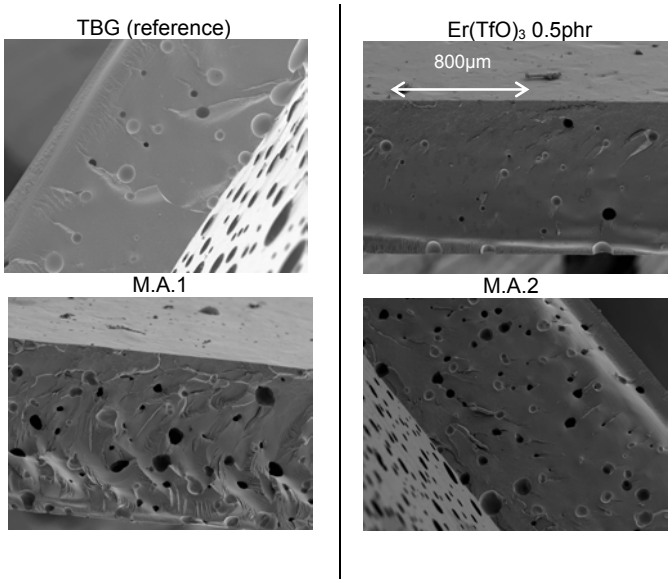

Fig. 3. SEM pictures at 75 magnifications.

3.4. Mechanical Properties

3.4.1. Shrinkage

In previous papers presented, we studied the evolution of the contraction during the curing by thermomechanical analysis [12, 15]. By this procedure it was observed that the addition of lactones to a cationic cured epoxy system lead to a significant reduction of the shrinkage after gelation, and the same conclusion could be extrapolated to this study. In the previous studies the samples were viscous liquids, very different to the powder coatings used in the present study, and this difference in the state of the

materials implied an experimental handicap which avoided us to perform the realization of the shrinkage measurements for powder coatings.

With respect to the global contraction of the materials during curing, shrinkage could be calculated from the determination of the densities of the materials before and after curing. However, the porosity which appears in the materials containing MA prevents the determination of a reliable shrinkage. It should be said, that the bubbles in the material are caused by the great increase in the viscosity of the sample (which entraps some air bubbles coming from the powder) and not by the change in the chemical bonding as is discussed in the introduction. Thus, the results of contraction calculated have no meaning at all.

3.4.2. DMTA

The change of the mechanical relaxation, as measured by the peak in the dynamic loss curve, and the change of the storage modulus is often used to characterize the behaviour of polymeric plasticizers and plasticized polymers [23].

Figures 4 and 5 show the loss tangent (tanδ) and the storage modulus (E') respectively versus temperature for the four different studied systems.

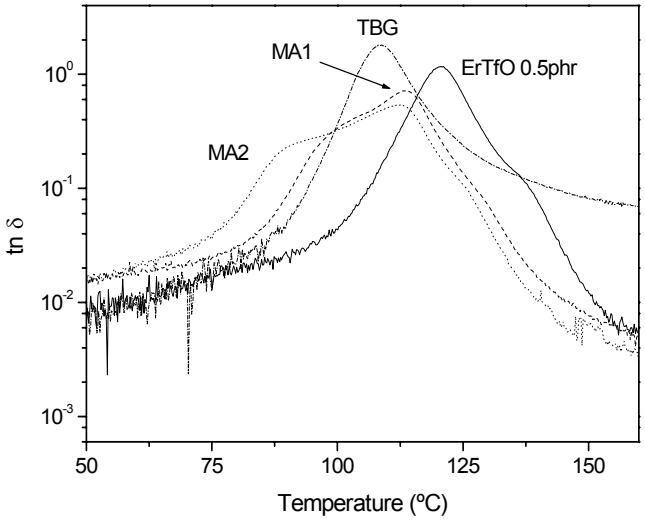

Fig. 4. Plot of the loss tangent (tanδ) versus temperature obtained by DMTA for the different studied clearcoats: epoxy resin/erbium triflate 0.5phr (—), epoxy resin/erbium triflate 0.5phr/Meldrum acid 3.3phr (---), epoxy resin/erbium triflate 0.5phr/Meldrum acid 5phr (···), and epoxy resin/TBG (-·-).

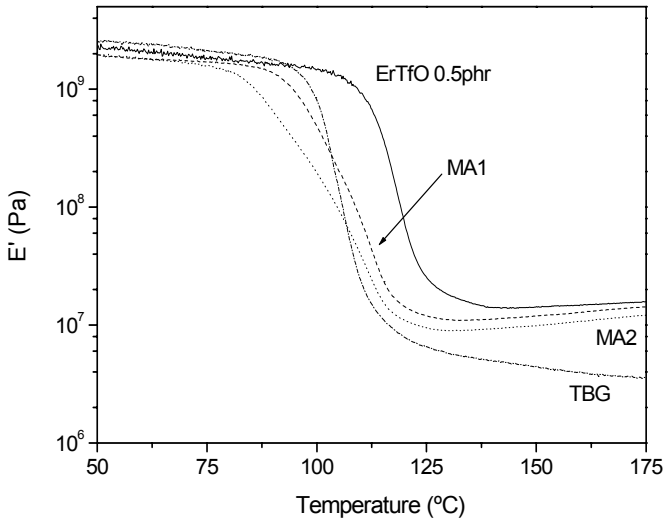

Fig. 5. Plot of the storage modulus (E') versus temperature obtained by DMTA for the different studied clearcoats: epoxy resin/erbium triflate 0.5phr (—), epoxy resin/erbium triflate 0.5phr/Meldrum acid 3.3phr (---), epoxy resin/erbium triflate 0.5phr/Meldrum acid 5phr (···), and epoxy resin/TBG (-·-).

When Meldrum acid was added to the thermosetting system the peak tanδ is broader and two relaxations appear which indicates an increase in the heterogeneity of the material, probably due to a different length of the chains between cross-links and to the formation of two different networked structures (one as a result of the homopolymerization of epoxides and another one originated by the co-polymerization of Meldrum acid with epoxides). As we can see in the figure, the higher the proportion of MA the broader is the tanδ curve. It should be considered that the formation of inhomogeneous materials depend on the reactivity of both co-monomers and on the initiator used which influences the kinetics of the elemental reactive processes represented in the Scheme 2.

As can be seen in table 2, when MA is added there is a decrease in the temperature at which the principal mechanical relaxation takes place (T_α decreases). This fact matches with those obtained by the measure of T_g with the DSC and reflects a diminution of the crosslinking density with longer chains between crosslinks with higher mobility and/or a more free volume in the network. This is translated to a less rigid system, which is the same result typically observed for the effect of plasticizers added into the system [23]. Moreover, the addition of MA diminishes the storage modulus (E'_{rubber} in table 2) which also implies that the material is less rigid which is in accordance to the results obtained with tanδ, due to the diminution of the crosslinking density.

On adding MA to the cationic systems the visco-elastic zone becomes broader and the higher the MA content the lower the temperature at which the relaxation begins (figure 4). This is related to a very different length of the chains between cross-links, caused by the co-polymerization process, which induces a higher inhomogeneous character to the material.

3.4.3. Average molecular weight between crosslinks ($\overline{M_c}$)

Apparent densities (ρ_{ap}) and values of $\overline{M}_c$ are collected in table 2. It can be observed as was expected from other studies with lactones [15] that the addition of Meldrum acid increases the average

molecular weight between cross-links. The SOE firstly formed is polymerized and introduces linear poly(ether-ester) structures between the cross-linking points, giving rise to a more opened network and more plasticized as was also observed from the T_g values and DMTA study. Despite these results, the reference system presents much more $\overline{M_c}$ than the samples with MA. This could be due to the inclusion of the aromatic ring from the TBG in the network and to the poly-condensation mechanism which is very different from the cationic one.

Figure 6 shows that there is a direct correlation between the length of the chains between cross-links and the transition temperatures T_g and T_α for the cationic thermosets. As usual, T_α values are higher than the T_g ones due to a different definition of glass transition and the experimental differences in the transition from the glassy to the rubbery states between both techniques (DSC and DMTA).

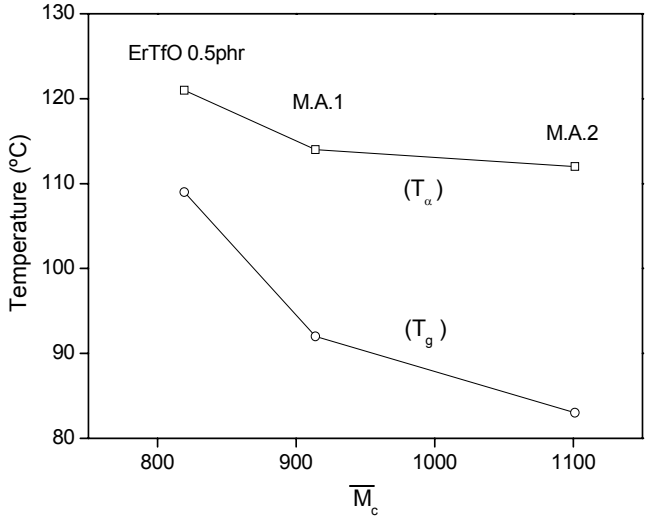

Fig. 6. Correlation between of $\overline{M_c}$ and transition temperatures (T_g and T_α) for the samples in which the Meldrum acid content is varied.

3.4.4. Stress-Strain

Figure 7 shows the stress-strain curves corresponding to the traction tests performed for the formulated coatings. Table 3 shows the parameters obtained from the mechanical tests: elastic modulus (E), elastic limit stress (σ_{el}), elastic limit strain (ε_{el}), maximum stress (σ_{max}), break stress (σ_{brk}), break strain (ε_{brk}), and toughness.

On comparing a homopolymerized system initiated by erbium triflate to those having Meldrum acid, it is observed a decrease in the break deformation (which implies lower ductility), lower toughness which implies that samples with Meldrum acid can absorb less energy before they break down, and slight decrease of the elastic modulus, that can be correlated to a decrease in the cross-linking density (higher $\overline{M_c}$).

Table 3. Mechanical properties from stress-strain tests

Sample	E (MPa)	σ_{le} (MPa)	ε_{le} (%)	σ_{max} (kN)	σ_{break} (MPa)	ε_{break} (%)	Toughness (MPa)
TBG	1881.3 ± 205.6	46.7 ± 1.49	2.36 ± 0.13	56.01 ± 1.07	49.4 ± 0.77	5.55 ± 0.28	2.32 ± 0.114
ErTfO 0.5	2328.1 ± 217.7	46.1 ± 2.82	2.40 ± 0.20	59.21 ± 0.54	57.5 ± 0.56	6.97 ± 1.26	3.35 ± 0.72
MA1	2114.2 ± 174.2	23.0 ± 1.10	0.77 ± 0.15	52.83 ± 0.26	49.6 ± 0.09	6.73 ± 0.76	2.95 ± 0.46
MA2	2219.6 ± 154.7	19.0 ± 1.00	0.42 ± 0.02	56.16 ± 0.60	52.0 ± 1.95	5.18 ± .0.19	2.36 ± 0.06

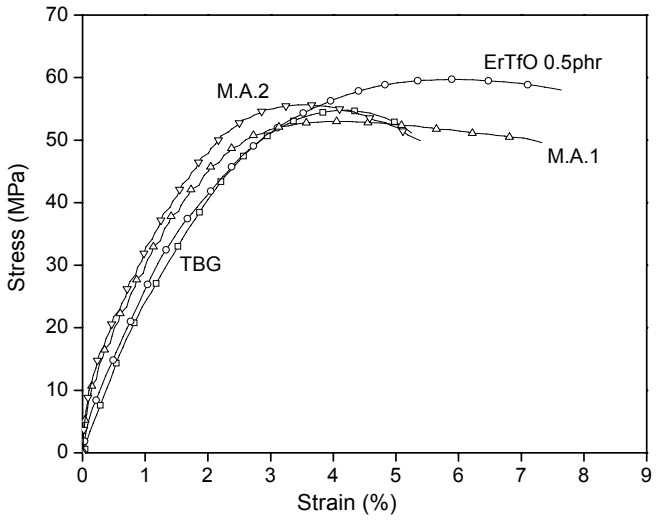

Fig. 7. Stress-strain curves of the studied clearcoats: epoxy resin/erbium triflate 0.5phr (O), epoxy resin/erbium triflate 0.5phr/Meldrum acid 3.3phr (Δ), epoxy resin/erbium triflate 0.5phr/Meldrum acid 5phr (∇), and epoxy resin/TBG (□).

Principal differences when MA was added can be found in the elastic limit with a decrease in the stress and especially in the strain. Similar results have been found with other plasticized epoxy systems [23].

3.4.5. Impact resistance

Figure 8 shows four pictures of the impacted samples at a height of 1m and with a mass of 1kg. It can be seen that the sample homopolymerized with erbium triflate shows no impact resistance (epoxy system coating breaks down due to the impact), probably due to the fact that the high shrinkage of the homopolymerized coatings gives rise to local stresses when it is applied on a steel substrate which results in a big increase in fragility.

When MA is added to that system the impact resistance is highly improved. The improvement obtained by adding MA can be attributed to its plasticizing effect in the network and/or to the less internal stress in the cured materials because the lower shrinkage produced after gelation. The reference system shows similar results to those presented by systems containing MA.

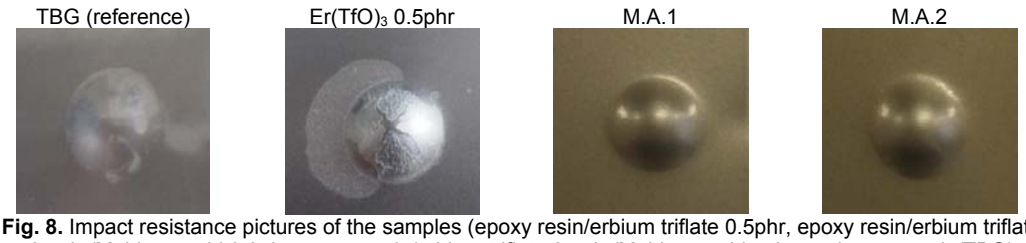

Fig. 8. Impact resistance pictures of the samples (epoxy resin/erbium triflate 0.5phr, epoxy resin/erbium triflate 0.5phr/Meldrum acid 3.3phr, epoxy resin/erbium triflate 0.5phr/Meldrum acid 5phr, and epoxy resin/TBG) applied on low carbon-steel panels tested at 1meter height with a 1kg mass dart.

3.4.6. Adhesion

Figure 9 shows the shear stress for the different samples. The system with TBG presents good adhesion (high σ_{shear}) probably due to the hydroxyl groups produced in the reaction (the higher the hydroxylic content, the higher the adhesion [24-27]) because the possibility to establish hydrogen bonds between the coating and the metal surface increases. There is a high improvement in adhesion on adding Meldrum acid to a system cured with erbium triflate. This fact could be due to the high polarity of the network and to the lower shrinkage after gelation obtained when using MA compared to the other systems, which reduces the internal stresses during curing and the formation of microcracks. Homopolymerized epoxy system presents the worst adhesion results due to the inexistence of hydroxylic groups, the less polar character of the network and the stress generated by the shrinkage in the curing process, which leads to warping.

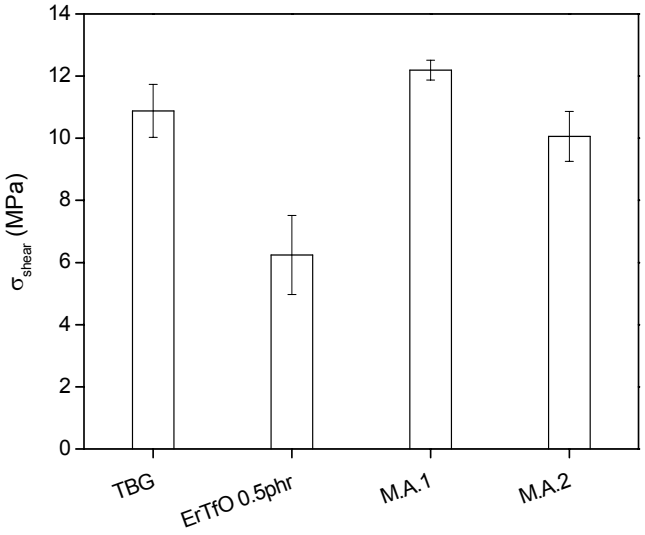

Fig. 9. Shear stress of the studied clearcoats: epoxy resin/erbium triflate 0.5phr, epoxy resin/erbium triflate 0.5phr/Meldrum acid 3.3phr, epoxy resin/erbium triflate 0.5phr/Meldrum acid 5phr, and epoxy resin/TBG.

4. Conclusions

The results obtained show that the use of erbium triflate as initiator of the homo-polymerization of DGEBA resins diminishes the curing temperature and time with respect to the reference system with

TBG but offers bad mechanical properties: low impact resistance, low adherence to the substrate, high contraction, and low mechanical properties.

In order to improve thermal and mechanical properties of homo-polymerized systems, Meldrum acid can be added to co-polymerize with the epoxy resin. The new systems containing Meldrum acid (3.3 and 5phr) are highly accelerated compared to reference systems (with TBG and only with erbium triflate), at the same time their adherence to metallic substrates, impact resistance and contraction are improved, therefore, they become a good alternative to the conventional powder coatings systems used in industry.

Acknowledgments

Authors would like to thank Ms Eva Romero and Ms Maite Rodríguez for their help in the development of this project. Authors are also grateful for the economic support in this work of CICYT (Comisión Internacional de Ciencia y Tecnología) and FEDER (Fondo Europeo de Desarrollo Regional) for the projects MAT 2000-0123-P4-03 and MAT 2005-01806.

1. J.K. Ivin, T. Saegusa, *Ring Opening Polymerization*: J.K. Ivin, T. Saegusa, Eds., Elsevier Science: New York, 1984; Vol. 1
2. S.G. Entelis, G.V. Korovina, *Makromol. Chem.,* 175 (1974) 1523
3. W. Tänzer, J.H. Wintzer, G. Müller, M. Fedtke, *Polym. Bull.,* 17 (1987) 31
4. R.O. Colclough, G.W. Gee, C.E. Higginson, J.B. Jackson, M. Litt, *J. Polym. Sci.,* 34 (1959) 171
5. S. Kobayashi, *Chem. Lett.,* (1991) 2187
6. S. Kobayashi, M. Sugiura, H. Kitagawa, W.W.-L. Lam, *Chem. Rev.,* 102 (2002) 2227
7. S. Kobayashi, Ed. Lanthanides: Chemistry and Use in Organic Synthesis; Topics in Organometallic Chemistry, Springer-Verlag: Berlin, 1999
8. *Expanding Monomers: Synthesis, Characterization and Applications*, R.K. Sadhir, M.R. Luck, Eds., CRC: Boca Raton, FL, 1992
9. S.J. García, X. Ramis, A. Serra, J. Suay, *Thermochim. Acta.,* 441 (2006) 45
10. S.J. García, X. Ramis, A. Serra, J. Suay, *J. Therm. Anal. Calorim.,* 83 (2) (2006) 429
11. S.J. García, A. Serra, X. Ramis, J. Suay, *J. Therm. Anal. Calorim.,* August (2006) Online-first
12. R. Giménez, X. Fernández-Francos, J.M. Salla, A. Serra, A. Mantecón, X. Ramis, *Polymer*, 46 (2005) 10637
13. W. J. Bailey, *J. Elastoplast.*, 5 (1973) 142
14. W.J. Bailey, R.L.-J. Sun, T. Katsuki, H. Endo, H. Iwama, R. Tsushima, K. Saigou, M. Bitritto, *Ring-Opening Polymerization,* T. Saegusa, E. Goethals, Eds., ACS Symposium Series 59, American Chemical Society: Washington, DC, 1977
15. C. Mas, X. Ramis, J.M. Salla, A. Mantecón, A. Serra, *J. Polym. Sci. Pol. Chem.*, 41 (2003) 2794
16. W. J. Bailey, *J. Macromol. Sci. Chem.*, 9 (1975) 849
17. M. Fedtke, J. Haufe, E. Kahlert, G. Müller, Angew. Makromol. Chem., 255 (1998) 53
18. C.Mas, A. Mantecón, A. Serra, X. Ramis, J.M. Salla, *J. Polym. Sci. Pol. Chem.,* 43 (2005) 2337
19. A.V. Tobolsky, D.W. Carlson, N. Indictor, *J. Polym. Sci.*, 54 (1960) 175
20. M. Ochi, K. Mimura, H. Motobe, *J. Adhesion Sci. and Techn.*, 8 (1994) 223
21. J.M. Martí-Martínez, M. Madrid-Vega, *Teoría de la adhesión, Tema 2: Propiedades de los adhesivos y los selladores antes del curado*, Loctite España
22. J.B. Rose, *J. Chem. Soc.,* (1956) 542
23. M.T. Rodríguez, S.J. García, R. Cabello, J.J. Gracenea, J.J. Suay, *J. Coat. Tech.,* 2 (7) (2005) 557
24. D. Greenfield, J.D. Scantleburry, *JCSE*, 3 (2000) paper5
25. E. Vaca-Cortés, M.A. Lorenzo, J.O. Jirsa, H.G. Wheat, R.L. Carrasquillo, *Adhesion testing of epoxy coating*, Centre for transportation research bureau of engineering research the university of Texas at Austin (1998)
26. N.I. Gaynes, *Testing of Organic Coatings*, Noyes Data Corp., Park Ridge, NJ (1977)
27. M.A. Lorenzo, *Experimental Methods for Evaluating Epoxy Coating Adhesion to Steel Reinforcement,* M.S. Thesis, The University of Texas at Austin (1997)

Anticorrosive properties of an epoxy-Meldrum acid cured system catalyzed by erbium III trifluromethanesulfonate

S. J. García[1,2] & J. Suay[2]

[1] Àrea de Ciència dels Materials i Enginyeria Metal·lúrgica, Departamento de Ingeniería de Sistemas Industriales y Diseño, Universitat Jaume I, Avda. Vicent Sos Baynat s/n, 12071 Castelló, Spain

[2] Centro de Biomateriales, Universitat Politècnica de València, Camino de Vera s/n, E-46071 Valencia, Spain

Progress in Organic Coatings

Enviado mayo de 2006. Aceptado septiembre 2006. In press

Abstract

New low curing temperature powder epoxy coatings cured with Meldrum acid and catalyzed by the use of erbium III trifluoromethanesulfonate have been formulated. Their curing kinetics and anticorrosive properties have been studied and compared with a system commonly used in industry (o-tolylbiguanide / epoxy resin), and with an epoxy powder coating homopolymerized by erbium III trifluoromethanesulfonate. Three different tests of anticorrosive properties (EIS, AC/DC/AC, and salt fog spray) have been used together with an adherence test, in order to establish the best system. Results show that systems crosslinked with Meldrum acid and catalyzed with erbium triflate present very fast curing kinetics and very good anticorrosive properties. The technique AC/DC/AC has shown its ability to evaluate properly and much faster than other techniques the anticorrosive properties of powder coatings.

Keywords: EIS, AC/DC/AC, biguanide, Meldrum acid, triflate, powder coating, salt fog spray

1. Introduction

Organic powder coatings are considered the best alternative for the reduction of volatile organic contents (VOCs) in the anticorrosive-coatings industry because they present VOC emissions lower to 4% [1, 2] while solvent-based paints present more than 60% of VOCs. Despite this big advantage, organic powder coatings present some limitations like the difficulty to be applied on thermo-sensible substrates as wood, plastic, or structural aluminium alloys (eg. aeronautic industry) due to the high temperatures used on their curing. For this reason it exists an interest on creating organic powder coating systems with low curing temperature and time together with good anticorrosive properties.

In previous studies it has been proposed the use of lanthanide triflates as initiators, thus promoting the homopolymerization of the resin [3, 4], as well as their use as catalysts for powder epoxy resins [5]. The kinetic studies showed that for epoxy systems homopolymerized using 0.5phr of erbium triflate, a total cure could be obtained at 130ºC for 25 minutes (this time and temperature being reduced when more initiator was employed). On the other hand, previous results not yet published [6, 7] showed that homopolymerized systems did not present very good anticorrosive properties probably due to the high shrinkage and low proportion of hydroxyl groups.

In thermostable coatings, shrinkage during curing (specially with fast curing kinetics) leads to poor adhesion to the substrate, delamination, microvoids and microcraks, which reduce the durability of the paint [8], thus, polymers obtained without shrinkage can be expected to have enhanced mechanical properties and longer service lives.

Bailey and coworkers [9, 10] introduced the term “expanding monomers”, which refer to monomers that lead to zero shrinkage or even positive expansion during polymerization. These monomers are generally bicyclics that open with the conversion of covalent bonds to van der Waals distances. The three principal requirements of expandable bicyclic monomers are: (1) they must have at least one common atom, which must, therefore, be fused or spiranic; (2) each ring must contain at least one heteroatom; and (3) the rings must not open symmetrically. Of the bicyclic compounds that fulfil these requirements, spiroorthoesters (SOEs) are some of the most commonly used.

SOEs are quite stable under alkaline conditions but undergo cationic ring-opening polymerization, which is the more suitable mechanism of polymerization for reducing shrinkage [11], with the presence of Lewis acid catalyst (such as lanthanide triflates).

Despite the polymerization of bifunctional SOEs leads to thermosetting materials with no volume change [12], their synthesizing cost is very high and then they can not be used directly. As SOEs can be obtained when reacting lactones and epoxides [13], it has been proposed the creation of epoxy networks by copolymerization of lactones with epoxy resins which can form an intermediate SOE, thus reducing the volume shrinkage during curing [11].

As the intermediate SOE forming reaction is slow without catalyst, the use of lanthanide triflates has been proposed to accelerate the system [11]. The reaction epoxy resin-lactone is very fast when catalyzed by lanthanide triflates, increasing the curing reaction when more catalyst is introduced [14].

One option of relatively low cost lactone is the Meldrum acid. This acid in presence of a lanthanide triflate should react quickly with the oxirane group of the epoxy resin giving as a result a SOE. From that moment on more reactions, described in the experimental section, can be expected.

Until now no organic powder coatings copolymerized by Meldrum acid with epoxy resin have been studied, neither from its mechanical, kinetic or thermal point of view nor from its anticorrosive properties. Since the point of view of anticorrosive properties it is expected that the Meldrum acid should give very good properties because of the low predicted shrinkage, which can promote better adhesion to the metallic surface and less delamination.

In order to study the anticorrosive properties of organic coatings, the most used experimental method is the so called salt fog spray. Nevertheless, this technique does not give quantitative information about the corrosion processes and an interpretation of the overall process itself. Another possibility to measure the anticorrosive properties is the use of techniques based on electrochemistry. Amongst these techniques, the most used is the electrochemical impedance spectroscopy (EIS) which has been proved to be a useful technique in the study of the corrosion performance of primers applied on metal substrates [15-22], although time is needed to perform this type of test because it takes days, weeks and sometimes months to obtain good results. As a response to these limitations a new electrochemical test based on the impedance of the system was developed by Hollaender et al. [23] for testing coated metals in food packaging consisting in a combination of DC and AC measurements (AC/DC/AC procedure) which has been successfully adapted and used by Suay , Rodríguez and García in liquid paints applied to steel substrates [24-26], and in cataphoretic paints for the automotive industry [27, 28]. Other works were this technique has been applied to study powder coatings are still under review but very good results were found.

In this work we focus on the study of the anticorrosive properties of an organic coating obtained by copolymerization of an epoxy powder resin with Meldrum acid in the presence of erbium triflate as catalyst. The curing kinetics was obtained, and results compared to other systems (orto-tolylbiguanide-TBG/epoxy, and a homopolymerized epoxy resin with lanthanide triflate).

To perform the kinetic study an isokinetic program from Metler-Toledo was used together with a dynamic scanning calorimeter. In order to study the anticorrosive properties three different techniques (EIS, AC/DC/AC, and salt fog spray) have been used. Is has also been studied the validity of the AC/DC/AC technique as a useful method on the formulation and determination of anticorrosive properties of powder paints in very short times, comparing it with other different evaluation procedures (EIS and Salt Fog Spray).

2. Experimental

2.1. Materials

Four different samples (see table 1) were prepared using a solid bisphenol-A based epoxy resin of medium molecular weight (scheme 1), 733 gr/eq. ep. (from Huntsman). A first sample, used as the reference one, was the epoxy resin polymerized in the ratio given by the producer with a Huntsman o-

tolylbiguanide (TBG), with an H^+ active equivalent weight of 37g/Eq. A second sample was homo-polymerized with 0.5phr (parts of initiator per hundred of resin, w/w) of Erbium III trifluoromethanesulfonate from Aldrich. Other two samples were crosslinked with Meldrum's acid in two different proportions (3.3 and 5 phr) using erbium triflate as catalyst. In order to perform the application of the samples on steel substrates and to avoid porosity 0.18phr of benzoine and 1.27phr of flux agent were added to the mixtures.

Table1. Composition of the samples studied and glass transition temperature after curing

Sample	Epoxy resin	TBG (phr)	$Er(TfO)_3$ (phr)	Meldrum Acid (phr)	Benzoine (phr)	Flux Agent (phr)	ΔH_{cur} (kJ/eq ep)	T_g (ºC)
TBG	100	4.8	-	-	0.18	1.27	65	95
ErTfO 0.5phr	100	-	0.5	-	0.18	1.27	76	109
M.A.1	100	-	0.5	3.3	0.18	1.27	71	92
M.A.2	100	-	0.5	5	0.18	1.27	67	83

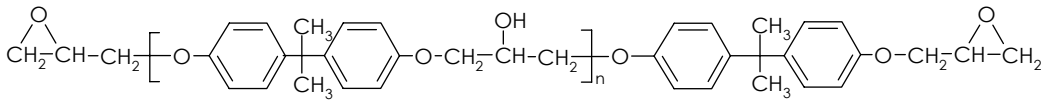

Scheme 1. DGEBA resin

Samples were pre-mixed and hand-shacked until good dispersion was afforded. After that, the material was extruded in a single screw extruder (Haake Rheomex 254), where operating conditions were 80 ºC along the extruder and 60rpm. After extruding, the material was grinded in an ultra-centrifugal mill ZM 100 and sieved at 100 micron, obtaining then the different powder coatings ready to be applied on steel substrates.

The different clearcoats were applied on cold-rolled low-carbon steel normalized tests panels (15 x 7.5 x 0.1 cm). All test panels were degreased with acetone, and paints were deposited by means of a corona electrostatic powder gun (powder coating equipment Easy 1-C), obtaining 10 panels of each sample. The clearcoats were totally cured for 15 minutes at 150ºC in an oven (25 minutes for the sample using TBG, reaching total cure). Curing conditions were established after the kinetic study of the systems. Thicknesses determined by an Elcometer were always within the range 60±5 µm.

Reactions taking place

Depending on the materials used, different chemical reactions during curing process can take place giving various networks with different structures and properties. Principal reactions are:

1. In epoxy systems using orto-tolylbiguanide the reactions taking place are those between amino and oxirane groups [29] (Scheme 2):

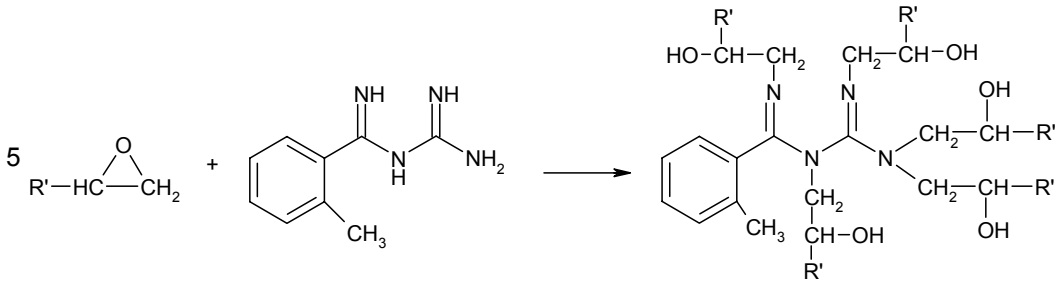

Scheme 2. Reaction o-tolylbiguanide / oxirane ring

This kind of reaction gives as a result the shrinkage of the system, nevertheless at the same time, a big number of hydroxide groups are formed which can promote the adhesion to the metallic substrate [30].

2. In systems homopolymerized by erbium triflate we can have two main reactions. Scheme 3 shows the reaction ACE which may be the most important, while reaction AM (scheme 4) is the secondary reaction which is probably increased when more triflate is added [3, 4].

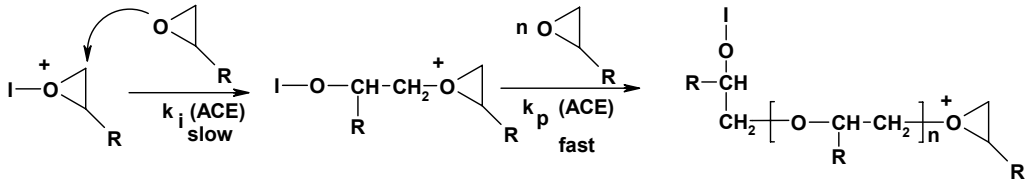

Scheme 3. Activated chain-end mechanism / ACE

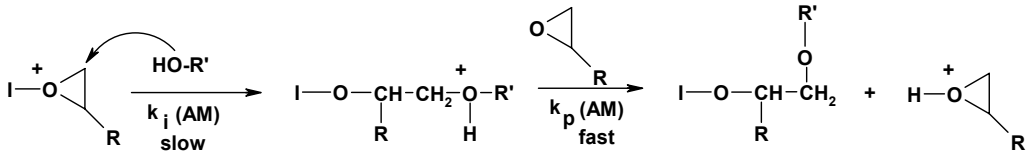

Scheme 4. Activated monomer mechanism / AM

This kind of reactions also carries to a shrinkage which is probably lower than in case 1. Moreover, these kind of reactions do not lead to an increase on hydroxyls, but leads to a highly crosslinked network and lowly plasticized (properties vary depending on the proportion of initiator used) [31].

3. The system where Meldrum acid has been used together with erbium triflate (or other lanthanide triflate) may lead to a very complex mixture of reactions [11, 32]. Firstly, the reaction between the Meldrum acid and the oxirane will happen leading to a SOE. This SOE will react with another oxirane group (copolymerization) or homopolymerize with another SOE (scheme 5). This last reaction will probably be secondary. Other possible reactions which probably will take place are reactions ACE and AM.

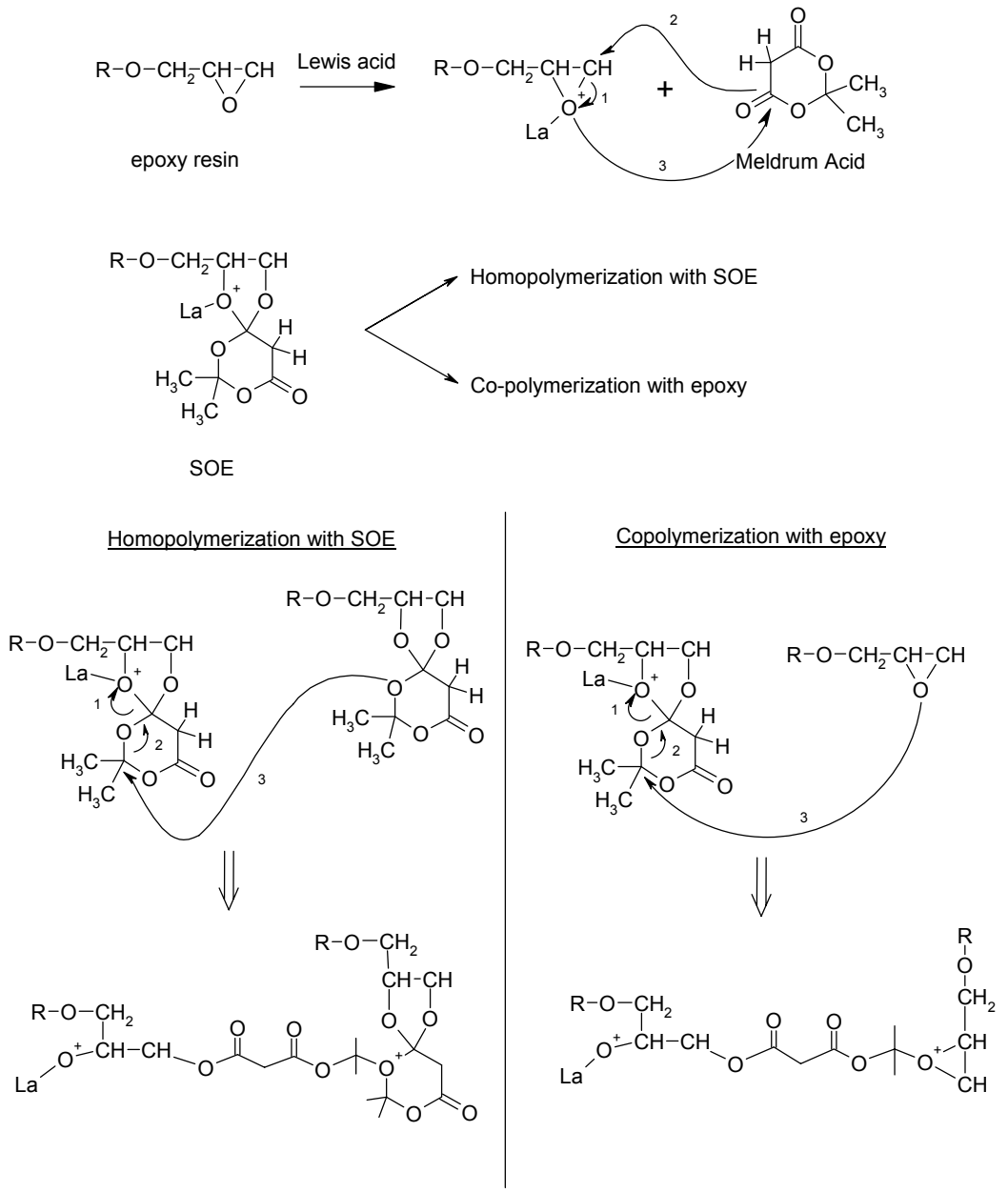

Scheme 5. Possible reactions Meldrum acid-epoxy in presence of lanthanide triflate

This kind of network does not present shrinkage; it even presents a slight expansion because of the opening of the SOE [11].

2.2. Testing Methods and Equipment

2.2.1. Thermal characterization

A Perkin Elmer DSC 7 differential scanning calorimeter was employed for dynamic scans in order to study the non isothermal curing process and apply results to isothermal curing. The samples were analyzed in covered aluminium pans, using high purity indium sample for calibration. A flow of 20 $cm^3 \cdot min^{-1}$ of argon was used as purge gas. The weight of the samples was between 8 and 9 mg. Non-isothermal scans were performed at rates of 2.5, 5, 10 and 15 $K \cdot min^{-1}$ to not-cured-samples of the four powder epoxy coatings. The scans were done at the range of temperature from 25 to 300ºC.

Isoconversional STARe software from Mettler-Toledo was used in order to calculate conversion degrees and kinetics of the processes.

Differential scanning calorimeter was also used to find the transition vitreous temperature (T_g) of the different cured samples. Scans were performed under the same conditions of the kinetic study using cured samples of 8mg weight, a scan rate of 10ºC/min at a range of 25-250ºC.

2.2.2. Accelerated cyclic test (salt fog spray)

The accelerated salt fog spray test was performed in accordance to ASTM B 117-85. In this test a cross is performed along the coating until the bare metal is reached. The samples are then introduced in a salt fog spray chamber where an alkaline fog is created with a 5% (in weight) NaCl water solution. The samples are collected at different periods of time and evaluated until a maximum of 300 hours of exposure. After each collection, the samples were dried, and blistering, corrosion and delamination were measured after 24h of ambient exposure. Delamination was evaluated after applying a tape of 40mm thick to one arm of the cross and peeling the clearcoat. Maximum value of delamination was 40mm.

2.2.3. Electrochemical impedance spectroscopy (EIS)

Electrochemical Impedance Spectroscopy (EIS) tests were carried out on coated samples exposed to 3.5% NaCl (by weight) in deionised water for periods up to ten months. The three-electrode electrochemical cell was obtained by sticking a glass cylinder on the sample sheet and filling it with the test solution. The exposed surface area was 16.6 cm^2. A carbon sheet acted as the counter electrode and an Ag/AgCl electrode was used as the reference one.

The AC impedance data were obtained at the free corrosion potential using an AUTOLAB PGSTAT30 potentiostat and a frequency response analyser. The impedance tests were carried out over a frequency range of 10^5 Hz down to $2 \cdot 10^{-3}$ Hz using a sinusoidal voltage of 10 mV as amplitude inside a Faraday cage in order to minimise external interferences on the system.

The equivalent circuit model, shown in Figure 1, was employed to analyze the EIS spectra. The circuit consisted on a working electrode (metal substrate), a reference electrode (Ag/AgCl), electrolyte resistance R_s, pore resistance R_{po}, constant phase element of the coating capacitance CPE_c (here on C_c), polarisation resistance R_p, and constant phase element of the double layer capacitance CPE_{dl} (here

on C_{dl}). The two CPE were used because the fitting was better than using capacitances in the equivalent circuit. The "n" value used to be between 0.7 and 1.

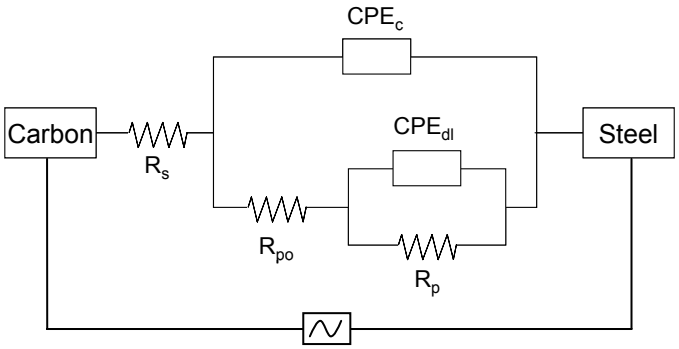

Fig. 1. Equivalent circuit used to model EIS and AC/DC/AC impedance data where passive parameters (R_s = electrolyte resistance, CPE_c = constant phase element of the coating capacitance, CPE_{dl} = constant phase element of the double layer capacitance, R_{po} = pore resistance, R_p = polarization resistance) can be defined.

Fitting the EIS data to the circuit by means of the Z-view software determined the values of the equivalent circuit elements. The chi-squared parameter of the fit was always below 0.1.

2.2.4. Equivalent circuit interpretation

It is generally assumed that there is a correlation between the elements of the equivalent circuit and the corrosion properties of the system [33].

Pore resistance R_{po} is a measure of the porosity and deterioration of the coating. R_{po} values have been usually related to the number of pores or capillary channels perpendicular to the substrate surface through which the electrolyte reaches the interface [34]. Although R_{po} can also increase with immersion time, probably as a result of pore or defect blockage by corrosion products, it usually decreases.

Some authors, as Walter [35, 36], have found three regions in the time-dependent trend of R_{po}. It initially decreases rapidly, then slowly (displaying a plateau) and then rapidly again, coinciding with the appearance of the second semi-circle. The plateau is explained by making the assumption that the number of pathways formed is approximately constant with time.

In order to calculate de capacitances of the systems it was used the Constant Phase Elements (CPE). Ideally a capacitor is formed by two conducting plates separated by a non-conducting media (dielectric), nevertheless capacitors in EIS experiments do not behave ideally (e.g. dielectric is not ideal). Instead, they act like constant phase elements becoming the impedance of the capacitor:

$$Z_{CPE} = A(j\omega)^{-n} \quad (1)$$

where,

A = the inverse of the capacitance given by a software

n = an exponent which equals 1 for a capacitor

For a CPE the exponent n is less than 1. In practice, it is better to treat n as an empirical constant with no real physical basis [37].

Having this into account, the results are presented as capacitances but with units $s^n/\Omega cm^2$ instead of those for effective/real capacitances ($s/\Omega cm^2$ or F/cm^2).

C_c is the capacitance of the coating and this should be a measure of water permeation into the coating.

The polarisation resistance R_p and double layer capacitance C_{dl} are two parameters used to specify the disbonding of the top coat and the onset of corrosion at the interface. The specific polarisation resistance is associated with the charge transfer behaviour of the metal substrate. R_p, like C_{dl}, can only be calculated well when at least two time constants are evident in the spectrum.

C_{dl}, the double layer capacitance, is a measure of the area over which the coating has disbonded. It can only be correctly measured at advanced stages of coating deterioration. The trend of C_{dl} is complex. A change in the C_{dl} value can be associated with the competition between disbonding and corrosion product accumulation at the interface. As water spreads at the interface and the delaminated area extends, there is an increase of the C_{dl} value. On the other hand, the accumulation of corrosion products at the interface reduces the area of the double layer capacitor, which will lead to a decrease in the C_{dl} value. Therefore, the change of trend in C_{dl} may depend on which factor, disbonding or corrosion product accumulation was more dominant during the corrosion process. However, it should be pointed out that both the increase and the decrease in C_{dl} are the results of the development of corrosion at the metal surface, while a constant C_{dl} is an indication of a stable interface [38].

2.2.5. AC/DC/AC test

The AC/DC/AC procedure (figure 2) is based on the application of a stress (DC) to a coated sample measuring the impedance (AC) of the system after it. This sequence stress/impedance is repeated several times until the system is totally damaged. In order to obtain more information about the coating itself and the whole system, a step of depolarization can be included for a given period (relaxation time). A first AC carried out as a normal EIS measurement gives an idea of the impedance of the system (Bode plots, and modelled characteristic parameters using Z-View and figure1). The relaxation time will give an idea of the evolution with time of the system after the applied stress, until it reaches again the steady state (graphics E_{oc} = f(time)).

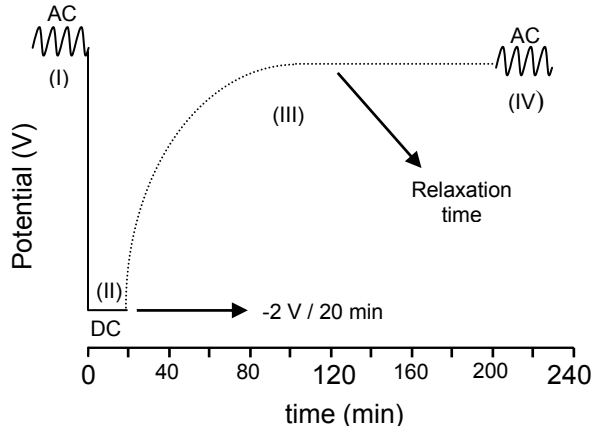

Fig. 2. AC/DC/AC test schematic figure versus time.

This test sequence is repeated at least 6 times, which means that about 24 hours are needed for performing this test. The AC/DC/AC procedure was absolutely automated in PGSTAT 30 AUTOLAB equipment.

This technique has its fundaments on the influence that the cathodic reaction of water hydrolysis (produced when the potential is more negative than -1.0 V (vs SCE) [39]) has on the adhesion because of the formation of H_2 (gas) and OH^-. The evolving of H_2 will increase local delaminations (figure 3) giving rise to the failure of the coating system (reflected on the variation of the impedance). When the cathodic reaction stops and the H_2 production has taken place, the normal electrochemical corrosion of the system happens in presence of electrolyte with production of iron oxides and hydroxides. On the other hand, the forced polarization makes that the double layer in the interface gets disturbed and needs reorganization, which is reflected on the variation of the potential at the relaxation process. At the same time, the different ions inside the coating will leave it producing charges equilibration and polymeric molecule dipoles reorganization producing also a variation on the potential. Thus the system is degraded by the loose of adherence (formation of H_2), the pore opening by the incoming of the different species from the electrolyte, and the formation of corrosion products by electrochemical processes.

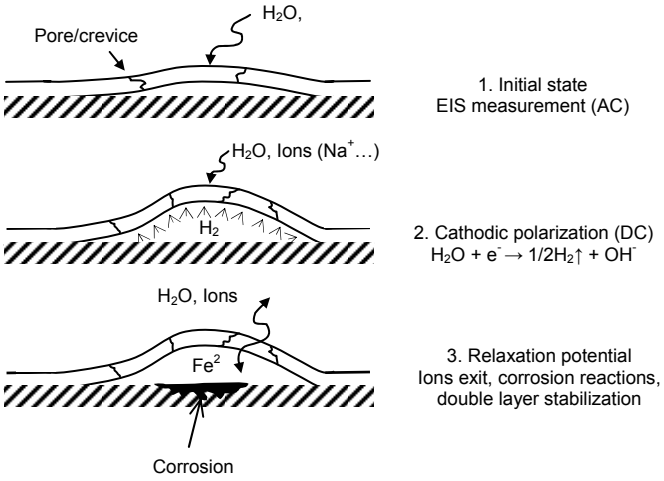

Fig. 3. Physic effect of AC/DC/AC test on a coated metallic substrate. Failure of an anticorrosive coating.

The AC/DC/AC procedure measures the quality of the coating and its adhesion by the study of the resistance that the system offers to its degradation with the cathodic polarizations. In this case of study the cathodic polarization (DC) was carried out for 20minutes at a constant voltage of -2V. Following that, the relaxation time was of 3 hours, and finally an EIS was applied under the conditions above mentioned. The test sequence was repeated six times (around 24hours of test) and was absolutely automated in PGSTAT 30 AUTOLAB equipment.

2.2.6. Adhesion Test

In order to have an overall idea of the influence of the triflates on the adhesion of the epoxy system, an adhesion test was carried out. Adhesion test was performed in accordance to ISO 4587 (1979). It

consists on the deposition of the powder clearcoat between two rectangular and cleaned steel substrates, giving rise to a glued area of 13x25mm. When the powder is deposited, the two rectangular substrates are fixed by means of two pincers and cured for 150ºC one hour. After the curing process and three days of ambient exposure, the samples were tested on an Instron Universal Test Machine 4469-H1907 (figure 4) at a traction speed of 1mm/min. The data of tension and deformation were registered. With the break force (F) and the glued area, the shear stress is obtained (σ_{shear} (MPa) = F/area), giving the adhesion of the clearcoats to the substrates. Almost all the specimens showed an adhesive failure type. Five probes of each sample were prepared and tested.

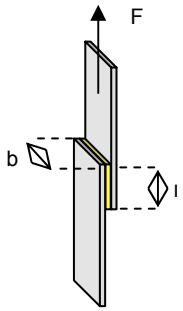

$\sigma_{shear} = F/b \cdot l$

Fig. 4. Scheme of an adhesion test. σ_{shear} calculus.

2.2.7. Morphology study

The morphology of the samples was studied with a scanning electron microscopy (SEM). Samples were frozen with liquid N_2 and hand broken. The measurements were carried out on a Jeol-JSM 6300 at 10kV.

3. Results and Discussion

3.1. Thermal characterization

Figure 5 shows the DSC-thermograms registered at a heating rate of 5K/min for the four different samples studied. The thermograms exhibit a small endothermic peak around 55ºC (where the T_g should be detected) probably related to the physical aging of the DGEBA. All the thermograms show a big exothermic peak at high temperatures (with its minimum between 130 and 160ºC) related to the curing reaction of the epoxy resin. It can be seen, that systems homopolymerized with erbium triflate shift the exotherm to minor temperatures compared to the reference sample DGEBA/TBG, demonstrating the acceleration effect of these Lewis acids. Moreover, when Meldrum Acid is added, there is a higher shift towards lower temperatures, meaning a higher increase of the reaction rate.

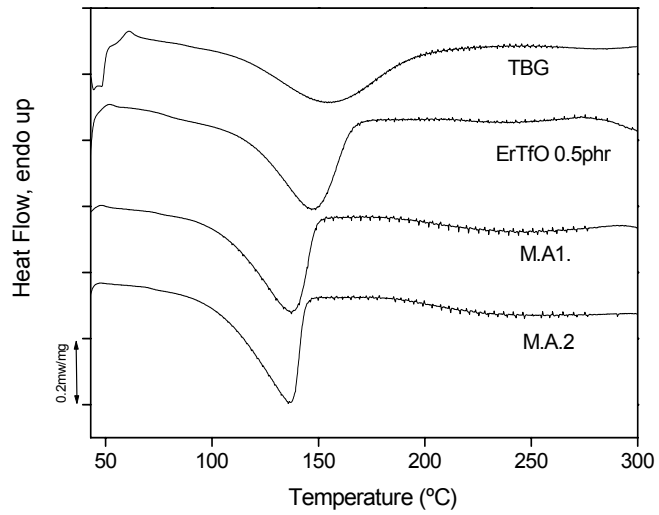

Fig. 5. Non-isothermal DSC thermograms at 5ºC/min of heating rate for mixtures epoxy resin/erbium triflate 0.5phr, epoxy resin/erbium triflate 0.5phr/Meldrum acid 3.3phr, epoxy resin/erbium triflate 0.5phr/Meldrum acid 5phr, and epoxy resin/TBG.

With the scans at different rates and the use of the STARe software form Metler-Toledo it can be obtained the curing enthalpies (table 1), the activation energy and the conversion as a function of temperature. Using the isoconversional method, graphics of conversion in function of temperature and time can be plotted (figure 6), where for a given conversion (in this case α=0.98) it is represented the curing time versus the curing temperature for all the samples, so a comparative idea of the curing kinetics can be figured out.

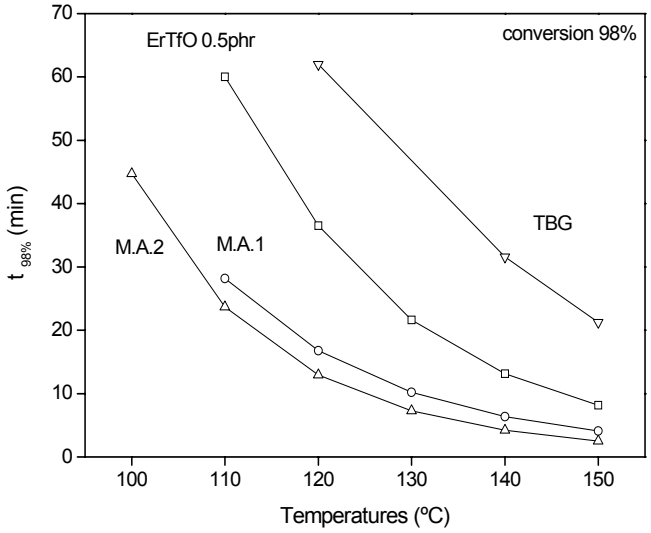

Fig. 6. Time-Temperature for a 98% conversion of the four different clearcoats: epoxy resin/erbium triflate 0.5phr (□), epoxy resin/erbium triflate 0.5phr/Meldrum acid 3.3phr (○), epoxy resin/erbium triflate 0.5phr/Meldrum acid 5phr (△), and epoxy resin/TBG (▽).

It can be seen that the use of Meldrum Acid as crosslinker catalyzed by erbium triflate leads to a very high reduction of the curing time and temperature. At the curing temperature of 120ºC the reduction of time is about 80% with respect to the reference system (TBG with resin), and around 60% with respect to a homopolymerized system ($Er(TfO)_3$ with resin).

This shows that from the point of view of the kinetics, a system crosslinked with Meldrum acid and catalyzed by 0.5phr erbium triflate represents a very good alternative to traditional systems, being a possible solution for the coating application to thermosensible substrates. The system can be cured at 110ºC for 25 minutes, meaning a high reduction of application costs (reducing curing temperature is one of the main objectives of the manufacturers). Lower curing temperatures can be afforded using a higher content of Meldrum acid.

Table 1 presents the different values of T_g. The use of Meldrum acid (M.A.) gives rise to lower T_g values than homopolymerizing the system with erbium triflate. This fact is due to the inclusion of the Meldrum acid on the network giving as a result longer chains between crosslinks. At the same time the addition of M.A. reacts with the epoxide obtaining a SOE which is opened in the curing process giving as a result a lower shrinked network. Thus, with M.A. the network is more opened and less crosslinked, while when using only erbium triflate the network is more crosslinked. The addition of M.A. has a plasticizing effect and reduces T_g of the system.

3.2. Adherence

In the adhesion test, figure 7, differences are detected between all the samples. The system homopolimerized with erbium triflate showed the lowest shear resistance, while the one with 3.3phr of M.A. shows the higher shear resistance meaning higher adhesion to the substrate. When more M.A. is added lower values of shear resistance are obtained, which could be due to a faster curing promoting local delaminations. The system with TBG probably presents good adhesion due to the hydroxyl groups produced in the reaction (the higher the OH^- content, the higher the adhesion [40-43]). There is a high improvement in adhesion when adding M.A. to a system cured with erbium triflate, this fact could be due to the lower shrinkage obtained when using M.A. compared to the other systems.

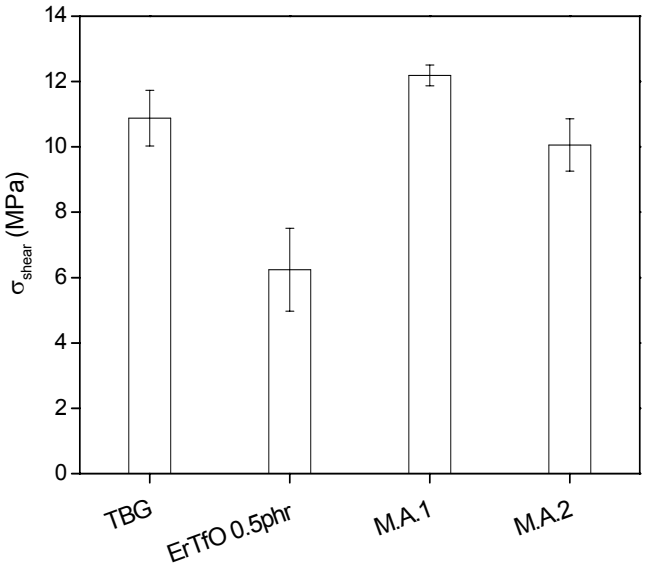

Fig. 7. Shear stress of the studied clearcoats: epoxy resin/erbium triflate 0.5phr, epoxy resin/erbium triflate 0.5phr/Meldrum acid 3.3phr, epoxy resin/erbium triflate 0.5phr/Meldrum acid 5phr, and epoxy resin/TBG.

3.3. SEM

Figure 8 shows the SEM-pictures of the four systems at 75 magnifications. The lowest porosity is obtained for a sample cured with TBG. When Meldrum acid is added to a system homopolymerized with erbium triflate there is an increase in porosity, being higher when more M.A. is added. This rising of the macroporosity is probably due to the fact that the faster the reaction the more the occluded air can be.

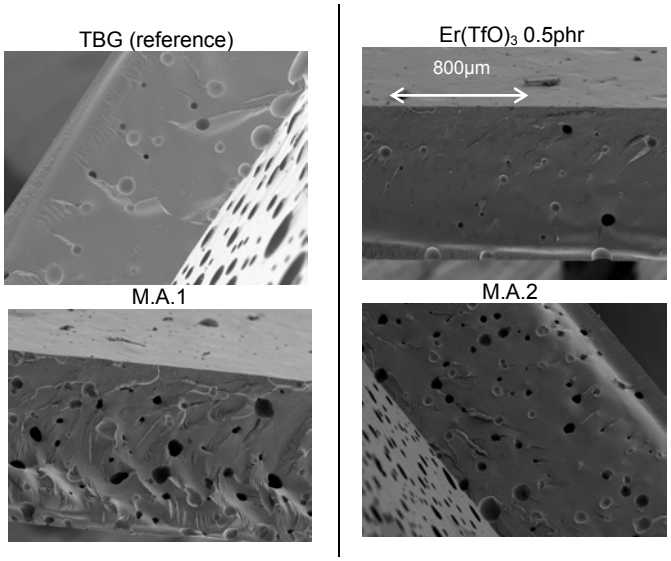

Fig. 8. SEM pictures at 75 magnifications.

3.4. Salt fog spray

Figure 9 presents pictures of the four samples after 214h of exposition to salt fog spray chamber, while figure 10 plots the delamination values versus time. It is clearly seen that the sample with 3.3phr of Meldrum acid (M.A.1) presents the lowest delamination and the lowest corrosion outside the cross. Sample M.A.2 presents very low delamination but some points of corrosion (pickling), as was expected because of the lower crosslinking density (and higher permeability) than the sample M.A.1. ErTfO0.5 sample showed regular delamination but very high pickling corrosion. Reference sample (TBG) showed almost no corrosion outside the cross but quite enough delamination. This fact could be due to the lower wet adhesion that the sample with TBG presents, although it presents very good dry adhesion. The loss of adhesion in wet conditions is due to the fact that water spreads under the film breaking the hydrogen bonds between the epoxy layer and the metal oxides [41]. It has to be pointed out that in the case of TBG, the adhesion to the metal is due to the hydrogen bond between OH and metal, while the catalized samples cured with Meldrum acid show adhesion because of the high polarity of the coatings.

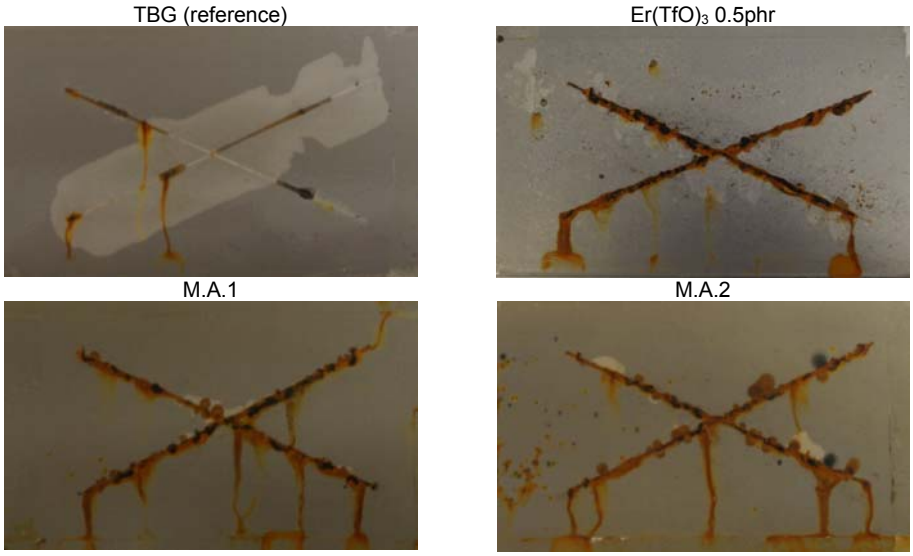

Fig. 9. Pictures of clearcoats: epoxy resin/erbium triflate 0.5phr, epoxy resin/erbium triflate 0.5phr/Meldrum acid 3.3phr, epoxy resin/erbium triflate 0.5phr/Meldrum acid 5phr, and epoxy resin/TBG after 214 hours of exposure to salt fog spray.

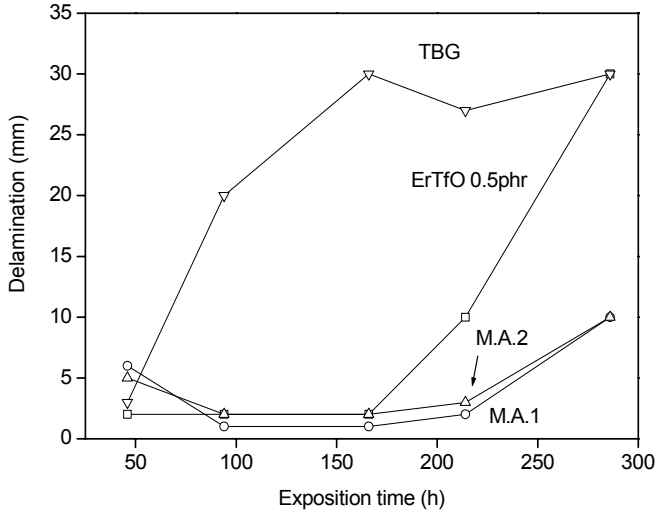

Fig. 10. Evolution of delamination with time of exposure of the different clearcoats, epoxy resin/erbium triflate 0.5phr (□), epoxy resin/erbium triflate 0.5phr/Meldrum acid 3.3phr (O), epoxy resin/erbium triflate 0.5phr/Meldrum acid 5phr (Δ), and epoxy resin/TBG (∇).

3.5. EIS (electrochemical impedance spectroscopy)

Figure 11 shows a Bode graphic of the impedance response (impedance modulus and phase angle versus frequency) of the four different prepared clearcoats exposed to 200 days to NaCl 3.5% in weight electrolyte. The higher modulus and phase angle is obtained for the reference system (TBG) followed by the samples with 5 and 3.3 phr of Meldrum acid (higher Meldrum acid leads to higher modulus and phase angle). The sample homopolymerized with 0.5phr $Er(TfO)_3$ shows the lower modulus and phase angle.

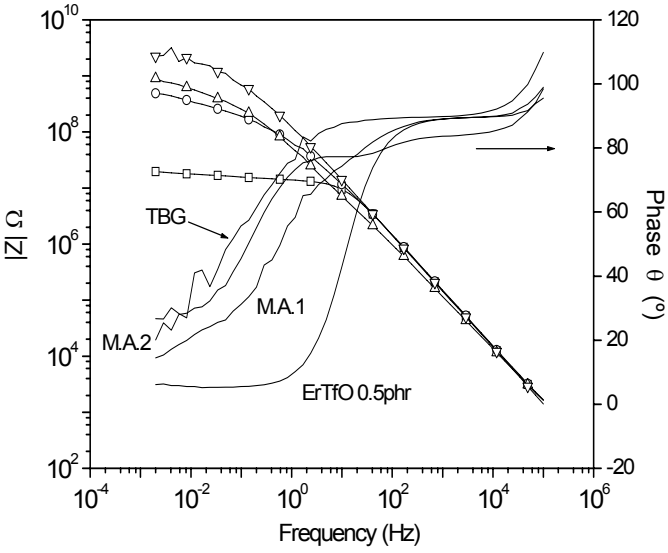

Fig. 11. Bode plot (impedance modulus and phase angle versus frequency) for different clearcoats epoxy resin/erbium triflate 0.5phr (□), epoxy resin/erbium triflate 0.5phr/Meldrum acid 3.3phr (○), epoxy resin/erbium triflate 0.5phr/Meldrum acid 5phr (Δ), and epoxy resin/TBG (∇) applied on metal substrates after 200 days' exposure to electrolyte (deionised water with 3.5% NaCl by weight). EIS test.

Figure 12a, 12b, 12c and 12d show the equivalent circuit parameters modelled for EIS results and corresponding to porous resistance R_{po}, coating capacitance C_c, polarization resistance R_p, and double layer capacitance C_{dl} respectively.

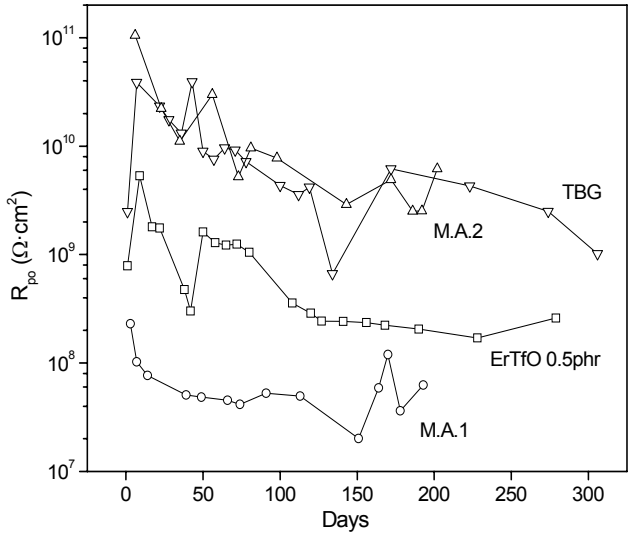

Fig. 12a. Evolution of porous resistance, R_{po}, versus time of exposure to electrolyte (deionised water with 3.5% NaCl by weight) for different clearcoats applied on metal substrates: epoxy resin/erbium triflate 0.5phr (□), epoxy resin/erbium triflate 0.5phr/Meldrum acid 3.3phr (○), epoxy resin/erbium triflate 0.5phr/Meldrum acid 5phr (Δ), and epoxy resin/TBG (∇). EIS test.

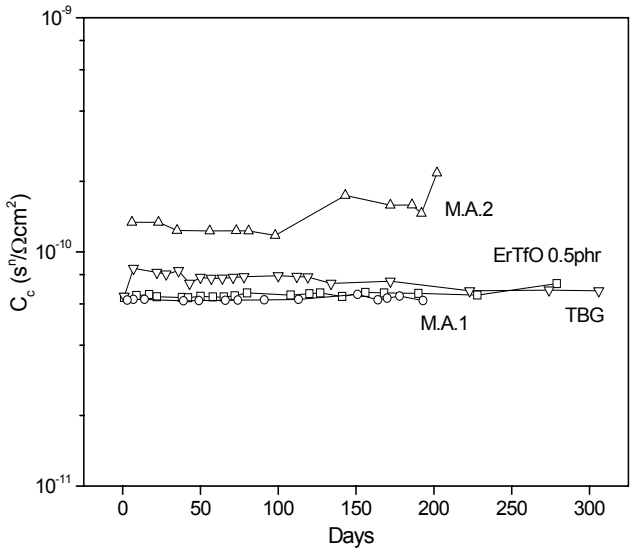

Fig. 12b. Evolution of coating capacitance, C_c, versus time of exposure to electrolyte (deionised water with 3.5% NaCl by weight) for different clearcoats applied on metal substrates: epoxy resin/erbium triflate 0.5phr (□), epoxy resin/erbium triflate 0.5phr/Meldrum acid 3.3phr (O), epoxy resin/erbium triflate 0.5phr/Meldrum acid 5phr (Δ), and epoxy resin/TBG (∇). EIS test.

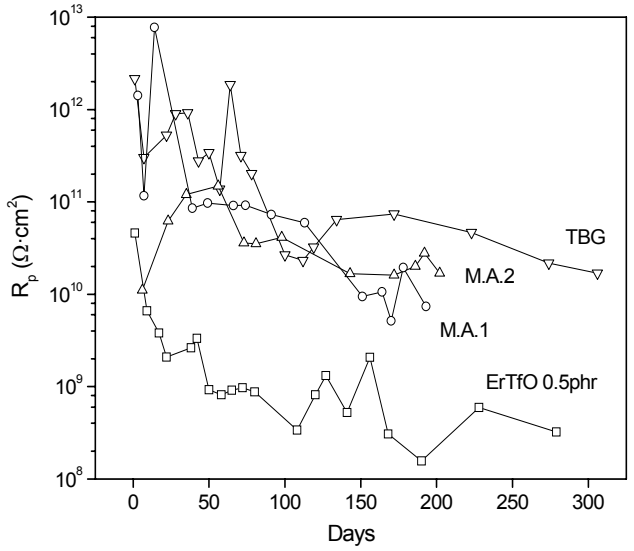

Fig. 12c. Evolution of polarization resistance, R_p, versus time of exposure to electrolyte (deionised water with 3.5% NaCl by weight) for different clearcoats applied on metal substrates: epoxy resin/erbium triflate 0.5phr (□), epoxy resin/erbium triflate 0.5phr/Meldrum acid 3.3phr (O), epoxy resin/erbium triflate 0.5phr/Meldrum acid 5phr (Δ), and epoxy resin/TBG (∇). EIS test.

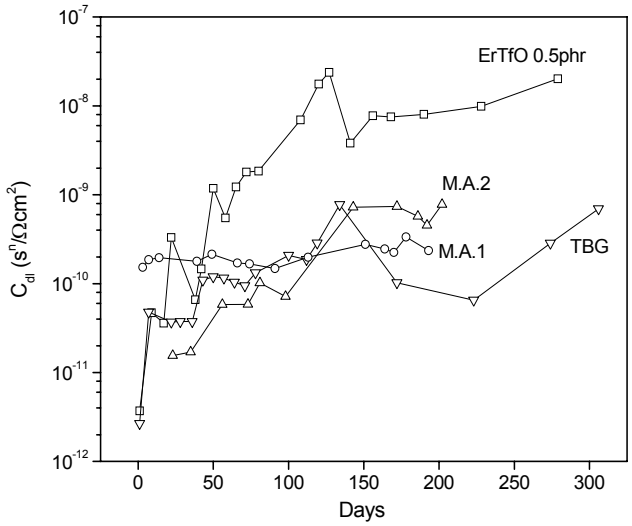

Fig. 12d. Evolution of double layer capacitance, C_{dl}, versus time of exposure to electrolyte (deionised water with 3.5% NaCl by weight) for different clearcoats applied on metal substrates: epoxy resin/erbium triflate 0.5phr (□), epoxy resin/erbium triflate 0.5phr/Meldrum acid 3.3phr (○), epoxy resin/erbium triflate 0.5phr/Meldrum acid 5phr (△), and epoxy resin/TBG (▽). EIS test.

Figures 12a and 12b (R_{po} and C_c), related to the coating's properties, show that the sample M.A.1 presents the lowest porous resistance while M.A.2 has the higher coating capacitance probably due to their lower crosslinking density (as can be seen in T_g values) and higher porosity. The plasticizing effect of the Meldrum acid leads to higher water content in the coating because the electrolyte can more easily penetrate in the film.

On the other hand the interface properties (figures 12c and 12d) showed that Meldrum acid samples had very good stability and low trend to delamination. The main reason for this behaviour can be a good adherence to the substrate and the absence of local delaminations in the curing reaction because very low shrinkage is obtained.

The best sample was the one cured with TBG because of its high resistance and low capacitances, while the worst one was the sample homopolimerized with erbium triflate 0.5phr.

.

3.5. AC/DC/AC test

Figure 13 shows a Bode graph (impedance modulus versus frequency) for the four different prepared clearcoats after 5 polarizations (DC). It can be seen that the sample homopolymerized with erbium triflate presents the worst impedance modulus at low frequencies, meaning a more active interface. There is almost no difference between samples cured with Meldrum acid catalyzed with erbium triflate and the reference sample (cured with TBG). This indicates an improvement in the coatings anticorrosive behaviour when adding Meldrum acid with respect to the sample with only erbium triflate.

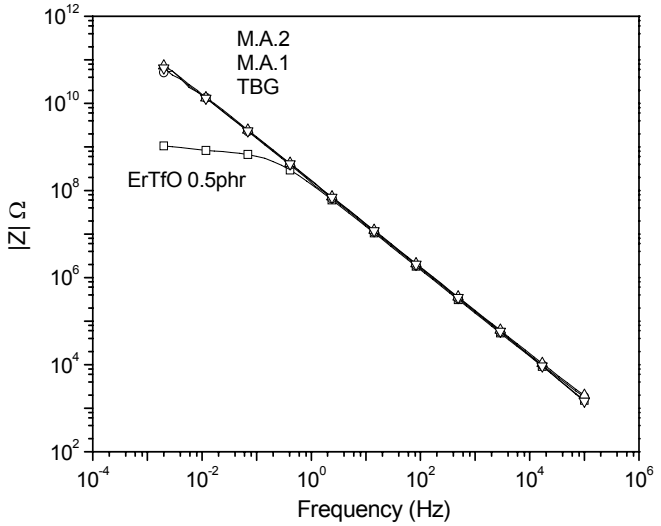

Fig. 13. Bode plot (impedance modulus versus frequency) for different clearcoats applied on metal substrates after 5 cathodic polarisations: epoxy resin/erbium triflate 0.5phr (□), epoxy resin/erbium triflate 0.5phr/Meldrum acid 3.3phr (○), epoxy resin/erbium triflate 0.5phr/Meldrum acid 5phr (△), and epoxy resin/TBG (▽). AC/DC/AC test..

In order to observe the differences between the coatings' behaviour, the impedance values can be fitted to an equivalent circuit (figure 1) and the specific parameters calculated. Figure 14a, 14b and 14c show the evolution of the equivalent circuit modelled parameters, R_{po}, R_p and C_{dl} respectively, with the number of cycles (polarizations) for the different clearcoats. C_c is not plotted because there was almost no difference between the samples, although sample with erbium triflate presents the highest coating capacitance. Maximum anticorrosive properties (higher resistances and lower capacitances) were obtained for the sample with 5phr of Meldrum acid catalyzed by erbium triflate, even if there are few differences between samples M.A.1, M.A.2 and TBG. The worst anticorrosive properties were obtained for the homopolymerized sample with erbium triflate.

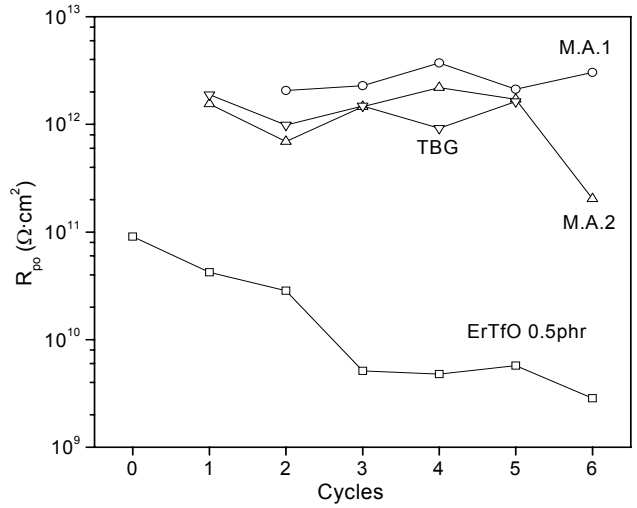

Fig. 14a. Evolution of pore resistance, R_{po}, versus cathodic polarizations for different clearcoats applied on metal substrates: epoxy resin/erbium triflate 0.5phr (□), epoxy resin/erbium triflate 0.5phr/Meldrum acid 3.3phr (○), epoxy resin/erbium triflate 0.5phr/Meldrum acid 5phr (△), and epoxy resin/TBG (▽). AC/DC/AC test.

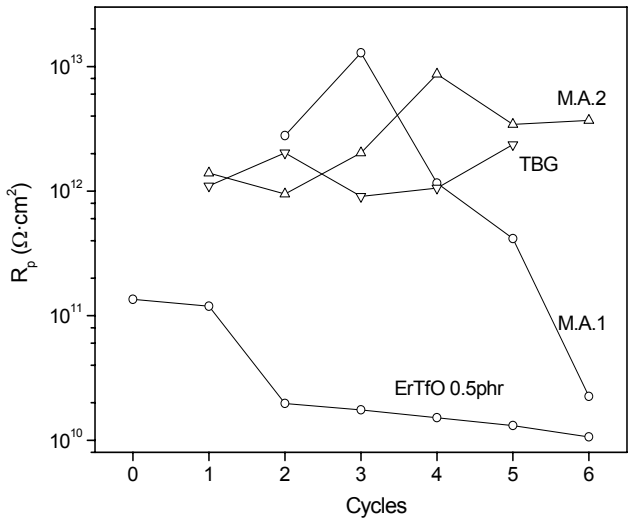

Fig. 14b. Evolution of polarization resistance, R_p, versus cathodic polarizations for different clearcoats applied on metal substrates: epoxy resin/erbium triflate 0.5phr (□), epoxy resin/erbium triflate 0.5phr/Meldrum acid 3.3phr (O), epoxy resin/erbium triflate 0.5phr/Meldrum acid 5phr (Δ), and epoxy resin/TBG (∇). AC/DC/AC test.

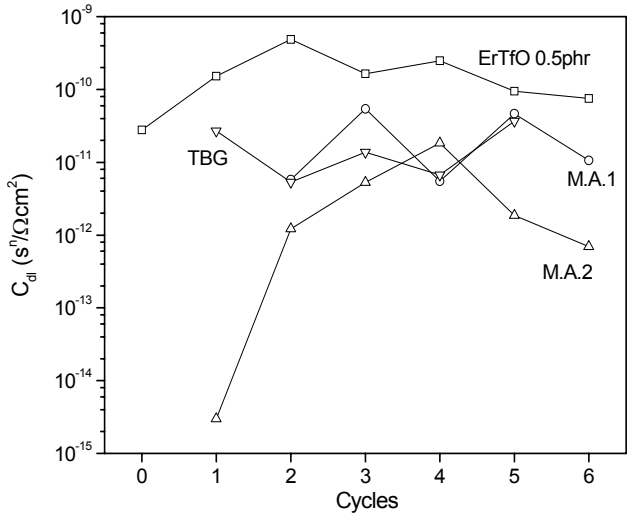

Fig. 14c. Evolution of the double layer capacitance, C_{dl}, versus cathodic polarizations for different clearcoats applied on metal substrates: epoxy resin/erbium triflate 0.5phr (□), epoxy resin/erbium triflate 0.5phr/Meldrum acid 3.3phr (O), epoxy resin/erbium triflate 0.5phr/Meldrum acid 5phr (Δ), and epoxy resin/TBG (∇). AC/DC/AC test.

4. Conclusions

Four different epoxy powder coatings have been formulated: one sample cured with o-tolylbiguanide and used as the reference system, another one homopolymerized with 0.5 of erbium triflate, and the other two polymerized with Meldrum acid in two different proportions (3.3 and 5phr) and catalyzed with 0.5 of erbium triflate.

The newly formulated systems using Meldrum acid and erbium triflate have given very good kinetic properties, lowering temperatures and times needed to cure the formulations (a reduction of 80% of the

curing time compared to a traditional system (with TBG)). Under industrial conditions, where the curing time must be between 20-25 minutes, a system using Meldrum acid 5phr/Erbium triflate 0.5phr reduces the curing temperature to 110ºC, while for a traditional system normally is 150-170ºC.

The use of the Meldrum acid gave rise to lower T_g values meaning a less crosslinked network, but at the same time with lower shrinkage (meaning less internal stresses in the coating).

In order to study the anticorrosive properties, three different evaluation tests have been applied: EIS, salt fog spray, and a new electrochemical test named AC/DC/AC. The results showed that samples using Meldrum acid offered the best anticorrosive properties (which increase with its addition). Samples homopolymerized with erbium triflate showed the worst anticorrosive properties.

The AC/DC/AC test has shown good correlation with EIS test but giving results in very short times (less than 24hours) and some coincidence with salt fog spray test (TBG samples showed quite different results between techniques), and giving objective information about the corrosive and degradation processes taking place in the coating. Nevertheless, future research in this direction should be done.

This work has proposed a new clearcoat using Meldrum acid as crosslinker together with a Lewis acid as catalyst with a very high improvement in curing conditions and very good anticorrosive behaviour.

Acknowledgements

Authors would like to thank Ms Eva Romero, Ms Àngels Serra, Mr Carlos Bonet, Mr Joseja Gracenea and Ms Maite Rodríguez for their help in the development of this project. Authors are also grateful for the economic support in this work of CICYT MAT 2000-0123-P4-03.

1. R.A. Dickie, D.R. Bauer, S.M. Ward, D.A. Wagner, *Prog. Org. Coat.,* 31 (1997) 209
2. S.S. Lee, H.Z.Y. Han, J.G. Hilborn, J.-A.E. Manson, *Prog. Org. Coat.,* 36 (1999) 79
3. S.J. García, X. Ramis, A. Serra, J. Suay, *Thermochim. Acta.,* 441 (2006) 45
4. S.J. García, X. Ramis, A. Serra, J. Suay, *J. Therm. Anal. Calorim.,* 83 (2) (2006) 429
5. S.J. García, A. Serra, X. Ramis, J. Suay, *J. Therm. Anal. Calorim.,* August (2006) Online-first
6. S.J. García, J. Suay, "Influence on the anticorrosive properties of the use of Erbium III Trifluoromethanesulfonate as initiator in an epoxy powder clearcoat", sent to *Corrosion Science*, May 2006
7. S.J. García J. Suay, "Epoxy powder clearcoats used for anticorrosive purposes cured with Ytterbium III Trifluoromethanesulfonate", *Corrosion*, (2006) In press
8. *"Expanding Monomers: Synthesis, Characterization and Applications",* R.K. Sadhir, M.R. Luck, Eds.; CRC: Boca Raton, FL, 1992
9. W.J. Bailey, *J. Elastoplast*, 5 (1973) 142
10. W.J. Bailey, R.L.-J. Sun, T. Katsuki, H. Endo, H. Iwama, R. Tsushima, K. Saigou, M.M. Bitritto, *"In Ring-Opening Polymerization*", T. Saegusa, E. Goethals, Eds.; ACS Symposium Series 59; American Chemical Society: Washington, DC, 1977
11. C. Mas, X. Ramis, J.M. Salla, A. Mantecón, A. Serra, *J. Polym. Sci. Pol. Chem.*, 41 (2003) 2794
12. W. J. Bailey, *J. Macromol. Sci. Chem*, 9 (1975) 849
13. M. Fedtke, J. Haufe, E. Kahlert, G. Müller, *Angew. Makromol. Chem.,* 255 (1998) 53
14. C.Mas, A. Mantecón, A. Serra, X. Ramis, J.M. Salla, *J. Polym. Sci. Pol. Chem.*, 43 (2005) 2337
15. F. Mansfeld, *J. Applied Electrochem.,* 25 (1995) 187
16. G.P. Bierwagen, *J. Coat. Tech.* 64 (1992) 71
17. B. Liu, Y. Li, H. Lin, C. Cao, *Acta Physico-Chimica Sinica.,* 17 (2001) 241
18. B.S. Skerry, C-T. Chen, C.J. Ray, *J. Coat. Tech.,* 64 (1992) 77
19. S. Gwori, K. Balakrishnan, *Prog. Org. Coat.,* 23 (1994) 363
20. M. Selvaraj, S. Guruviah, *Prog. Org. Coat.,* 28 (1996) 271

21. L.S. Hernández, B. del Amo, R. Romagnoli, *Anti-Corrosion Methods and Materials* ,46 (1999) 198
22. X.Liu, H. Lu, J. Shao, P. Wan, S. Zhang, *Materials and Corrosion,* 46 (1995) 33
23. J. Hollaender, C.A. Schiller, W. Strunz, *Food additives and contaminants,* 14, 6-7 (1999) 617
24. M.T. Rodriguez, J.J. Gracenea, J.J. Saura, J.J. Suay, *Prog. Org. Coat.,* 50 (2004) 68
25. J.J. Suay, M.T. Rodriguez, K.A. Razzaq, J.J. Carpio, J.J. Saura, *Prog. Org. Coat.,* 46 (2003) 121
26. M.T. Rodriguez, J.J. Gracenea, S.J. García, J.J. Saura, J.J. Suay, *Prog. Org. Coat.,* 50 (2004) 123
27. S.J. García, M. Rodríguez, R. Izquierdo, F. Romero, J. Suay, "Validity of an electrochemical accelerated technique (ac/dc/ac) for rapid assessment of automotive primers", *Corr. Sci.,* (2006) In press
28. S.J. García, M.T. Rodríguez, R. Izquierdo, J. Suay, "Evaluation of cure temperature effects in cataphoretic automotive primers by electrochemical techniques", *Corr. Sci.,* (2006) In press
29. M. Ochi, K. Mimura, H. Motobe, *J. Adhesion Sci. and Techn.,* 8 (1994) 223
30. J.M. Martí-Martínez, M. Madrid-Vega, *Teoría de la adhesión, Tema 2: Propiedades de los adhesivos y los selladores antes del curado*, Loctite España
31. C.Mas, A. Serra, A. Mantecón, J.M. Salla, X. Ramis, *Macromol. Chem. Phys.*, 202 (2001) 2554
32. C.Mas, A. Mantecón, A. Serra, X. Ramis, J.M. Salla, *J. Polym. Sci. Pol. Chem.*, 42 (2004) 3782
33. F. Mansfeld, *Electrochim. Acta*, 38 (1993)
34. A. Amirudin, D. Thierry, *Prog. Org. Coat.,* 26 (1995) 1
35. G.W. Walter, *J. Electroanal. Chem.,* 118 (1981) 259
36. G.W. Walter, *Corros. Sci.,* 26 (9) (1986) 681
37. Gamry Instruments, "*Electrochemical Impedance Spectroscopy Primer*", www.gamry.com
38. N. Tang, W.J. Ooij, G. Górecki, *Prog. Org. Coat.,* 30 (1997) 255
39. H. Leidheiser, *J. Adhesion Sci. Tech.,* 1 (1987) 79
40. D. Greenfield, J.D. Scantleburry, *JCSE*, 3 (2000) paper5
41. E. Vaca-Cortés, M.A. Lorenzo, J.O. Jirsa, H.G. Wheat, R.L. Carrasquillo, *Adhesion testing of epoxy coating*, Centre for transportation research bureau of engineering research the university of Texas at Austin (1998)
42. N.I. Gaynes, *Testing of Organic Coatings*, Noyes Data Corp., Park Ridge, NJ (1977)
43. M.A. Lorenzo, *Experimental Methods for Evaluating Epoxy Coating Adhesion to Steel Reinforcement,* M.S. Thesis, The University of Texas at Austin (1997)

VI. CONCLUSIONES

6.1. CONCLUSIONES

De la investigación realizada en el desarrollo de esta tesis doctoral se pueden extraer las siguientes conclusiones:

1. En este estudio se ha intentado optimizar las propiedades anticorrosivas de una imprimación cataforética mediante el estudio de la influencia que dos variables del proceso de aplicación (temperatura de curado y potencial de deposición) tienen sobre la protección final del recubrimiento. Las mejores propiedades se han encontrado cuando la temperatura de curado se encuentra en el intervalo 165-185ºC y el potencial de deposición entre 270 y 320V. Las propiedades anticorrosivas disminuyen significativamente cuando se emplean condiciones de aplicación fuera de estos intervalos.
2. Se ha formulado y producido recubrimientos en polvo mediante la utilización de triflatos de lantánido (de erbio e iterbio) en sistemas epoxi como agentes de curado. Una vez los sistemas han sido producidos se ha obtenido su cinética de curado y se han caracterizado sus propiedades térmicas, mecánicas y anticorrosivas.
3. El estudio muestra que los triflatos de lantánido en proporciones de alrededor de 1phr pueden ser una alternativa interesante a los sistemas convencionales utilizados en industria (que utilizan como agente de curado diciandiamida o sus derivados, como la o-tolilbiguanida). Proporciones fuera de este intervalo en triflato de lantánido no dan lugar a recubrimientos de buenas propiedades, si bien la adición de estos compuestos en mayores proporciones dan lugar a cinéticas de reacción más rápidas.
4. A fin de mejorar las posibilidades del uso de triflatos de lantánido en recubrimientos anticorrosivos en polvo se introdujo el ácido de Meldrum que en reacción con resina epoxi en presencia de un ácido de Lewis da lugar a un monómero expandible capaz de suplir las carencias de los sistemas homopolimerizados, creándose así nuevos sistemas de los que fueron igualmente estudiados sus propiedades cinéticas, térmicas, mecánicas y anticorrosivas.
5. Los sistemas propuestos epoxi / ácido de Meldrum (3.3 y 5 phr) / triflato de erbio (0.5 phr) han demostrado ser un buen punto de partida para desarrollar sistemas alternativos a los convencionales, ofreciendo muy bajas temperaturas y tiempos de curado, elevadas prestaciones mecánicas así como elevada protección anticorrosiva.
6. Se ha desarrollado y ampliado el conocimiento de una técnica electroquímica de evaluación anticorrosiva acelerada (AC/DC/AC). Para ello, ésta se ha aplicado a recubrimientos en polvo y cataforéticos. Los resultados obtenidos se han comparado con aquellos que otras técnicas, EIS y resistencia a niebla salina, ofrecen. A pesar de pequeñas desviaciones, la técnica electroquímica acelerada AC/DC/AC, muestra resultados similares a los de otras técnicas, pero en tiempos mucho menores (inferiores a 24horas).

6.2. TRABAJOS FUTUROS

A raíz del estudio realizado en el transcurso de esta tesis doctoral y de los resultados obtenidos, es conveniente destacar el interés que los sistemas epoxi/ácido de Meldrum/triflato de erbio ofrecen como recubrimientos orgánicos en polvo de rápido curado. Por esto, futuros esfuerzos podrían ir dirigidos a la optimización de estos sistemas, tanto en proporciones de componentes como en condiciones de curado. La introducción de pigmentos y cargas para completar el sistema anticorrosivo se plantea necesaria en futuros trabajos relacionados. En el aspecto experimental se podría estudiar con más profundidad la contracción de las muestras en su proceso de curado resolviendo los problemas experimentales encontrados.

Por otro lado, la técnica electroquímica acelerada AC/DC/AC objeto de estudio en esta tesis doctoral requeriría la elaboración de un modelo estadístico de correlación con ensayos acelerados tradicionales como la resistencia a la niebla salina y electroquímicos.